1993

High-Temperature High-Pressure Carbon Dioxide Removal From Coal Gas.

Arpaden Silaban
Louisiana State University and Agricultural & Mechanical College

Order Number 9401568

High-temperature high-pressure CO_2 removal from coal gas

Silaban, Arpaden, Ph.D.

The Louisiana State University and Agricultural and Mechanical Col., 1993

U·M·I
300 N. Zeeb Rd.
Ann Arbor, MI 48106

HIGH-TEMPERATURE HIGH-PRESSURE CO_2 REMOVAL FROM COAL GAS

A Dissertation

Submitted to the Graduate Faculty of the
Louisiana State University and
Agricultural and Mechanical College
in partial fulfillment of the
requirements for the degree of
Doctor of Philosophy

in

The Department of Chemical Engineering

by
Arpaden Silaban
Engineer, University of Sriwijaya, 1980
M.S. in Ch.E., Louisiana State University, 1989
May 1993

Debata baen donganmi. Lao mangula ulaonmu.
Baen Ibana haposanmu. Sai paserep rohami.
Debata baen donganmi. Debata baen donganmi.
(..Sian Ende Huria No. 66)

Acknowledgements

I would like to express my appreciation to Alumni Professor Douglas P. Harrison as my major advisor. His initiation, patience, encouragement, and guidance throughout this study are greatly acknowledged.

Thanks are also due to Professors Frank R. Groves, Jr, Arthur M. Sterling, and Geoffrey L. Price and Associate Professor Kerry M. Dooley of the Chemical Engineering Department, and to Associate Professor Willem H. Koppenol of the Department of Chemistry for serving as members of examining committee. Their helpful suggestions and guidance are appreciated.

I wish to thank Indonesian government via University of Sriwijaya, Palembang, Indonesia, for financial support during my study in the United States. In particular, thanks are due to Professor H. Machmud Hasjim who always supports and encourages me especially during my final year of study. My appreciation is also due to Ir. Nawawi Machmud, Ir. H. Ali Fasya Ismail, M.Eng., and Dr. Ir. Syarifuddin Ismail.

I also would like to thank the Department of Chemical Engineering for their financial support during my final semester at LSU.

I am grateful to my friends and fellow graduate students Muhammad Youvial, Marcel Narcida, and Chun Han who shared with me during the course of my laboratory work. My

appreciation also goes to Paul Rodriguez from the machine shop who always provided me the help during my difficult times on experimental problems. The help from my student workers Brandt D. and Matt H. Schumacher are greatly appreciated.

Finally, my deepest gratitude and love are extended to my wife, Doorce S. Batubara, and my son, Athens Gomes Partogi Silaban, who always encourage, motivate, and, most importantly, pray everyday during our stay at LSU.

TABLE OF CONTENTS

LIST OF TABLES

LIST OF FIGURES

Abstract

The noncatalytic gas-solid reaction between $CO_2(g)$ and $CaO(s)$ to form $CaCO_3(s)$ has been studied at high temperature and high pressure (HTHP) using a thermobalance reactor. This reaction could serve as the basis for a HTHP process for the separation of CO_2 from coal-derived gas.

The kinetics of the calcination and carbonation reactions were studied as a function of temperature, pressure, CO_2 concentration, and background gas composition. Three sorbent precursors which produced CaO having a wide range of structural properties were selected for detailed kinetic studies. They were (i) reagent grade calcium carbonate, (ii) reagent grade calcium acetate, and (iii) commercial grade dolomite containing essentially equimolar quantities of $CaCO_3$ and $MgCO_3$. Multicyle runs were conducted in order to have a better understanding of sorbent durability. Almost complete carbonation was possible using both calcium acetate and dolomite sorbent precursors; carbonation was incomplete when calcium carbonate precursor was used.

The following operating conditions were found to be most appropriate:

Calcination temperature: 750°C

Calcination pressure : 1 - 15 atm

Calcination atmosphere : any inert gas with low CO_2 partial pressure

Carbonation temperature : 650 - 750°C

Carbonation pressure : 15 atm

Carbonation atmosphere : any sulfur-free or low-sulfur coal gas

When sulfur-free simulated coal gas was tested, improved sorbent reactivity, capacity, and capacity maintenance were observed. The increase in reactivity was consistent with a higher concentration of CO_2, possibly formed by the water-gas shift reaction.

The distributed pore size model (Christman and Edgar, 1983) was used to analyze the carbonation results using the reagent grade calcium carbonate precursor. Good agreement between the model and experiment was achieved for runs at 650°C with varying CO_2 mol fraction and reaction pressure. At different carbonation temperatures, however, it was necessary to assign zero activation energies to the intrinsic rate constant and product layer diffusion coefficient in order to match the experimental data. Both of these parameters should have quite large activation energies.

Chapter 1

Introduction

Improved coal gasification technology is important if the vast reserves of coal available world-wide are to be used in a manner which is economically attractive and environmentally acceptable. A number of studies have focused on the improvement of energy efficiency in coal gasification for electric power generation. Integrated gasification combined-cycle (IGCC) power plants are reported to have an energy efficiency as high as 42.7% while the integration of currently available gasification processes with molten carbonate fuel cells (MCFCs) is expected to have 52.5% energy efficiency (Holt, 1991). These efficiency values may be compared to typical 37% efficiencies achieved in current pulverized coal fired power plants.

While the improved energy efficiency of coal gasification can be achieved, reducing or removing the adverse environmental impact associated with coal utilization has also been a major concern. Removal of trace gas impurities such as H_2S, COS, and NO_x is necessary before coal-gases are used in further processes. Conventional removal of these trace contaminants is accomplished by wet scrubbing operations which require that the hot coal-gas be cooled to near ambient temperature before treatment. The low-temperature wet removal causes a loss in thermal

efficiency and additional capital equipment cost for necessary heat exchangers is inevitably required. Further improvements in overall efficiency would be possible if contaminant removal could be accomplished at elevated temperature.

Contaminants in the coal gas, such as sulfur and nitrogen species, particulate matter, and trace metals and alkali, are detrimental to the operation of both turbines and fuel cells. These contaminants must be removed in order to reduce the capital cost and, at the same time, increase the overall cycle efficiency for the power plant. Removal of H_2S to less than 10 ppmv can minimize the corrosion of turbine blades. Removal of H_2S to less than 1 ppmv may be necessary to avoid the poisoning of electrodes in molten carbonate fuel cells (Gangwal *et al.*, 1989).

For a number of years research at LSU has focused on high-temperature coal-gas desulfurization based upon the noncatalytic gas-solid reaction between H_2S and appropriate metal oxides. Westmoreland and Harrison (1976) performed a preliminary thermodynamic analysis of various metal oxides as candidate sorbents for gas desulfurization. Using the free energy minimization method, they reported that eleven candidate solids based upon the metals Fe, Zn, Mo, Mn, V, Ca, Sr, Ba, Co, Cu, and W were thermodynamically feasible for high temperature desulfurization of low-Btu gas. Westmoreland *et al.* (1977) then performed comparative kinetic studies of

the high temperature reaction between H_2S and selected metal oxides (MnO, ZnO, CaO, and V_2O_3) over the temperature range of 300-800°C in a thermogravimetric analyzer. Gibson and Harrison (1980) studied the kinetics of the reaction between H_2S and ZnO pellets in a microbalance over the temperature range of 375-800°C. Rapid and essentially complete reaction was observed in the temperature range of 600-700°C while slow decomposition of ZnO with subsequent zinc vaporization was observed near 800°C. At temperatures below 600°C, the reaction stopped well before total ZnO conversion was obtained. Ranade and Harrison (1981) examined the effect of structural property changes during the ZnO-H_2S reaction.

Focht *et al.* (1988) studied the kinetics of the reaction between zinc ferrite, $ZnFe_2O_4$, and H_2S in the temperature range of 500-700°C. Reduced zinc ferrite in the form of ZnO plus Fe_3O_4 was found to be capable of rapid and complete reaction with H_2S at the temperatures of interest. More interestingly, Focht *et al.* (1989) reported that zinc ferrite sorbents were capable of being regenerated and subjected to a number of cycles without suffering a major activity loss. Woods *et al.* (1990) investigated the single pellet reaction between H_2S and zinc oxide-titanium oxide sorbents in an electrobalance reactor at the temperature range of 670-760°C. The addition of titanium oxide was believed to reduce the tendency for zinc oxide reduction and subsequent volatilization of metallic zinc, thereby increasing the

maximum sorbent operating temperature. Woods *et al.* (1991) also studied the reaction kinetics of another zinc ferrite sorbent having different structural properties using a thermogravimetric reactor as a function of temperature, pressure, gas composition, and sorbent radius over the temperature range of 500-700°C. H_2S concentration, reaction pressure, and sorbent radius had a strong effect on sulfidation kinetics. The sulfidation kinetics, however, were essentially independent of temperature in the 500-700°C range. More recently, Silaban *et al.* (1991) investigated zinc ferrite sorbents prepared using a number of formulation recipes and induration conditions with the objective of determining which sorbent formulations had a high reactivity and, most importantly, durability.

Similar research has been carried out by a number of researchers at other locations. Lew (1990) and Lew *et al.* (1992a), for example, studied the potential benefit of reduction and sulfidation of zinc titanate compared to zinc oxide solids. It was found that zinc titanate was reduced more slowly to volatile elemental zinc than pure zinc oxide.

H_2S removal using metal oxides at high temperature has also been tested in larger scale reactors. Grindley and Steinfeld (1981) studied the desulfurization of simulated coal gas using zinc ferrite sorbents in a fixed-bed reactor. They reported that zinc ferrite sorbents were capable of reducing H_2S to 5 ppm. Sorbents other than zinc ferrite (zinc

titanate, zinc copper ferrite, copper aluminate, etc.) have been tested in a fixed-bed at the bench-scale level using a simulated coal gas (Gangwal *et al.*, 1988). Zinc titanate was shown to be a promising sorbent at up to 150°F higher operating temperature than zinc ferrite. Pilot scale tests of a hot gas cleanup system using zinc ferrite were also performed by KRW Energy System, Inc. (Schmidt *et al.*, 1988), the M.W. Kellog Company (Buckman *et al.*, 1988), GE Environmental Services (Cook *et al.*, 1988), and Texaco Inc. (Robin *et al.*, 1988).

While the removal of trace components from coal gases at high temperature has been studied extensively and has proven to be feasible, it is also desirable to separate bulk gasifier products in order to achieve further improvements in gasification process efficiency and economics. The U.S. Department of Energy has identified the need for bulk separation processes which would operate within a temperature range of 100-700°C. Typical bulk gas components produced from coal gasification are carbon dioxide, carbon monoxide, hydrogen, nitrogen, and methane.

1.1 Bulk Removal of CO_2 at High Temperature

Bulk removal of CO_2 can improve the performance of several downstream processes which utilize the coal gas. Examples are increased heating value of the fuel gas, increased efficiency of the shift conversion process for

production of hydrogen or methanol and ammonia synthesis gas, and the improved operation of molten carbonate fuel cells. The production of hydrogen will be described as an example.

Coupling the well-known shift reaction for hydrogen production with CO_2 removal at high temperature could improve the efficiency of the process. Consider the water-gas shift reaction:

$$CO + H_2O \rightleftharpoons CO_2 + H_2 \qquad (1.1)$$

Multiple catalytic reactors are normally required because the exothermic reaction is highly reversible. The "high" temperature shift catalyst , which normally operates in the 350-450°C range, consists of chromia-promoted iron oxide. The "low" temperature catalyst, operating at the temperature range of 200-250°C, consists of copper and zinc oxides supported on Al_2O_3. A serious problem associated with low temperature catalysts is the possibility of catalyst poisoning by sulfur compounds. This problem could be more serious when the synthesis gas is derived from coal gasification because of the sulfur content.

Removing the CO_2 as it is formed will avoid the equilibrium limitation and increase the yield of H_2. This can be done by direct coupling between reaction (1.1) and reaction (1.2):

$$CaO_{(s)} + CO_{2(g)} \rightleftharpoons CaCO_{3(s)} \qquad (1.2)$$

The concept of simultaneous high-temperature CO_2 removal and shift reaction was first proposed by Gluud *et al.* (1931) and later revived by Squires (1967). However, the concept was not economically competitive at that time due to the availability of reliable and low-cost methods of CO_2 removal near ambient temperature.

A brief thermodynamic analysis will illustrate the potential of combining the high temperature shift reaction with CO_2 removal. The equilibrium constant for the shift reaction (1.1) is

$$Kp_1 = \frac{p_{CO_2}\, p_{H_2}}{p_{CO} p_{H_2O}} \qquad (1\text{-}1)$$

Kp_1 as a function of temperature may be calculated using the thermochemical constants of Barin and Knacke (1973):

$$\log_{10} Kp_1 = a + bT + cT^2 + dT^3 + eT^4 \qquad (1\text{-}2)$$

where a = 10.56, b = -2.9E-02, c = 3.06E-05, d = -1.41E-08, and e = 2.07E-12. The equilibrium constant for reaction (1.2) is

$$Kp_2 = \frac{1}{p_{CO_2}} \qquad (1\text{-}3)$$

Kp_2 can be expressed as a function of temperature (Barin and Knacke, 1973):

$$\log_{10} Kp_2 = a + bT + cT^2 + dT^3 + eT^4 \qquad (1\text{-}4)$$

where a = 47.69, b = -0.13, c = 0.14E-03, d = -0.75E-07, and

e = 0.15E-10. An expression for the overall equilibrium for the combined reactions is

$$K_a = Kp_1\, Kp_2 = \frac{P_{H_2}}{P_{CO}\, P_{H_2O}} \qquad (1\text{-}5)$$

Figure 1.1 illustrates the equilibrium calculation for a typical synthesis gas composition consisting of 18.9%(mol) H_2, 3.0% CO, 2.5% CO_2, and 75.6% H_2O. At 723 K, for example, the equilibrium fractional conversion of CO without using CaO for CO_2 removal (curve A) is only 93%. Using the combined reactions at 1 atm (curve B), the equilibrium CO conversion is essentially complete for all temperatures less than about 800 K. Moreover, at 22.1 atm (curve C) essentially complete CO conversion is feasible to about 900 K. When the $CaCO_3$ decomposition temperature is approached, the equilibrium CO_2 pressure increases and equilibrium CO conversion approaches the level corresponding to the shift reaction alone.

As a second example, separation of CO_2 from coal-derived gas before being fed to a molten carbonate fuel cell can improve the overall system efficiency. Figure 1.2 (from Hauserman *et al.*, 1991) shows a diagram of a conceptual advanced gasification and molten carbonate fuel cell system. "Clean" coal-derived gas is sent to a CO_2 separation section leaving H_2 and CO which are sent to the anode part of a molten carbonate fuel cell while the separated CO_2 is directed to the cathode. This approach can improve the

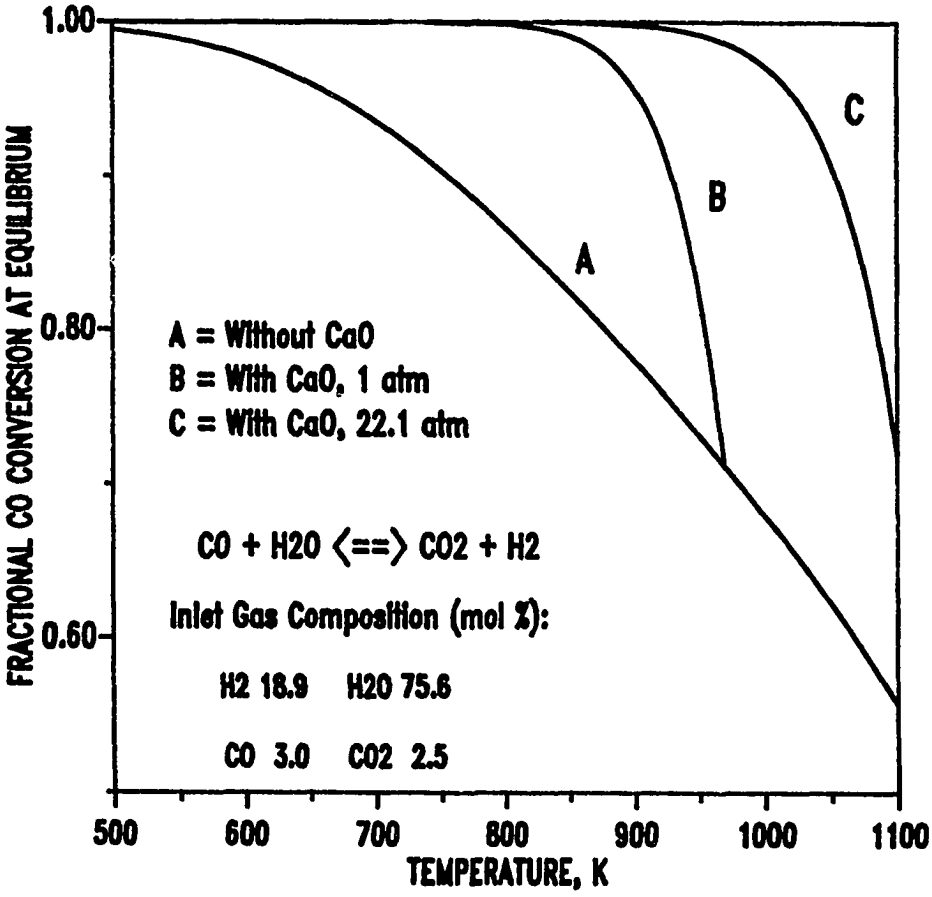

Figure 1.1 Equilibrium CO Conversion for the Simultaneous Water-Gas Shift and Carbonation Reactions

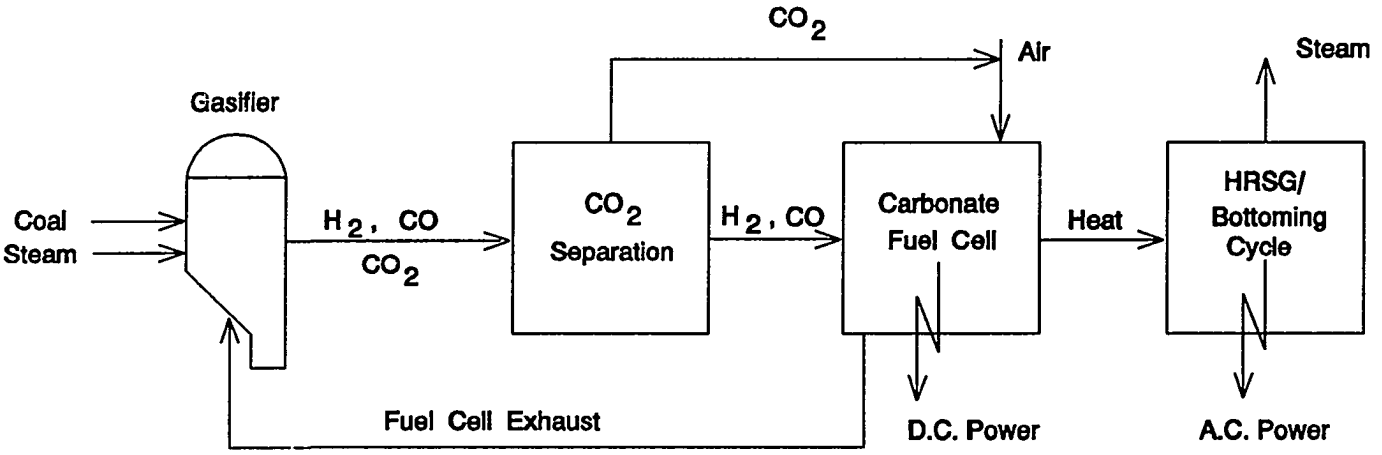

Figure 1.2 Advanced Gasification / Carbonate Fuel Cell System
(from Hauserman et al., 1991)

overall efficiency from about 46% without CO_2 separation to about 53% with CO_2 separation (Hauserman *et al.*, 1991).

1.2 Objectives of Current Study

High temperature CO_2 removal from simulated coal-gas has been studied by utilizing the reversible noncatalytic gas-solid reaction with calcium oxide, reaction (1-2). Figure 1.3 shows calculated values of the equilibrium ptressure of CO_2 over CaO for the temperature range of 773 to 1273 K using Gibbs free energy data from Hougen *et al.* (1959). In many gasification processes the product gas is at a temperature of 500 to 700°C and a pressure of 5 atm or higher. With a relatively high CO_2 content in the gasifier product (e.g., 15 volume%) CO_2 removal (forward reaction) is favored at the above temperatures and pressures. Moreover, the reverse reaction may be accomplished by lowering the operating pressure, reducing CO_2 partial pressure, and/or increasing the operating temperature. For coal gas entering at 650°C, 15 atm and containing 15% CO_2, for example, it is theoretically possible to achieve 99.6% CO_2 removal. With lower temperatures, higher pressures, and/or higher inlet CO_2 concentrations, greater CO_2 removal efficiencies are theoretically possible.

The objective of this research has been to determine the technical feasibility of CO_2 separation using a CaO-based sorbent at high temperature and high pressure by performing

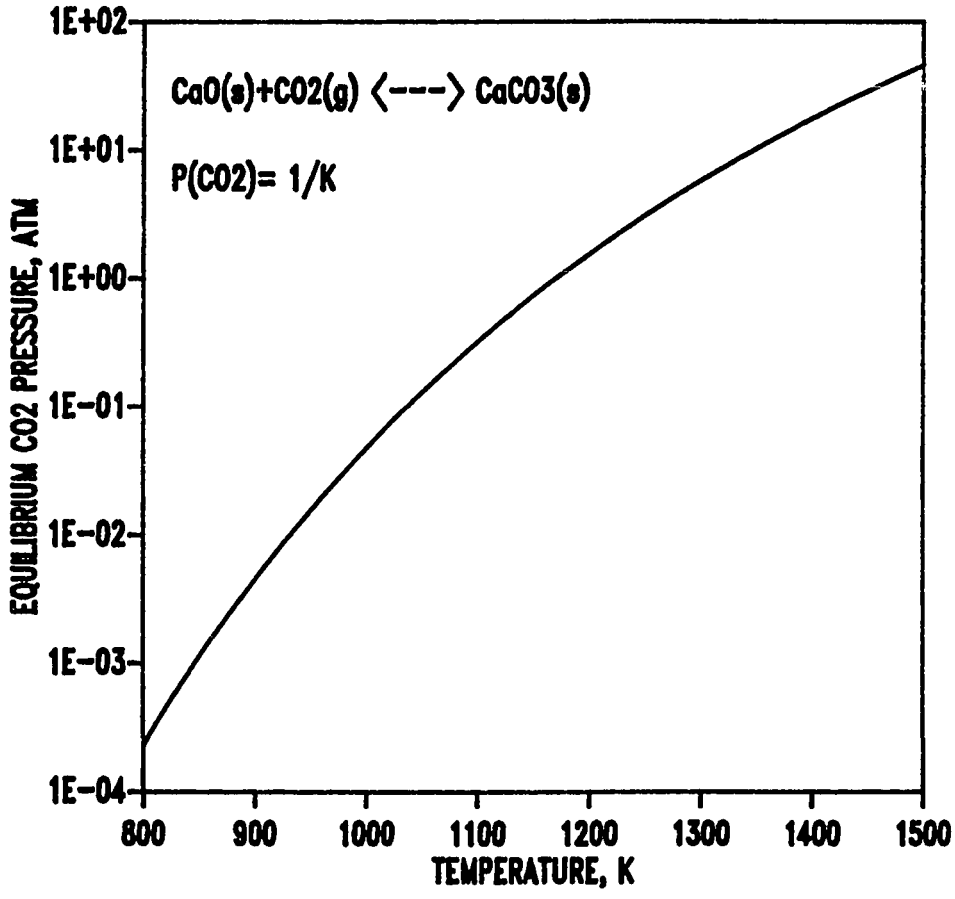

Figure 1.3. Equilibrium CO_2 Pressure as a Function of Temperature

kinetic studies to determine the effect of operating conditions, sorbent properties, and multicycle operation in laboratory scale equipment.

Structural properties of "fresh" sorbents and after being subjected to various reaction conditions, from the related study of Narcida (1992), are used to support the kinetic studies.

In addition, the experimental results have been analyzed using an appropriate gas-solid reaction model in order to better understand the behavior of the reaction.

Chapter 2

Literature Review

The literature review focuses on three major areas. The first concerns previous studies on carbonation of CaO-based materials. The second major area concerns the structural property changes which occur during calcination of $CaCO_3$ and subsequent carbonation of CaO. The discussion includes the similar behavior associated with the CaO + SO_2 reaction. Numerous studies of this reaction have been performed due to the need for removing sulfur compounds in flue gas desulfurization. Finally, mathematical models for describing the reaction between a gas and a porous solid whose structural properties change will be reviewed.

2.1 Carbonation of CaO-based Materials

The possibility of using the carbonation reaction for CO_2 removal was considered at least as early as the 1920s. Gluud *et al.* (1931) patented a process for producing hydrogen via the water-shift reaction using calcined dolomite as a combination shift catalyst-CO_2 sorbent in a fixed bed reactor. They found that MgO served as a catalyst in CO conversion while CaO reacted with CO_2 to form $CaCO_3$. Squires (1967) revived the concept and suggested the use of dual fluidized-bed reactors to permit steady-state operation and overcome other problems associated with Gluud's concept. The

CO_2 acceptor process (Curran *et al.*, 1967) was based upon the simultaneous removal of H_2S and CO_2 from coal-derived gases. Dolomite was again used as the solid sorbent. Since each of these studies was process oriented, essentially no fundamental kinetics data were reported.

Dedman and Owen (1962) performed a more fundamental study of the carbonation of CaO. They studied the reaction at the temperature range of 100-600°C using various CO_2 pressures. The reaction of CO_2 with calcined limestone occured in two stages; a very rapid initial reaction was followed by an abrupt transition to a much slower reaction well before all calcium was reacted. The rapid stage was reported to be due to chemisorption and reaction of CO_2 on the surface while the slower reaction stage was due to the diffusion of the gases in pores at the lower temperature and migration of the ions at higher temperature (above 300°C).

Barker (1973) examined the reaction between CO_2 and CaO at 866°C in a thermogravimetric analyzer using calcium carbonate of particle diameter of 2 to 20 microns. Figure 2.1 shows the typical response found when $CaCO_3$ was subjected to multiple calcination and carbonation cycles. As seen in the figure, calcination was always complete (56 weight %). The carbonation reaction, however, was initially rapid and after reacting to approximately 72% carbonation, the reaction rate quickly dropped off well short of completion. 98% carbonation was achieved after 24 hours. Barker also found that

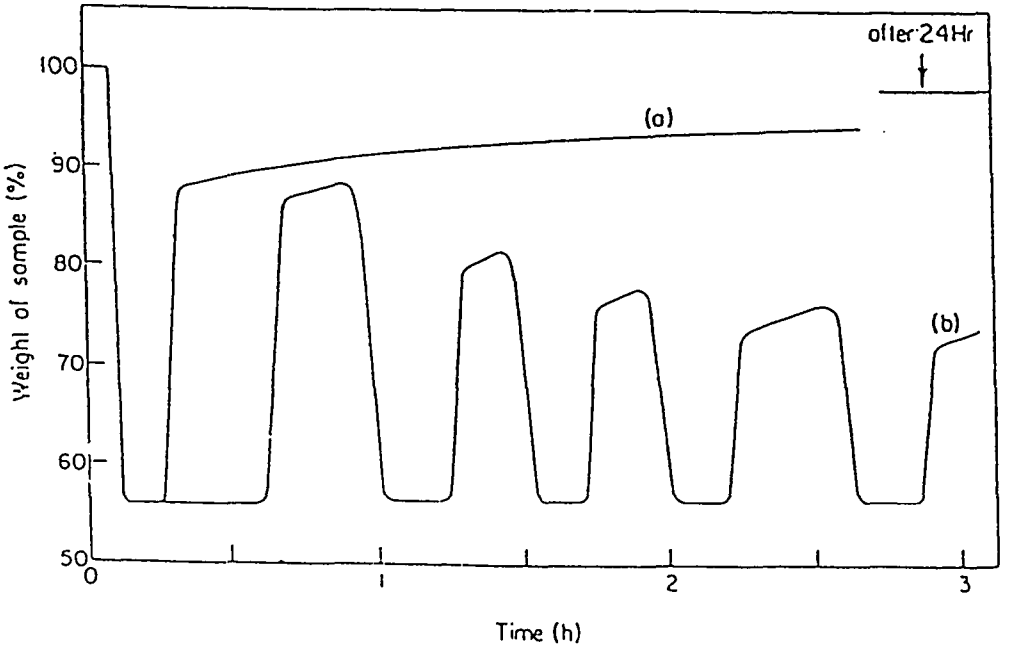

Figure 2.1 $CaCO_3$ Calcination and Recarbonation
(a) 24 hr. Recarbonation
(b) Multiple Short Cycles
(from Barker, 1973)

carbonation gradually decreased with multiple cycles as a result of the loss of pore volume in the CaO and possibly sintering of the carbonate. In a subsequent study, Barker (1974) utilized very small particles (diameter of about 20 nm) in order to achieve complete carbonation with no deterioration as the number of cycles increased. While complete reaction was achieved, the use of such a particle size is commercially difficult.

Delucia (1985) studied multicycle carbonation runs in a TGA at atmospheric pressure over the temperature range of 50 to 800°C. Calcined samples were reported to have a smaller particle volume than the starting calcium carbonate materials. The particles shrank from 7.4 to 24%, depending on calcination conditions. The reactivity of the particles also declined 10 to 25% per cycle. The multicycle decline was similar to that reported by Barker (1973).

Bhatia and Perlmutter (1983) studied the carbonation reaction over the temperature range of 400 to 725°C in a thermogravimetric analyzer at atmospheric pressure. They reported similar behavior, an initially rapid reaction controlled by the surface resistance followed by a much slower reaction controlled by product layer diffusion.

The incomplete reaction during the carbonation phase can be explained by considering structural property changes in the course of reaction. Precursor calcium carbonate or limestones are effectively nonporous. During calcination,

product gas CO_2 must escape from the solid structure thereby creating pores within the solid CaO. In principle, the pore volume created during calcination should be sufficient so that complete recarbonation of the CaO could occur. In practice, however, recarbonation occurs preferentially near the particle exterior and the surface porosity approaches zero preventing CO_2 from reaching unreacted CaO at the interior of the particle. During the slow reaction phase either CO_2 must diffuse through a nonporous carbonate layer or unreacted CaO must diffuse outward to complete the reaction with CO_2.

By preventing pore closure during the carbonation reaction, it is expected that the extent of reaction would increase. Dhupe *et al.* (1987) and Dhupe and Gokarn (1990) added metallurgical-grade silicon powder to CaO as an inert material. After 3 hours, 78% carbonation was achieved for calcined $CaCO_3$ with 70% inert material compared to only about 45% conversion for pure CaO. An optimum inert composition was proposed in order to achieve the maximum capacity, but with no clear explanation.

Beruto *et al.* (1988) studied the use of calcium precursor materials other than $CaCO_3$ which, upon calcination, would increase the initial porosity of CaO and allow complete carbonation. Calcium acetate and calcium oxalate were used as the CaO precursors. With calcium acetate precursor, 90% carbonation was achieved in less than 1½ hours, compared to

60% carbonation using calcium carbonate precursor at the same reaction conditions.

Oakeson and Cutler (1979) studied the diffusion-controlled reaction using nonporous CaO in a microbalance over the temperature range of 853 to 1044°C under CO_2 pressure between 2.35 and 24.89 atm. The carbonation reaction rapidly became diffusion-controlled as $CaCO_3$ built up on the surface of CaO. The carbonation rate was found to be a function of the CO_2 pressure and temperature. The pressure dependence was reported to follow a Langmuir-type adsorption isotherm with the diffusion activation energy of 29 ± 6 kcal/mol.

Finally, Mess (1989) investigated product layer diffusion in the carbonation reaction in a TGA under CO_2 pressure up to 12 atm over the temperature range of 550 - 1050°C using nonporous CaO particles. At high temperatures (>900°C), the reaction rate decreased with time and was first order in CO_2 concentration with respect to its equilibrium concentration after 600 minutes. The activation energy of steady state diffusion was reported to be 56.9 kcal/mol.

2.2 Structural Property Changes During Calcination of $CaCO_3$

As dicussed previously, calcination of $CaCO_3$-based materials creates pores within the solid product CaO. However, the recarbonation extent is obviously dependent upon

the structural properties (i.e. surface area, pore volume, and pore-size distribution) created during calcination.

In a related study, Narcida (1992) measured structural properties resulting from the calcination and carbonation of three calcium-based sorbents: (i) reagent grade calcium carbonate, (ii) reagent grade calcium acetate, and (iii) commercial dolomite. Table 2-1 summarizes the surface areas and pore volumes of the sorbents and their precursors using calcination conditions of 750°C in 1 atm N_2 for 1 hour. The low surface area and pore volume of the precursors illustrate their essentially nonporous character. After calcination, both surface area and pore volume increase significantly as volatile components are driven from the solid. It is interesting to note that calcium acetate precursor experiences the greatest increase in pore volume. This is attributed to its higher initial volatile content and the fact that calcination occurs in three distinct steps: (i) removal of water of hydration at 100-300°C, (ii) decomposition of calcium acetate into calcium carbonate at about 600°C, and finally (iii) decomposition of calcium carbonate into calcium oxide at about 700°C.

The pore-size distributions of the three sorbents emphasize the above results. Figures 2.2, 2.3, and 2.4 (Narcida, 1992) show the pore-size distributions of reagent grade calcium carbonate, reagent grade calcium acetate, and commercial dolomite, respectively, along with their calcined

Table 2-1

Structural Properties of Test Sorbents

	$CaCO_3$	Ca-Acetate	Dolomite
Surface Area (m^2/g)			
Initial	0.9	3.8	1.7
First Calcination[1]	18.5	23.2	14.4
First Carbonation[2]	1.1	3.8	6.4
Pore Volume[3] (cm^3/g)			
Initial	0.00	0.06	0.05
First Calcination[1]	0.25	0.96	0.40
First Carbonation[2]	0.00	0.15	0.15
Second Calcination	0.19	0.79	0.38

[1] Calcined at 750°C, 1 atm in N_2 for 1 hour

[2] Carbonated at 750°C, 1 atm, 15% CO_2/N_2 for 1 hour

[3] Pore diameter range from 0.02 to 1.0 microns

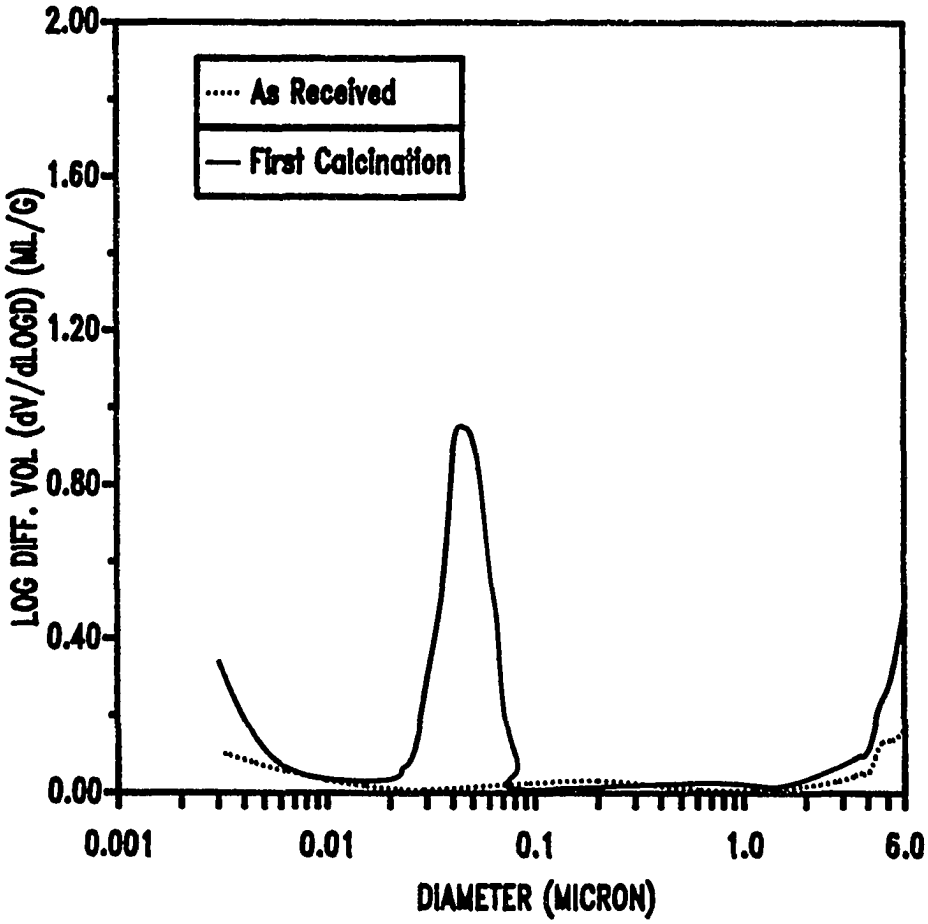

Figure 2.2 Pore Size Distribution of As-Received Calcium Carbonate and after Calcination at 750°C in N_2 Atmosphere for 1 hour (Narcida, 1992)

products, CaO. As shown in Figure 2.2, pores with diameters of 0.02 - 0.08 μm are created during the calcination of calcium carbonate. Calcination of hydrated calcium acetate occurs in three steps, with each step contributing to the final structure, as shown in Figure 2.3. First, removal of water of hydration at 300°C produces pores in the range of 2 - 8 μm. Second, decomposition of calcium acetate into calcium carbonate (shown as 550°C calcination) creates a broad distribution of pores with a peak at 0.8 μm. Finally, upon decomposition of calcium carbonate into calcium oxide (shown by the curve labeled Calcined at 750°C) two ranges of pore sizes are formed; the larger pores cover a wide range of diameters between 0.1 - 6 μm and the smaller pores have an average diameter of 0.035 μm. The calcination of commercial dolomite releases gaseous CO_2 from both $MgCO_3$ and $CaCO_3$ decomposition. As shown in Figure 2.4, this calcination produces a bimodal pore size distribution with average diameters of 3 μm and 0.05 μm, respectively.

It is interesting to note that the pores in the 0.02 - 0.08 μm diameter range are common to all calcined precursors. The small pores may be represented as those as being formed during the final decomposition of $CaCO_3$ into CaO. Even though the scales on y-axis of Figures 2.2, 2.3, and 2.4 are different, the intensity of the 0.02 - 0.08 μm diameter range is essentially the same.

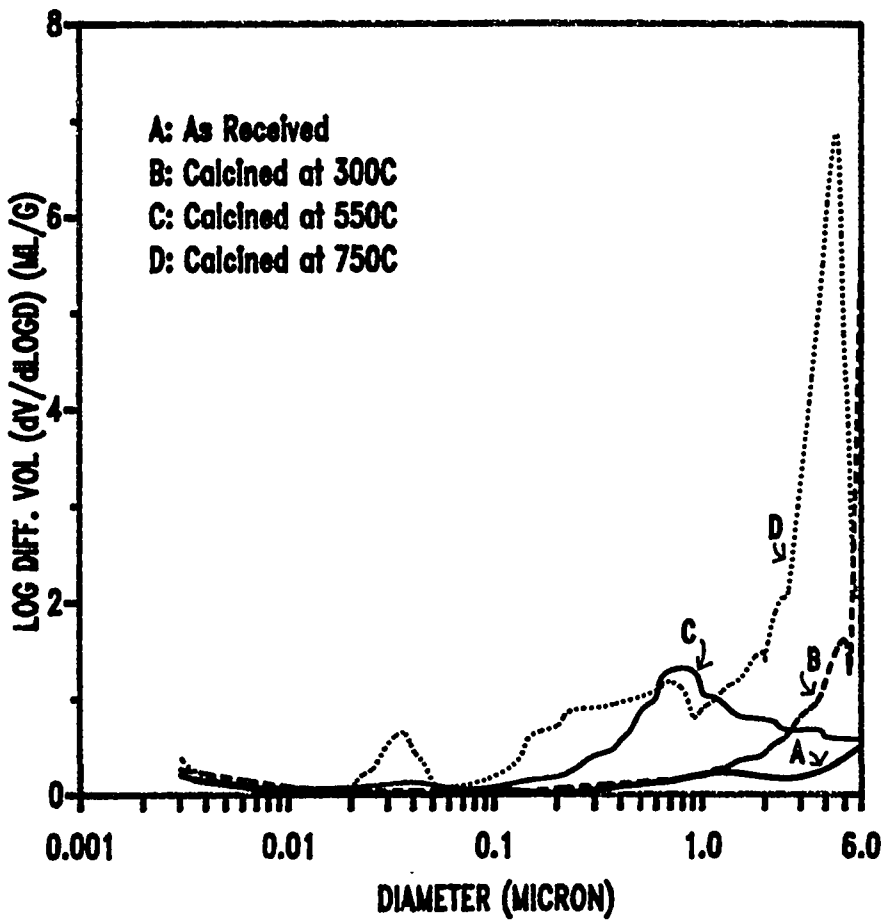

Figure 2.3 Pore Size Distribution of As-Received Calcium Acetate and after Calcination Temperatures in N_2 Atmosphere (Narcida, 1992)

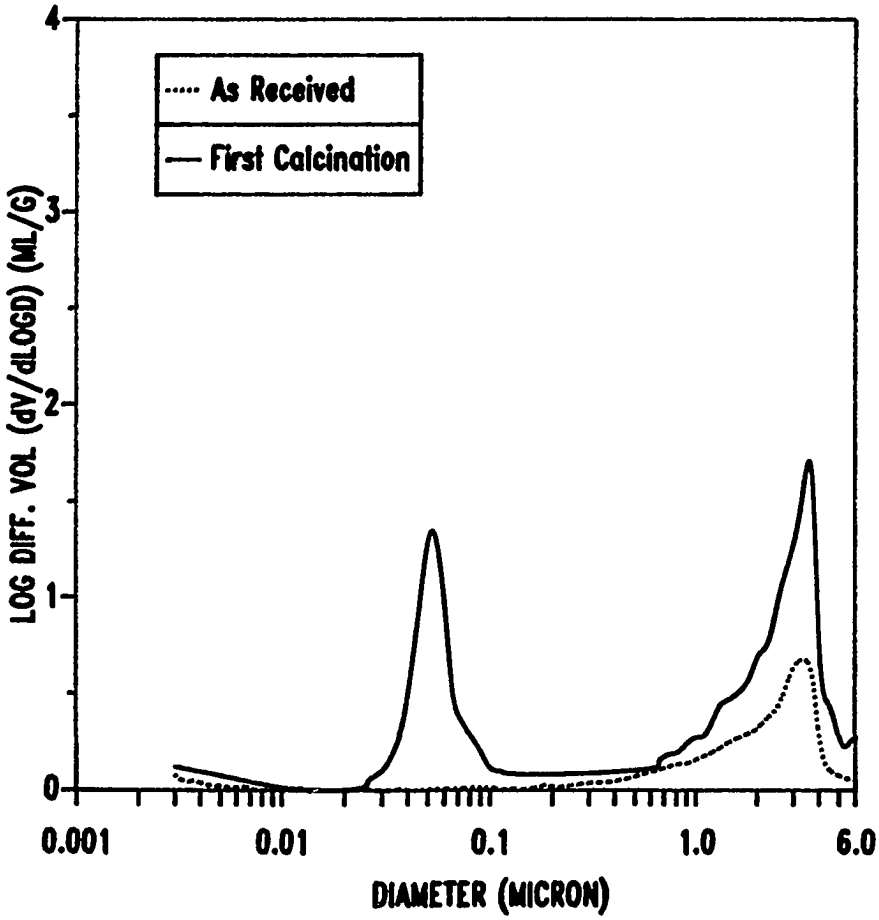

Figure 2.4 Pore Size Distribution of As-Received Dolomite and after Calcination at 750°C in N_2 Atmosphere for 1 hour (Narcida, 1992)

A similar phenomenon occurs during the calcination of $CaCO_3$ and subsequent sulfation of CaO in flue gas desulphurization processes, which have been studied in a great detail. As a guide to this study, important structural effects associated with this reaction are discussed below.

Hartman *et al.* (1978) reported that the porosity of the calcined $CaCO_3$ was a strong function of the porosity of the natural rock precursors. Limestones, chalks, and marls were tested. Subsequent sulfation results, as shown in Figure 2.5, illustrate the importance of the calcine porosity on the sulfation reaction. Using nonporous limestone ($\epsilon_{LS} = 0$), the fractional sulfation was less than 0.30 after 60 minutes. The moderate porosity chalk ($\epsilon_{LS} = 0.27$) resulted in about 0.60 to 0.70 fractional sulfation after 60 minutes, while the calcine from the high porosity marl ($\epsilon_{LS} = 0.71$) was completely sulfated in approximately 20 minutes. Ulerich et al. (1978) reported that the sulfation capacity of calcined limestone was improved when calcination produced larger pore diameters. Calcination at 900°C and 0.8 atm CO_2 pressure was found to have the highest sulfation capacity.

Dogu (1981) reported that the reactivity of calcined limestone for SO_2 removal increased as the calcination temperature increased from 750 to 950°C. The improvement was attributed to an increase in the pore size of the calcined limestone. Zakarnitis and Sotirchos (1989) reported similar results, and concluded that the sulfation behavior of

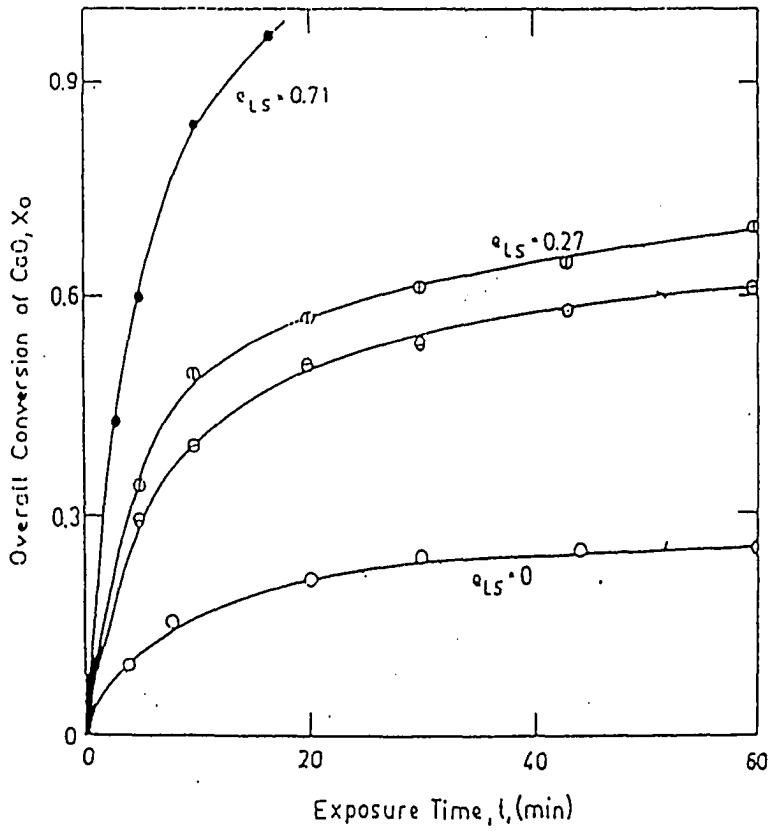

Figure 2.5 Variation of Sulfation Rate with the Porosity of Natural Rock (from Hartman *et al.*, 1978)

calcined limestone particles was dependent not only on internal surface area and porosity, but also on the pore-size distribution and interconnectedness of the pores.

The effect of calcination conditions on the structural properties of calcined $CaCO_3$-based materials has been studied. For example, Borgwardt (1989) reported that the surface area of calcined $CaCO_3$ was strongly dependent on temperature and the presence of impurities. Fuertes *et al.* (1991) studied the changes in surface area and pore size during the sintering of CaO samples. The presence of CO_2 caused a reduction in surface area and an increase in pore size. The pore volume and porosity of CaO particles was not affected by sintering.

2.3 Modeling of Noncatalytic Gas-Solid Reactions

A number of models analyzing the behavior of nancatalytic gas-solid reactions have been developed. The noncatalytic gas-solid reaction usually proceeds through the following steps:

(i) mass transfer of gaseous reactants from the bulk gas phase to the exterior surface of the solid particle,

(ii) diffusion of gaseous reactants through the pores of the solid,

(iii) diffusion of gaseous reactants through the product layer, and

(iv) chemical reaction between gas and solid reactants.

A brief introduction to simple gas-solid reaction models will be presented first. Such models assume constant solid structural properties and, therefore, are not applicable to CaO carbonation. Variable property models which might be applied to CaO carbonation will then be discussed.

2.3.1 Unreacted Core Model

The unreacted core model (Yagi and Kunii, 1955) is the simplest of the gas-solid reaction models. It assumes that the reaction occurs at a sharp interface between the solid reactant and product. Initially the interface is at the outer surface of the solid, but as the reaction progresses, the interface moves into the interior leaving behind a completely reacted product layer (see Figure 2.6). This model is limited to systems in which the solid reactant is nonporous or for the cases in which internal diffusion controls the reaction rate. It is interesting to note that the unreacted core model equations have an analytical solution making it possible to analyze the effects of the individual resistances.

2.3.2 Volumetric Model

The volumetric, or homogeneous model, describes gas-solid reaction systems in which the reaction occurs homogeneously throughout the solid (Ausman and Watson, 1962; Wen, 1968). This behavior occurs in highly porous solids where the chemical reaction resistance is much greater than

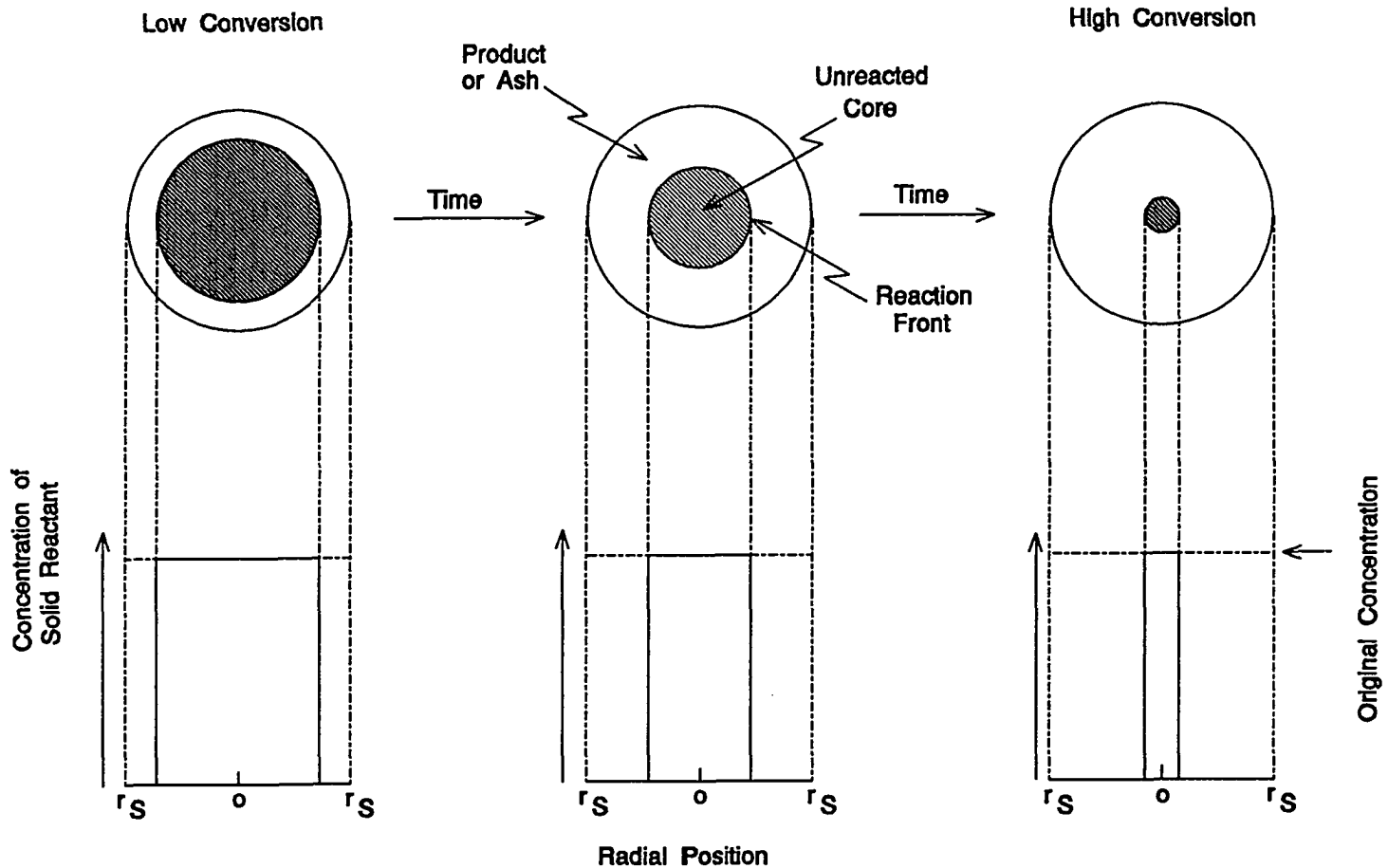

Figure 2.6 Schematic of the unreacted core model

the resistance due to internal diffusion. Figure 2.7 shows a schematic diagram of the model. In contrast with the unreacted core model, the volumetric model equations require numerical solution of the gas phase and solid phase material balances to obtain the time-conversion relationship.

2.3.3 Constant Property Grain Models

Grain models assume that the reacting solid consists of a matrix of very small grains (see Figure 2.8). The space between the grains constitutes the porous network. The model assumes that the overall grain sizes remain constant during the reaction. The reactant gas is transported to the surface of the particle from the bulk gas stream, diffuses between the grains, then through the solid product layer surrounding each grain, and reacts at the reaction interface. The reaction takes place within the grain according to the unreacted core model. These models were extensively developed by Szekely and coworkers (Szekely and Evans, 1970, 1971; Sohn and Szekely, 1972; Szekely *et al.*, 1973).

2.3.4 Constant Property Pore Model

Szekely and Evans (1970) also proposed a constant property pore model. The reacting solid is considered to be semi-infinite containing pores of uniform radius (see Figures 2.9a and 2.9b). The gaseous concentration is assumed to be constant at the mouth of the pore. The reactant gas diffuses

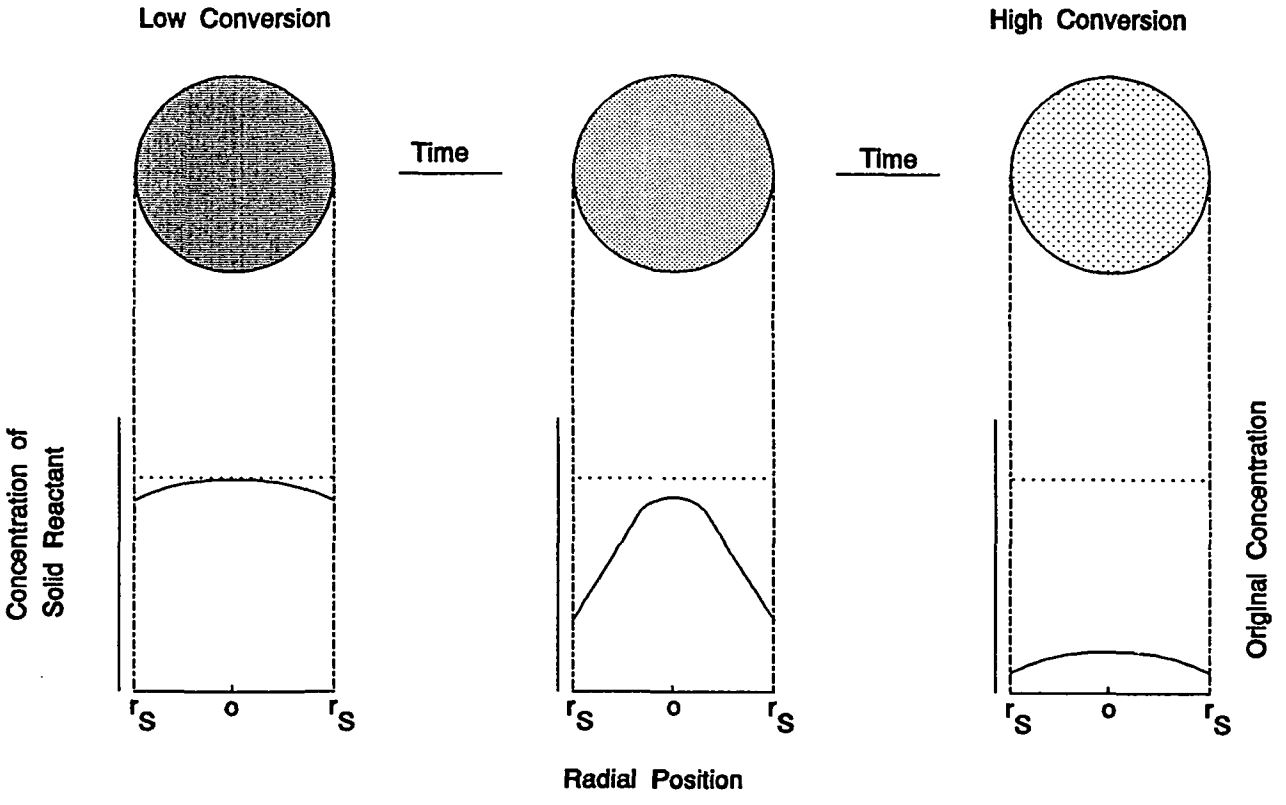

Figure 2.7 Schematic of the Volumetric Model

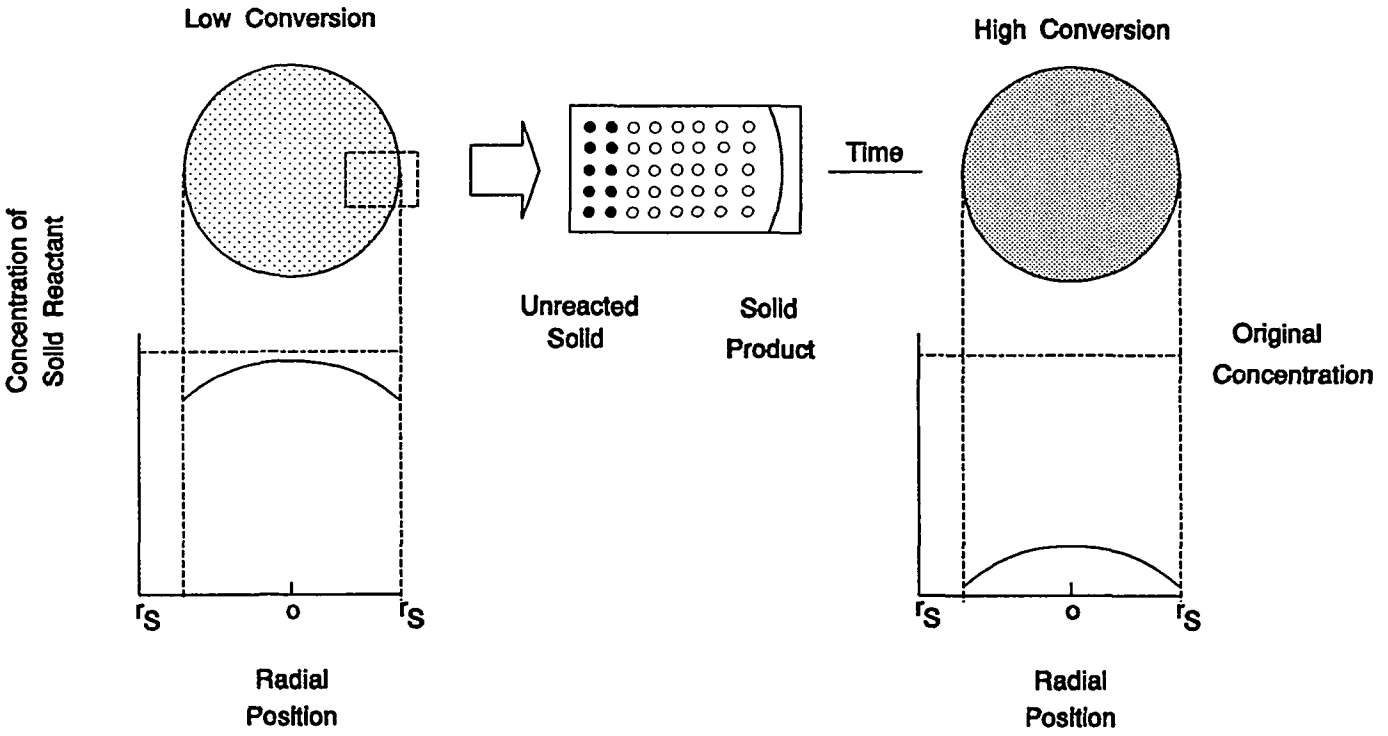

Figure 2.8 Schematic of the grain model

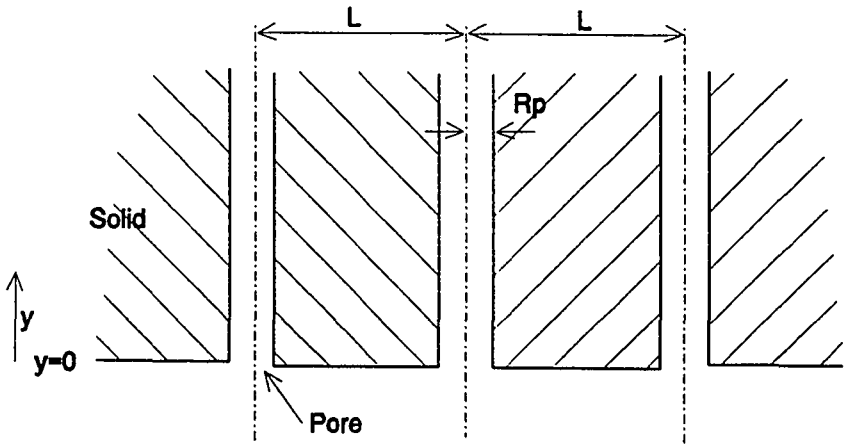

Figure 2.9a Schematic Representation of the Pore Model

(From Szekely and Evans, 1970)

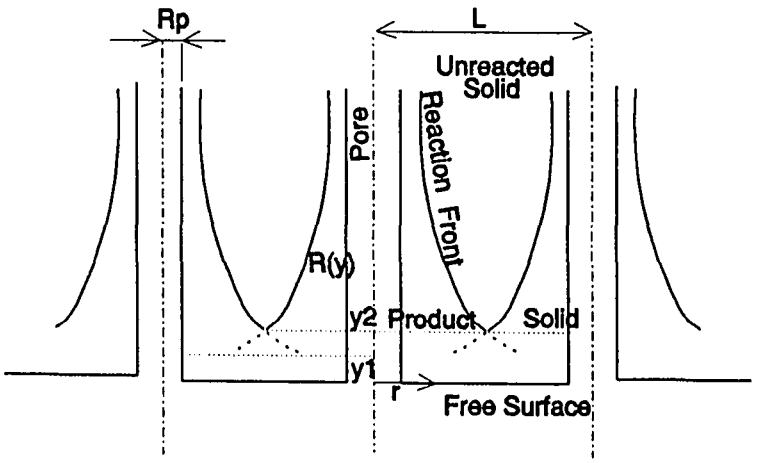

Figure 2.9b The Reaction Front in the Pore Model

(From Szekely and Evans, 1970)

axially through the pore and initially reacts with solid at the pore wall. Subsequently, a solid product layer is formed and, consequently, reactant gas must diffuse radially through this product layer. This causes the thickness of the product layer to be greater near the pore mouth (free surface) as shown in Figure 2.9b.

2.4 Modeling of Noncatalytic Gas-Solid Reactions with Structural Property Changes

In noncatalytic gas-solid reactions, when the molar volume of solid product is greater or smaller than the molar volume of solid reactant, the structural properties of the solid are expected to change. For example, for the reaction of current interest, the solid reactant CaO, having a molar volume of 16.8 cm^3/g, reacts with gaseous CO_2 to produce solid $CaCO_3$ having a molar volume of 36.9 cm^3/g. Depending upon the initial solid structure, the reaction may cease well below the theoretical maximum conversion as a result of the structural changes during the reaction.

A number of models to describe noncatalytic gas-solid reactions undergoing structural property changes have been developed, and the models may be classified into two groups: grain models and pore models.

2.4.1 Grain Models with Structural Changes

Hartman and Coughlin (1976) modified the constant property grain model in describing the sulfation of CaO. The pellet porosity was considered to decrease as the reaction proceeded. This caused the gas diffusion resistance within the pellet to increase. The model did predict the reaction "die-off" as observed experimentally (Hartman and Coughlin, 1974).

Georgakis *et al.*(1979) also modified the grain model by considering changes in the porosity of the pellet during the reaction. The porosity changes were attributed to the formation of a product layer on the grains which caused the grain diameter to increase as a result of differences in the molar volumes of reactant and product solids.

Ranade and Harrison (1979, 1981) developed the modified grain model to account for structural changes due to sintering and chemical reaction. Figure 2.10a illustrates the initial condition of grains, while Figure 10.2b illustrates the sintering which occurs during the reaction. The solid reactant was assumed spherical and was composed of microscopic spherical grains which reacted according to the unreacted core model. During the course of reaction, the specific surface area of the pellet and the grain density changed causing the change in grain radius. Sintering caused the adjacent grains to combine (see Figure 2.10b), thereby increasing the size of the grains and reducing their number.

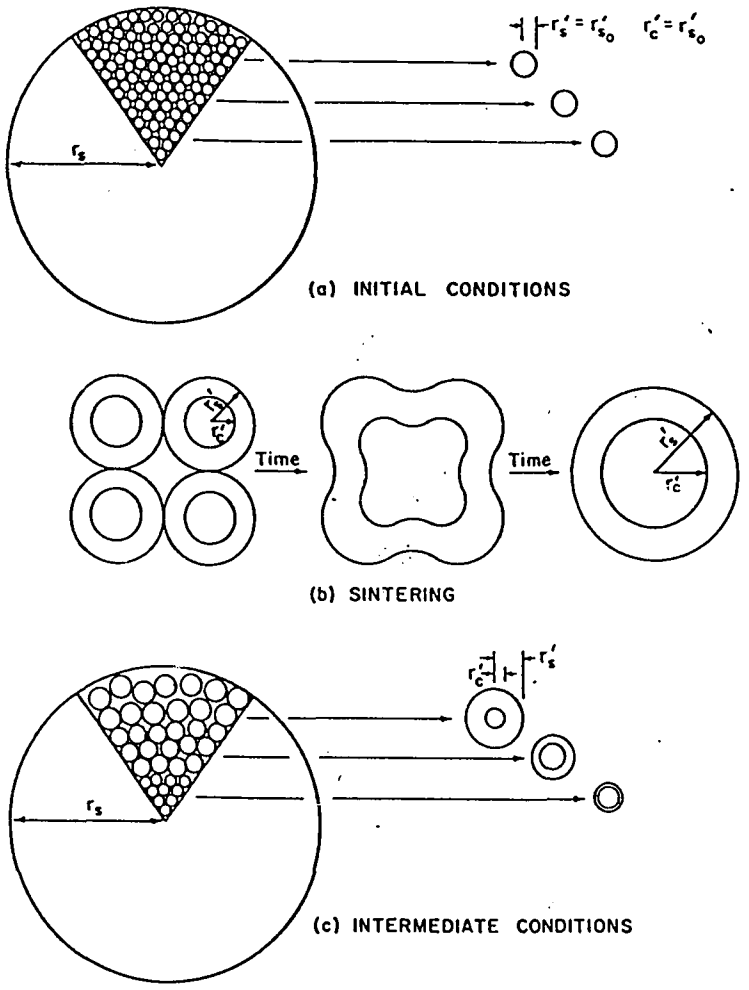

Figure 2.10 Modified Grain Model with Structural Changes Due to Sintering and Chemical Reaction (Ranade and Harrison, 1979)

Significant improvement was achieved in matching the experimental data for the reaction between H_2S and ZnO as compared to the constant property grain model.

Sotirchos and Yu (1988) developed a structural model by allowing grains to overlap. The porous solid was represented by a population of randomly overlapping grains of distributed size which react according to a shrinking core model.

2.4.2 Pore Models with Structural Changes

Ramachandran and Smith (1977) developed a single pore model for predicting the conversion-time relationship for noncatalytic gas-solid reactions. The model focused on the structural changes taking place in a single pore which was representative of the changes in the pellet. Figure 2.10 shows a cyclindrical pore of initial radius r. The single pore has a length *l*, and the solid reactant associated with that pore has an overall radius λ. The model considers the influence of pore diffusion, diffusion through the product layer, and surface reaction. When a significant gas concentration gradient along the pore exists (i.e. pore diffusion is an important resistance), a product layer of thickness $(\delta_1+\delta_2)$, as shown in Figure 2.11 is formed at position x. δ_1 and δ_2 are maximum at the pore mouth, x = 0. Consequently, the reaction can be stopped before complete conversion due to pore plugging at the mouth of the pore. The model was applied to the experimental conversion-time

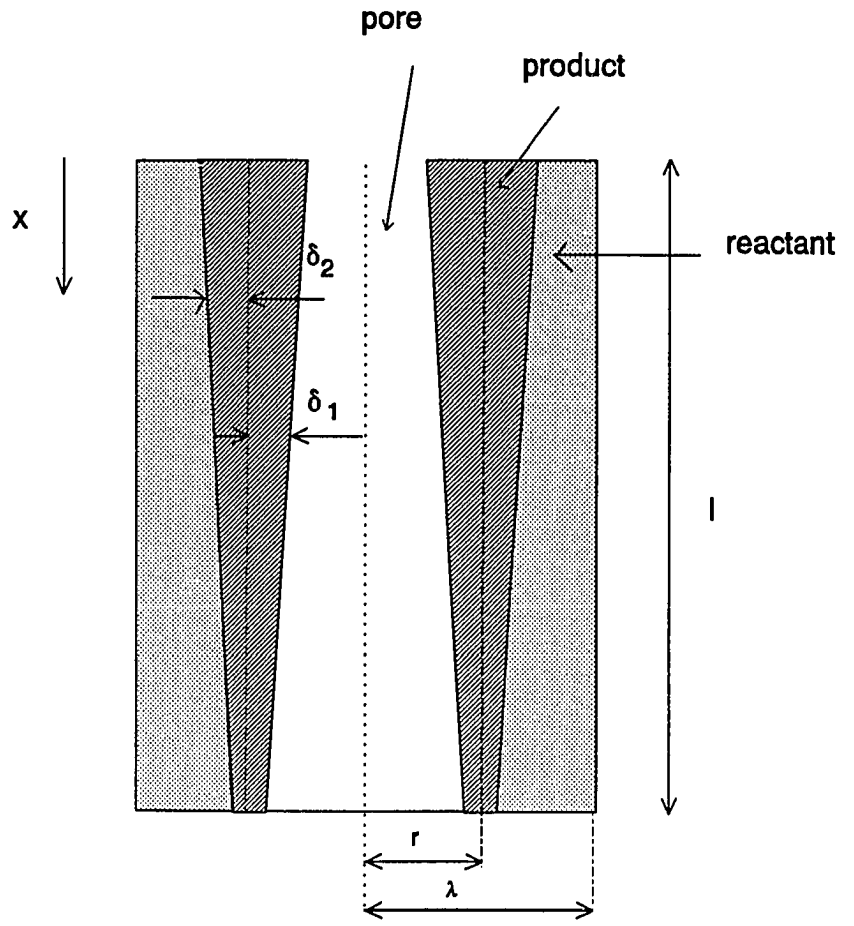

Figure 2.11 Geometrical View of Single Pore Model
(From Ramachandran and Smith, 1977)

data by Hartman and Coughlin (1974). There was good agreement between the model and experiment at the early stages, but the model overpredicted conversion as the reaction time increased.

Chrostowski and Georgakis (1978) independently developed a single pore model similar to that of Ramachandran and Smith (1977). The model considered effective diffusion coefficient (combination of molecular and Knudsen diffusion coefficients) changes due to the decrease in pore size as the product layer built up during the reaction. The model was, however, not able to improve the quantitative agreement to the experimental data of Hartman and Coughlin (1974). Lee (1980) analyzed the single pore model for a parallel-plate pore. The model was simplified to produce an analytical solution between conversion and time. Shankar and Yortsos (1983) also simplified the single pore model and obtained an asymptotic solution. The model was applied for large values of the Thiele modulus corresponding to pore diffusion control or narrow pores.

Bhatia and Perlmutter (1980, 1981) developed a so-called random pore model which allowed for variation of pore structure during the reaction. The model introduced a structural parameter which was a function of the type of pore size distribution. Pore overlapping was allowed to occur. The model was applied to CaO sulfation (Bhatia and Perlmutter, 1981) and carbonation of CaO (Bhatia and Perlmutter, 1983).

A similar model was developed independently by Gavalas (1980).

Sotirchos and Yu (1985) developed a structural model for gas-solid reactions with solid product which allowed pore closure. The model considered the effect of pore overlap on diffusion in the product layer and on the evolution of the pore surface and of the solid product-reactant interface, but did not allow for formation of inaccessible pore space. The pore structure was represented as a population of infinitely long cylindrical capillaries. Yu and Sotirchos (1987) then extended the model to allow the formation of inaccessible pore space by considering pore structures as a network of finite cylindrical capillaries. Percolation theory was used to describe the formation of inaccessible pores.

The grain and pore models discussed above were developed by considering the solid structure to have an average grain or pore size. Christman and Edgar (1983) developed a so-called distributed pore size model to describe the evolution of pore size distribution as the reaction occurred by using population balance techniques. The model accounted for four resistances to the overall reaction: mass transfer of reactive gas into the pellet, pore diffusion within the pellet, product layer diffusion, and surface reaction. A detailed explanation of this model will be presented in Chapter 8.

Sahimi *et al.* (1990) recently reviewed the noncatalytic gas-solid reaction models. They emphasized the use of percolation theory to account for the effect of dead ends, tortuous paths, and the interconnectivity of the pores. Yortsos and Sharma (1986), Reyes and Jensen (1987), and Yu and Sotirchos (1987) developed percolation-based models for describing the incomplete reactions which occur in noncatalytic gas-solid reactions.

Chapter 3

Experimental Apparatus and Procedure

The equipment and procedure used to collect experimental data in this research are described in this chapter. First, the atmospheric pressure electrobalance used for preliminary studies is presented. Second, the high pressure electrobalance reactor system will be described along with experimental difficulties encountered when using water vapor at high pressure in the electrobalance. The modification to the reactor vessel to overcome the problem is also presented. A description of materials and the gas delivery systems will follow. Finally, the procedure followed during a typical run using the high pressure electrobance is described.

3.1 Atmospheric Thermogravimetric Analyzer

An atmospheric pressure electrobalance reactor system was used during preliminary screening studies to compare the performance of different sorbents and determine appropriate calcination and carbonation temperatures. Figure 3.1 shows a diagram of the atmospheric pressure electrobalance system. The system consists of a Cahn 2000 Electrobalance equipped with a temperature programmer/controller (MicRicon), a Bascom-Turner 113-DC data center, and a gas flow control center. All gases were obtained from high purity cylinders and the flows were regulated by calibrated rotameters. Inert

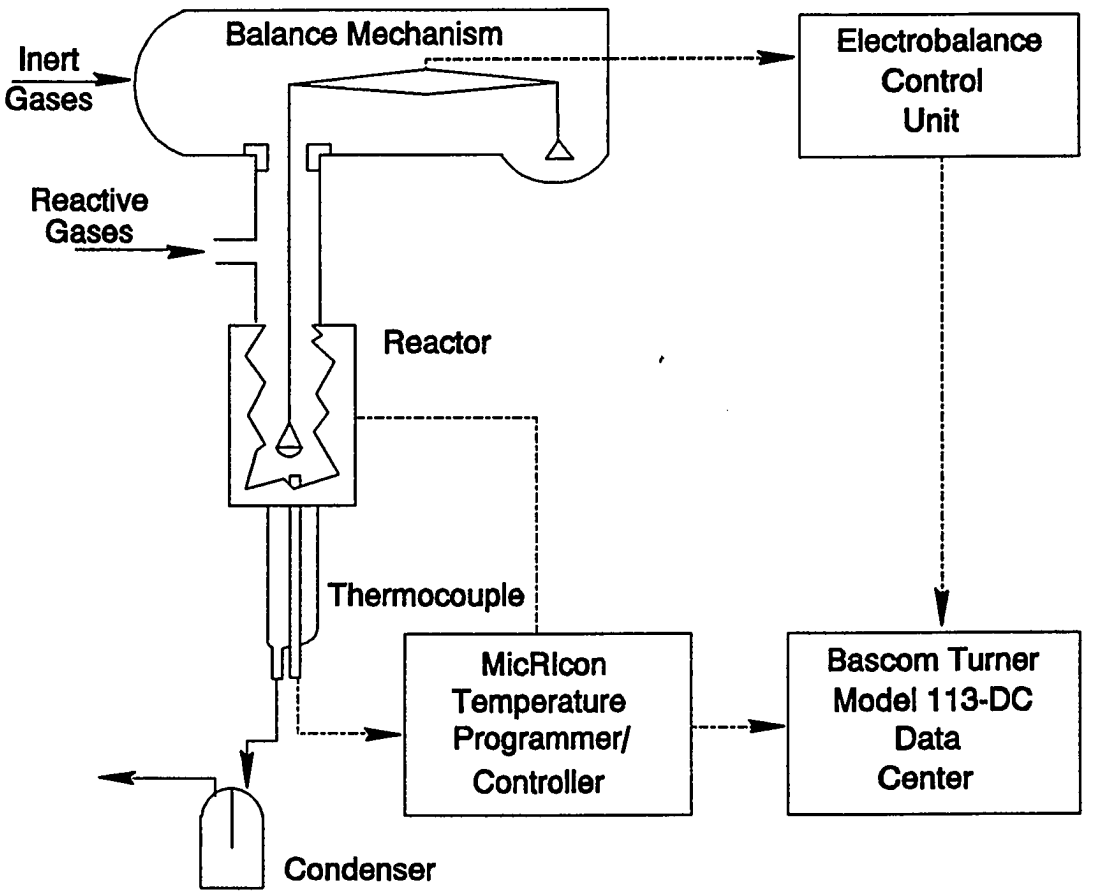

Figure 3.1 Schematic of the Atmospheric Pressure Electrobalance System

gas was added through the upper flow path to blanket the balance mechanism and prevent corrosive gas from reaching the balance mechanism. Additional inert and reactive gases were premixed and entered the reactor through the side arm of the hangdown tube. The combined gases flowed downward over the sample, passed through a condenser, and were vented to a laboratory hood. Water was introduced to the reactive gas stream using a Harvard Apparatus Model 944 precision syringe pump. To induce water vaporation, the line was heated at the point where water mixed with the reactive gases. The reactive gas feed line was also heated until it reached the reaction furnace to prevent water condensation.

Reaction temperature was monitored using a chromel-alumel thermocouple positioned about ¼ inch below the sample container. The thermocouple signal was transmitted to the MicRicon temperature programmer/controller. The thermocouple signal and the sample mass signal from the electrobalance were transmitted to the Bascom-Turner data system where results were stored on diskette and/or plotted on an x-y plotter.

A typical atmospheric pressure electrobalance response curve for one complete calcination and carbonation is shown in Figure 3.2. The sample was heated at 50°C/min to 750°C. Initial calcination, corresponding to the solid weight loss, was observed at a temperature of about 725°C, and calcination was complete approximately 30 minutes after the final

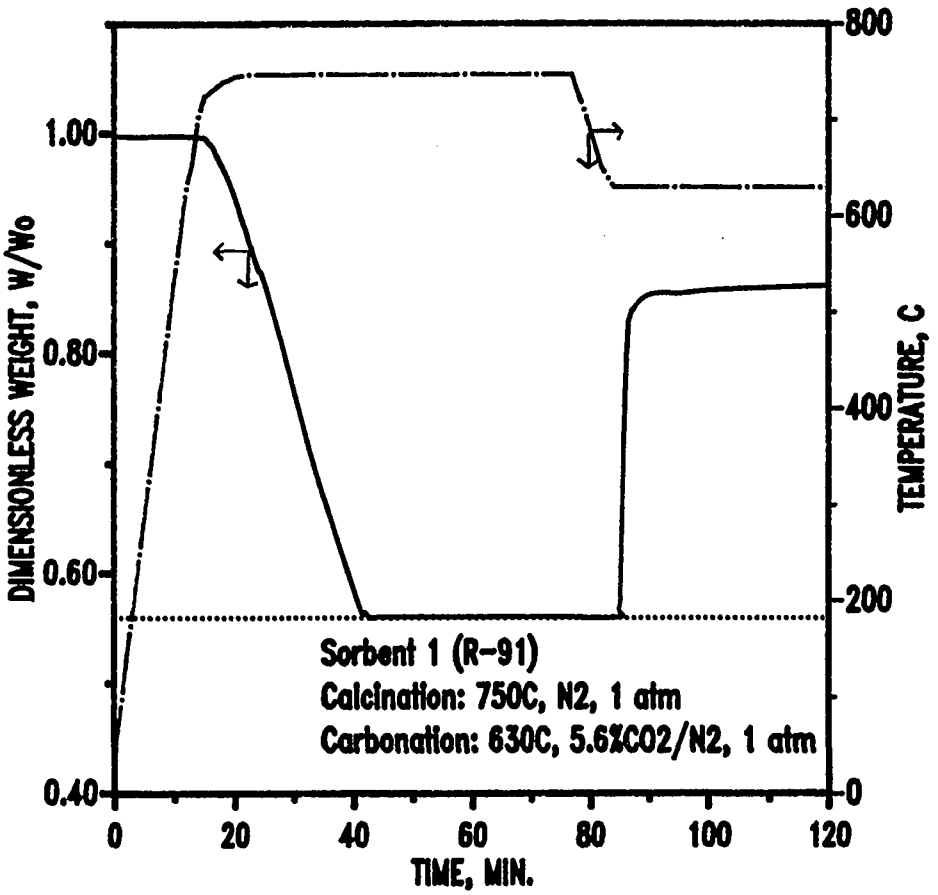

Figure 3.2 Typical Response of Atmospheric Pressure TGA

temperature of 750°C was reached. The sample weight at the end of the calcination cycle was equal to the theoretical value of W/Wo = 0.56 which corresponds to the complete conversion of $CaCO_3$ to CaO. Temperature was then adjusted to 630°C and the recarbonation phase was initiated by introducing 5.6% (vol) CO_2 in N_2. The rate of recarbonation was quite rapid for two minutes to W/Wo = 0.84. Thereafter the recarbonation rate became slow and the final W/Wo value was only about 0.86 when the run was terminated 35 minutes after carbonation began.

3.2 High Pressure Electrobalance Reactor System

The high pressure electrobalance reactor system is the primary equipment used in this research. Figure 3.3 shows a diagram of this reactor system which consists of a Cahn Model 1100 high pressure balance and its balance mechanism housing, a Cahn Model 1000 electrobalance controller, a gas feed system, and a furnace housing.

The Cahn pressure balance model C-1100 is the key component of the system. The housing and hangdown tube are constructed of 316 stainless steel capable of operating up to 1500 psi at 600°C. Two black anodized spacers are inserted in the balance mechanism housing to minimize dead volume. The balance is connected to the Cahn Model 1000 electrobalance controller having 100 g capacity and 10 μg sensivity. The

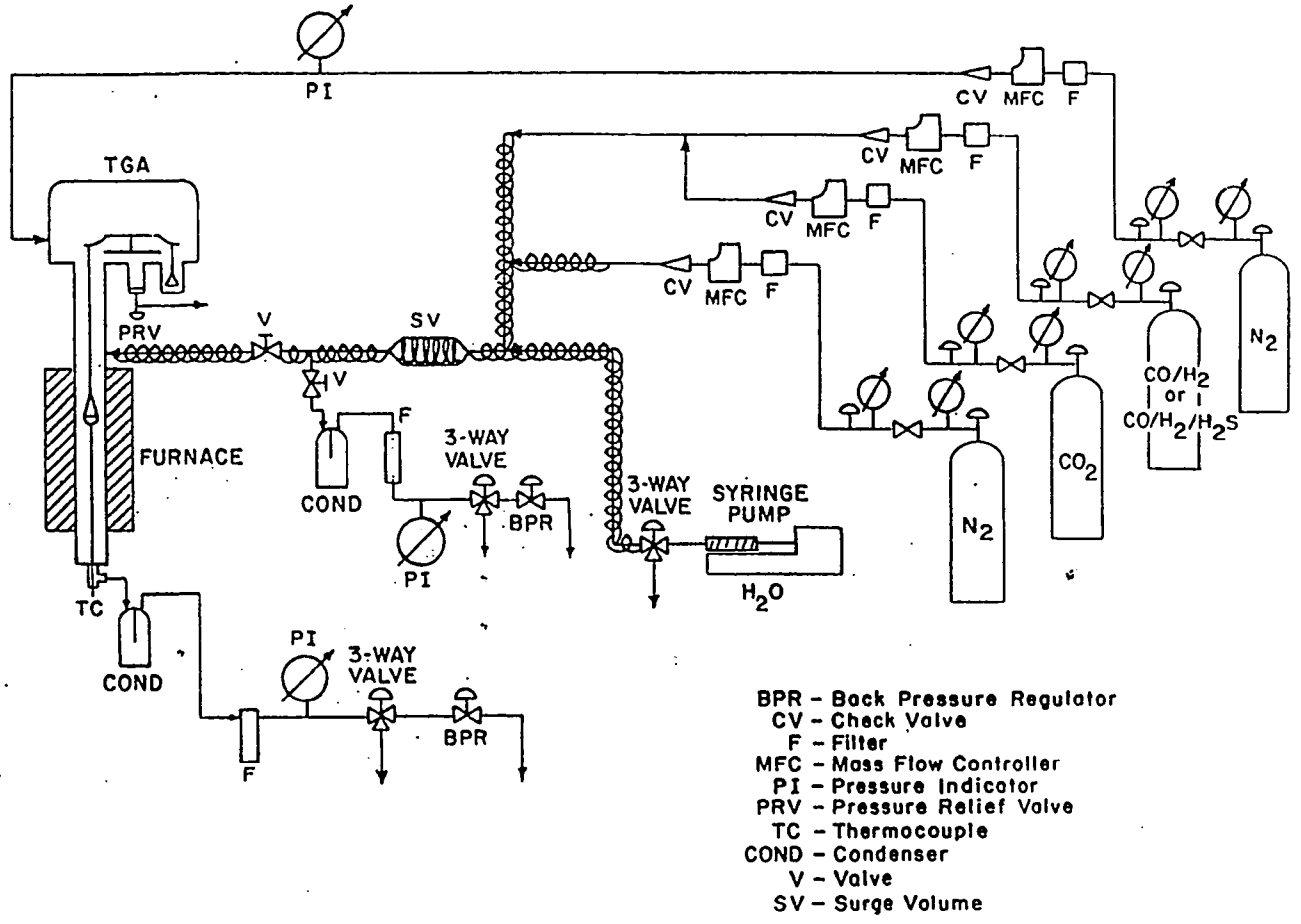

Figure 3.3 Schematic Diagram of High Pressure TGA

Table 3-1

Cahn 1000 Performance Specifications

Capacity	: 100 g
Mechanical Tare	: 100 g
Electrical Tare	: 10 g
Sensitivity	: 1 μg
Repeatability	: 10E-5 of total load on both pans
Ultimate Repeatability	: 1.5 μg
Temperature Stability	: Between 20 and 26°C
Recorder Zero Agreement	
Between Ranges	: 0.5% of Range
Calibration Range Agreement	: 0.2% of Range
Linearity	: 0.025% of Range
Accuracy	: 0.1% of Meter and Recorder Range (MRR) + 1.5E-4 of Weight Suppression Range (WSR)
Maximum Weight Change	: 10 g
Bakeout Temperature	: 125°C maximum

specifications of the Cahn Model 1000 electrobalance are illustrated in Table 3-1.

The solid sample was placed on a 9 mm-diameter bowl-type platinum container which was suspended inside the reactor hangdown tube from the electrobalance using a nichrome hangdown wire. Temperature measurement was provided by a K-type thermocouple placed about 1¼ inch directly below the sample container. The reactor temperature was maintained using a single zone split-tube furnace (Applied Test System Series 3210) equipped with a single zone temperature controller (Model 2010) and CFE Model 2040 limit controller. The temperature controller is microprocessor programmable with capability of up to 8 ramp-and-soak intervals and up to 254 cycles. The limit controller is designed to shut down the furnace system when the furnace temperature exceeds 1000°C.

The feed gas system consists of N_2 gas to the balance mechanism housing, and N_2, CO_2, and CO/H_2 or $CO/H_2/H_2S$ gases to the side arm of the hangdown tube. Each gas is fed from a high pressure cylinder through a gas filter, a high pressure mass flow controller (Porter Instrument Model 201), and a check valve. Water vapor is generated by supplying water from a high pressure syringe pump (Harvard Apparatus Model 909). The feed line leading to the side arm of the reactor hangdown tube is heated to induce water vaporation. A surge volume consisting of a 300 ml high pressure sampling bomb is included in the syringe pump exit line to dampen steam flow

variations. Combined gases flow downward over the solid reactant and exit from the bottom of the hangdown tube.

Exit gases pass through a condenser immersed in an ice bath followed by a filter, and are vented either through a three-way valve for atmospheric pressure runs or through a back-pressure regulator for high pressure runs. An identical condenser and filter arrangement is provided in the side arm gas feed line so that flow rate, composition, and pressure may be adjusted while reactant gas bypasses the reactor.

Data of solid sample weight, reactor temperature, and furnace temperature are acquired using an IBM PC with a 286 processor. A data interface package and software (supplied by Laboratory Technologies Corporation) were used for data acquisition and processing.

A typical electrobalance response curve through one complete calcination and carbonation cycle using reagent grade $CaCO_3$ (Sorbent 1) is shown in Figure 3.4. 11.8 mg of $CaCO_3$ were heated at a rate of approximately 5°C/minute to 750°C in N_2 at 1 atm. Due to the large reactor tube mass, a nonlinear response occured for the first 50 minutes of the heating cycle. However, the heating rate approached linearity before the calcination began.

The sample weight showed a small apparent increase during the early heating period prior to the beginning of calcination. This apparent weight increase was due to

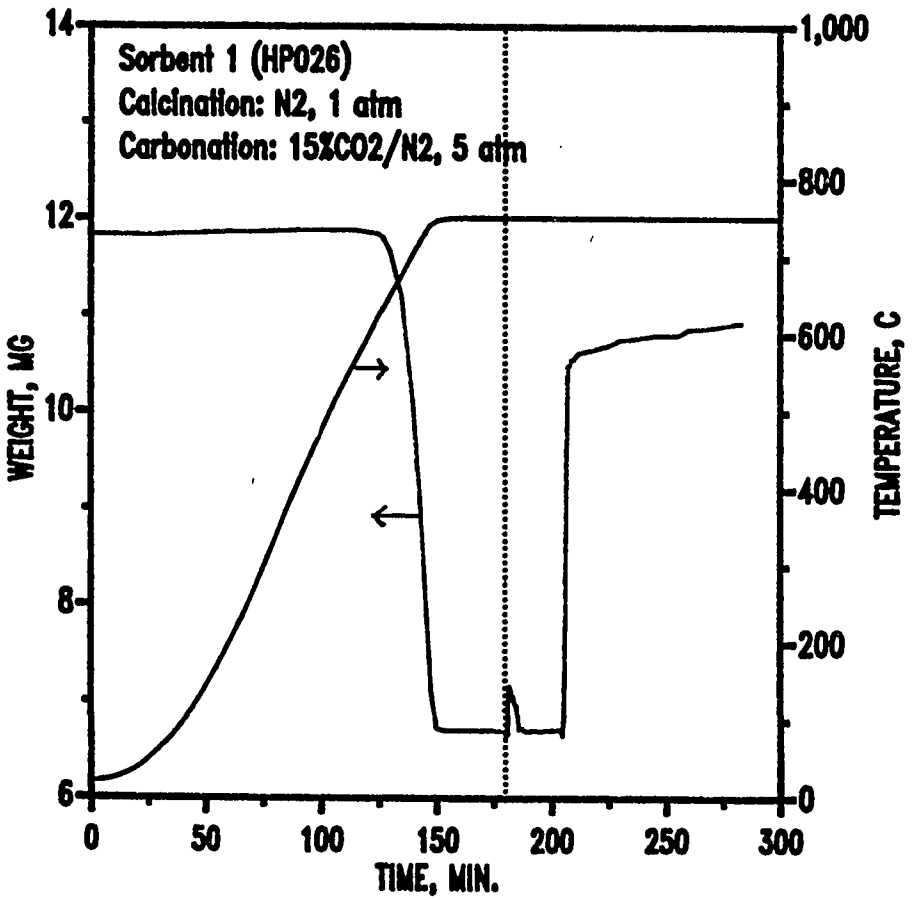

Figure 3.4 Typical High Pressure Response

increased aerodynamic drag exerted by the flowing N_2 as the temperature increased.

Calcination began after 125 minutes at the temperature of approximately 650°C and was complete after 150 minutes when the temperature reached 750°C. The sample weight of 6.6 mg at the end of calcination corresponds to the theoretical weight associated with the complete decomposition of pure $CaCO_3$ to CaO (44% weight loss).

After 180 minutes, the reactor pressure was increased to 5 atm of N_2 in preparation for carbonation. As shown in Figure 3.4, pressurization produced a temporary upset in the measured sample weight. Once the final pressure of 5 atm was reached, the sample weight stabilized at 6.6 mg. After 210 minutes, the reactive gas composed of 15%CO_2 in N_2 was introduced to the reactor tube. The carbonation reaction began immediately as indicated by the solid weight increase to 10.5 mg within approximately two minutes. Thereafter, the rate became quite slow and a maximum weight of 11.0 mg was reached when the run was terminated after 280 minutes. The 10.5 and 11.0 mg weights correspond to fractional carbonations of 0.75 and 0.85, respectively. These typical results are consistent with previous results reported in the literature (Barker, 1973, 1974; Bhatia and Perlmutter, 1983).

The high pressure reactor system described above worked well in runs at all pressures when no H_2O was included in the carbonation gas. In addition, no experimental problems were

encountered using H_2O at atmospheric pressure. However, severe experimental problems were found when high pressure carbonation runs with steam in the carbonation gas were attempted.

A typical electrobalance response during the carbonation cycle of a run in which 10% steam was introduced at 5 atm is shown in Figure 3.5. For approximately 30 minutes, carbonation proceeded in a normal manner; rapid initial reaction was followed by the expected abrupt transition to the very slow reaction after 5 minutes. At about 30 minutes, however, an abrupt solid weight loss of about 4 mg was recorded. Five minutes later, another 4 mg of solid was lost. The run was terminated after two additional weight losses occured. Only about 0.5 mg of sorbent remained in the sample pan. The actual solid loss was confirmed after the reactor was cooled and opened for inspection.

Steam condensation on the inside of the reactor hangdown tube in the cool zone where the hang-down tube joined the balance housing was believed to be the cause of the problem. During the carbonation phase using steam, the reactive gas gradually diffused upward to the cool zone when water vapor condensed and fell periodically into the hot zone where almost instantaneous vaporization occured. This produced a pressure wave of sufficient magnitude to dislodge solid from the sample pan. The problem was not encountered in atmospheric pressure runs since the volumetric flow rate of

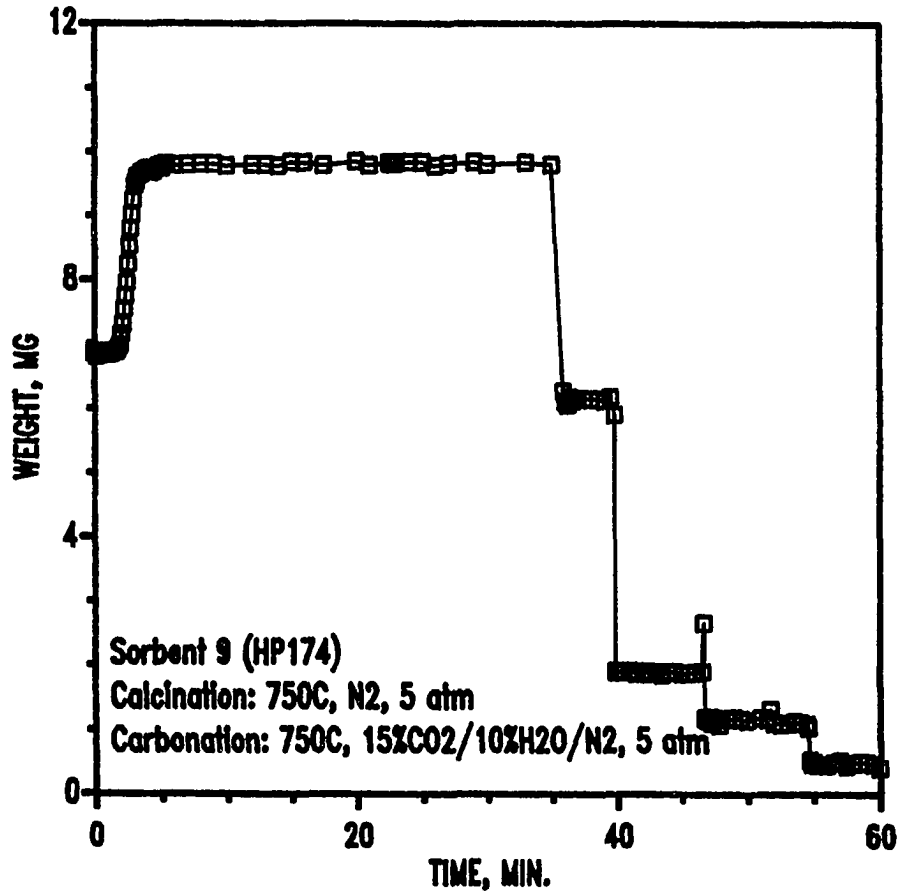

Figure 3.5 Typical Response Using Water Vapor

inert gas through the balance housing was sufficient to prevent steam from diffusing upward to the cool zone. At elevated pressures, the volumetric flow rate of inert gas was insufficient to prevent back diffusion of steam.

The above problem was solved by machining a close-fitting stainless steel rod which was inserted into the upper portion of the hangdown tube where it joined the balance housing. A diagram of the hangdown tube with insert is shown in Figure 3.6. The upper portion of the insert was attached by a press fit to the flange which attaches to the balance housing. The hang-down tube fit over the insert and the teflon sleeve sealed against the walls of the hang-down tube to prevent steam from reaching the upper cooler sections. A small hole was drilled through the wall of the insert to allow pressure equalization above and below the teflon sleeve.

Several runs were attempted after modification of the hangdown tube. There was no evidence of dislodging the sample from the sample pan. It was discovered, however, that a small amount of water condensation along the hangdown wire in the cooler regions was still occuring. While the amount of condensate was quite small and no droplets were formed, the condensate produced a small increase in apparent sample weight, thereby causing an error in the kinetic results. The open area of the gas outlet from the insert tube was reduced

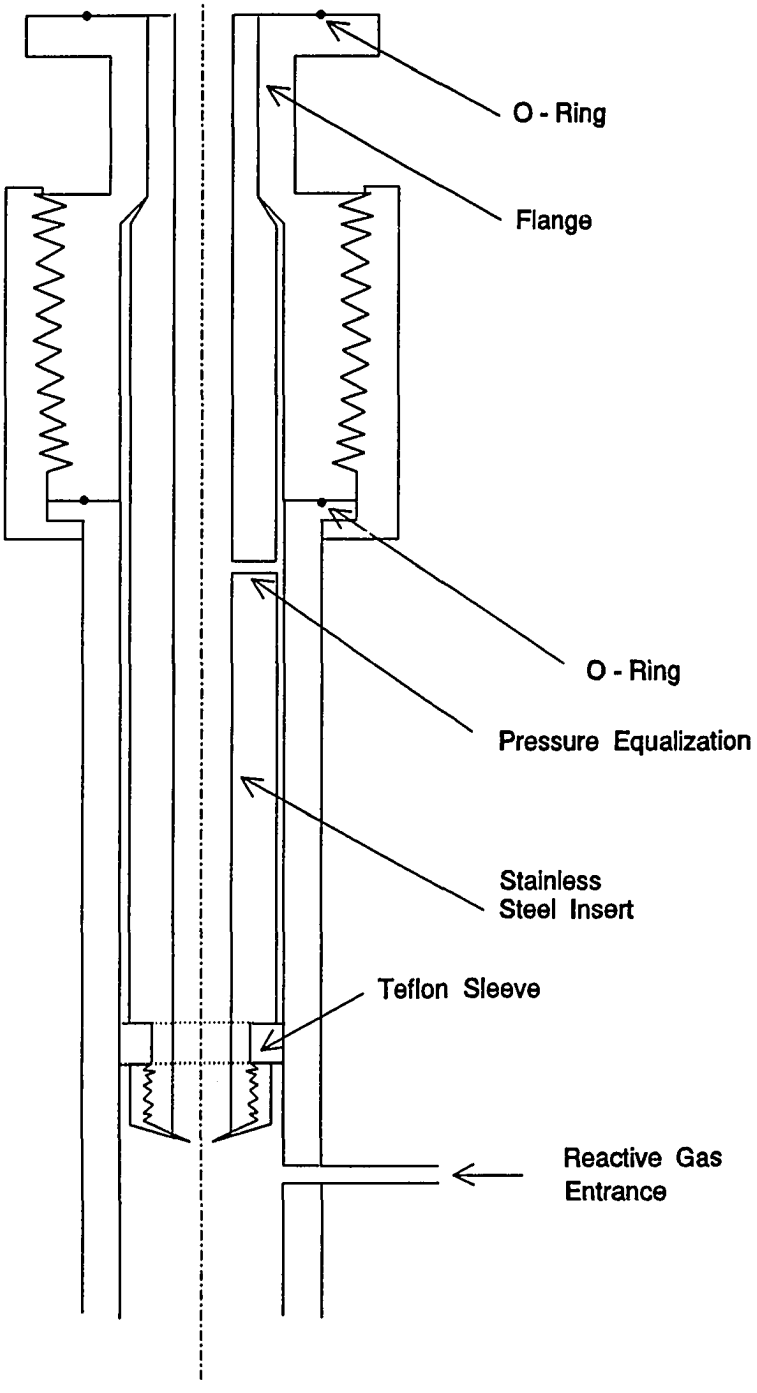

Figure 3.6 Diagram of the Insert Added to the Hangdown Tube to Prevent Steam Condensation

to prevent steam from back-diffusing up the insert (see Figure 3.6). No further experimental problems were encountered.

Figure 3.7 compares the results of a run using the original insert with the larger opening with results of a run after reducing the diameter of the opening. The insert having the larger opening was used in run HP193; a small but steady weight gain in the 5 to 22 minute time span is evident. At 22 minutes, the reactive gas (including steam) flow was stopped in preparation for the second calcination cycle. An apparent weight loss caused by evaporation of water from the hang-down tube resulted. In Run HP205, the inside diameter of the opening was reduced and there was essentially no weight gain in the 5 to 25 minute time span. Reactive gases were stopped after 25 minutes and no weight loss occured. Indeed, after 35 minutes the sample weights were effectively the same in both runs. The second calcination cycle was initiated after about 40 minutes, and the calcination curves for both runs were effectively identical.

3.3 Materials

Gases were obtained from high purity gas cylinders. In most runs nitrogen (99.96% purity), carbon dioxide (99.9% purity), and a mixture consisting of 67.3%CO/32.7%H_2 were used. A mixture of 32%H_2, 65%CO, and 3%H_2S was used in a

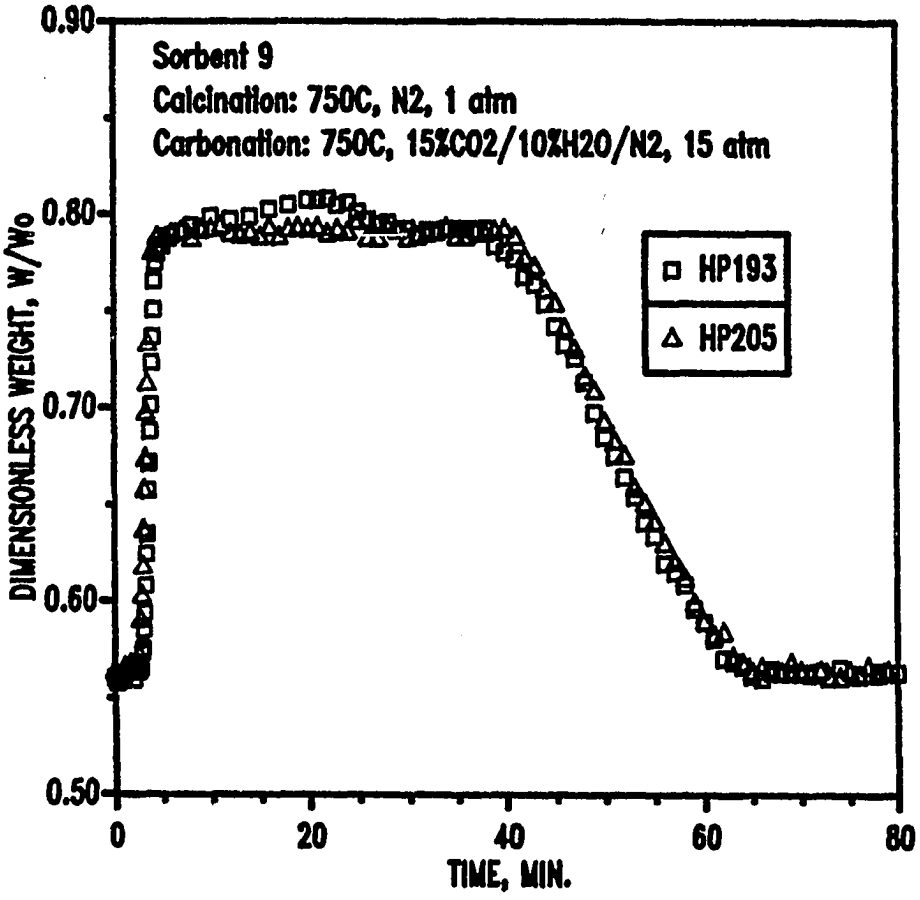

Figure 3.7 TGA Response Using Water Vapor

limited number of tests to determine the effect of H_2S on the carbonation reaction.

A total of nine calcium-based sorbent precursors were used in preliminary studies. Table 3-2 presents a general description of the sorbents. Reagent-grade calcium carbonate (sorbent 1), calcium acetate (sorbent 7), and calcium sulfate (sorbent 8) were supplied by Mallinckrodt Chemicals. Sorbents 2 through 6 were all commercial-grade $CaCO_3$ obtained from producing quarries. Commercial dolomite (sorbent 9) contained approximately equal molar quantity of $MgCO_3$ and $CaCO_3$.

As a result of preliminary screening tests, sorbents 1, 7, and 9 were selected for detailed studies. The complete chemical analysis of these materials is presented in Tables 3-3, 3-4, and 3-5.

All commercial sorbents were received as relatively large chunks. These materials were oven dried for 24 hours, crushed in a mortar, and then screened with the -400 mesh (< 38 μm diameter) fraction used in reaction tests. The reagent grade materials were in fine powder form. These materials were sieved directly and the -400 mesh fraction used in reaction tests.

3.4 Experimental Procedure Using High Pressure Electrobalance

Approximately 12 mg. of sorbent precursor was added to the sample pan and suspended on the hangdown wire from the

Table 3-2

Description of Calcium-Based Sorbent Precursors

Sorbent	General Description	Source
1	Reagent grade calcium carbonate, $CaCO_3$	Mallinckrodt Chemicals
2	Marl from producing quarry	Gifford-Hill Co. Harleyville, SC
3	Chalk from producing quarry	United Cement Co. Artesia, MS
4	Chalk from producing quarry	Texas Crushed Stone Co. Georgetown, TX
5	Limestone from newly developed quarry in Yucatan, Mexico	Vulcan Materials Co., Houston, TX
6	Chalk from producing quarry	Gifford-Hill Co. Midlothian, TX
7	Reagent grade calcium acetate, $Ca(C_2H_3O_2)_2 . x\ H_2O$	Mallinckrodt Chemicals
8	Reagent grade calcium sulfate, $CaSO_4 . 2\ H_2O$	Mallinckrodt Chemicals
9	Dolomite, $CaCO_3.MgCO_3$	National Lime Co. Findley, OH

Table 3-3

Chemical Analysis of Reagent Grade $CaCO_3$ (as Reported by Mallinckrodt)

CaCO3	99.97% (after 2 hours at 285°C)
Alkalinity	Passes Test
Ammonium (NH_4)	0.002%
Barium (Ba)	0.002%
Chloride (Cl)	0.001%
Fluoride (F)	0.0009%
Heavy Metals (as Pb)	0.0005%
Insoluble in HCl and NH_4OH ppt	0.00025%
Iron (Fe)	< 0.0002%
Magnesium (Mg)	0.0006%
Other Alkalis	Passes test
Oxidizing Substances (as NO_3)	< 0.005%
Potassium (K)	0.0006%
Silica (SiO_2)	< 0.0006%
Silicon (Si)	0.0003%
Sodium (Na)	0.002%
Strontium (Sr)	0.006%
Sulfate (SO_4)	< 0.0025%

Table 3-4

Chemical Analysis of Reagent Grade Calcium Acetate (as Reported by Mallinckrodt)

$Ca(C_2H_3O_2)_2$	> 91.47%
Barium (Ba)	< 0.005%
Chloride (Cl)	< 0.001%
Heavy Metals (as Pb)	< 0.001%
Iron (Fe)	< 0.001%
Magnesium and Alkali Salts	< 0.2%
Sulfate (SO_4)	< 0.01%
Water	8.3%

Table 3-5
Chemical Analysis of Dolomite
(as Reported by National Lime Co., Findley, OH)

Component	Weight %
$CaCO_3$	54.5
$MgCO_3$	45.0
SiO_2	0.2
Fe_2O_3	0.07
Al_2O_3	0.08
S	0.03
Other	0.12

Loss on Ignition after Calcination at 1800°F - 47.4%

balance. N_2 from a high pressure cylinder was fed using a mass flow controller adjusted at 2 liter/min to build up the desired operating pressure in the reactor system. The pressure was controlled using a back pressure regulator. During this time, the gas line was heated to insure vaporation of water. The liquid water flow rate from the high pressure syringe pump was adjusted and checked by bypassing the water flow to a graduated cylinder. After the temperature along the gas feed line was steady, the water was switched to mix with the reactive gases. After about 15 minutes, the reactive gas line was switched to a back pressure regulator to build up the same pressure as the reactor system. The total flow rate of reactive gases was 200 ml/min (STP).

After the reactor system reached the appropriate pressure, the N_2 gas flow rate to the balance housing was reduced to 300 ml/min (STP). About 10 minutes later, power was supplied to the furnace to initiate heating at a rate of approximately 5°C/minute.

The sample weight and temperature were monitored during the heating period. Approximately 30 minutes after calcination was complete, the reactive gases were introduced to the reactor to initiate the carbonation reaction. At the end of carbonation cycle, the power supply to the furnace was shut off and the reactor was depressurized by very slowly switching the 3-way valve to the atmosphere. The water supply from high pressure syringe pump was immediately stopped.

After the reactor cooled to about 400°C, a temperature at which calcination would not occur, the reactive gas flow rate was stopped. N_2 flow through the reactive gas line was maintained for sufficient time to purge the reaction gases. About 10 minutes later, the N_2 gas flow rate to the balance housing and through the side-arm was reduced to about 20 ml/min.

After the reactor reached room temperature, the sample container was unloaded, weighed using a Sartorius balance, and cleaned. The empty pan was again loaded to the balance to measure the empty-pan weight for comparison to the weight before the run.

The experimental procedure described above was followed for one complete calcination and carbonation cycle with the same operating pressure for both phases. If the calcination phase was at atmospheric pressure and carbonation phase was at elevated pressure (see Figure 3.2), the reactor system was pressurized after the calcination was complete with the procedure similar to that described above.

Many of the experimental tests using the high pressure electrobalance system were continued for several cycles. The experimental procedure was similar but involved additional switching of reactive gases between reactor and the by-pass lines between the calcination and carbonation cycles.

Chapter 4

Experimental Results:

Reaction Screening Tests

This chapter deals with the preliminary studies which investigated the effect of operating conditions as well as screened potential sorbent precursors. Operating conditions included the effect of calcination temperature, carbonation temperature, and background gas composition. Reagent grade $CaCO_3$ was used in these tests. The results of these tests suggested the operating conditions which were used for screening of sorbent precursors. Three out of nine sorbent precursors were selected for further kinetic studies. They were: (i) reagent grade $CaCO_3$ considered as a standard sorbent, (ii) reagent grade calcium acetate, and (iii) commercial grade dolomite having essentially equal molar quantities of $MgCO_3$ and $CaCO_3$.

The preliminary studies used the atmospheric pressure thermogravimetric analyzer while the high pressure TGA was being acquired. It is necessary, however, to point out that the atmospheric pressure TGA experienced a problem in temperature measurement. The actual temperature was about 20 to 30°C below the temperature reading from the temperature controller. Since this effort was only for preliminary studies, the temperature problem did not significantly affect the preliminary analysis. In addition, the preliminary

results were excluded in detailed studies discussed in the next chapters. Controller temperature is reported in the following.

4.1 Effect of Temperature

Figure 4.1 shows the effect of temperature on the calcination reaction. Calcination was carried out in N_2 at 1 atm using a heating rate of 50°C/minute to the indicated temperature and isothermal thereafter. The calcination rate is a strong function of temperature. Calcination was very slow at 600°C, and the rate increased with temperature. Calcination was complete after about 25 minutes at 845°C and after about 200 minutes (not shown) at 660°C. These results showed that complete calcination could be achieved in a relatively short time at temperatures as low as 710°C.

The effect of carbonation temperature is shown in Figure 4.2. All sorbents were previously calcined at 750°C in 1 atm of N_2. Carbonation was at 1 atm in 5.6% CO_2/N_2. Each run showed the typical initial rapid reaction phase followed by an abrupt change to a slow reaction phase, in agreement with previous results reported in literature (Dedman and Owen, 1962; Barker, 1973, 1974; Bhatia and Perlmutter, 1983). It can also be seen that the end of the rapid carbonation phase is a strong function of temperature suggesting that the rate was controlled by the diffusion of gas into the product layer of $CaCO_3$. The final fractional carbonations at 430°C and

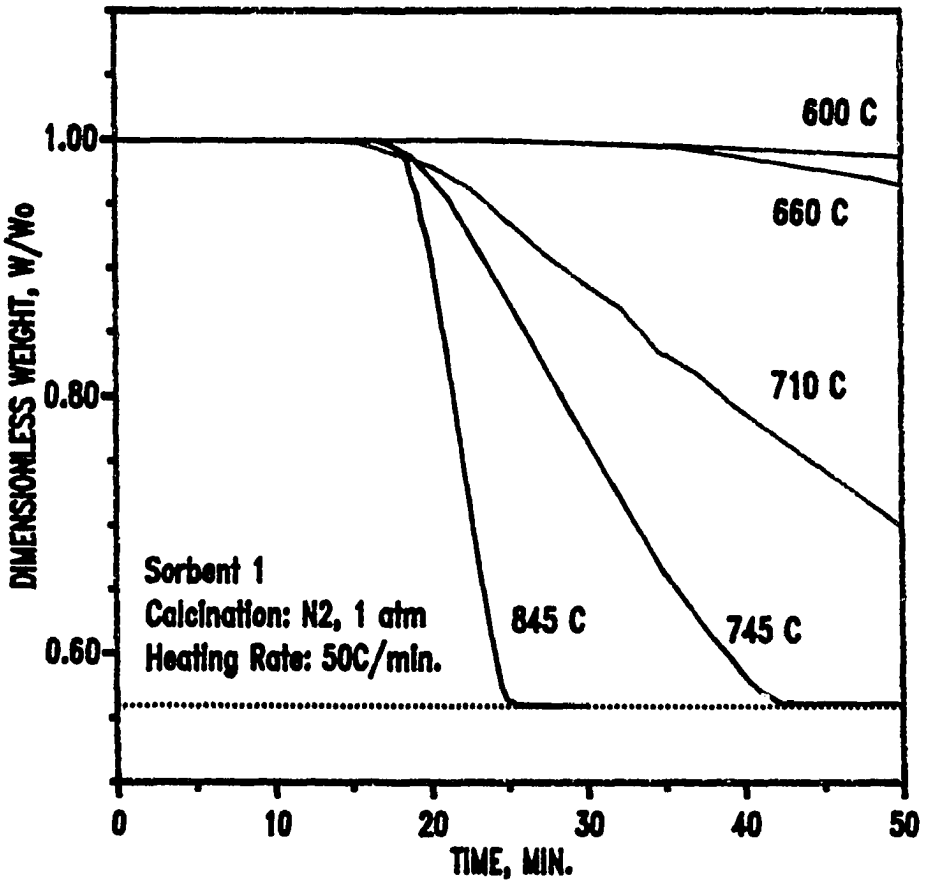

Figure 4.1 Effect of Temperature on Calcination Kinetics; Sorbent 1

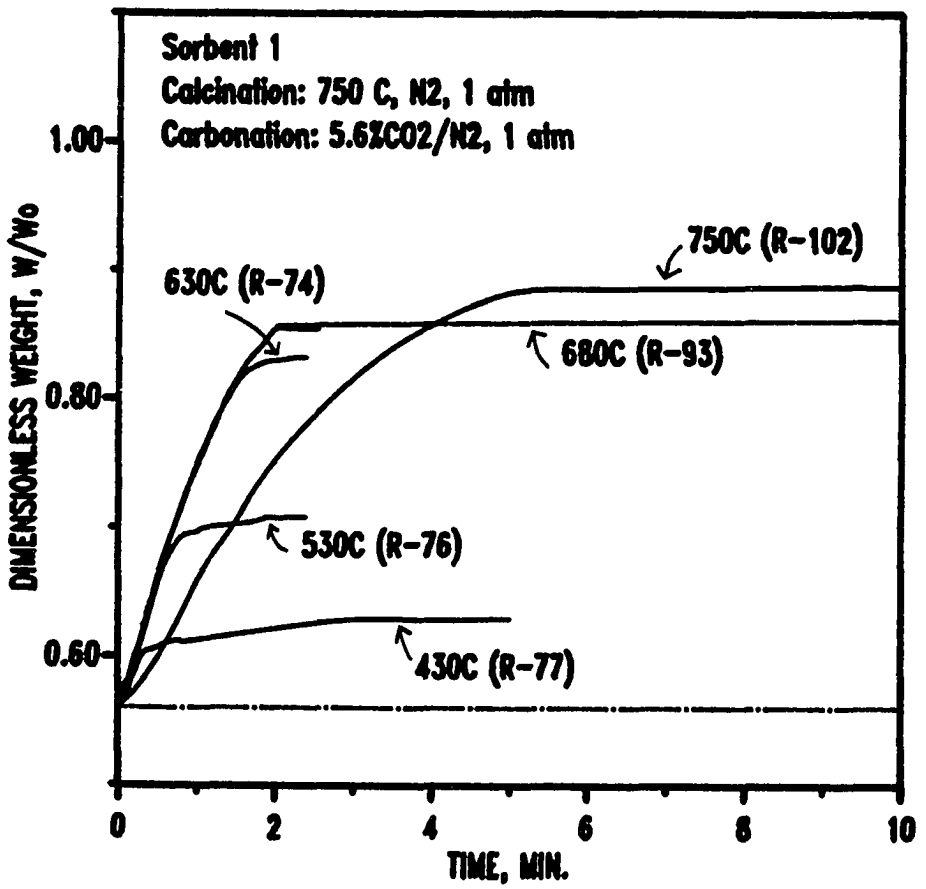

Figure 4.2 Effect of Temperature on Carbonation Kinetics: Sorbent 1

750°C were 0.16 and 0.75, respectively. The global rate during the rapid reaction phase was approximately equal in the temperature range 430 to 680°C, and the decrease in the global reaction rate at 750°C can be attributed to the fact that the actual partial pressure of CO_2 was only slightly greater that the equilibrium partial pressure at this temperature.

Figure 4.3 shows the carbonation reaction behavior in a test extended to 24 hours. Calcination was carried out at 895°C in 1 atm of N_2 followed by carbonation at 710°C in 15% CO_2/N_2. The rapid reaction phase ended at W/Wo = 0.85, corresponding to fractional carbonation of 0.66. After 24 hours, W/Wo gradually increased from 0.85 to 0.93 (84% carbonation). This test showed that the carbonation reaction never stopped completely.

4.2 The Effect of Gas Composition

The effect of CO_2 concentration on the carbonation reaction is shown in Figure 4.4. The reactive gases consisted of CO_2 and N_2 only. An expected strong dependence of carbonation rate during the initial rapid reaction phase was confirmed. However, there was relatively little difference in the carbonation level at the end of the run.

The effect of background gas components, CO and H_2, is shown in Figure 4.5. This gas composition includes all major components present in coal-gas except steam. The addition of

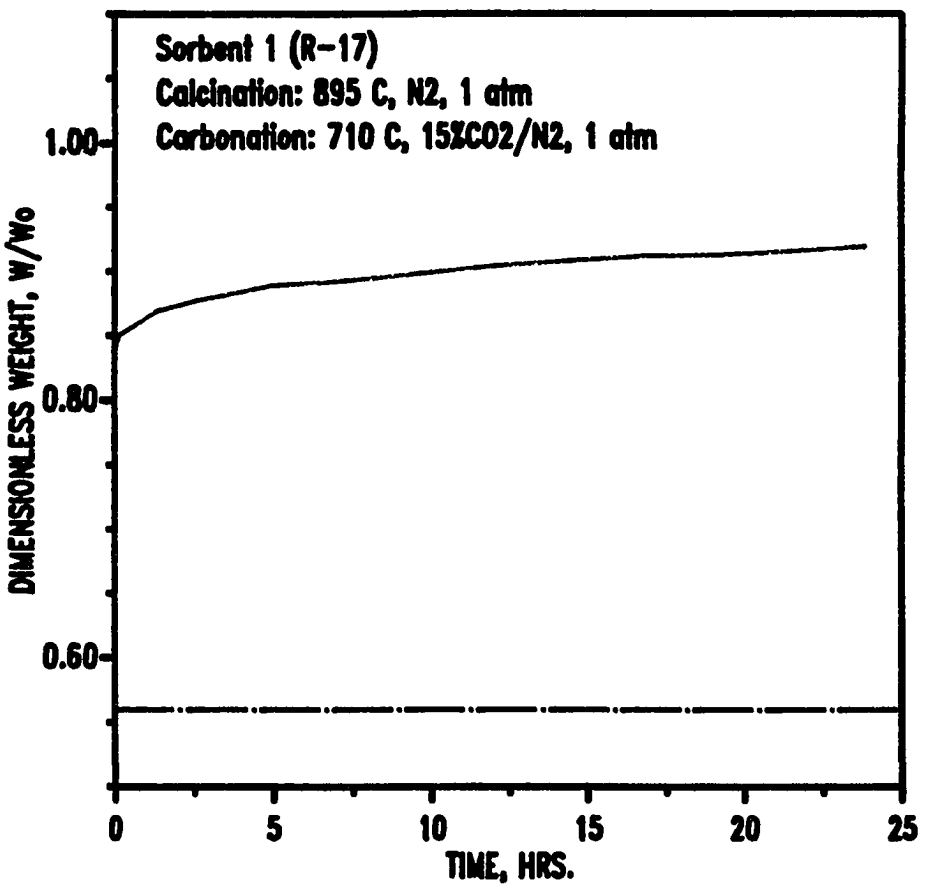

Figure 4.3 Long-Term Carbonation Results; Sorbent 1

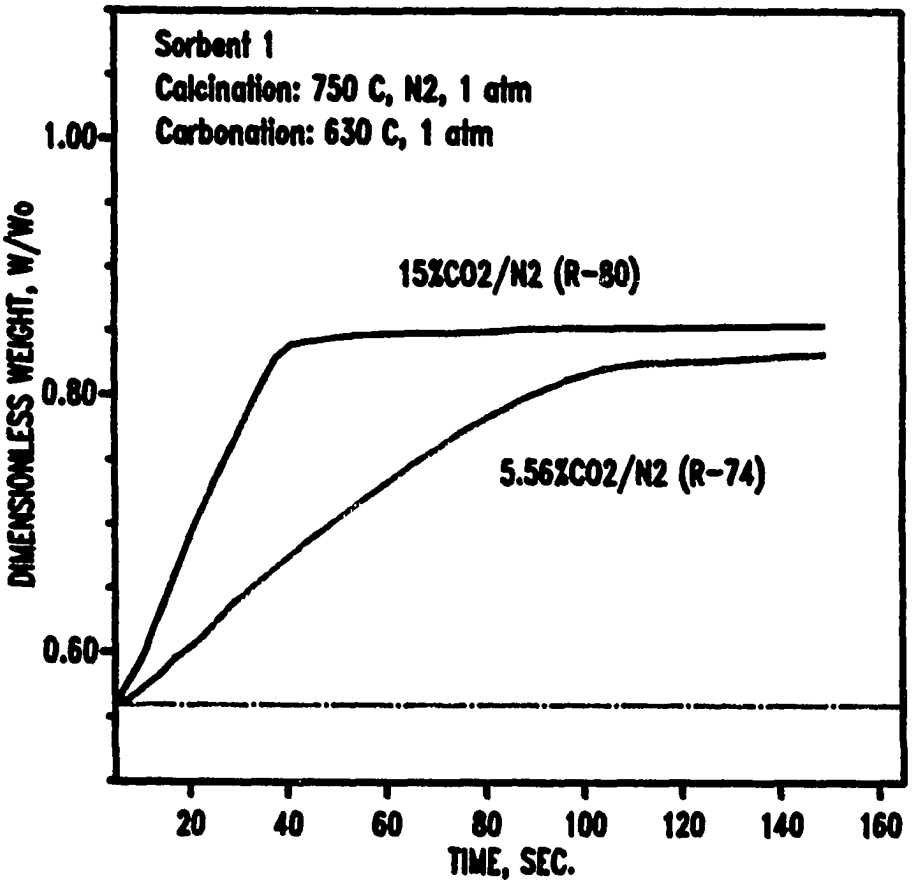

Figure 4.4 Effect of CO_2 Concentration on Carbonation Kinetics; Sorbent 1

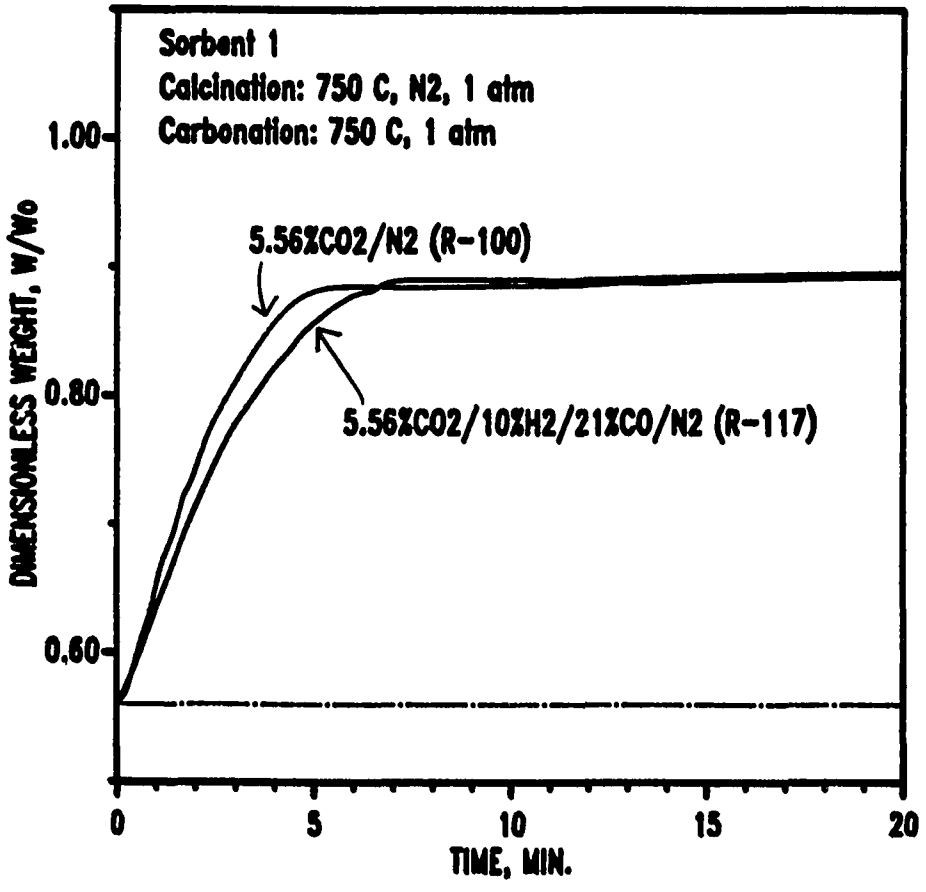

Figure 4.5 Effect of Gas Composition on Carbonation Kinetics; Addition of CO and H_2, Sorbent 1

CO and H_2 appears to result in a slight decrease in the rapid reaction rate, but the rapid reaction period ends at essentially the same level of W/Wo.

The addition of steam to complete the simulated coal-gas composition produced a dramatic increase in the carbonation rate during the rapid reaction phase as shown in Figure 4.6. Two possible reasons for the rate increase were considered. First, since all components required for the water-gas shift reaction were present, the occurrence of this reaction would increase the CO_2 concentration above that of the feed gas; hence the rate during the rapid reaction phase would increase. Second, H_2O might simply serve to enhance the rate of the rapid reaction phase. In order to help distinguish between these possibilities, an additional run in which the reaction gas consisted of 8.9% CO_2 in N_2 was carried out. Calculations showed that if the simulated coal gas feed was allowed to be in shift equilibrium, the CO_2 composition would be increased to approximately 9%. As shown in Figure 4.6, the rates for the two tests were approximately equal. While the evidence is indirect, there is the suggestion that the shift reaction occurs simultaneously with carbonation when the necessary shift components are present.

Other evidence of the occurrence of the shift reaction is shown in Figure 4.7. In run R-134, the CO_2 feed concentration was held constant while the background gas composition was changed ten minutes into the run. Initially

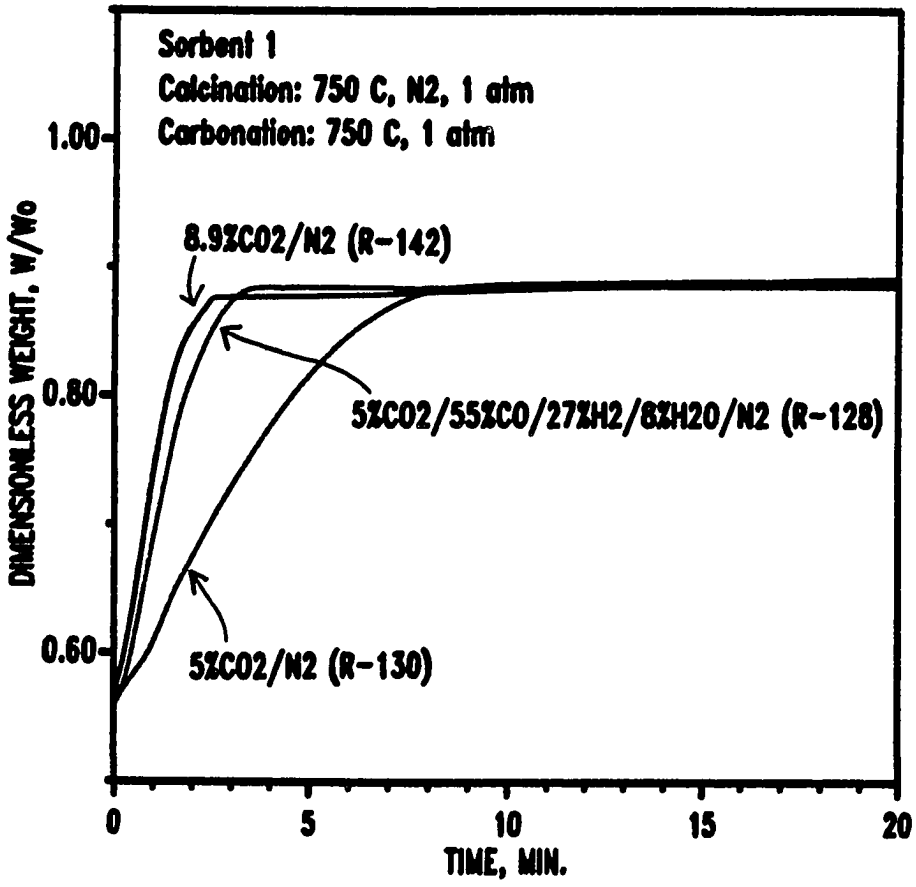

Figure 4.6 Testing for the presence of the Shift Reaction; Sorbent 1

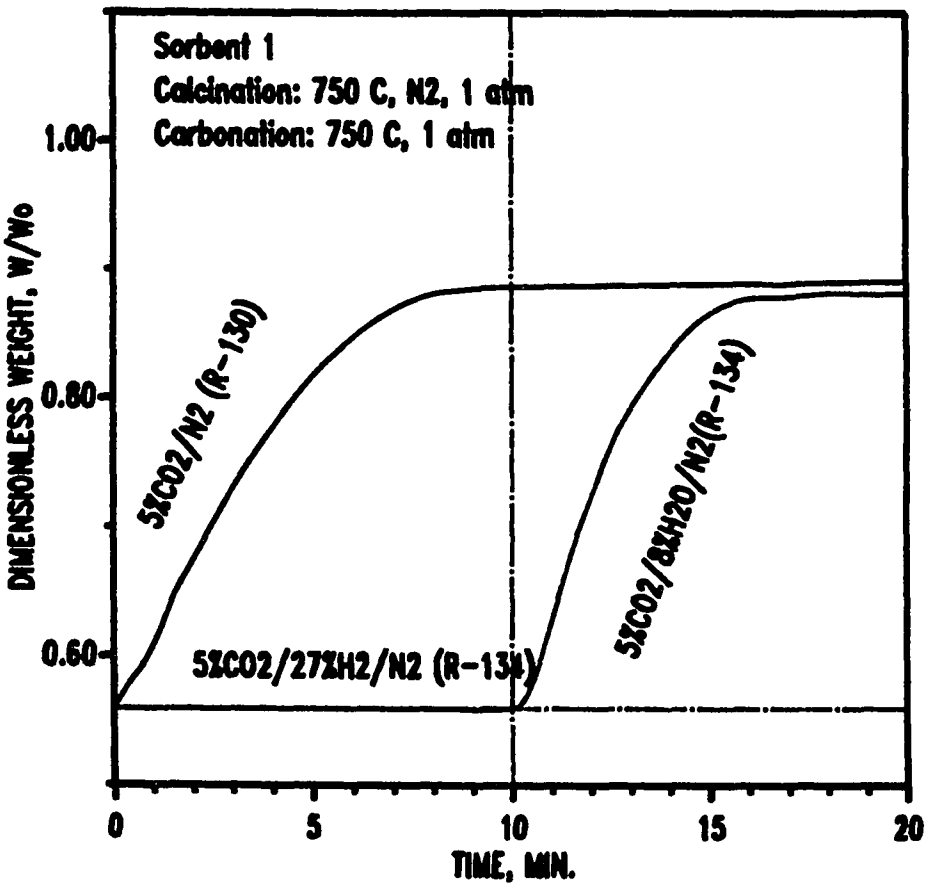

Figure 4.7 Carbonation Kinetics with Constant CO_2 Concentration and Varying Background Gas Composition; Sorbent 1

the feed gas consisted of 5%CO_2/27%H_2/68%N_2, and no carbonation occurred. This gas composition included the components (H_2 and CO_2) for the reverse shift reaction which would result in an equilibrated gas composition below equilibrium CO_2 pressure for the carbonation reaction. After 10 minutes, H_2O was substituted for H_2 to prevent the reverse shift reaction. Carbonation began immediately and proceeded to a W/Wo value approximately equal to that observed using the simple CO_2/N_2 composition.

Results of one final test (R-144) showing the importance of background gas composition are shown in Figure 4.8. The feed gas contained no CO_2 but did contain the shift reactants CO and H_2O. The observed weight increase proves that carbonation did occur, and the only reasonable source of CO_2 was from the shift reaction. Carbonation was transitory, however, as the W/Wo value reached a maximum of approximately 0.68 after 10 minutes and declined thereafter. This behavior is consistent with CaO serving as a shift catalyst. Early in the test when most of the sorbent was in the oxide form, the shift reaction produced CO_2 which subsequently reacted to form $CaCO_3$. Once an appreciable quantity of $CaCO_3$ was formed, the catalytic effect diminished, less CO_2 was formed, and $CaCO_3$ began to decompose.

The evidence of the water gas shift reaction combined with CO_2 removal in the presence of CaO sorbent observed in this preliminary study was indirect. In order to obtain

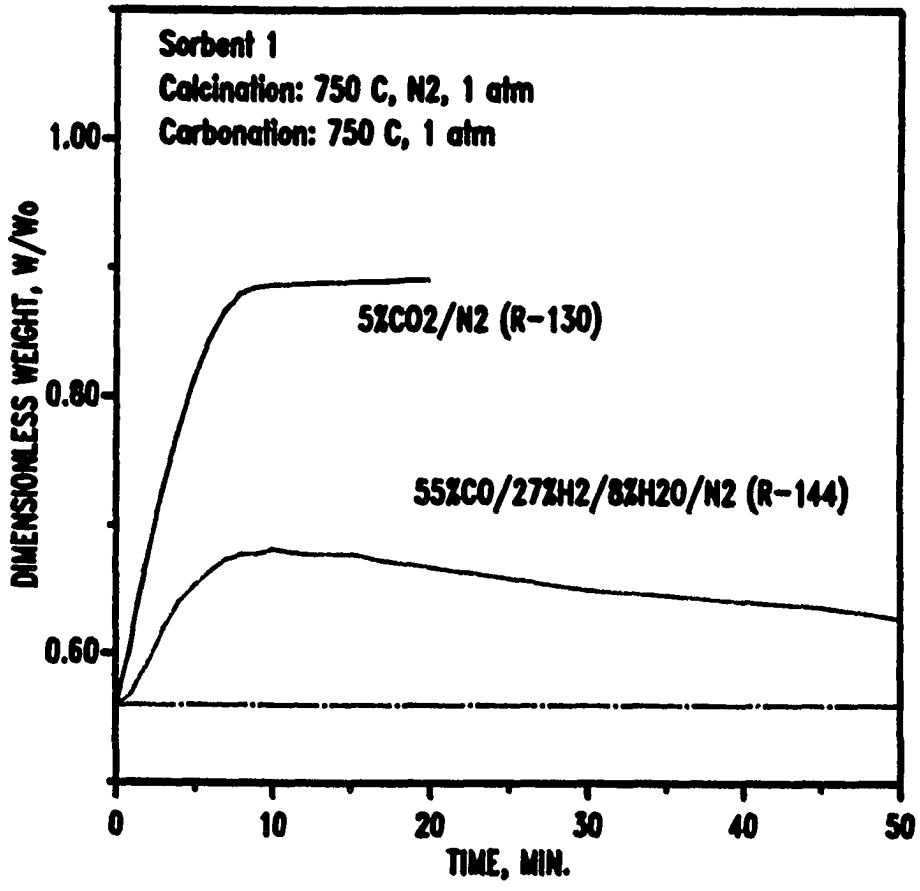

Figure 4.8 Carbonation with No CO_2 in the Feed Gas; Sorbent 1

direct evidence of the occurrence of the water-gas shift reaction, a more detailed study involving gas analysis will be necessary. It will also be important to determine whether the shift reaction is homogeneous or is catalyzed by solid CaO. A number of metals and metal oxides are reported to be active shift catalysts (see, for example, Rofer-DePoorter, 1984). CaO, however, is not included. Gauthier (1909) reported that the shift reaction could occur homogeneously at conditions of interest in this study. Gluud *et al.* (1931) reported that MgO had a catalytic effect on the shift reaction.

The combined reactions, however, create problems for the current study in that the CO_2 concentration in contact with the CaO sorbents is not equal to the feed gas composition whenever shift reaction components are present. Therefore, the simple reactive gas containing only CO_2 and N_2 was used for comparison of test sorbents and detailed kinetic studies of the selected sorbents. The effect of the background gas composition will be discussed once again in Chapter 7.

4.3 Comparison of Test Sorbents

Calcination results for the six calcium carbonate precursors (sorbents 1 to 6) are compared in Figures 4.9 and 4.10. Sorbent 1 results are included in both figures for reference purposes. Note that all sorbents were calcined at the same conditions. As shown in the figures, all calcination

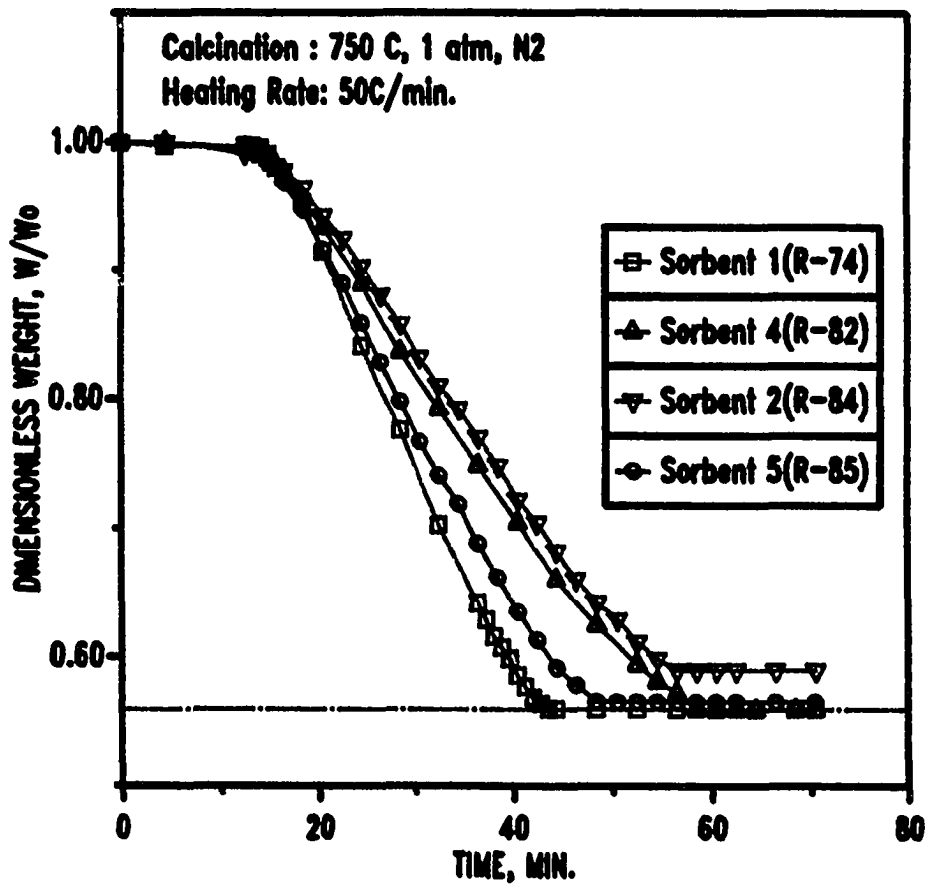

Figure 4.9 Comparison of Calcination Kinetics; Sorbents 1, 2, 4, and 5

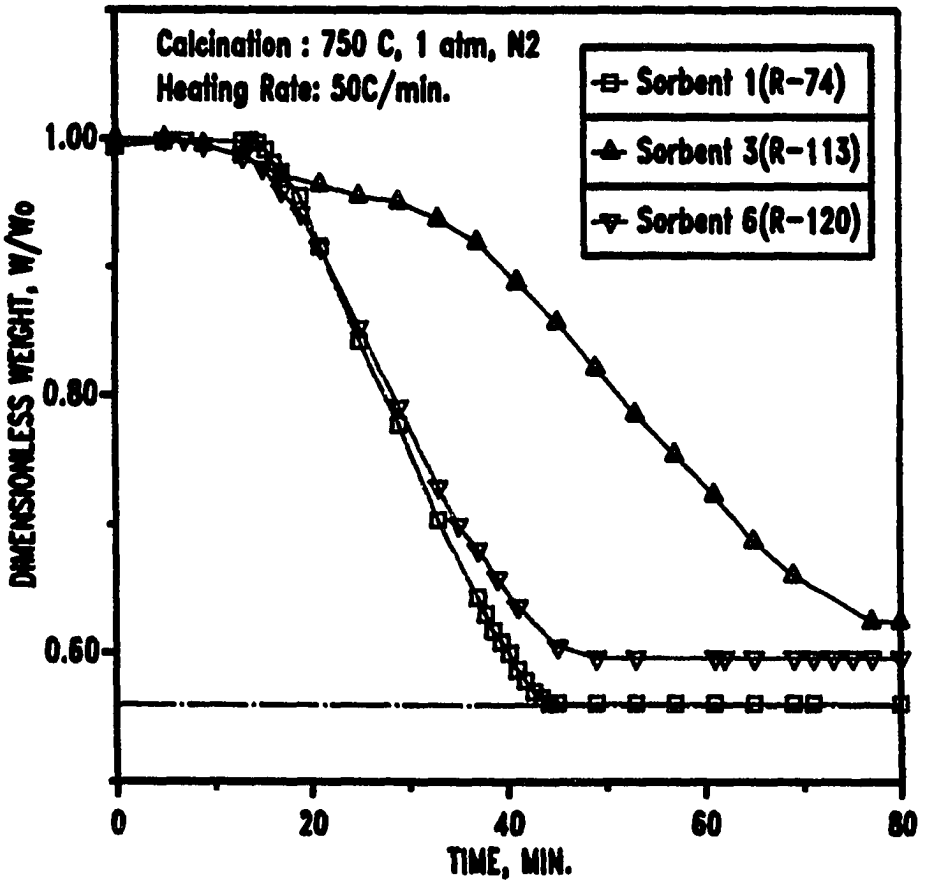

Figure 4.10 Comparison of Calcination Kinetics; Sorbents 1, 3, and 6

results were qualitatively similar. The calcination rate became appreciable at about 625°C. Complete calcination, corresponding to constant W/Wo values, occurred in the range of 43 to 75 minutes. The difference in time for complete calcination was attributed primarily to particle size effects. Differences in W/Wo at complete calcination were due to differences in purity. While the final weight of sorbent 1 (pure $CaCO_3$) was quite close to the theoretical value of 0.56, the final values for other sorbents were in the range from 0.56 to 0.64.

Carbonation results of the six sorbents are shown in Figures 4.11 and 4.12. Data for sorbent 1 are again included in both figures for reference. Note that the carbonation reaction for tests shown in Figure 4.11 was stopped after 2½ minutes, while the reaction was allowed to proceed for 20 minutes for the Figure 4.12 tests. Longer time was needed at at 750°C (Figure 4.12) since the equilibrium CO_2 pressure approached to actual CO_2 pressure. Differences in the initial values of W/Wo were due to differences in final calcination results. Each carbonation curve is similar. The final values of W/Wo ranged from 0.82 to 0.85 at 630°C (Figure 4.11) while the final W/Wo values at 750°C tests (Figure 4.12) were all approximately 0.89.

The carbonation results for marl (sorbent 2) and chalk (sorbents 3,4, and 6) sorbent precursors were unexpected. Hartman *et al.* (1978) reported that the reactivity of chalks

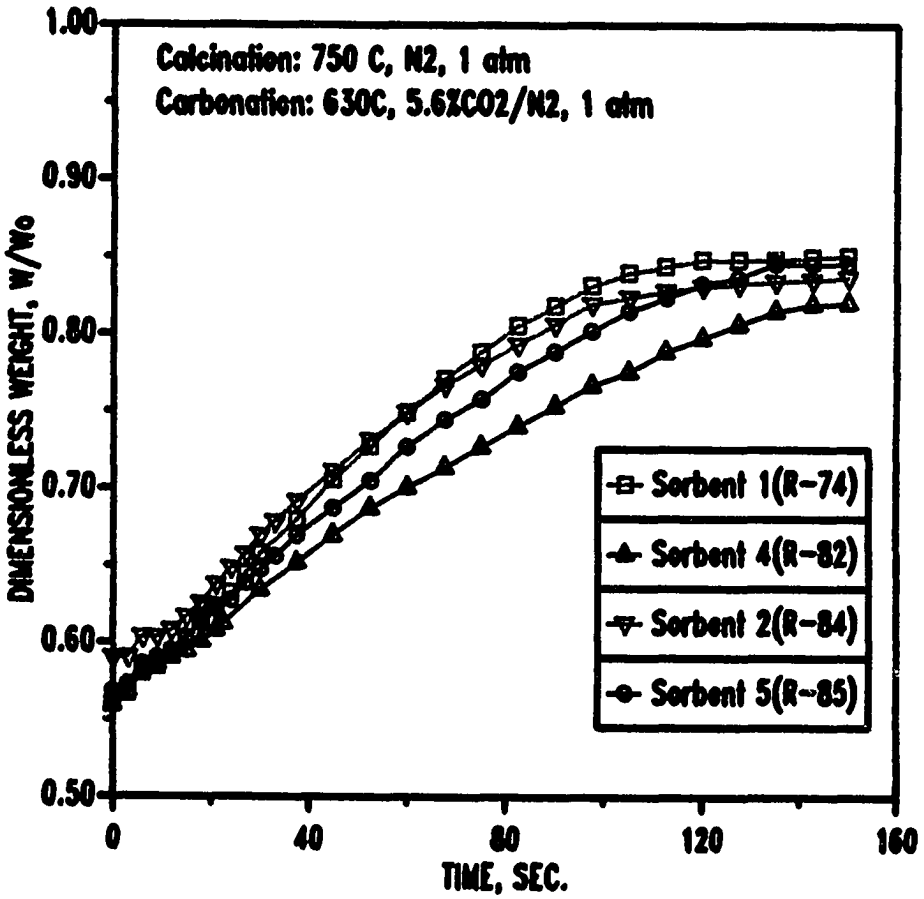

Figure 4.11 Comparison of Carbonation Kinetics; Sorbents 1, 2, 4, and 5

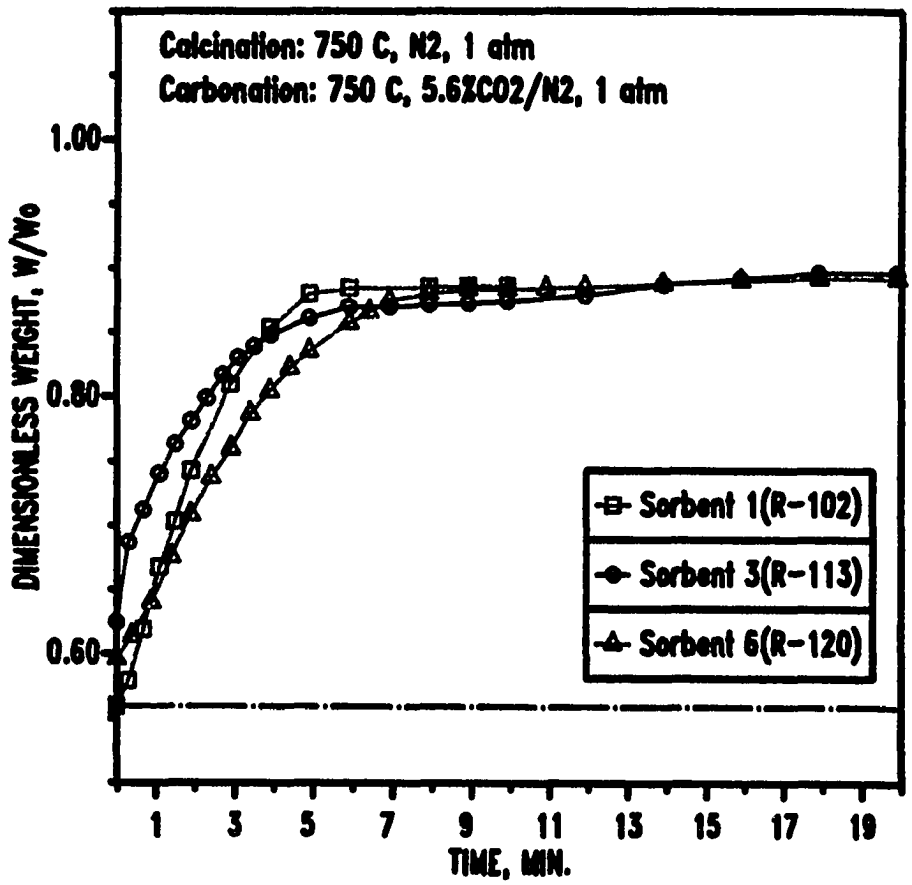

Figure 4.12 Comparison of Carbonation Kinetics; Sorbents 1, 3, and 6

and marls was significantly greater than the reactivity of limestone in their sulfation studies. The reactivity increases were attributed to the greater porosity of CaO formed from chalks and marls. However, as seen in the figures, the carbonation behavior of all sorbents was similar to that of the reagent grade $CaCO_3$.

An alternate approach to increasing sorbent reactivity was tested by the use of sorbents 7, 8, and 9. Sorbents 7 and 8, consisting of reagent grades of calcium acetate and calcium sulfate, respectively, were selected based upon the logic that decomposition of the precursor would involve driving off a significantly increased quantity of volatile material leaving CaO sorbent with increased pore volume and, presumably, greater carbonation reactivity.

Figure 4.13 shows calcination and carbonation results for one complete cycle of sorbent 7. Although the high pressure electrobalance was used, both calcination and carbonation were at one atmosphere. The precursor, $Ca(C_2H_3O_2)_2.xH_2O$ containing 8.3% H_2O, was heated in N_2 as shown. Water of hydration was driven off in two increments in the temperature range 100-300°C, leaving $Ca(C_2H_3O_2)_2$ with W/Wo ≈ 0.92. Acetate decomposition began at about 370°C and a constant weight plateau was reached at 500°C with W/Wo ≈ 0.58, corresponding to $CaCO_3$ formed from the original hydrated calcium acetate. Additional weight loss to W/Wo = 0.325 occurred in the vicinity of 750°C. No further weight

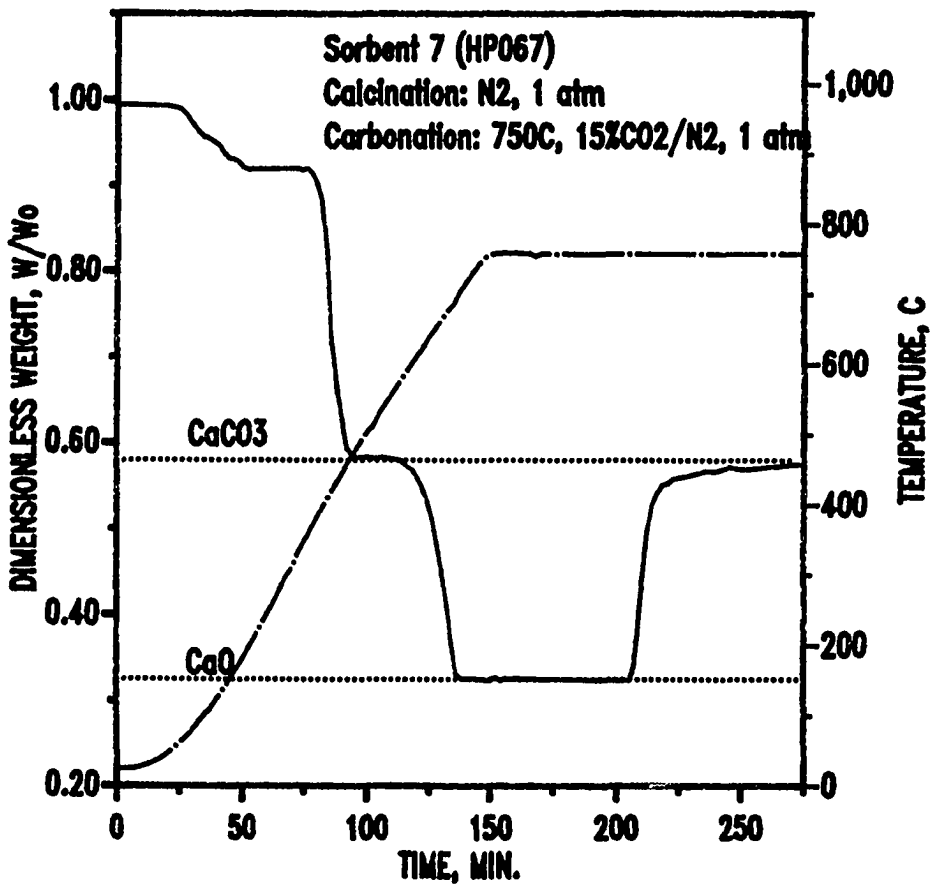

Figure 4.13 Decomposition and Carbonation Kinetics; Sorbent 7

loss occurred during 60 minutes in N_2 at 750°C, and the final weight corresponded to the theoretical value for the production of CaO from calcium acetate containing 8.3% H_2O. When carbonation was initiated after 210 minutes, the weight gain was rapid and the final value of W/Wo = 0.57 corresponded closely to the value expected for total conversion of CaO to $CaCO_3$ (W/Wo = 0.58).

Decomposition of hydrated calcium sulfate, $CaSO_4.2H_2O$ (sorbent 8), is illustrated in Figure 4.14. The atmosphere during $CaSO_4$ decomposition was 50% N_2 - 50% H_2, with the hydrogen added to promote the removal of sulfur as H_2S. H_2O was driven-off at about 300°C. $CaSO_4$ began to decompose after approximately 80 minutes at about 900°C. Instead of forming CaO, the final decomposition product was CaS. After 130 minutes, the carbonation gas was introduced, and CaS, as shown in the figure, had no carbonation activity. Hydrated calcium sulfate, therefore, could not be considered as a sorbent precursor.

Sorbent 9 was a commercial dolomite containing approximately equal molar quantities of $CaCO_3$ and $MgCO_3$ obtained from National Lime Co. (see Table 3-5). Dolomite was chosen to test the effect of magnesium on the reactions. Calcination of both $CaCO_3$ and $MgCO_3$ should contribute to increased porosity in the mixed oxide product. At the carbonation conditions of interest, MgO will not react with CO_2 so that the pores created by $MgCO_3$ calcination should

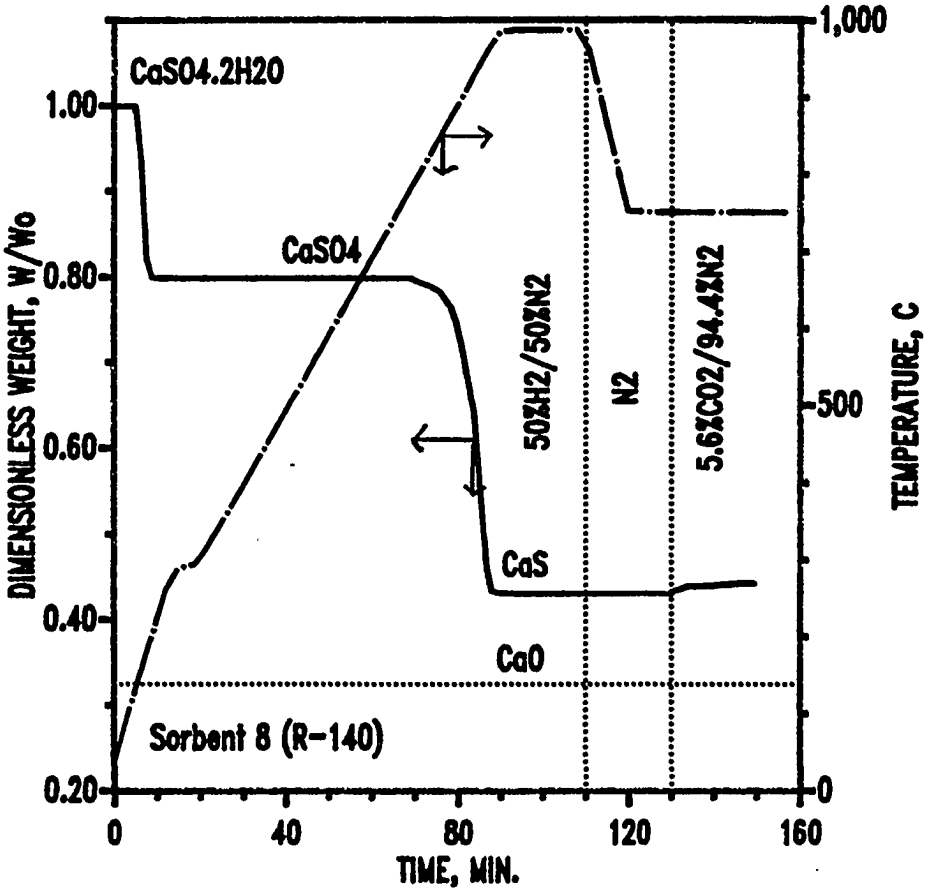

Figure 4.14 Decomposition of Calcium Sulfate; Sorbent 8

remain open and prevent the pore closure experienced by pure $CaCO_3$. Figure 4.15 shows the results for one complete calcination-carbonation cycle of sorbent 9. Calcination began at approximately 450°C and was complete at about the time the sample reached the desired final temperature of 750°C. Calcination of $MgCO_3$ should occur at lower temperature, followed by calcination of $CaCO_3$. However, no clearcut distinction in the weight loss curve associated with $MgCO_3$ and $CaCO_3$ decomposition was observed. The final value of W/Wo = 0.525 corresponded closely to the loss on ignition value reported by National Lime, and represented complete conversion of $CaCO_3$ and $MgCO_3$ to CaO and MgO.

Carbonation was carried out in 15% CO_2/N_2 at 750°C and 1 atm. Carbonation behavior was qualitatively similar to that exhibited by other sorbents. A rapid initial reaction period lasting less than 5 minutes was followed by an abrupt transition to a slow reaction phase. The transition, however, occurred at W/Wo $\approx$ 0.73, which corresponds to a fractional calcium carbonation of 0.85, significantly higher than that observed using pure $CaCO_3$. After one hour of carbonation reaction, the W/Wo value was 0.75, which corresponds to 0.93 fractional carbonation of calcium.

From the above test results, three sorbents were chosen to be studied in a greater detail. Sorbent 1 served as the standard sorbent. Sorbent 7 was selected due to the high porosity created during calcination which caused high

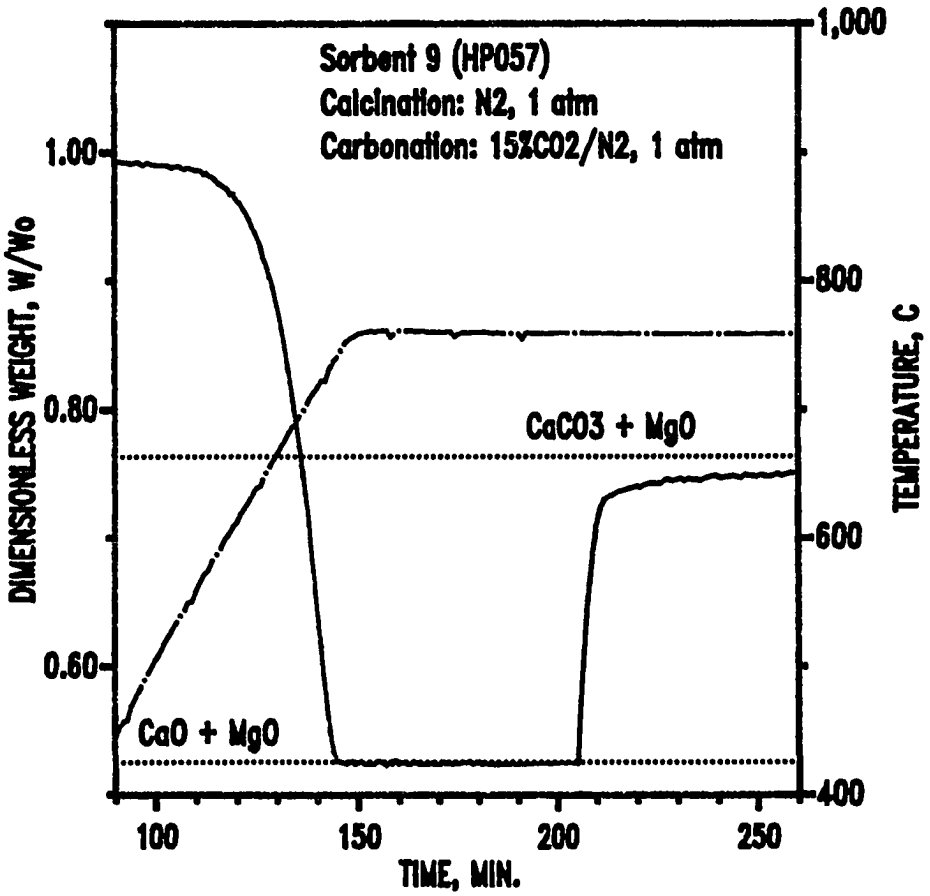

Figure 4.15 Calcination and Carbonation Kinetics; Sorbent 9

carbonation reactivity. Sorbent 9 was chosen because decomposition of $MgCO_3$ to MgO helps create "extra" pore volume during calcination, hence increasing the carbonation reactivity. In addition, related studies by Narcida (1992) showed that the three sorbents produced a wide variation of structural property changes during their calcination and carbonation reactions, as discussed in Chapter 2.

Figure 4.16 provides a direct comparison of first-cycle carbonation behavior of the three sorbents at the same carbonation conditions. While each sorbent exhibits qualitatively similar behavior, it is clear that sorbents 7 and 9 can achieve greater than 90% carbonation compared to only 80% carbonation for sorbent 1.

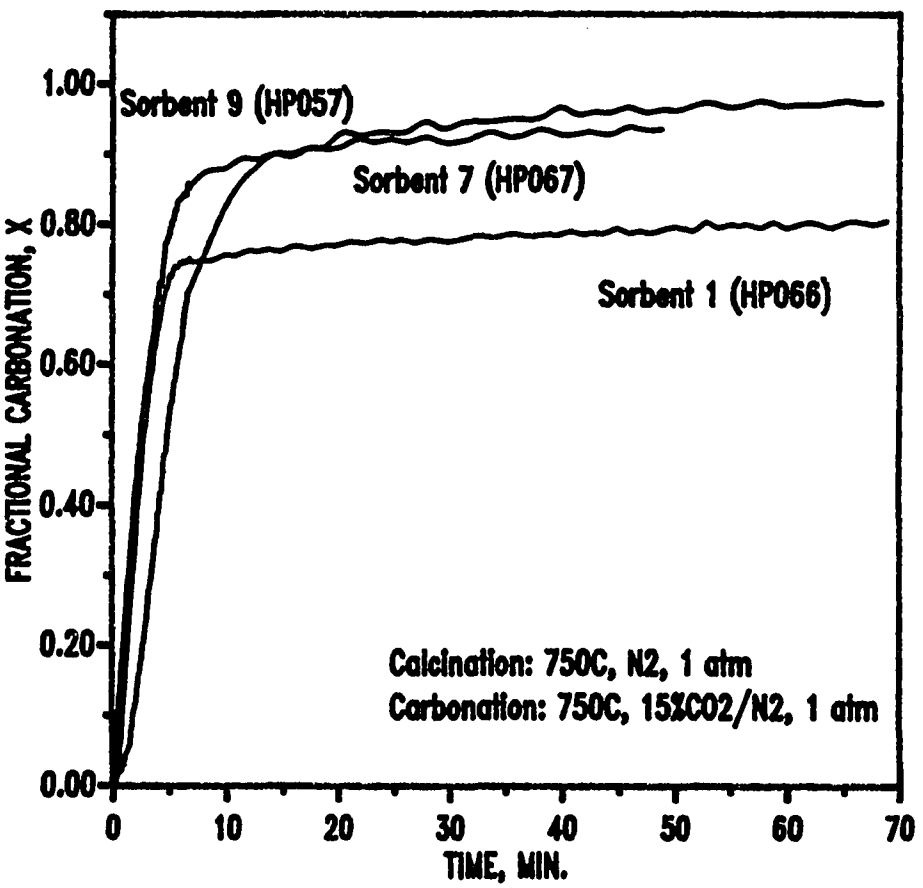

Figure 4.16 Comparison of First-Cycle Carbonation Kinetics; Sorbents 1, 7, and 9

Chapter 5

Experimental Results:

Two-Cycle Reaction Studies

This chapter focuses on studies of two-cycle calcination-carbonation kinetics of the three base sorbents, selected in the previous chapter, as a function of temperature, pressure, and CO_2 gas composition. Table 5-1 shows the reaction parameters tested in this study. Calcination pressure was one atmosphere and the calcination gas was pure nitrogen. As discussed later in Chapter 6, calcination pressure does not significantly affect the carbonation performance. As a result of Table 5-1, the complete matrix consists of 243 tests. However, due to reaction equilibrium considerations and on the basis of results from the earlier tests, only 98 tests were actually carried out. In addition to determining the effect of reaction parameters, the two-cycle tests provided preliminary information on sorbent durability which is a primary concern of commercial use.

The complete test matrix is shown in Tables 5-2, 5-3, and 5-4 for sorbents 1, 7, and 9, respectively. The 98 runs which were completed are designated in these tables by run number. Duplicate runs were made periodically as indicated to check reaction reproducibility.

Table 5-1

Two-Cycle Reaction Parameters

Parameter	No. of Parameter Levels	Conditions
Calcination Temperature	3	750, 825, and 900°C
Carbonation Temperature	3	550, 650, and 750°C
Carbonation Pressure	3	1, 5, and 15 atm
CO_2 Mol Fraction	3	0.01, 0.05, and 0.15
Base Sorbent	3	Sorbent 1, Sorbent 7, and Sorbent 9

Table 5-2
Matrix of Two-Cycle Runs for Sorbent 1

Calcin. Temp. (°C)	Carbon. Temp. (°C)	Carbon. CO_2 (% Vol)	Carbonation Pressure		
			1 atm	5 atm	15 atm
900	750	15	HP048	HP082	HP040
900	750	5	***	***	***
900	750	1	***	***	***
900	650	15	HP084	HP096	***
900	650	5	***	***	***
900	650	1	***	***	***
900	550	15	HP083	HP099	***
900	550	5	HP085	***	***
900	550	1	HP086	***	***
825	750	15	HP047	HP113	HP039
825	750	5	***	***	***
825	750	1	***	***	***
825	650	15	HP045	HP117	HP134
825	650	5	HP051	***	***
825	650	1	***	***	***
825	550	15	HP125	HP120	***
825	550	5	HP129	***	***
825	550	1	HP126	***	***
750	750	15	HP066 HP095	HP063	HP032
750	750	5	***	***	HP034
750	750	1	***	***	HP033
750	650	15	HP046	HP097	HP141
750	650	5	HP043	***	***
750	650	1	***	***	HP133 HP137
750	550	15	HP049	HP098	HP139
750	550	5	HP130	***	***

Table 5-3
Matrix of Two-Cycle Runs for Sorbent 7

Calcin. Temp. (°C)	Carbon. Temp. (°C)	Carbon. CO_2 (% Vol)	Carbonation Pressure		
			1 atm	5 atm	15 atm
900	750	15	HP055	***	HP076
900	750	5	***	HP109	***
900	750	1	***	***	***
900	650	15	***	***	HP091
900	650	5	***	***	***
900	650	1	***	***	***
900	550	15	***	***	HP100
900	550	5	***	***	***
900	550	1	***	***	***
825	750	15	HP053	***	HP106
825	750	5	***	HP108	***
825	750	1	***	***	***
825	650	15	HP054	***	HP121
825	650	5	HP052	HP118	***
825	650	1	***	***	***
825	550	15	HP123	***	HP127
825	550	5	***	HP131	***
825	550	1	***	***	***
750	750	15	HP067 HP068	HP064	HP036
750	750	5	***	HP124	HP037
750	750	1	***	***	HP038
750	650	15	HP056	HP110	HP101
750	650	5	***	***	***
750	650	1	***	HP147	***
750	550	15	HP061	HP144	HP128
750	550	5	HP093	***	***
750	550	1	HP060	HP145	***

Table 5-4
Matrix of Two-Cycle Runs for Sorbent 9

Calcin. Temp. (°C)	Carbon. Temp. (°C)	Carbon. CO_2 (% Vol)	Carbonation Pressure		
			1 atm	5 atm	15 atm
900	750	15	HP062	***	HP077
900	750	5	***	***	HP088
900	750	1	***	***	HP087
900	650	15	***	***	***
900	650	5	***	***	***
900	650	1	***	***	HP090
900	550	15	***	***	***
900	550	5	***	***	***
900	550	1	***	***	HP089
825	750	15	HP078	HP112	HP103
825	750	5	***	***	***
825	750	1	***	***	HP135
825	650	15	***	***	HP115
825	650	5	***	***	HP132
825	650	1	***	***	HP116
825	550	15	***	***	***
825	550	5	***	***	***
825	550	1	***	***	HP122
750	750	15	HP057 HP105	HP069	HP075
750	750	5	***	***	HP092
750	750	1	***	***	HP080
750	650	15	HP071	HP111	HP136
750	650	5	HP072	***	***
750	650	1	***	***	HP102
750	550	15	HP073	HP143	HP140
750	550	5	HP074	***	HP142
750	550	1	HP094	***	HP114

The electrobalance response through two complete cycles for duplicate tests using sorbent 9 (HP057 and HP105) is shown in Figure 5.1. Both samples were calcined at 750°C and 1 atm N_2. Carbonation was carried out in 15% CO_2/N_2 at 750°C and 1 atm. Calcination of the dolomite precursor consisting of 54.5% $CaCO_3$ and 45% $MgCO_3$ (mass %) produced the final value of W/Wo = 0.528 which corresponds to complete calcination of $CaCO_3$ and $MgCO_3$ to CaO and MgO. Complete calcination was achieved in both cycles of both tests. Carbonation gas consisting of 15% CO_2 in N_2 was introduced after 210 minutes. Carbonation was quite rapid initially but after 5 minutes the rate decreased abruptly and was quite slow thereafter. After carbonation for 40 minutes, fractional carbonation for the two cycles of the two tests varied from 0.90 to 0.93. As seen in the figure, the reproducibility was quite good, and is typical of all cases in which repeat tests were carried out.

5.1 Reactivity and Capacity Indices

Because of the large amount of experimental data acquired in each run, it was necessary to develop a means of reducing the data to a more manageable form to permit direct comparison of results and to evaluate the effect of the reaction parameters. Therefore, indices based upon fractional carbonation at equivalent reaction times in both the early rapid reaction phase and the final slow reaction phase were developed to provide this comparison basis. Selection of the

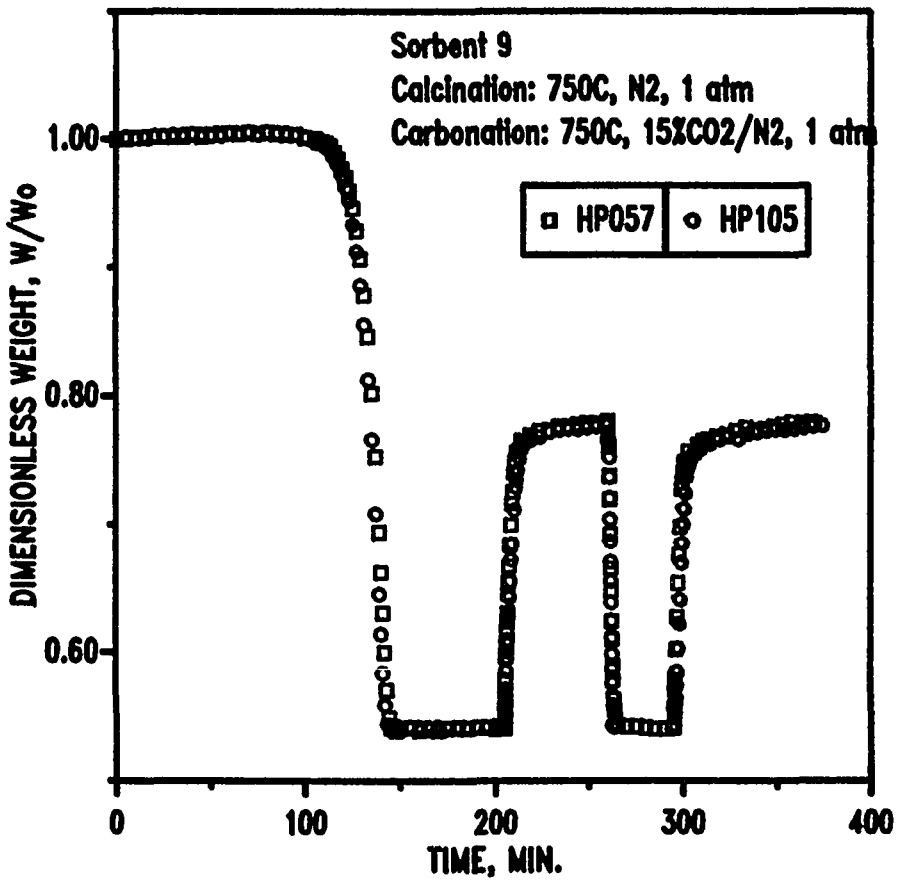

Figure 5.1 Reaction Reproducibility of Two Calcination-Carbonation Cycles for Sorbent 9

appropriate reaction time for the slow phase represented no major problem since the slope of the weight-time curve for each run approached zero during the latter stages. Selection of the proper time for comparing results in the rapid reaction phase, however, was complicated by two factors. The first was associated with a time lag between opening the reactive gas valve in the reactor sidearm and the sample being exposed to the full reactive gas concentration. The second factor was the large slope of the weight-time curve early in the reaction. A relatively small time error would result in a large error in the index.

This problem was solved by evaluating the lag time, t_o, associated with each run as described below. Figure 5.2 shows the general response of the weight-time curve during a carbonation cycle. Low CO_2 mol fraction at high pressure was chosen to accentuate the time lag. t = 0 corresponds to opening the sidearm reactive gas valve. There was no reaction for approximately 5 minutes thereafter. In next couple of minutes the reaction rate gradually increased and after about 7 minutes there was a period in which the weight-time curve was essentially linear. During the first 5 minutes the sorbent was exposed to essentially no CO_2; between 5 and 7 minutes the CO_2 concentration increased from zero to its steady-state value (1% vol). The duration of the unsteady state period was found to a strong function of pressure and a weak function of temperature and CO_2 mol fraction. The lag

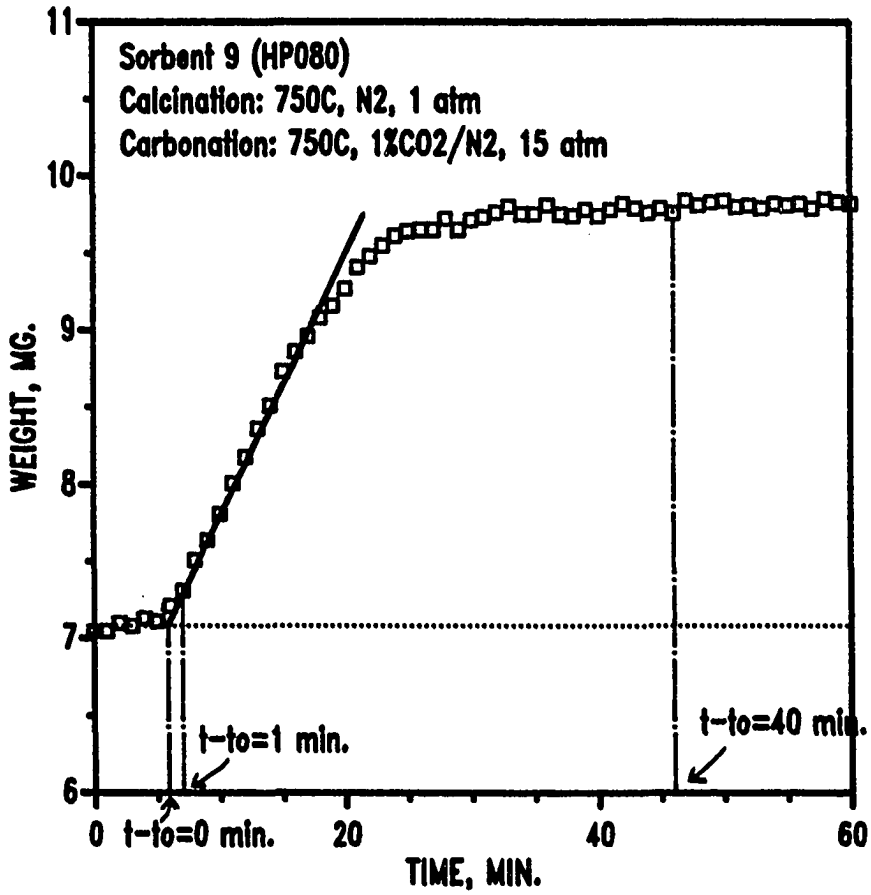

Figure 5.2 Determination of the Time Lag, t_o, during Carbonation Reaction

time t_o shown in Figure 5.2 was obtained by extrapolating the linear portion of the weight-time curve to the initial weight. Constant values of $(t-t_o)$, therefore, were taken to represent equivalent reaction time. Table 5-5 summarizes the t_o values for the first and second cycles for each set of reaction conditions. No dependence of t_o on either calcination temperature or sorbent precursor was found except for carbonation at 750°C, 1 atm, and 15% CO_2, reaction conditions which were quite close to the equilibrium conditions for carbonation. Therefore, multiple table entries are included for these conditions. In other cases there are two t_o values for each set of reaction conditions. These represent cycles 1 and 2, respectively. There is either no change or a slight increase in t_o in the second cycle. The overall values range from 6.9 minutes at high temperature, high pressure, and low CO_2 mol fraction to 0.2 minutes at low temperature, low pressure, and high CO_2 mol fraction. Each entry represents the average value from all runs at the particular set of conditions.

Values of fractional carbonation at fixed values of $(t-t_o)$ were used to compare the kinetics of different runs. As a result of trial-and-error comparison, $(t-t_o) = 1$ minute was chosen as the most suitable time for comparing kinetics during the initial reaction phase, while $(t-t_o) = 40$ minutes was chosen to compare the slow reaction phase. In Figure 5.2, for example, the rapid phase lasts for several minutes and

Table 5-5

Summary of the Lag Time, t_o, at Various Reaction Conditions

Carbonation Temperature (°C)	% CO_2	t_o (min) Carbonation Pressure 1 atm	5 atm	15 atm
750	15	0.6/* (S-1) 1.4/* (S-7) 0.3/* (S-9)	0.9/1.0	0.9/1.0
750	5	***	2.2/2.2	2.2/2.2
750	1	***	***	6.8/6.9
650	15	0.2/0.3	0.7/0.8	1.2/1.3
650	5	0.3/0.4	0.9/1.0	1.5/1.5
650	1	***	2.0/2.5	2.7/3.0
550	15	0.2/0.3	0.7/0.7	1.1/1.1
550	5	0.3/0.3	0.7/0.7	1.5/1.3
550	1	0.2/0.3	1.3/1.3	2.0/2.1

(*)

Calcination Temperature (°C)	t_o (min) S-1	S-7	S-9
900	1.4	1.7	1.3
825	1.3	1.1	0.5
750	0.7	0.9	1.0
750	0.8	0.9	0.5

(***) no tests were made at these conditions due to reaction equilibrium considerations

values of $(t-t_o)$ > 1 minute could be used. However, at high CO_2 concentration and low pressure, the rapid reaction phase terminates much sooner and values of fractional carbonation at $(t-t_o)$ > 1 minute would be inappropriate. The choice of $(t-t_o)$ = 40 minutes to compare the slow reaction phase is arbitrary. It is obvious from Figure 5.2 that the rate of increase in fractional carbonation is quite slow in the vicinity of 40 minutes, and approximately the same fractional carbonation values would be obtained over a range of times.

In the following discussion, the terms reactivity, reactivity maintenance, capacity, and capacity maintenance are used. These are defined as follows:

Reactivity, R_i - fractional carbonation after $(t-t_o)$ = 1 minute in cycle i.

Capacity, C_i - fractional carbonation after $(t-t_o)$ = 40 minutes in cycle i.

Reactivity Maintenance, R_{ij} - ratio of reactivity in cycle j to reactivity in cycle 1.

Capacity Maintenance, C_{ij} - ratio of capacity in cycle j to capacity in cycle 1.

Experimental reactivity results for the two-cycle test series are summarized in Tables 5-6, 5-7, and 5-8 for sorbents 1, 7, and 9, respectively. Note that the arrangement in these tables corresponds to the test matrix in Tables 5-2, 5-3, and 5-4. The two entries in each position correspond to cycles 1 and 2, respectively. For example, in the first

Table 5-6
Matrix of First and Second Cycle Reactivity for Sorbent 1

Calcin. Temp. (°C)	Carbon. Temp. (°C)	Carbon. CO_2 (% Vol)	Carbonation Pressure		
			1 atm	5 atm	15 atm
900	750	15	.21/.11	.56/.47	.37/.32
900	750	5	***	***	***
900	750	1	***	***	***
900	650	15	.65/.41	.59/.40	***
900	650	5	***	***	***
900	650	1	***	***	***
900	550	15	.56/.14	.55/.16	***
900	550	5	.43/.19	***	***
900	550	1	.16/.06	***	***
825	750	15	.22/.14	.56/.56	.39/.37
825	750	5	***	***	***
825	750	1	***	***	***
825	650	15	.68/.50	.52/.43	.38/.37
825	650	5	.30/.17	***	***
825	650	1	***	***	***
825	550	15	.60/.41	.51/.36	***
825	550	5	.45/.24	***	***
825	550	1	.11/.08	***	***
750	750	15	.23/.22 .20/.18	.51/.52	.37/.39
750	750	5	***	***	.21/.21
750	750	1	***	***	.10/.09
750	650	15	.67/.55	.63/.53	.42/.43
750	650	5	.25/.27	***	***
750	650	1	***	***	.15/.10 .10/.11
750	550	15	.63/.49	.57/.43	.41/.33
750	550	5	.47/.40	***	***
750	550	1	.05/.04	***	***

Table 5-7
Matrix of First and Cycle Reactivity
for Sorbent 7

Calcin. Temp. (°C)	Carbon. Temp. (°C)	Carbon. CO_2 (% Vol)	Carbonation Pressure		
			1 atm	5 atm	15 atm
900	750	15	.13/.08	***	.59/.48
900	750	5	***	.30/.29	***
900	750	1	***	***	***
900	650	15	***	***	.61/.41
900	650	5	***	***	***
900	650	1	***	***	***
900	550	15	***	***	.47/.18
900	550	5	***	***	***
900	550	1	***	***	***
825	750	15	.13/.27	***	.51/.57
825	750	5	***	.24/.25	***
825	750	1	***	***	***
825	650	15	.76/.40	***	.47/.51
825	650	5	.42/.20	.43/.33	***
825	650	1	***	***	***
825	550	15	.54/.43	***	.44/.35
825	550	5	***	.48/.24	***
825	550	1	***	***	***
750	750	15	.13/.29 .08/.28	.72/.72	.55/.60
750	750	5	***	.25/.27	.32/.27
750	750	1	***	***	.07/.10
750	650	15	.75/.68	.79/.73	.55/.58
750	650	5	***	***	***
750	650	1	***	.10/.11	***
750	550	15	.62/.57	.58/.53	.48/.42
750	550	5	.54/.47	***	***
750	550	1	.08/.07	.11/.11	***

Table 5-8
Matrix of First and Second Cycle Reactivity for Sorbent 9

Calcin. Temp. (°C)	Carbon. Temp. (°C)	Carbon. CO_2 (% Vol)	Carbonation Pressure		
			1 atm	5 atm	15 atm
900	750	15	.15/.13	***	.53/.44
900	750	5	***	***	.28/.23
900	750	1	***	***	.05/.00
900	650	15	***	***	***
900	650	5	***	***	***
900	650	1	***	***	.12/.15
900	550	15	***	***	***
900	550	5	***	***	***
900	550	1	***	***	.11/.12
825	750	15	.20/.14	.73/.61	.38/.36
825	750	5	***	***	***
825	750	1	***	***	.08/.07
825	650	15	***	***	.50/.42
825	650	5	***	***	.28/.26
825	650	1	***	***	.07/.11
825	550	15	***	***	***
825	550	5	***	***	***
825	550	1	***	***	.09/.11
750	750	15	.23/.19 .17/.15	.69/.71	.51/.48
750	750	5	***	***	.32/.25
750	750	1	***	***	.16/.05
750	650	15	.80/.68	.72/.66	.49/.54
750	650	5	.34/.33	***	***
750	650	1	***	***	.11/.08
750	550	15	.73/.49	.70/.44	.41/.33
750	550	5	.49/.40	***	.27/.19
750	550	1	.11/.10	***	.13/.11

matrix position of Table 5-6 the value of reactivity for cycle 1 is 0.21 while that for cycle 2 is 0.11. The reactivity maintenance in this case is R_{12} = 0.11/0.21 = 0.52, indicating a rather severe decrease at these reaction conditions. Increased second-cycle reactivity was observed in a number of instances. For example, from Table 5-7 using sorbent 7 at 750°C calcination and carbonation temperatures, 15 atm carbonation pressure, and 0.15 mol fraction CO_2 in the carbonation gas, the sorbent reactivity increased from R_1 = 0.55 to R_2 = 0.60, yielding R_{12} = 1.09.

Tables 5-9, 5-10, and 5-11 summarize the comparable results for sorbent capacity. The two entries in each matrix position represent results from cycles 1 and 2. For example, the first entry for sorbent 1 (Table 5-9) shows C_1 = 0.77 and C_2 = 0.57 to give the capacity maintenance (C_{12}) of 0.74. The capacity results in the tables show, for most test conditions, small to quite significant capacity loss in the second cycle ($C_{12} < 1.0$). In a few cases, however, a slight increase in capacity was observed. For example, for sorbent 9 (Table 5-11) at a calcination temperature of 750°C, and carbonation conditions of 650°C, 5 atm, and 15% CO_2, C_1 = 0.93 and C_2 = 0.94 yielding C_{12} = 1.01. Since the maximum value of C_i = 1.0, there is little opportunity for an increase in the capacity maintenance index when complete carbonation is closely approached.

Table 5-9
Matrix of First and Second Cycle Capacity for Sorbent 1

Calcin. Temp. (°C)	Carbon. Temp. (°C)	Carbon. CO_2 (% Vol)	Carbonation Pressure		
			1 atm	5 atm	15 atm
900	750	15	.77/.57	.76/.58	.77/.62
900	750	5	***	***	***
900	750	1	***	***	***
900	650	15	.70/.46	.71/.49	***
900	650	5	***	***	***
900	650	1	***	***	***
900	550	15	.60/.35	.60/.37	***
900	550	5	.63/.41	***	***
900	550	1	.62/.45	***	***
825	750	15	.78/.60	.76/.66	.78/.64
825	750	5	***	***	***
825	750	1	***	***	***
825	650	15	.74/.56	.67/.49	.64/.48
825	650	5	.74/.54	***	***
825	650	1	***	***	***
825	550	15	.63/.44	.58/.39	***
825	550	5	.62/.41	***	***
825	550	1	.65/.48	***	***
750	750	15	.79/.68 .78/.67	.81/.70	.77/.66
750	750	5	***	***	.77/.67
750	750	1	***	***	.77/.65
750	650	15	.73/.59	.71/.57	.67/.54
750	650	5	.76/.60	***	***
750	650	1	***	***	.75/.60 .71/.58
750	550	15	.67/.52	.62/.48	.60/.43
750	550	5	.63/.47	***	***
750	550	1	.72/.52	***	.62/.48

Table 5-10
Matrix of First and Second Cycle Capacity for Sorbent 7

Calcin. Temp. (°C)	Carbon. Temp. (°C)	Carbon. CO_2 (% Vol)	Carbonation Pressure		
			1 atm	5 atm	15 atm
900	750	15	.94/.81	***	.96/.94
900	750	5	***	.86/.89	***
900	750	1	***	***	***
900	650	15	***	***	.94/.76
900	650	5	***	***	***
900	650	1	***	***	***
900	550	15	***	***	.93/.46
900	550	5	***	***	***
900	550	1	***	***	***
825	750	15	.94/.87	***	.98/.95
825	750	5	***	.91/.97	***
825	750	1	***	***	***
825	650	15	.92/.72	***	.93/.88
825	650	5	.89/.86	.95/.94	***
825	650	1	***	***	***
825	550	15	.91/.54	***	.94/.51
825	550	5	***	.93/.59	***
825	550	1	***	***	***
750	750	15	.95/.94 .95/.93	1.0/.95	.98/.94
750	750	5	***	.97/.92	.97/.94
750	750	1	***	***	.93/.90
750	650	15	.92/.91	.92/.93	.95/.95
750	650	5	***	***	***
750	650	1	***	.92/.90	***
750	550	15	.92/.75	.94/.73	.94/.73
750	550	5	.94/.76	***	***
750	550	1	.88/.67	.90/.69	***

Table 5-11
Matrix of First and Second Cycle Capacity for Sorbent 9

Calcin. Temp. (°C)	Carbon. Temp. (°C)	Carbon. CO_2 (% Vol)	Carbonation Pressure		
			1 atm	5 atm	15 atm
900	750	15	.92/.84	***	.92/.89
900	750	5	***	***	.93/.89
900	750	1	***	***	.90/.84
900	650	15	***	***	***
900	650	5	***	***	***
900	650	1	***	***	.87/.84
900	550	15	***	***	***
900	550	5	***	***	***
900	550	1	***	***	.84/.68
825	750	15	.94/.90	.92/.94	.94/.93
825	750	5	***	***	***
825	750	1	***	***	.97/.92
825	650	15	***	***	.94/.91
825	650	5	***	***	.93/.87
825	650	1	***	***	.95/.91
825	550	15	***	***	***
825	550	5	***	***	***
825	550	1	***	***	.90/.73
750	750	15	.93/.91 .92/.90	.98/.97	.96/.96
750	750	5	***	***	.96/.95
750	750	1	***	***	.93/.90
750	650	15	.95/.96	.93/.94	.96/.93
750	650	5	.94/.94	***	***
750	650	1	***	***	.95/.93
750	550	15	.91/.78	.93/.79	.90/.78
750	550	5	.90/.75	***	.92/.61
750	550	1	.86/.69	***	.90/.74

These index values permit the effect of individual reaction parameters to be evaluated and allow direct comparison of the performance of the three sorbents under equivalent reaction conditions. These evaluations are discussed in the following sections.

5.2 Reaction Parameter Evaluation

5.2.1 The Effect of Calcination Temperature

Reactivity and capacity results suggest that the lowest calcination temperature, 750°C, should be used. Higher calcination temperature, in particular 900°C, has an adverse effect on both reactivity and capacity. Figures 5.3, 5.4, 5.5, and 5.6 illustrate the effect of calcination temperature on reactivity and capacity performance. All runs in these figures were carried out at the same carbonation conditions. Of the twelve curves represented in Figures 5.3 and 5.4, eleven exhibit a negative slope. Only the first-cycle reactivity of sorbent 7 (Figure 5.3) shows slightly improved performance following high calcination temperature. The magnitudes of the negative slopes are greater in the second cycle (Figure 5.4) suggesting that the adverse effect of high calcination temperature increases with increased number of cycles. These second cycle results are emphasized in Figures 5.5 and 5.6 where two-cycle reactivity maintenance and capacity maintenance are plotted against calcination temperature.

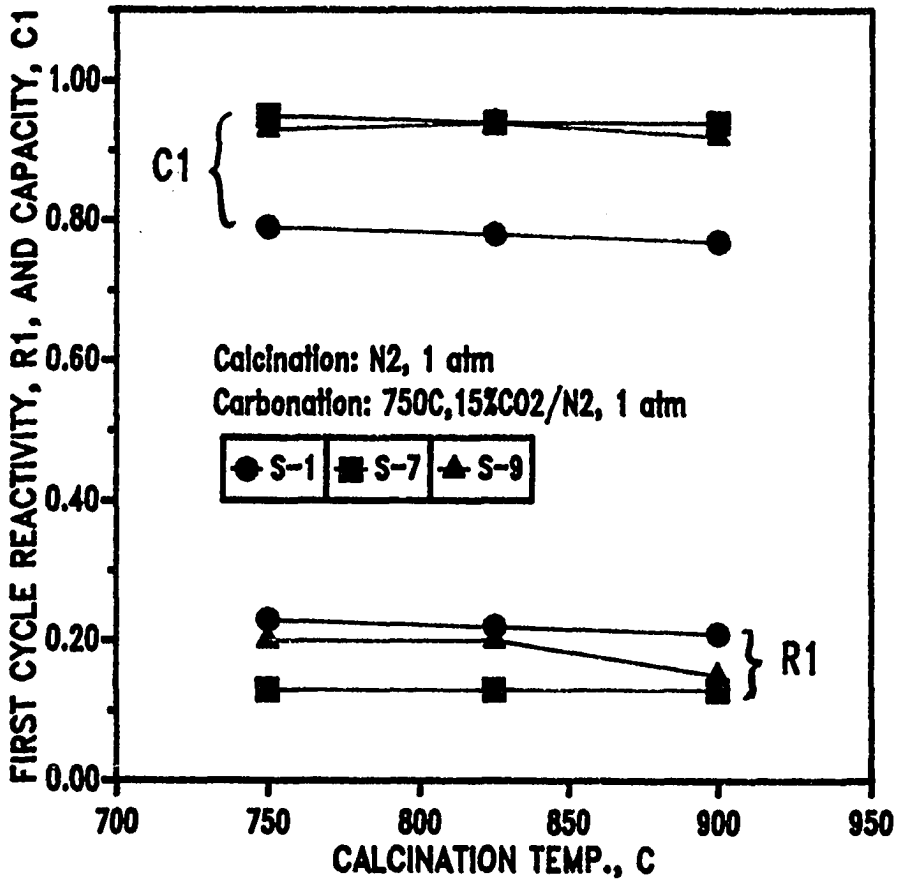

Figure 5.3 Effect of Calcination Temperature on First-Cycle Reactivity and Capacity

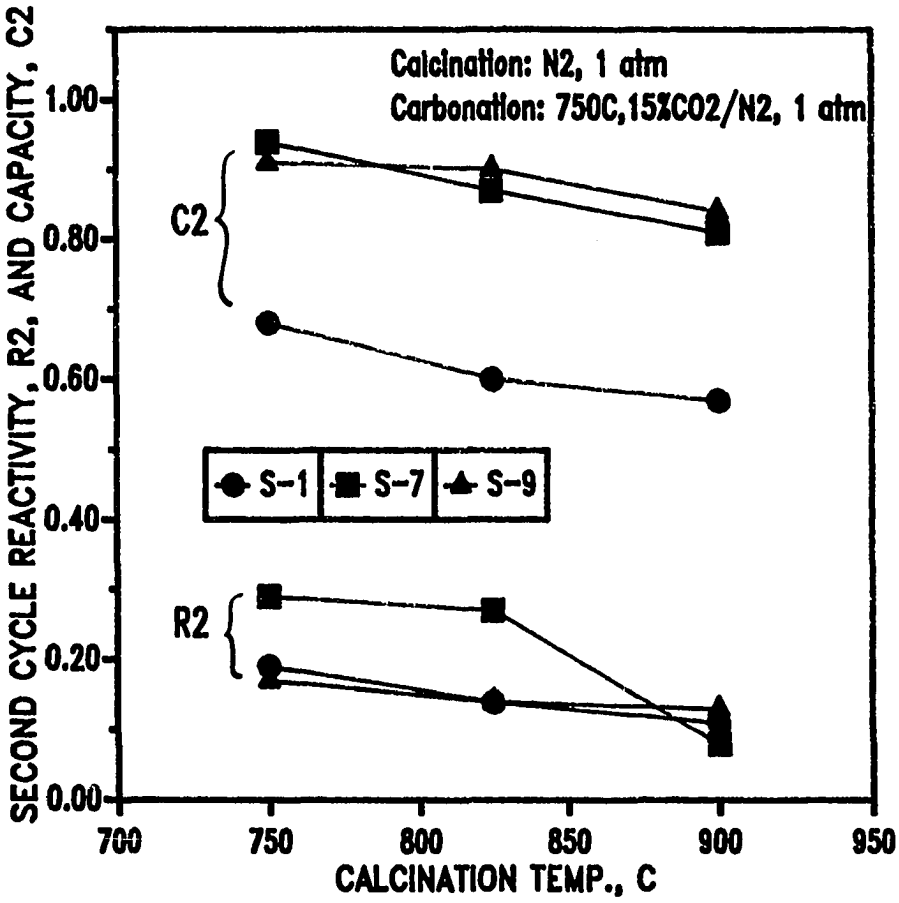

Figure 5.4 Effect of Calcination Temperature on Second-Cycle Reactivity and Capacity

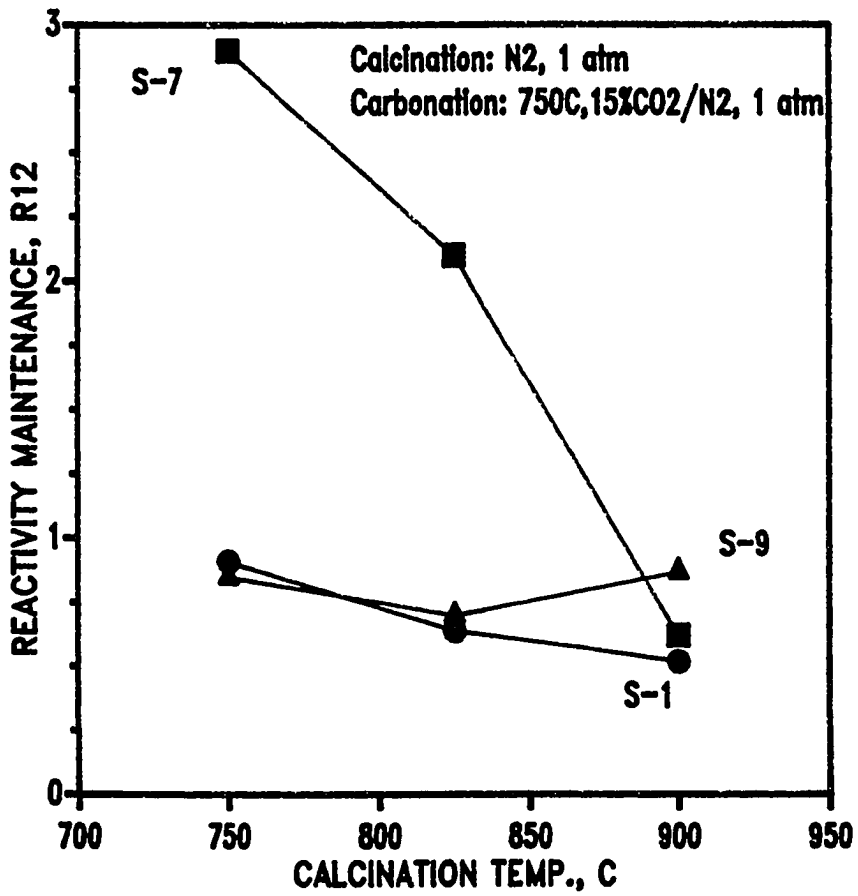

Figure 5.5 Effect of Calcination Temperature on Reactivity Maintenance

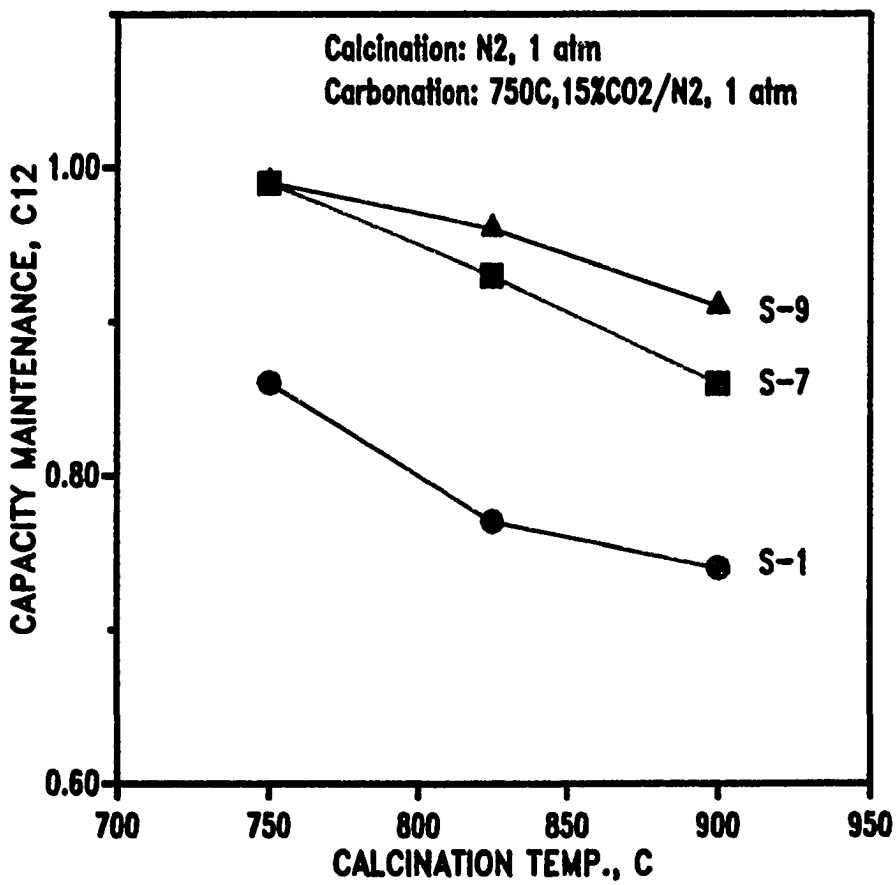

Figure 5.6 Effect of Calcination Temperature on Capacity Maintenance

There are 19 sets of data at which a complete comparison of the effect of the three calcination temperatures at constant carbonation conditions is possible. The advantages associated with low calcination temperature are most apparent with respect to first-cycle capacity, C_1, and capacity maintenance, C_{12}. In 15 of the 19 data sets, the lowest calcination temperature resulted in the highest value for these indices. Conversely, in 15 of the 19 cases the highest calcination temperature resulted in the lowest indices values.

5.2.2 The Effect of Carbonation Temperature

In evaluating the effect of carbonation temperature on the reaction characteristics, the equilibrium CO_2 partial pressure at the temperature of interest must be considered. A number of tests were eliminated in the matrix (Tables 5-2, 5-3, and 5-4) due to the equilibrium restrictions. Even at conditions where tests were carried out, one must be aware of equilibrium when interpreting the results. At 750°C the equilibrium CO_2 pressure is about 0.08 atm. At 1 atm total pressure no reaction will occur when either 1% or 5% CO_2 is included in the carbonation gas; the effective CO_2 pressure in 15% CO_2 is reduced by about one-half. At 550°C, however, the equilibrium CO_2 pressure is sufficiently small that even data at 1 atm total pressure and 1% CO_2 is free from equilibrium restrictions.

Figure 5.7 illustrates the effect of carbonation temperature on first cycle reactivity, R_1. Note that the large decrease in reactivity at 750°C is due to the equilibrium CO_2 pressure, as mentioned above. At 550°C and 650°C the equilibrium CO_2 pressure is small compared to the actual CO_2 pressure, and as shown in Figure 5.7, there is a small increase in reactivity with temperature. Figure 5.8 shows a more realistic view of the effect of carbonation temperature on reactivity. Note that the equilibrium CO_2 pressure is very small compared to the actual 2.25 atm CO_2 partial pressure. As shown in the figure, there is a small increase in reactivity through the entire temperature range for sorbents 7 and 9, but a small decrease in reactivity for sorbent 1 between 650°C and 750°C. The overall lack of a strong temperature dependence suggests that the reactivity is influenced more by transport resistances than the surface chemical reaction.

The most surprising effect of carbonation temperature was an apparent sharp decrease in capacity maintenance, C_{12}, at the lowest carbonation temperature of 550°C. Table 5-12 summarizes the average and standard deviation values of first-cycle capacity (C_1), second-cycle capacity (C_2), and capacity maintenance (C_{12}) for all equivalent data sets from Tables 5-9, 5-10, and 5-11. Each sorbent shows a significant drop in capacity maintenance at 550°C compared to the higher temperatures. A caution in interpreting the Table 5-12

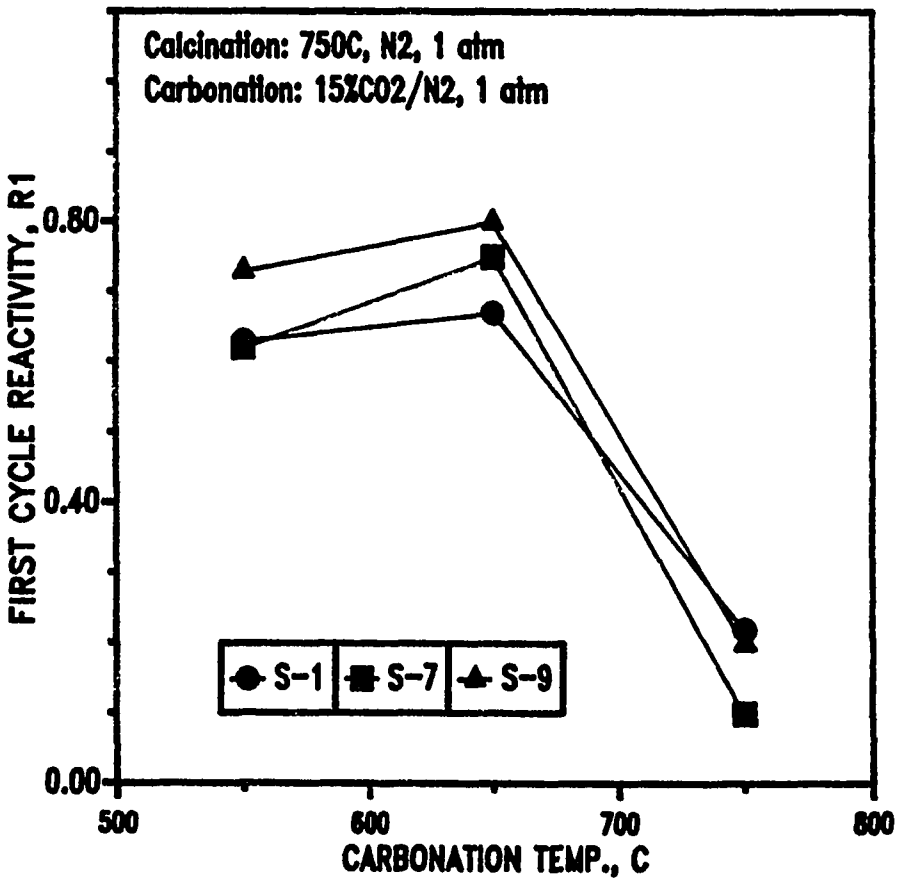

Figure 5.7 Effect of Carbonation Temperature on First-Cycle Reactivity; Carbonation at 1 atm in 15% CO_2/N_2

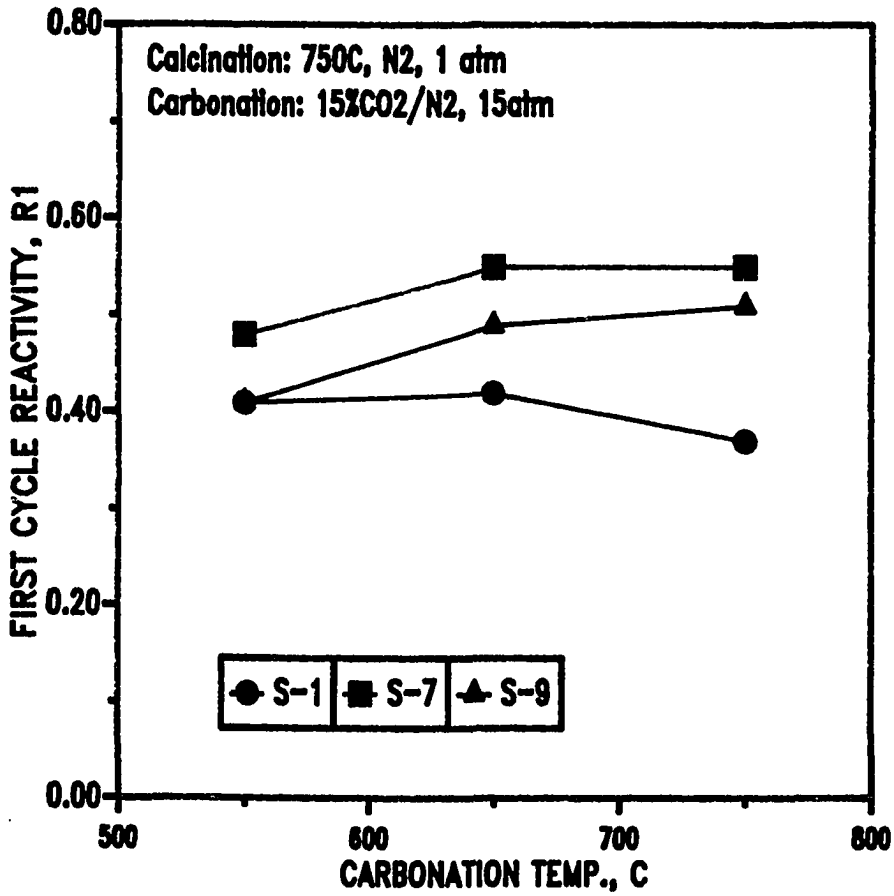

Figure 5.8 Effect of Carbonation Temperature on First-Cycle Reactivity; Carbonation at 15 atm in 15% CO_2/N_2

Table 5-12
The Average and Standard Deviation Values of First and Second Cycle Capacity and its Capacity Maintenance for Sorbents 1, 7, and 9

Carbonation Temperature (°C)	No.of Data Sets	First-Cycle Capacity (C_1)	Second-Cycle Capacity (C_2)	Capacity Maintenance (C_{12})
Sorbent 1	8			
750		0.78±0.02	0.64±0.05	0.82
650		0.71±0.03	0.54±0.05	0.76
550		0.62±0.03	0.43±0.06	0.69
Sorbent 7	7			
750		0.96±0.03	0.94±0.03	0.98
650		0.93±0.02	0.87±0.09	0.94
550		0.93±0.03	0.62±0.12	0.67
Sorbent 9	6			
750		0.95±0.03	0.92±0.04	0.97
650		0.94±0.03	0.92±0.04	0.98
550		0.90±0.03	0.75±0.04	0.83

entries is necessary. The only valid comparison is of the effect of carbonation temperature on an individual sorbent; in this case the data sets are equivalent. It is not valid to compare the performance of the three sorbents at a fixed carbonation temperature since the data sets involved in such a comparison would not be equivalent. A general trend to low C_{12} values at the lowest carbonation temperature is shown in Figure 5-9.

Other researchers have also reported unexpected results at carbonation temperatures near 550°C. Bhatia and Perlmutter (1983) reported a change in activation energy for product layer diffusion at 515°C suggesting a change in the reaction mechanism. Anderson (1969) also reported a similar change in activation energy for CO_2 exchange with calcite grains at 550°C. Mess (1989) reported a unique result from carbonation of nonporous CaO particles at 550°C. Based on SEM micrographs, he observed that nonporous CaO particles carbonated at 550°C had completely different product structure than particles carbonated at higher temperature. He observed that the surface of the particles contained many small crystallites of approximately 1 μm size which protruded from the product layer. This caused much rougher particle surfaces than those carbonated at 600°C or above. Unlike carbonation results at higher temperature, grain boundaries were not observed at 550°C carbonation temperature.

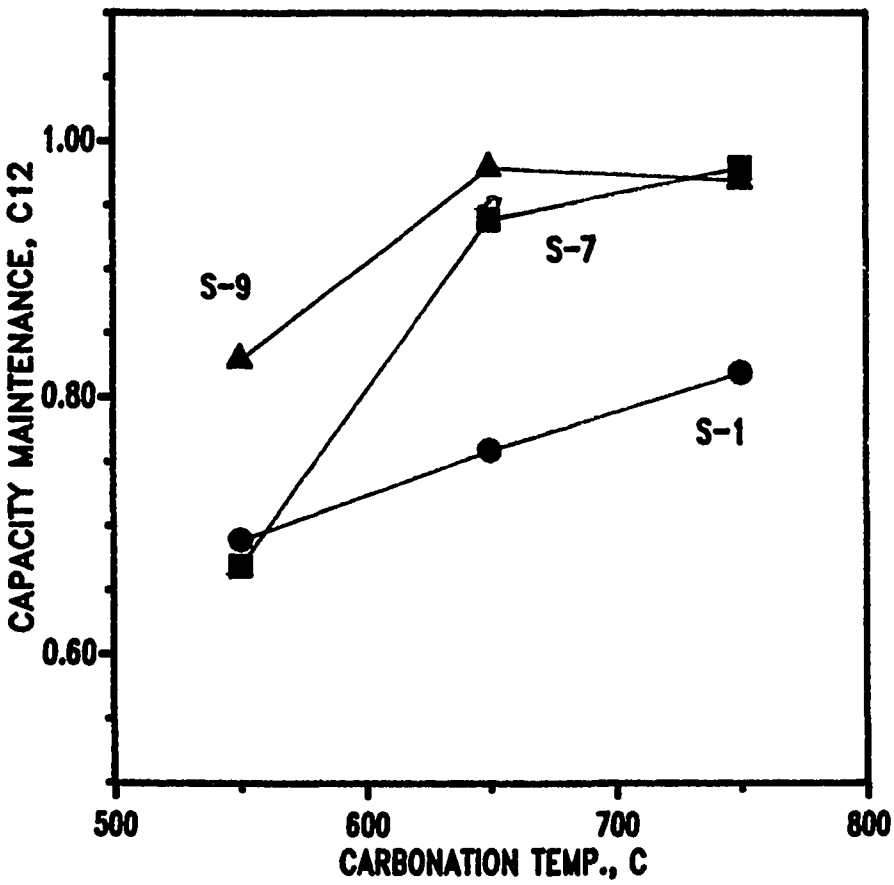

Figure 5.9 Effect of Carbonation Temperature on Average Capacity Maintenance

Carbonation temperatures of 650 and 750°C for sorbents 7 and 9 show little difference in capacity and capacity maintenance. As seen in Table 5-12, the average values of capacity for both sorbents are 0.90 or above for both cycle 1 and cycle 2 at 650 and 750°C (except for second-cycle capacity of sorbent 7 at 650°C). Sorbent 1, however, shows a significant decrease of capacity (from C_1 = 0.78 to C_2 = 0.64 at 750°C and from C_1 = 0.71 to C_2 = 0.54 at 650°C).

5.2.3 The Effect of Carbonation Pressure

Like carbonation temperature, the effect of pressure on the carbonation equilibrium must be considered. The effect of carbonation pressure on first-cycle reactivity, R_1, is shown in Figure 5.10. The calcination temperature was 750°C, and the carbonation conditions were 550°C and 15 atm in 15% CO_2 where the equilibrium effects were negligible. The reactivity decreases with increasing pressure for all three sorbents.

The fact that reactivity decreases with increasing carbonation pressure is consistent with the previous conclusion that transport resistances are important in establishing reactivity. If surface rate was controlling, one would expect an increase in reactivity with pressure since CO_2 concentration is directly proportional to pressure. In contrast, both mass transfer coefficient and effective diffusivity decrease with increasing pressure so that transport resistances would produce the observed effect.

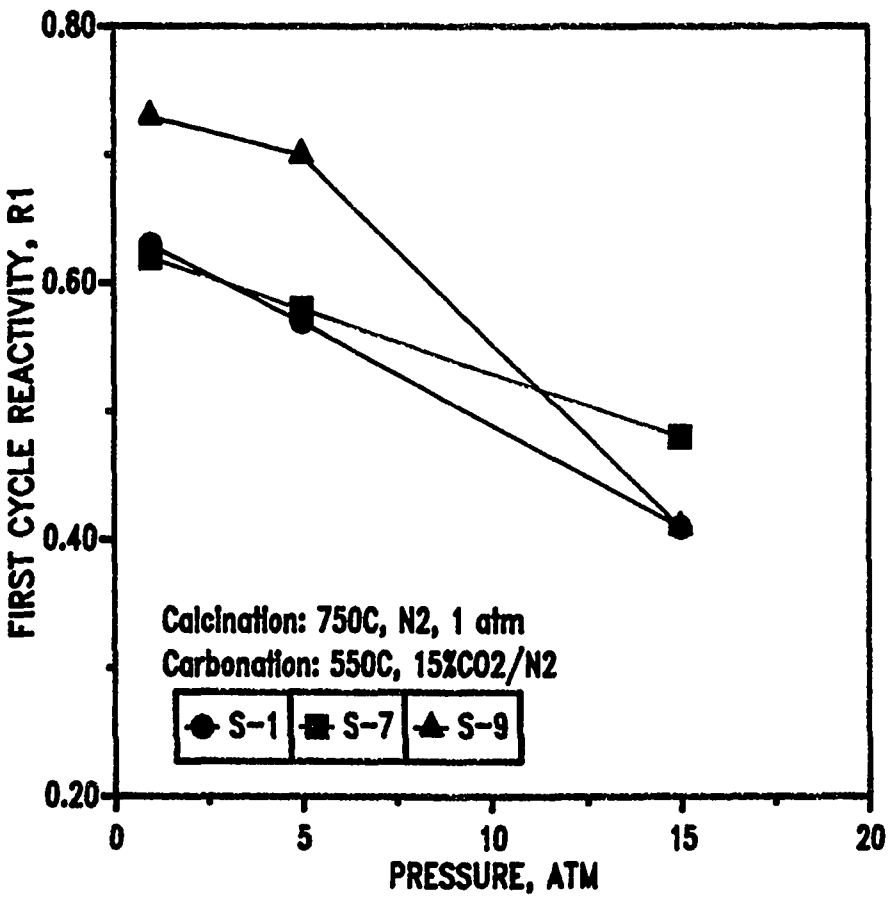

Figure 5.10 Effect of Carbonation Pressure on First-Cycle Reactivity

Reaction pressure has little effect on sorbent capacity in either cycle, or on capacity maintenance. The capacity maintenance behavior is illustrated in Figure 5.11. The calcination temperature was 750°C, and the carbonation was in 15% CO_2 at 650°C. The curves are approximately horizontal for each of the three sorbents with values of C_{12} in the range of 0.97 to 1.01 for sorbents 7 and 9 compared to about 0.81 for sorbent 1. Eleven out of 13 equivalent data sets available for this direct comparison show essentially no effect of operating pressure on capacity maintenance.

5.2.4 The Effect of CO_2 Mol Fraction

Figure 5.12 illustrates the effect of CO_2 mol fraction on first-cycle reactivity, R_1. Calcination was carried out at 750°C, and carbonation was at 750°C and 15 atm. As expected, the reactivity increases with increasing CO_2 mol fraction. The absence of a linear dependence throughout the entire mol fraction range is also reasonable. At the lowest CO_2 mol fraction, the values of R_1 are in the range of 0.07 to 0.15; an increase in R_1 by a factor of 15 is impossible. In other words, reactivity is not a diferential but an integral function.

Sorbent capacity, on the other hand, is essentially independent of CO_2 mol fraction as illustrated in Figure 5.13. Note that the reaction conditions are the same as in Figure 5.12. The data for all three sorbents are almost

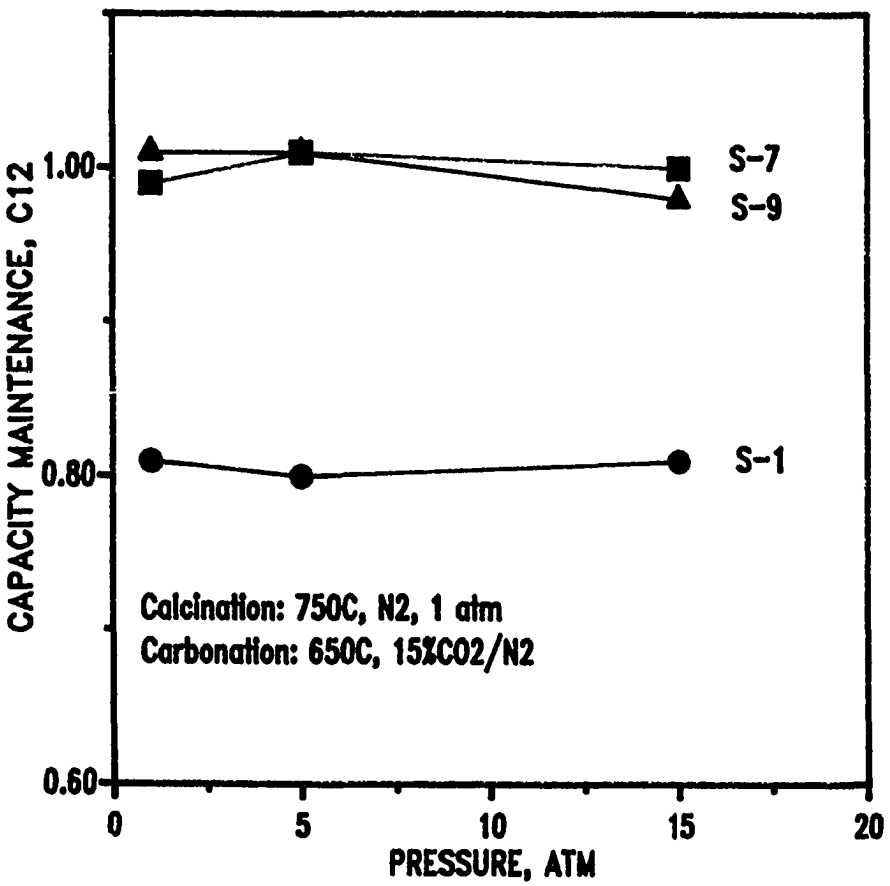

Figure 5.11 Effect of Carbonation Pressure on Capacity Maintenance

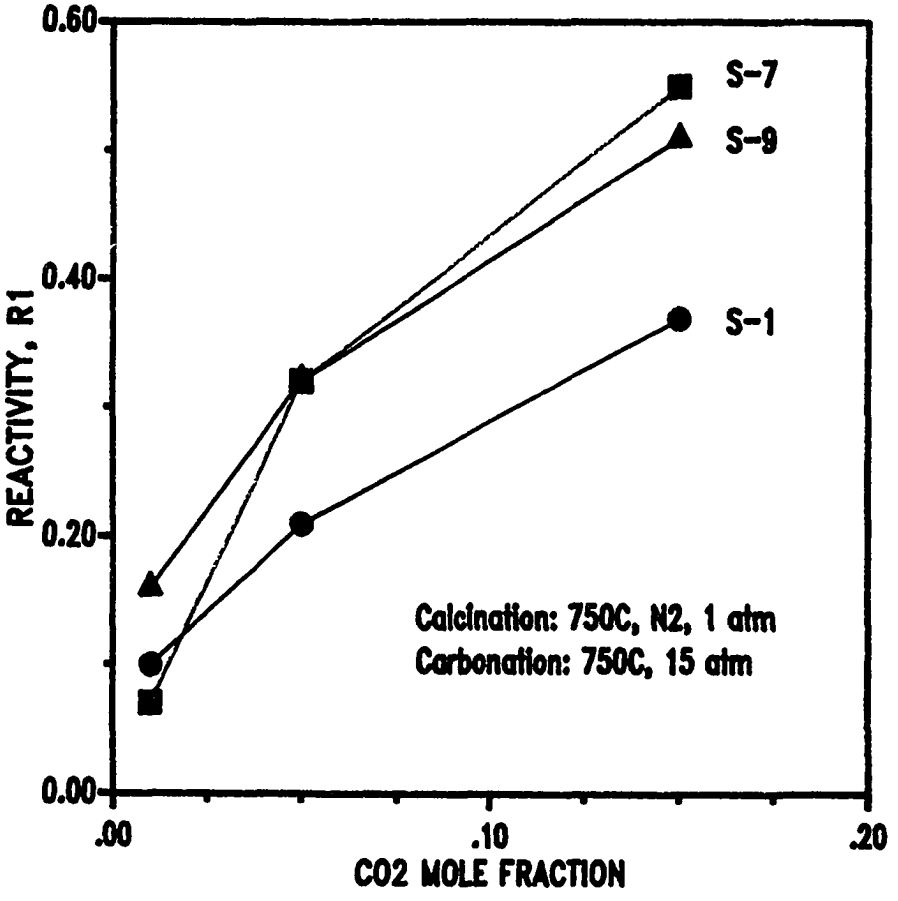

Figure 5.12 Effect of CO_2 Mol Fraction on First-Cycle Reactivity

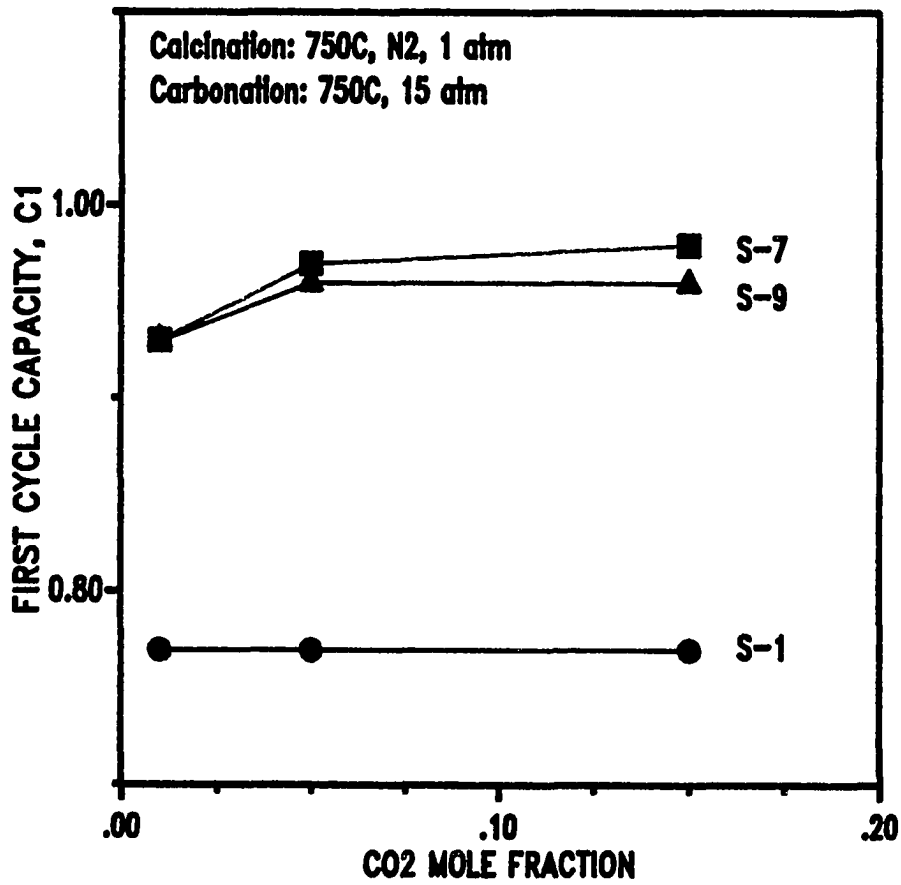

Figure 5.13 Effect of CO_2 Mol Fraction on First-Cycle Capacity

horizontal, with slightly lower values of C_1 for sorbents 7 and 9 at 0.01 mol fraction due to the slow progress of the reaction at low concentration and high pressure. In other words, at these conditions the reaction was so slow that the 40 minute reaction time was not sufficient to establish sorbent capacity.

5.3 Direct Comparison of Base Sorbents

There are 18 sets of reaction conditions at which all three sorbents were tested. Four of the 18 data sets were excluded in reactivity comparisons because the reaction conditions were quite close to the equilibrium conditions. However, these data were included in capacity and capacity maintenance comparisons since CO_2 mol fraction has little effect on capacity.

Sorbents 7 and 9 have a clear advantage over sorbent 1 in terms of both capacity and capacity maintenance. All 18 direct comparisons show that both sorbents 7 and 9 have first-cycle capacities of 0.90 or above. For sorbent 1, on the other hand, the first-cycle capacity ranges from 0.60 to 0.81. Moreover, sorbents 7 and 9 have better capacity maintenance than sorbent 1. The C_{12} values of sorbent 1 range from 0.72 to 0.86 while sorbents 7 and 9 have C_{12} values from 0.76 to 1.01 and from 0.80 to 1.01, respectively.

Since first-cycle carbonation for sorbents 7 and 9 is almost complete (conversion of 0.90 or above), it is

difficult to make direct comparisons between the two sorbents. However, sorbent 9 exhibits slightly higher values of capacity maintenance. Of 18 data sets available for direct comparison, 13 data sets confirm that sorbent 9 has a slight advantage in term of capacity maintenance.

Capacity results for sorbent 9 can be somewhat misleading. Capacity is a measure of fractional calcium utilization, which provides an unambiguous basis for comparison of sorbents 1 and 7, since both are essentially pure CaO at the beginning of the carbonation cycle. Sorbent 9, however, at the beginning of carbonation contains more than 40% (wt) inerts, primarily MgO. Therefore, on the basis of unit mass of total sorbent, the CO_2 capacity of sorbent 9 is much less than that of either sorbent 1 or sorbent 7. This subject will be discussed in more detail in Chapter 7.

In order to compare the reactivity of the three sorbents it is necessary to exclude four of the 18 equivalent data sets due to equilibrium considerations. Thirteen out of the remaining 14 data sets show that sorbent 7 and sorbent 9 exhibit a higher reactivity in both cycles 1 and 2 than sorbent 1. This behavior is attributed to the differences in structural properties of each sorbent discussed in Chapter 2 (Narcida,1992). There are no first-cycle significant reactivity differences between sorbent 7 and sorbent 9. This conclusion has been confirmed using a statistical analysis based on the method of hypothesis testing (Bethea *et al.*,

1975) with the confidence level of 95%. Using the same test, sorbent 7 has a slightly higher reactivity maintenance than sorbent 9.

5.4 Optimum Reaction Conditions

As a result of the two-cycle reaction studies, it is possible to define the conditions at which a CaO-based high temperature, high pressure CO_2 separation process should operate:

Calcination Temperature	750°C
Carbonation Temperature	650 - 750°C
Carbonation Pressure	15 atm
% CO_2 in Carbonation Gas	15

Calcination should be carried out at the lowest possible temperature (about 750°C) to minimize sorbent deterioration and to avoid the normal operational problems associated with higher temperature. Carbonation at 550°C should be avoided because of the negative effect on capacity maintenance. Carbonation at 650°C is desirable because it will permit higher equilibrium fractional CO_2 removal. However, values of the reactivity and capacity indices indicate that 750°C carbonation temperature is also acceptable. The lack of a narrowly defined optimum carbonation temperature may be advantageous from the standpoint of reactor design and control because of the exothermic nature of the carbonation reaction.

Carbonation pressure will be dictated by the gasification process which is likely to operate at 15 atm or more. High pressure is favorable for high equilibrium CO_2 removal, and the experimental studies have shown no adverse effect of high pressure other than a decrease in reactivity. In a commercial process, sorbent capacity and, in particular, capacity maintenance are more important than reactivity. The inlet CO_2 mol fraction will also be determined by the gasification process. No adverse kinetic effects of high CO_2 concentration have been detected, and high inlet concentration is advantageous for high fractional CO_2 removal. At the most favorable carbonation conditions, namely 650°C, 15 atm, and 15% CO_2 in the inlet gas, the theoretical CO_2 removal efficiency exceeds 99.5%.

Chapter 6

Experimental Results:

Detailed Parametric Studies

More detailed investigations of calcination and carbonation reaction parameters are discussed in this chapter. All previous calcination runs were carried out at 1 atm in N_2. Calcination at elevated pressure has been studied in order to investigate its effect on carbonation kinetics. It has been shown that calcination at 900°C must be avoided and calcination at 750°C produced the best carbonation results. Additional runs using calcination temperatures as low as 650°C have been carried out. The effect of low calcination temperature on carbonation performance will be discussed. Previous tests showed that carbonation temperatures of 650 or 750°C produce similar carbonation results. Additional carbonation temperatures have been studied in order to have a more complete understanding of this parameter. Finally, the effect of CO_2 concentration in the calcination gas on the carbonation reaction is discussed.

6.1 Effect of Calcination Pressure

Figure 6.1 compares the calcination results using sorbent 9 at calcination pressures of 1 atm (HP146) and 15 atm (HP153). The high pressure delays the start of calcination and decreases the calcination rate by a small

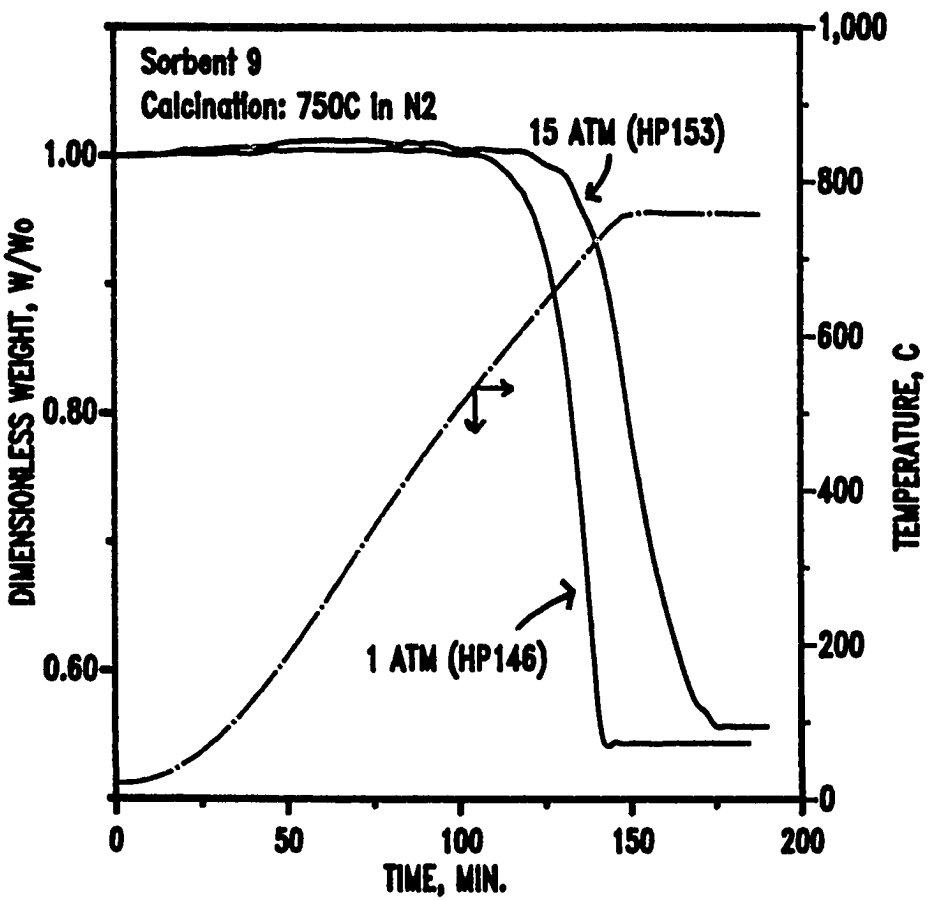

Figure 6.1 Comparison of Calcination Kinetics at Different Pressure; Sorbent 9

amount. Nevertheless, effectively complete calcination was achieved in a reasonable amount of time. Figure 6.2 compares the subsequent first-cycle carbonation kinetics of sorbent 7 at 750°C, 15 atm, and in 15% CO_2 following calcination at 1, 5, and 15 atm. There is essentially no effect of calcination pressure on carbonation reactivity, and little, if any, effect on first-cycle capacity.

6.2 Effect of Calcination Temperature

It was confirmed previously that calcination at 900°C should be avoided, and that calcination at 750°C leads to improved carbonation performance. Lower calcination temperatures of 700 and 650°C were studied in order to confirm the above conclusion and to determine the minimum possible calcination temperature. Low calcination pressure (1 atm) was required in order to achieve calcination at lower temperature. Figure 6.3 shows the calcination curves for sorbent 7 at lower temperatures with the 750°C calcination results included for comparison. Temperature was increased at a rate of approximately 5°C/min until the indicated final temperature was reached and held constant thereafter. Minor differences in calcination behavior were observed between 700 and 750°C, but the final step in the overall calcination process of sorbent 7 at 650°C (decomposition of $CaCO_3$ to CaO) was quite slow. The rate of weight loss was so slow that after 410 minutes the rate was accelerated by increasing

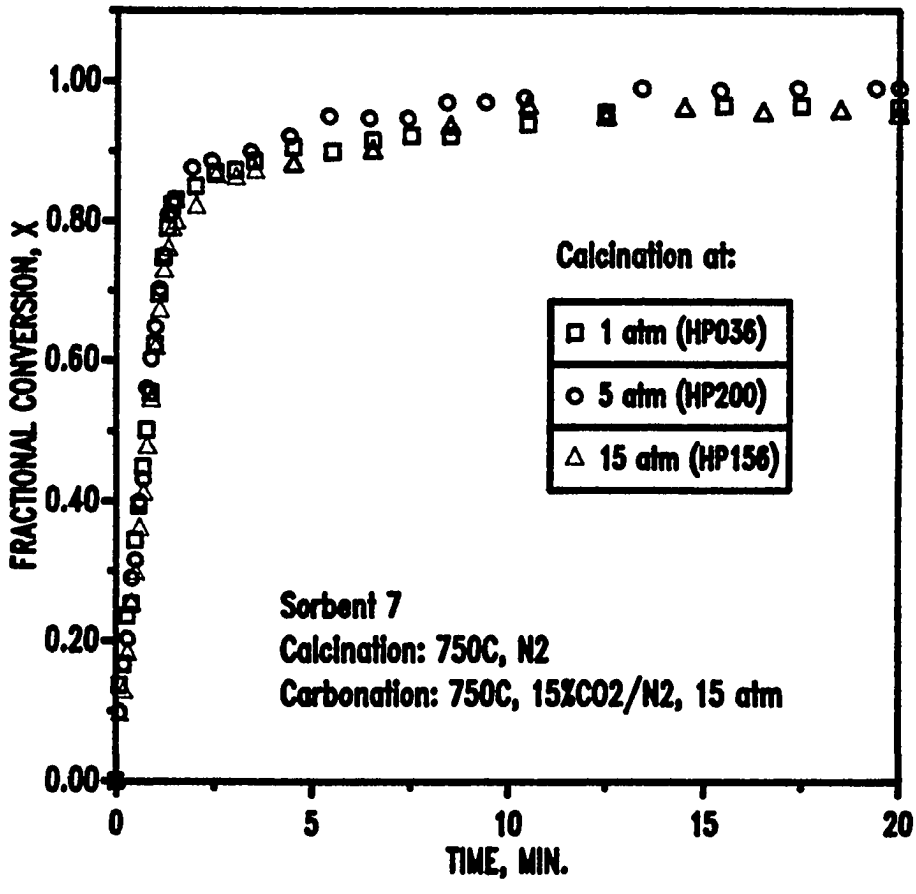

Figure 6.2 Effect of Calcination Pressure on First-Cycle Carbonation Kinetics; Sorbent 7

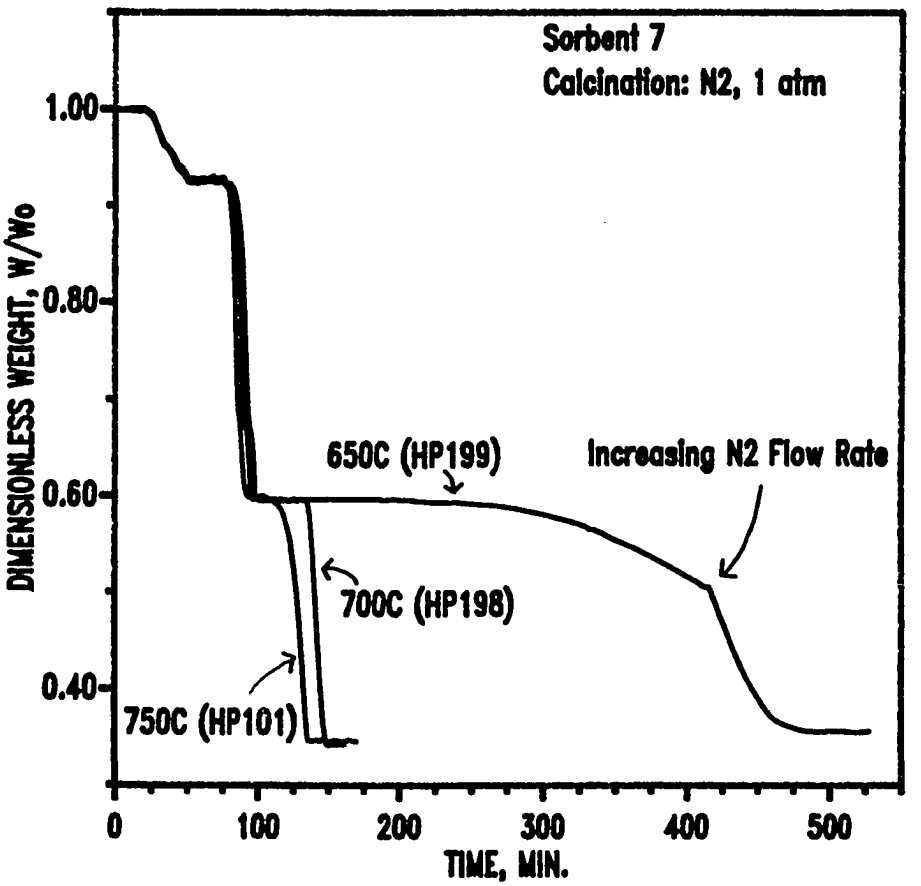

Figure 6.3 Calcination Kinetics as a Function of Temperature; Sorbent 7

N_2 flow from 300 ml/min to 500 ml/min (STP). Complete calcination was achieved after approximately 8½ hours.

First-cycle carbonation results at 650°C, 15 atm, in 15% CO_2/N_2 following calcination at the three lower temperatures are shown in Figure 6.4. The curves are almost coincident indicating that there is little effect of lower calcination temperature on either sorbent reactivity or capacity. Likewise, there was little difference in the two-cycle carbonation capacity maintenance following low calcination temperature. Figure 6.5 shows that the values of C_{12} are effectively 1.0 at each of the three lower calcination temperatures. Note that the adverse effect of higher calcination temperature (825 and 900°C) which was established in the previous chapter is included for comparison purposes.

6.3 Effect of Carbonation Temperature

The additional carbonation temperatures of 600 and 700°C were studied using sorbent 9 following calcination at 750°C, 1 atm. Figure 6.6 shows the first-cycle fractional conversion versus time results for five carbonation temperatures. The time scale is limited to 20 minutes in this figure in order to emphasize the initial rate period. All tests show the characteristic rapid initial rate followed by the abrupt transition to the slow rate. The initial rates at 550, 600, and 650°C are quite similar. A slight decrease in initial

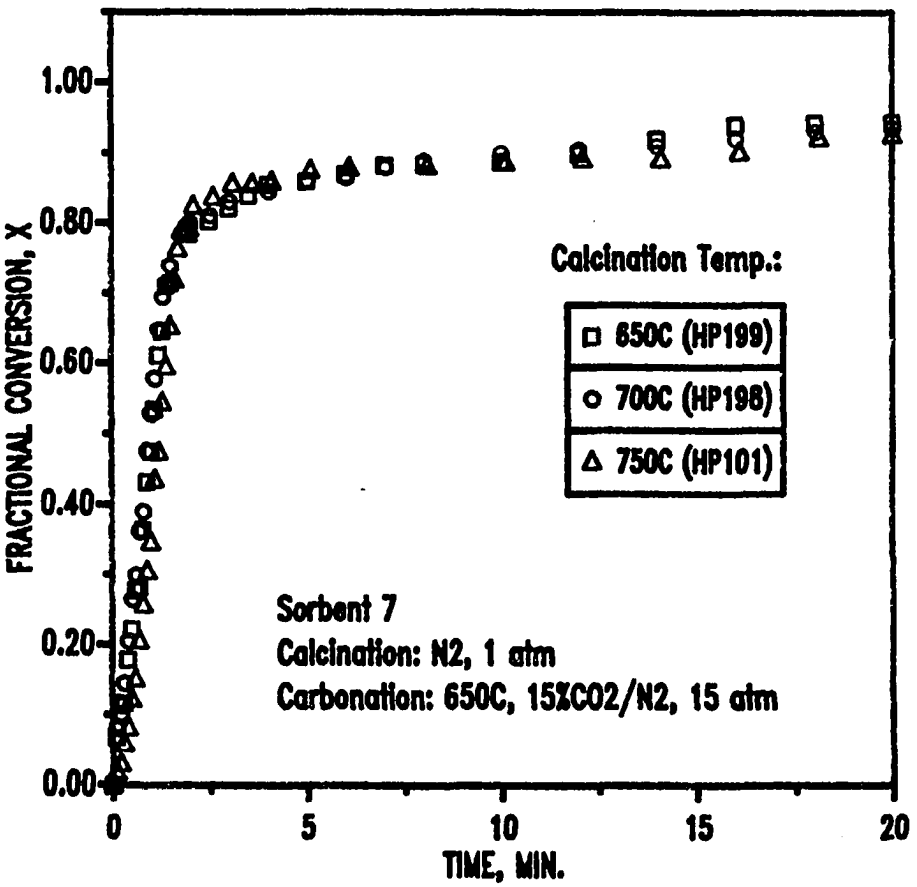

Figure 6.4 Effect of Calcination Temperature on First-Cycle Carbonation Kinetics; Sorbent 7

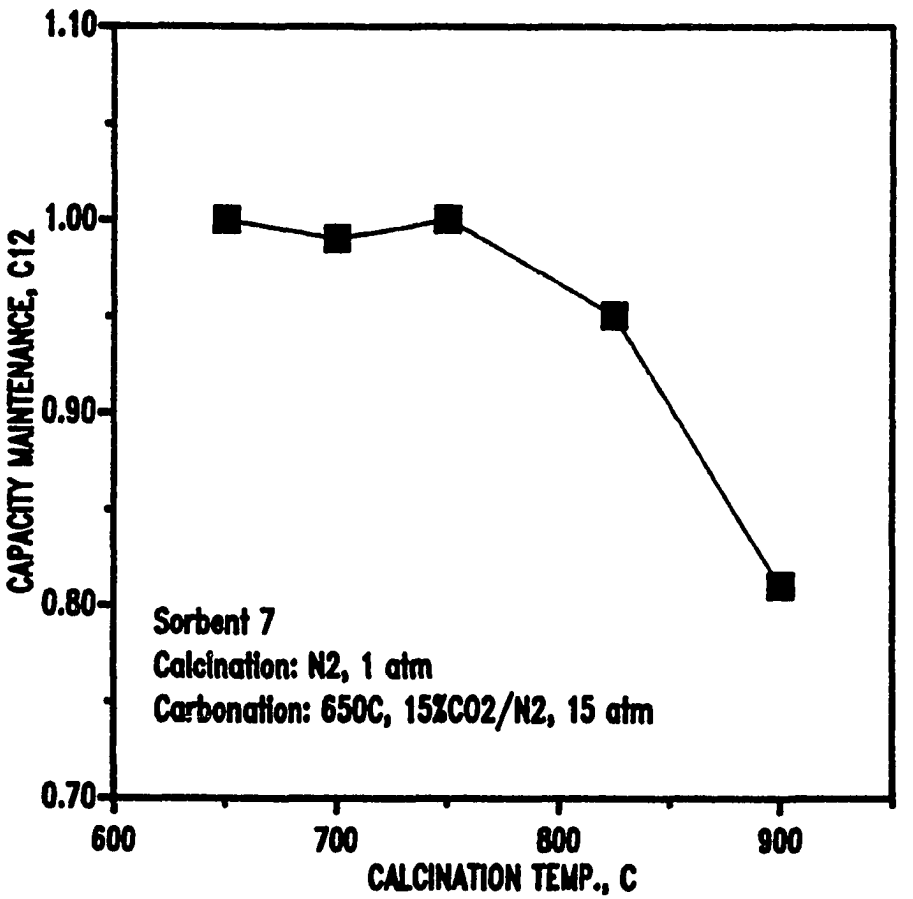

Figure 6.5 Effect of Calcination Temperature on Capacity Maintenance; Sorbent 7

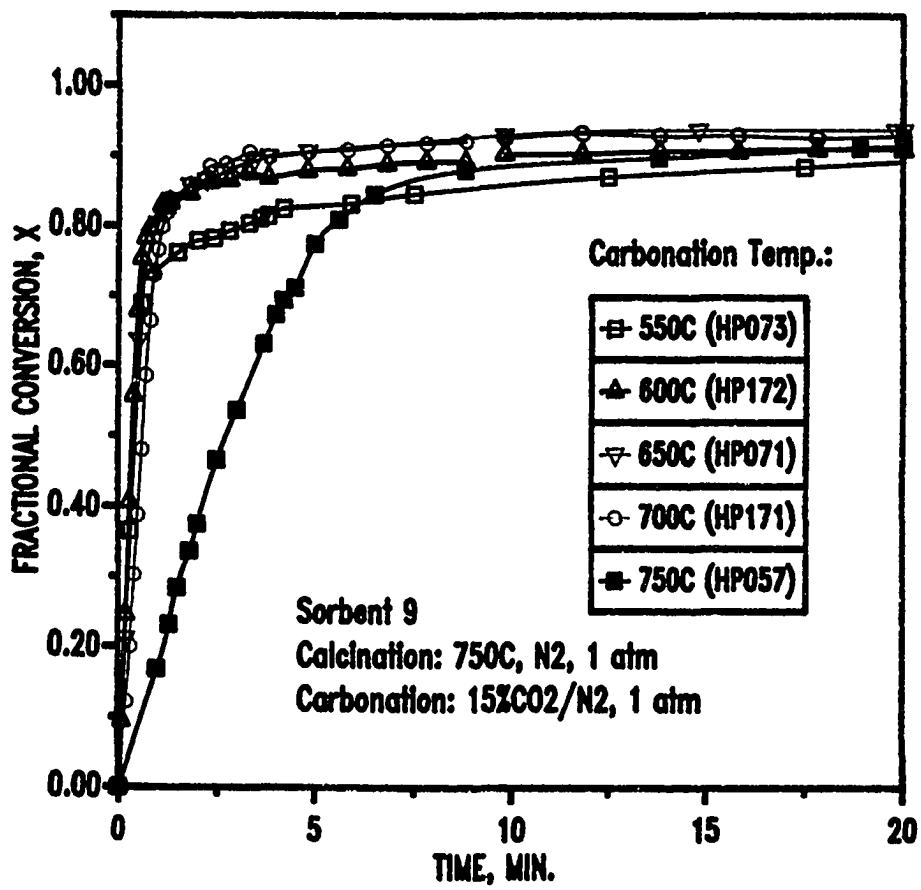

Figure 6.6 Effect of Temperature on Carbonation Kinetics During Early Phases of the Reaction; Sorbent 9.

rate is obvious at 700°C, and at 750°C the initial rate is significantly lower. This result is due to the increasing importance of equilibrium CO_2 pressure with increasing temperature. At the three lower temperatures the equilibrium CO_2 pressure is negligible compared to the 0.15 atm actual CO_2 pressure. At 700°C the equilibrium pressure is just becoming important, and at 750°C the equilibrium pressure is approximately one-half the actual pressure. The transition from the rapid to the slow reaction phase occurred more gradually at 750°C. At the lowest temperature of 550°C, the transition occurred at lower conversion and the fractional carbonation remained lower throughout the early part of the reaction. However, after 40 minutes (not shown) the fractional conversion were similar, and the capacity values for the five tests were 0.92, 0.92, 0.96, 0.93, and 0.93 for 550, 600, 650, 700, and 750°C, respectively. Figure 6.7 shows the carbonation temperature effect on capacity maintenance. The capacity maintenance at 600°C lies between previously determined values at 550 and 650°C. Similarly, the capacity maintenance at 700°C lies between the previously determined values at 650 and 750°C. All C_{12} values in the temperature of 650-750°C range are 0.98 or above.

Figure 6.8 illustrates the effect of a still lower carbonation temperature (450°C) using sorbent 7 following calcination at 750°C, 1 atm, in N_2. Initial carbonation rates are similar for all temperatures. The abrupt transition to

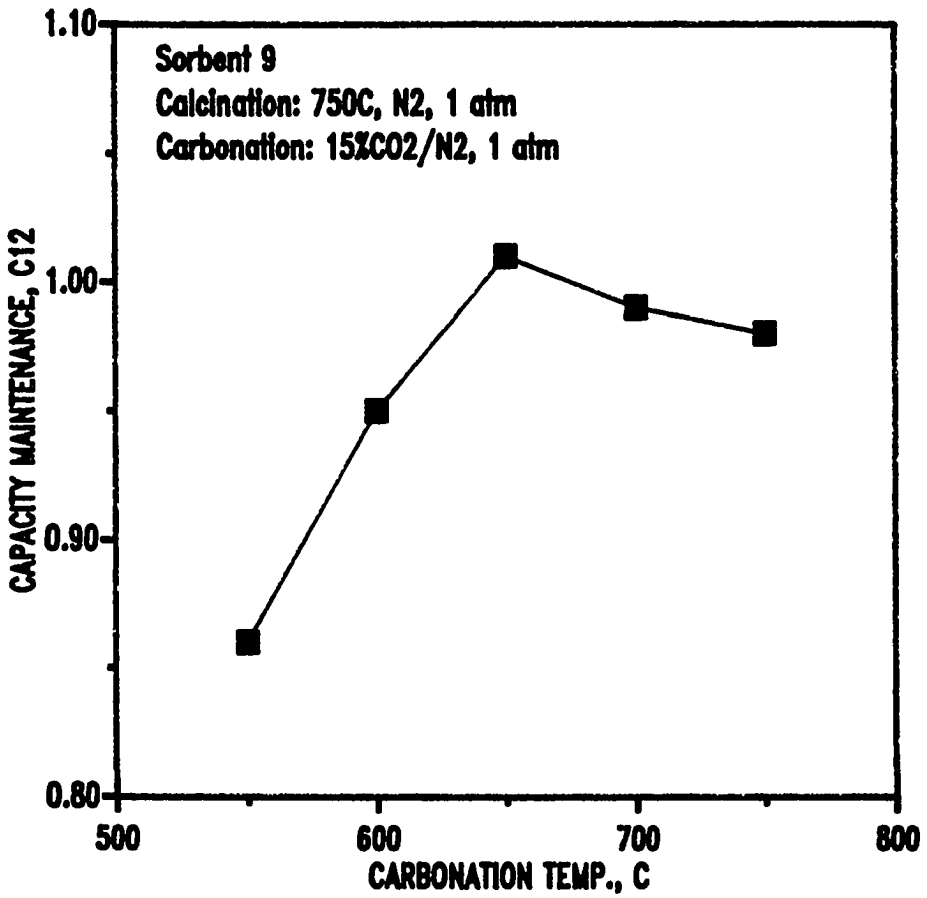

Figure 6.7 Effect of Carbonation Temperature on Capacity Maintenance; Sorbent 9

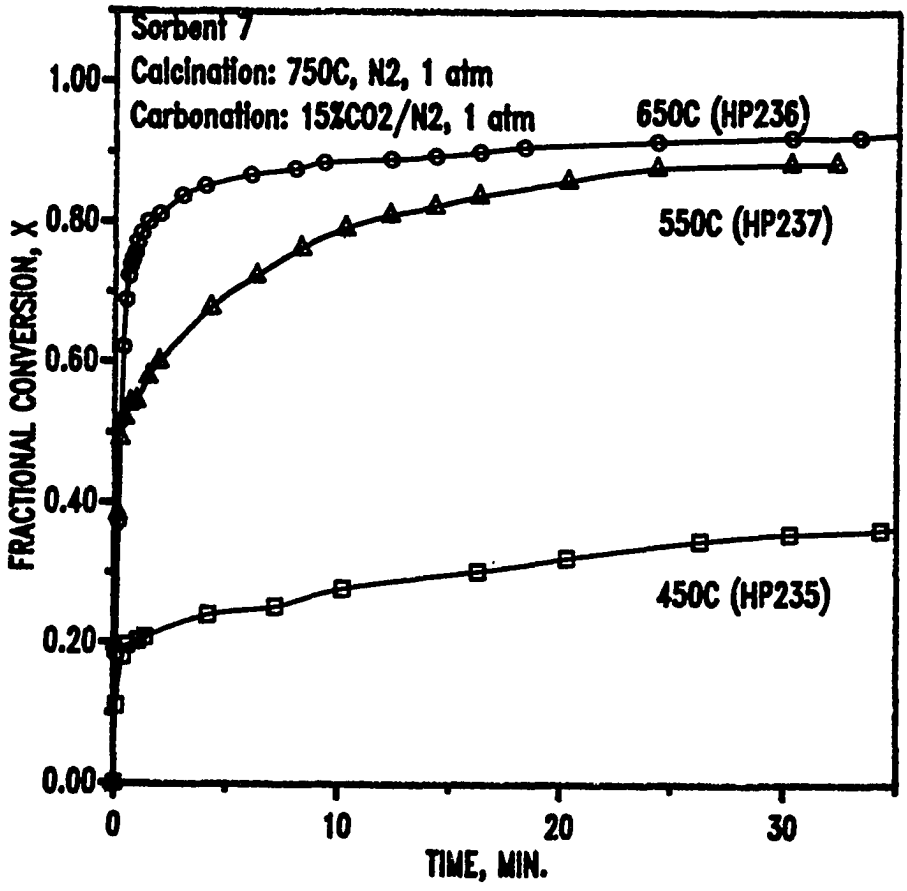

Figure 6.8 Effect of Temperature on Carbonation Kinetics; Sorbent 7

the slow rate, on the other hand, is very distinct for each carbonation temperature. At a carbonation temperature of 450°C, the fractional conversion was about 0.20 at the transition, and after 30 minutes the conversion only reached 0.36. This compares to transition fractional conversions of 0.52 and 0.78, and conversions of 0.88 and 0.92 after 30 minutes at 550 and 650°C, respectively. The low capacity value at 450°C carbonation temperature is attributed to the product layer diffusion controlling the reaction almost immediately. The product layer diffusion coefficient is known to be strongly temperature dependent (Bhatia and Perlmutter, 1983; DeLucia, 1985).

Figure 6.9 shows the effect of carbonation temperature on capacity maintenance for sorbent 7 following calcination at 750°C and 1 atm N_2. Carbonation was carried out at 1 atm in 15% CO_2/N_2. Note that results from two tests are provided at 550°C carbonation temperature, two at 650°C, and three at 750°C. The significant result here is that the capacity maintenance at 450°C is less than the previously measured low values at 550°C. On the other hand, C_{12} values at the temperatures of 650 and 750°C are essentially 1.0, in agreement with the results for sorbent 9. Figure 6.10 shows the effect of higher carbonation temperatures (800 and 850°C) on capacity maintenance using sorbent 7. Calcination was carried out at 750°C and 1 atm N_2 followed by carbonation at 15 atm in 15% CO_2/N_2. High pressure was required in order to

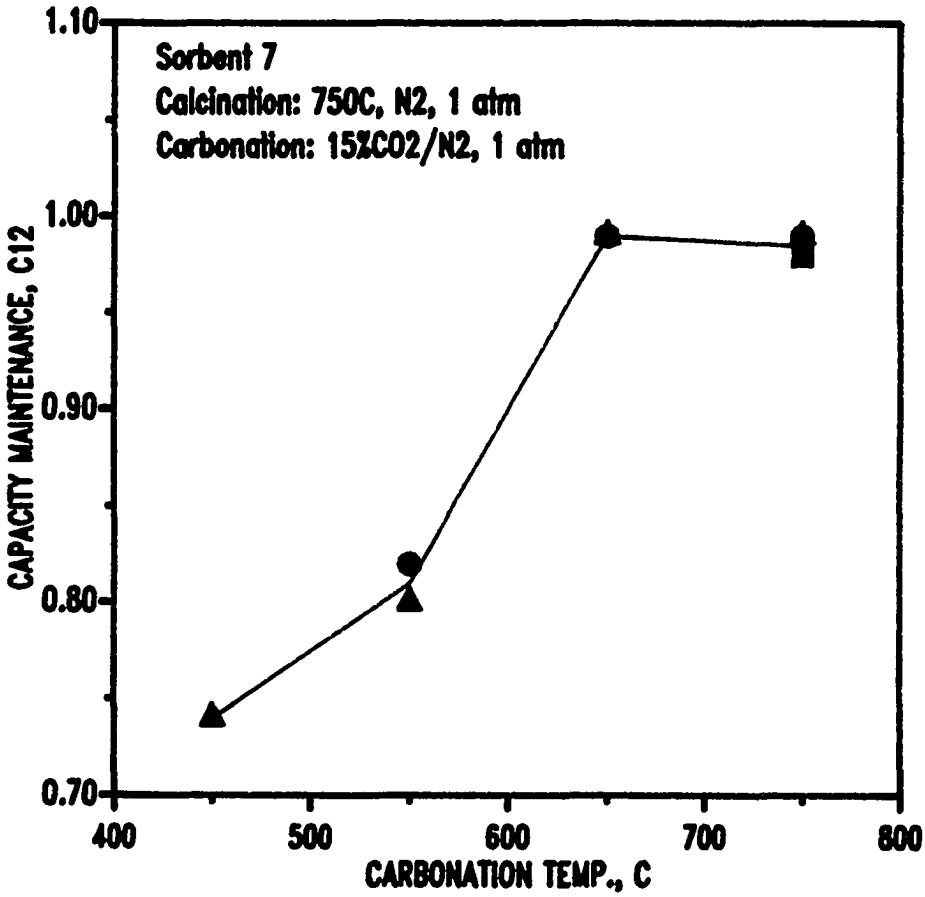

Figure 6.9 Effect of Carbonation Temperature on Capacity Maintenance; Sorbent 7.

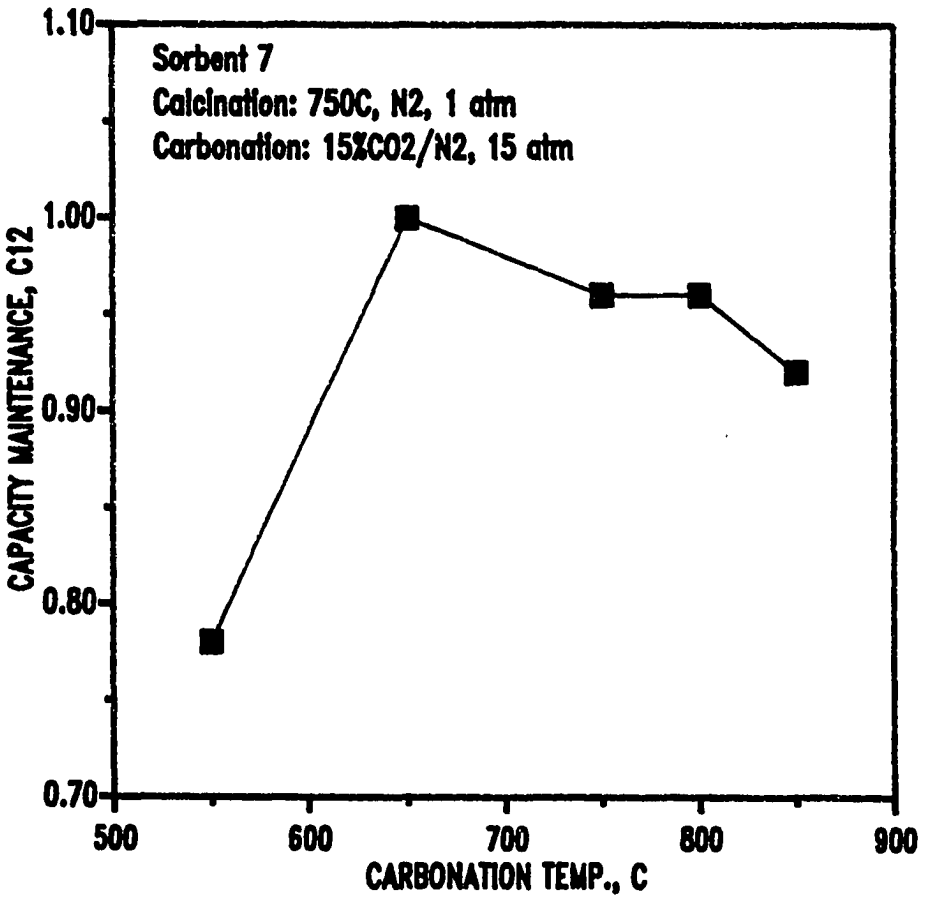

Figure 6.10 Effect of Carbonation Temperature on Capacity Maintenance; Sorbent 7

achieve carbonation at the higher temperatures. Essentially no decrease in C_{12} was observed at 800°C and the decrease at 850°C was relatively small. The result at 850°C, where C_{12} = 0.92, was superior to the result at 550°C, where C_{12} = 0.78. These higher temperature results are encouraging in that they suggest no major loss in performance for temperature excursions of as much as 100°C above the normal maximum temperature of 750°C. Such a margin of safety is desirable in any exothermic reaction system.

6.4 Effect of Calcination Gas Atmosphere

Figure 6.11 shows the calcination results using sorbent 1 under different gas atmospheres. Curve A (HP048) represents calcination in 1 atm N_2. As seen in the figure, calcination started at the temperature of approximately 610°C, and complete calcination was achieved at approximately 730°C. Curve B (HP079) represents calcination at 1 atm in 20% CO_2/N_2. Due to the the presence of CO_2, calcination did not begin until 800°C and was complete in a relatively short time at about 860°C. In Curve C (HP070) the sorbent was heated in 100% CO_2 to 880°C followed by calcination in 20% CO_2/N_2 between 880 and 900°C. In all three tests, the temperature was held at 900°C for 20 minutes and then was cooled to 750°C before the subsequent carbonation. Carbonation was carried out at 750°C and 1 atm in 15% CO_2/N_2. Figure 6.12 compares the carbonation kinetics for the three tests. The sorbent calcined

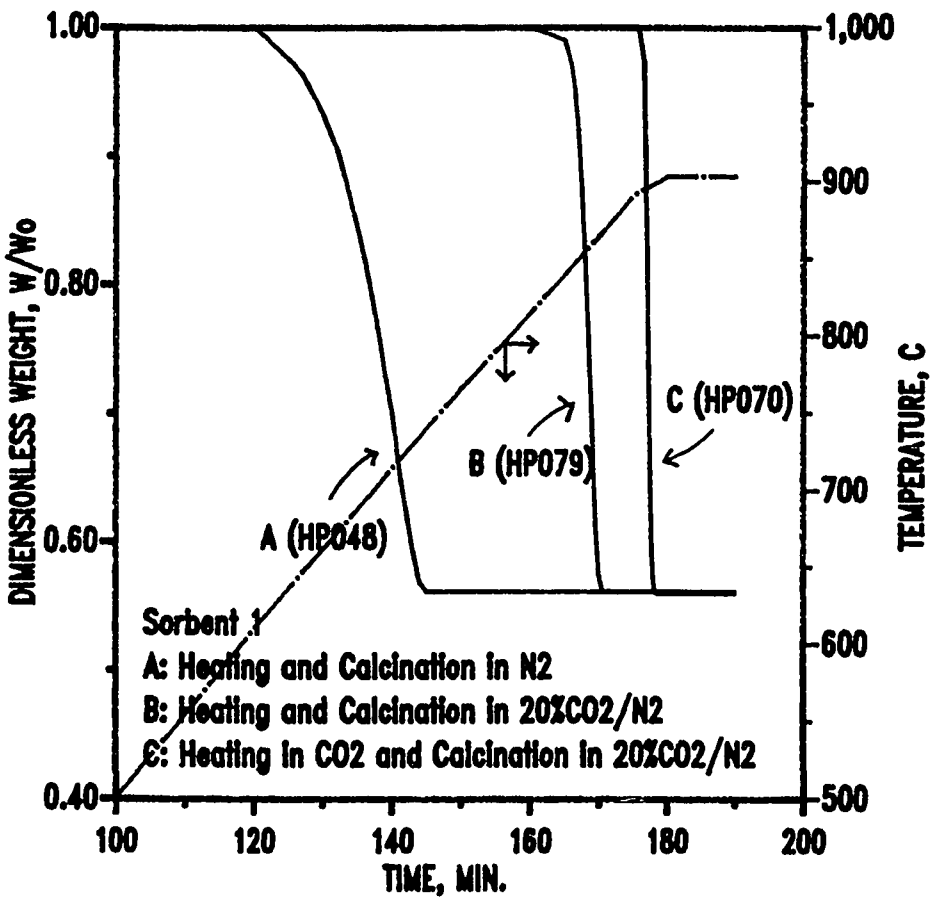

Figure 6.11 Effect of Gas Atmosphere on Calcination Kinetics; Calcination at 900°C, Sorbent 1

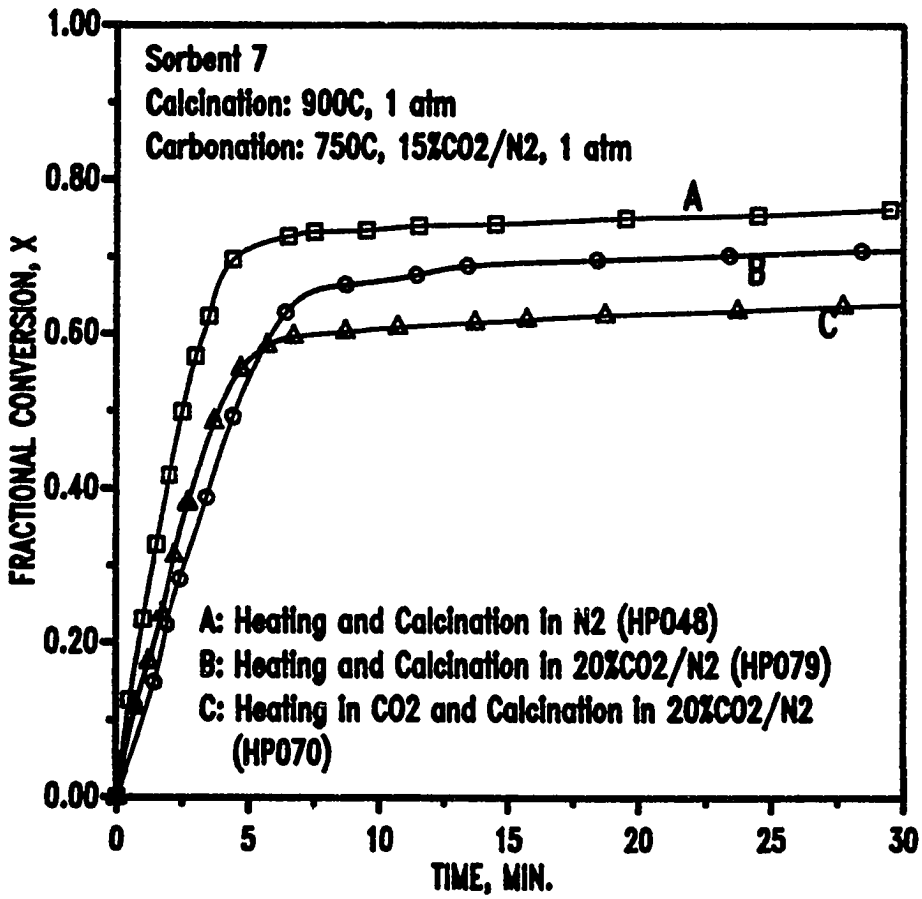

Figure 6.12 Effect of Calcination Gas Atmosphere on First-Cycle Carbonation Kinetics; Calcination at 900°C, Sorbent 1

in N_2 (HP048) had the highest reactivity and capacity. Sorbents calcined in the presence of CO_2 experienced reduced reactivity and capacity (HP070 and HP079). The decrease is attributed to the fact that CO_2 enhances the sintering process which causes a surface area reduction and an increase in the pore diameter distribution.

After the first-cycle carbonation, each sorbent was recalcined by heating to 900°C using the same gas atmosphere as the first-cycle calcination. Second-cycle carbonation at 750°C and 1 atm in 15% CO_2/N_2 then followed. The second-cycle capacity decrease was more pronounced for sorbents calcined in an atmosphere containing CO_2. The capacity of the sorbent which was calcined in N_2 (HP048) decreased from $C_1 = 0.77$ to $C_2 = 0.57$ ($C_{12} = 0.74$), while the sorbent heated and calcined in 20% CO_2/N_2 (HP079) exhibited a capacity decrease from $C_1 = 0.72$ to $C_2 = 0.46$ ($C_{12} = 0.64$). The sorbent which was heated in 100% CO_2 and calcined in 20% CO_2/N_2 (HP070) suffered a capacity decrease from $C_1 = 0.65$ to $C_2 = 0.42$ ($C_{12} = 0.65$).

A number of investigators have reported that the presence of CO_2 during calcination at high temperature (900°C or above) affects the structural properties of the product CaO. Bhatia and Perlmutter (1983) reported that the pore diameters of CaO created during calcination of $CaCO_3$ at 910°C were increased and the distribution of pore diameters narrowed as the CO_2 content of the calcination gas increased. A reduction of surface area was also observed with increasing

CO_2 content. DeLucia (1985) reported that the pore volume of CaO formed from decomposition of $CaCO_3$ at 940°C in 1 atm CO_2 was 27% less than the theoretical pore volume, and the pore diameters were about 2.5 times larger than CaO formed from decomposition of $CaCO_3$ at 800°C in N_2. Borgwardt (1989b) reported that CO_2 accelerated CaO sintering which caused a reduction of surface area and porosity. Fuertes *et al.* (1991) also reported a similar effect due to the presence of CO_2 on CaO at 900°C.

Figure 6.13 shows the calcination results using sorbent 1 in different gas atmospheres at 825°C and 1 atm. Curve A (HP047) represents calcination in N_2. Calcination started at about 600°C, and complete calcination was achieved after about 145 minutes at about 740°C. Curve B (HP081) represents calcination in 15% CO_2/N_2. Due to the presence of CO_2, calcination started just as the temperature reached 825°C, and complete calcination was achieved after about 180 minutes. The subsequent first-cycle carbonation results are shown in Figure 6.14. The presence of 15% CO_2 in the calcination gas decreased the carbonation reactivity, but had essentially no effect on capacity. The first-cycle capacity (C_1) was 0.78 and 0.79 for HP047 and HP081, respectively, while the second-cycle capacity (C_2) of HP047 was 0.60 compared to 0.58 for HP081.

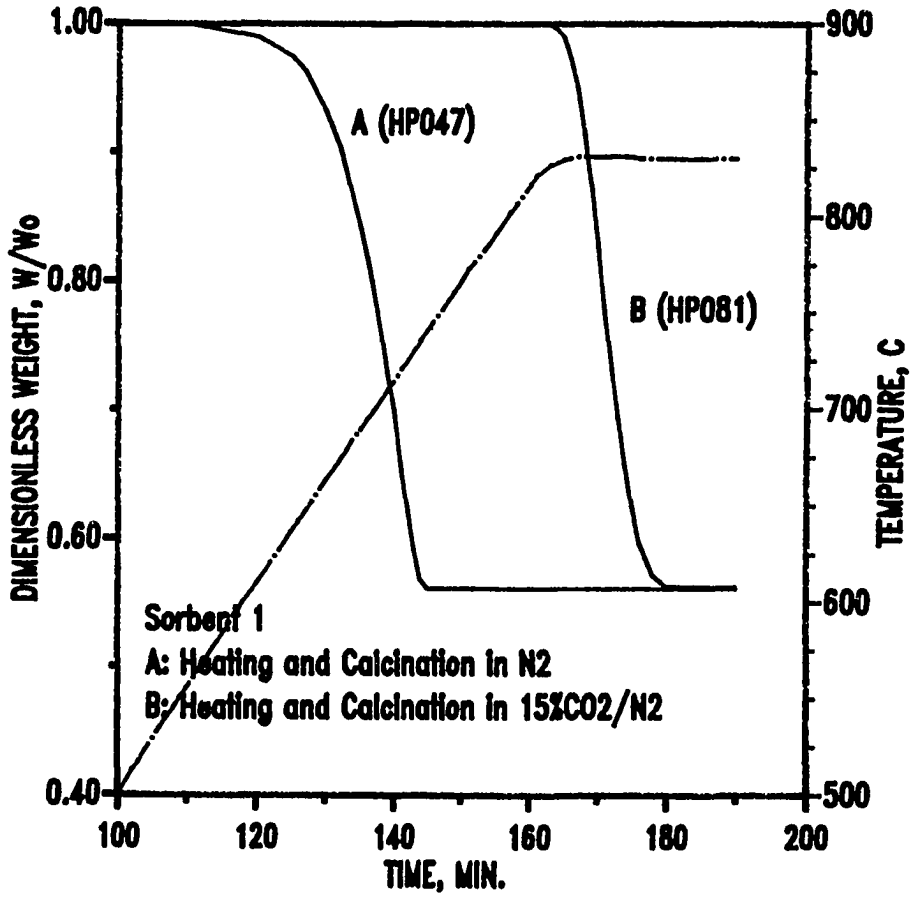

Figure 6.13 Effect of Gas Atmosphere on Calcination Kinetics; Calcination at 825°C, Sorbent 1

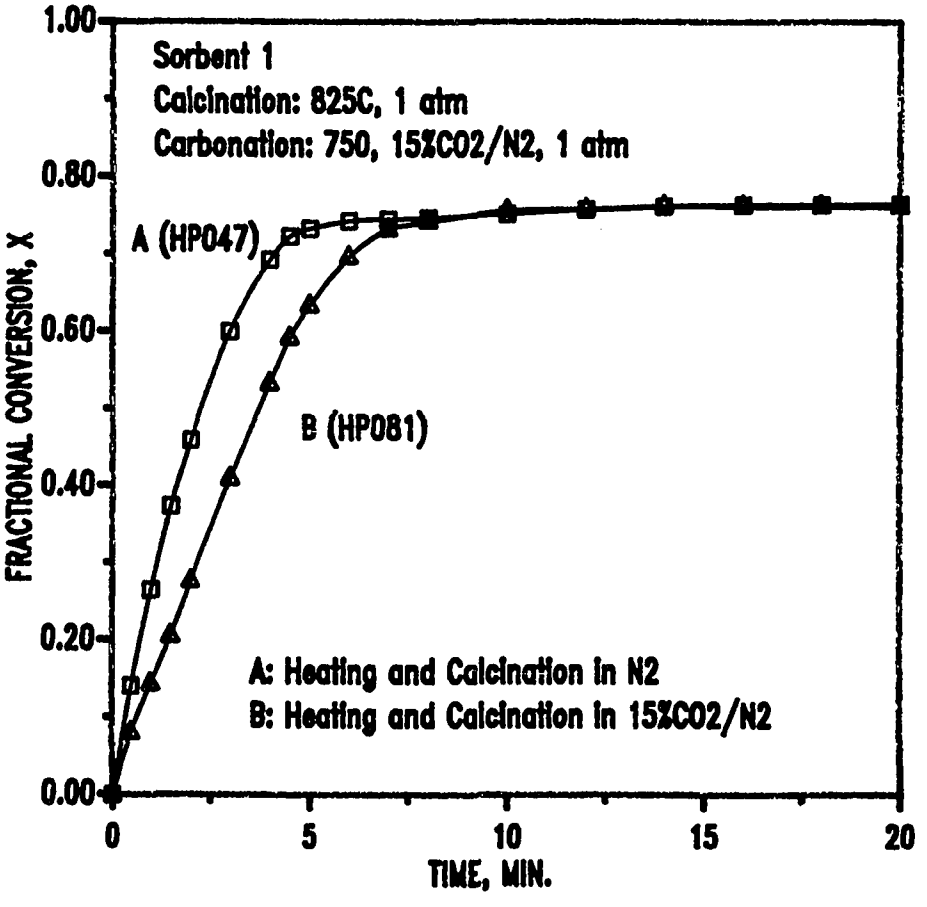

Figure 6.14 Effect of Calcination Gas Atmosphere on First-Cycle Carbonation Kinetics; Calcination at 825°C, Sorbent 1

Figure 6.15 shows calcination results using sorbent 1 in different gas atmosphere at 750°C and 1 atm. The presence of CO_2 during heating period prevented calcination at 750°C (curve A). After about 150 minutes the gas was switched to N_2 in order to initiate calcination, which was completed in only about 5 minutes. Curve B (HP066) represents heating and calcination in N_2. The calcination started at approximately 600°C and was completed at about 730°C. The subsequent first-cycle carbonation results are shown in Figure 6.16. There is essentially no effect of calcination atmosphere at 750°C on reactivity, and little, if any, effect on capacity. The capacity maintenance (C_{12}) for runs HP066 and HP065 was found to be 0.68 and 0.69, respectively, indicating no effect of CO_2 in the calcination gas at 750°C.

In summary, an adverse effect of CO_2 in the calcination gas on the carbonation cycle obviously exists at 900°C. However, At 825°C or lower, the presence of CO_2 in the calcination gas appears to have very little effect on either capacity or capacity maintenance during subsequent carbonation.

6.5 Conclusions

These additional tests confirm the results and trends established in the detailed two-cycle reaction studies discussed in the previous chapter. Carbonation temperatures in the 650-750°C range are desirable, although periodic

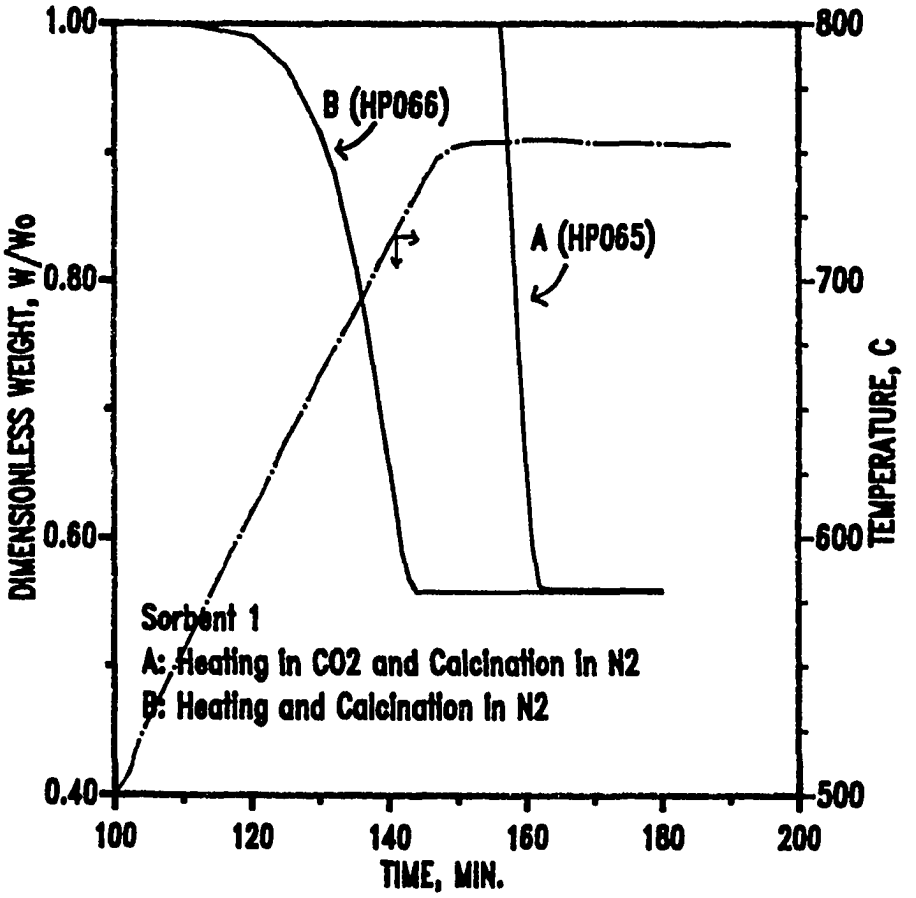

Figure 6.15 Effect of Gas Atmosphere on Calcination Kinetics; Calcination at 750°C, Sorbent 1

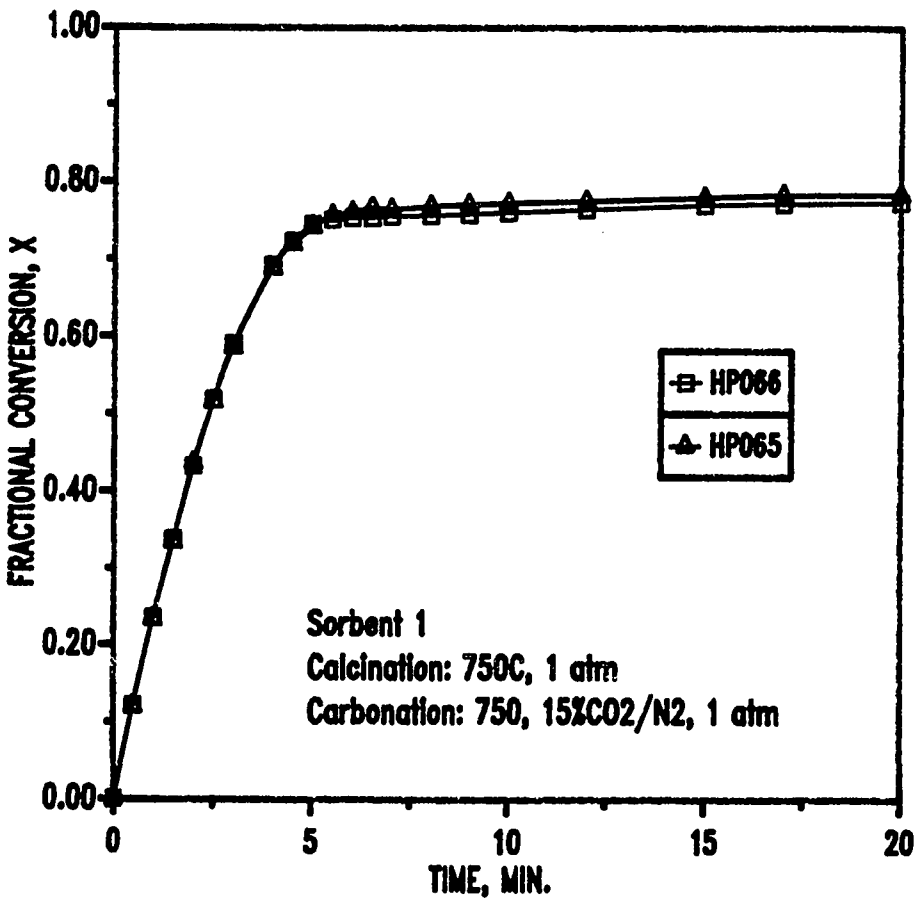

Figure 6.16 Effect of Calcination Gas Atmosphere on First-Cycle Carbonation Kinetics; Calcination at 750°C, Sorbent 1

excursions to 800°C or higher seem to have no major immediate adverse effect. Calcination temperatures as low as 700°C at 1 atmosphere appear feasible. However, the calcination reaction is endothermic, and lower temperature excursions must be avoided since the calcination rate becomes extremely slow at 650°C. It is also been confirmed that the presence of CO_2 in the calcination gas at 900°C affects the carbonation cycle. However, CO_2 present in calcination at 825°C or lower has been found to have little effect on either capacity or capacity maintenance in the carbonation reaction.

High pressure calcination is feasible at a temperature of approximately 750°C. Moreover, reactivity, capacity, and capacity maintenance for the subsequent carbonation reaction show no adverse effect of calcination pressure. This opens the possibility of operating a commercial process with equal pressures and temperatures in the carbonation and calcination phases. Calcination can be achieved simply by reducing the CO_2 partial pressure in the gas.

Chapter 7

Experimental Results:

Multicycle Studies

More detailed results on sorbent durability are presented in this chapter. Multicyle runs were carried out in order to extend and confirm the previous determinations of sorbent durability through two cycles. Results of five-cycle calcination and carbonation runs using sorbents 1, 7, and 9 are first discussed to provide direct comparisons of carbonation reactivity and capacity throughout the cycles.

In the following sections the times used to evaluate reactivity and capacity are changed. These changes are made for two reasons. First, since the CO_2 concentration used in most multicycle runs was significantly higher than the equilibrium CO_2 concentration, the early rapid reaction phase was almost over at $(t-t_o)$ = 1 min. The reactivity time of $(t-t_o)$ = ½ min was chosen to ensure that the reactivity comparisons were well within the rapid reaction period. Secondly, the total time required to complete a five-cycle or ten-cycle test needed to be reduced. Therefore, the capacity was redefined to be the fractional conversion at $(t-t_o)$ = 20 min instead of 40 min. Since the global reaction rate in the 20 to 40 min time period is quite low, the shorter time produces only a small change in the capacity values. It is necessary to point out that reactivity and capacity values

used in section 7.1 were determined using the original values of $(t-t_o)$ = 1 min and 40 min, respectively, since in these 1 atm tests the actual CO_2 pressure during carbonation was 0.15 atm compared to about 0.08 atm at equilibrium. The new time bases are used beginning in section 7.2.

In addition to extending the tests through multiple cycles, the effects of calcination pressure, carbonation temperature, and background gas composition have been investigated. Background gas composition was varied in a step-wise manner. First, H_2O was introduced into the CO_2-N_2 gas and then a simulated coal gas containing CO_2, CO, H_2, H_2O, and N_2 was tested. In the end, a small amount of H_2S was added to the simulated coal gas. In the final set of experiments, favorable reaction conditions were selected and the tests were extended to ten cycles.

7.1 Comparison of Sorbent Performance on Five-Cycle Runs

Five-cycle runs using sorbents 1, 7, and 9 were carried out at the following reaction conditions: calcination at 750°C and 1 atm N_2 followed by carbonation at 750°C and 1 atm in 15% CO_2/N_2. Figure 7.1 shows the sorbent 1 results in the form of the raw weight-time data. Note that first-cycle calcination data are not included in this figure. Complete calcination was achieved in all cycles, and each carbonation cycle exhibited the rapid initial rate followed by an abrupt transition to a slow rate. The transition occurred at

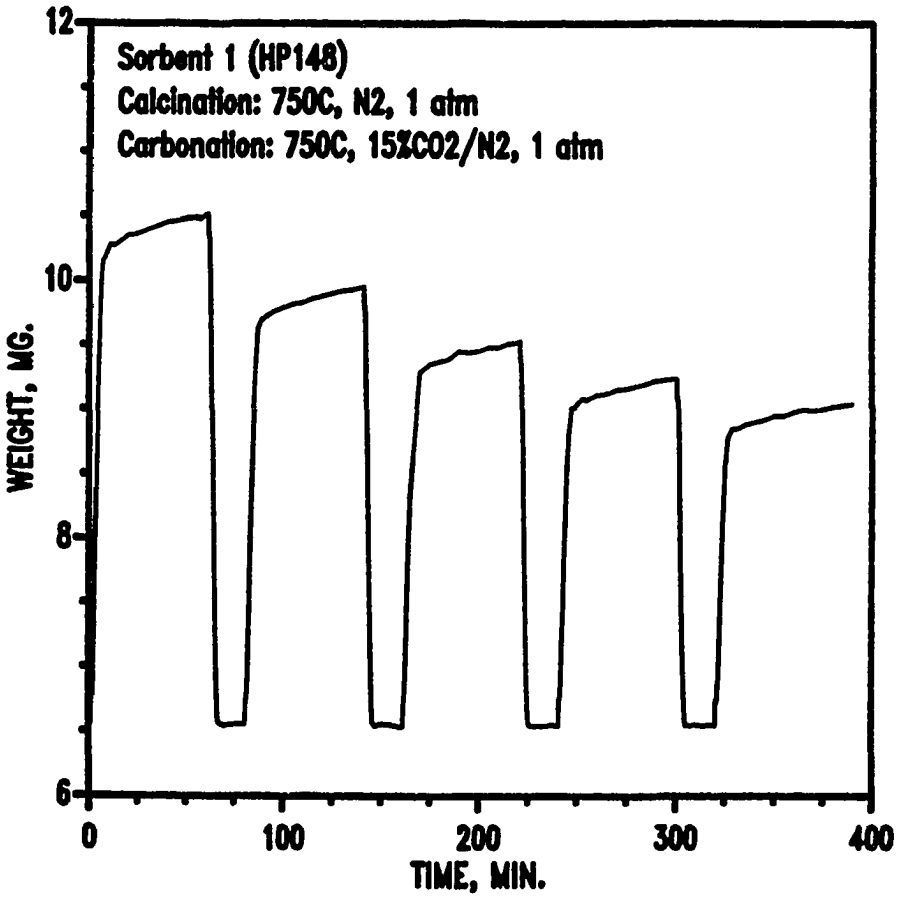

Figure 7.1 Calcination-Carbonation Results for Sorbent 1 Through Five Cycles

successively smaller sorbent weight in each cycle. These results confirm the previous sorbent 1 tests where the capacity deteriorated in the second cycle. This behavior is similar to results of other investigators when calcium carbonate or limestone was used as the sorbent precursor. Figure 7.2 compares the capacity, C_i, of sorbent 1 with results reported by Barker (1973) and Delucia (1985). Although the specific sorbents used and reaction conditions were somewhat different in each study, the trends were remarkably similar.

Results of five-cycle carbonation kinetics of sorbent 7 are shown in Figure 7.3. Two important results are illustrated. First, there is a marked increase in the early rapid reaction rate between cycles 1 and 2. Thereafter, the reaction rate in the early stages remained approximately constant in cycles 2 through 5. The slow stages of the reaction exhibit a small but continuous decrease in carbonation capacity with cycle number.

Five-cycle runs using sorbent 9 exhibit excellent sorbent stability as shown in Figure 7.4. The initial rapid rate is essentially equal in each of the five cycles. There is a small decrease in capacity between cycles 1 and 2, with essentially no decrease thereafter.

Comparisons based only on calcium utilization are somewhat misleading because the inert MgO present in calcined sorbent 9 reduces the CO_2 capacity per unit mass of sorbent.

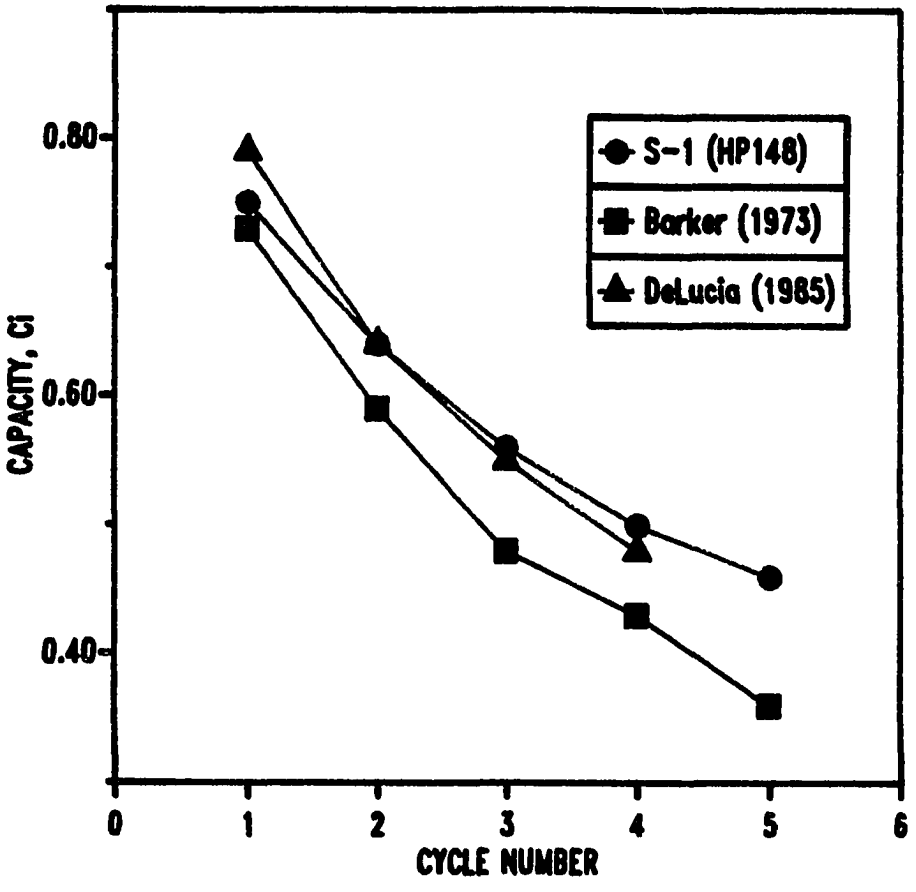

Figure 7.2 Comparison of Capacity Decrease for Sorbent 1 with Literature Results at Similar Reaction Conditions

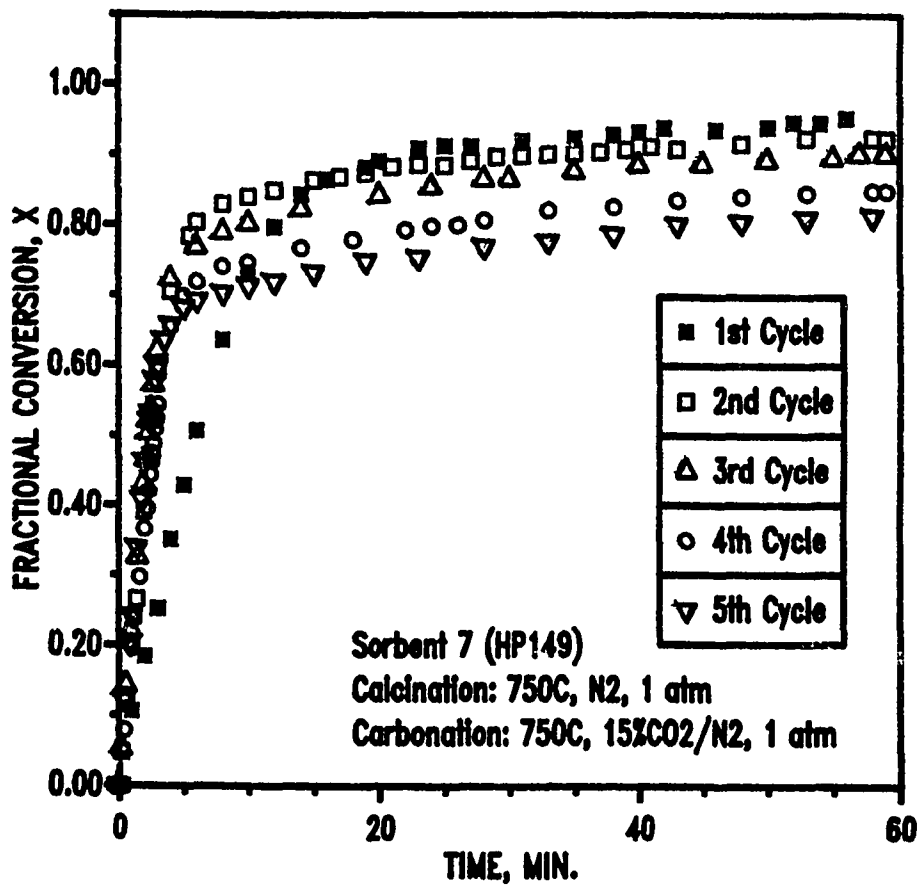

Figure 7.3 Carbonation Results for Sorbent 7 Through Five Cycles

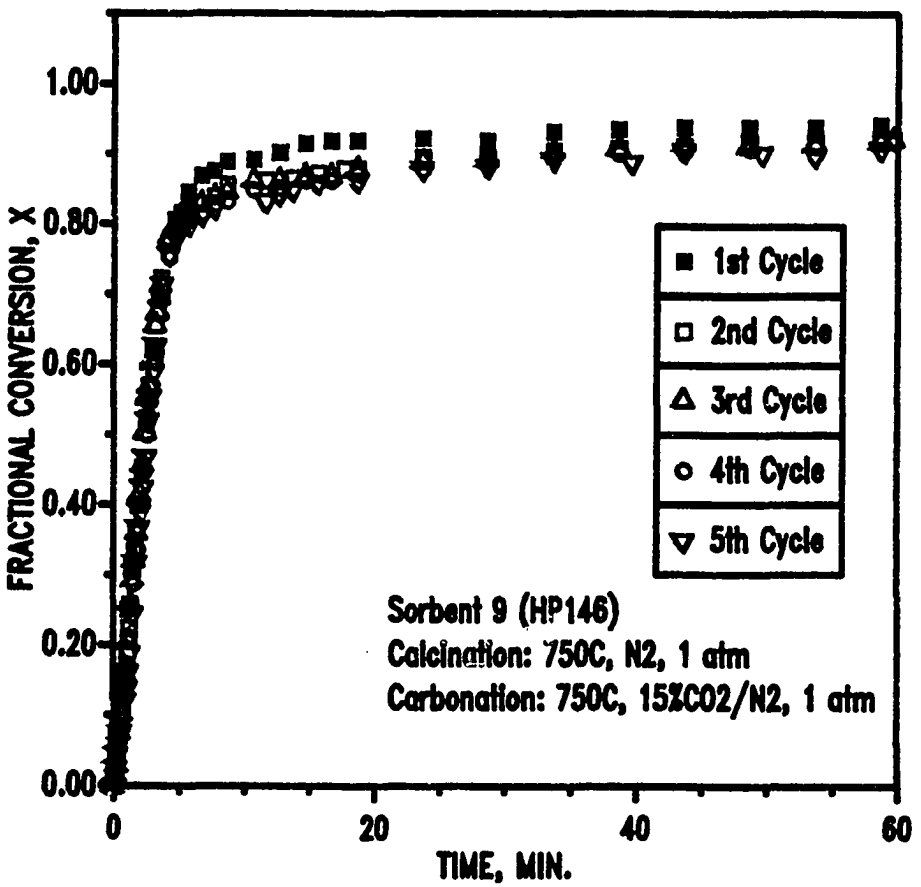

Figure 7.4 Carbonation Results for Sorbent 9 Through Five Cycles

Figure 7.5 compares the capacities of the sorbents expressed as grams of CO_2 per gram of sorbent. Data for four sorbents, 1, 7, and 9 plus a calcium magnesium acetate (CMA) obtained from Chevron Chemical, are included. Calcined CMA is composed of approximately 2MgO:1CaO (molar ratio).

The theoretical capacity of both sorbents 1 and 7, which are essentially 100% CaO, is 0.79 gram CO_2/gram sorbent. As shown in Figure 7.5, sorbent 7 approaches this value in cycle 1 and then experiences a slow capacity decrease in subsequent cycles. The capacity of sorbent 1 is considerably less than theoretical in cycle 1, and the rate of decrease in subsequent cycles is greater than that experienced by sorbent 7. Sorbent 9, with equimolar CaO and MgO, has a theoretical capacity of 0.46 gram CO_2/gram sorbent. The experimental capacity approaches this level in each of the five cycles. As shown in the figure, by cycle 4 the capacity of sorbent 9 exceeded that of sorbent 1. Sorbent CMA has a theoretical capacity of 0.32 gram CO_2/gram sorbent. Although the measured capacity is significantly below theoretical, the capacity maintenance is quite good as shown by the horizontal line, and is comparable to that of sorbent 9. This similarity suggests that the presence of MgO is important not only for providing open pore structure, but also for stabilizing the structure for multicycle operation.

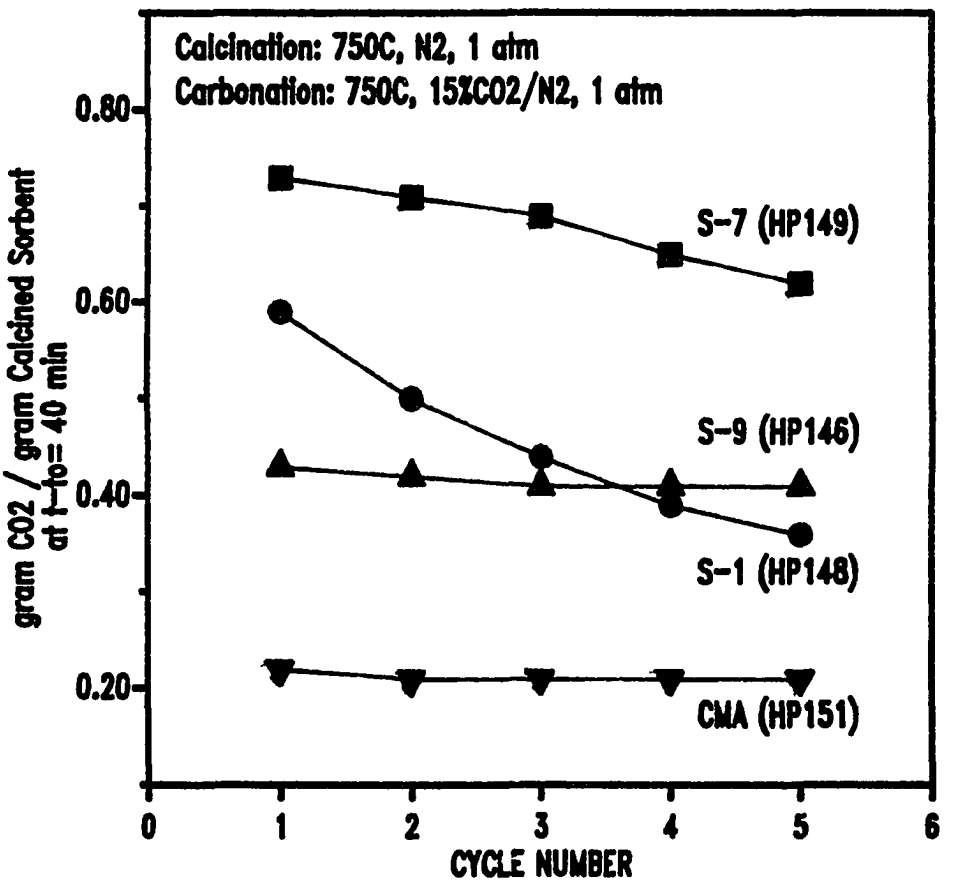

Figure 7.5 CO_2 Capacity per Gram of Sorbent for Four Sorbents as a Function of Cycle Number

7.2 Effect of Calcination Pressure

Figures 7.6 and 7.7 show the reactivity and capacity results versus cycle number as a function of calcination pressure using sorbents 7 and 9, respectively. Calcination was at 750°C in N_2, and carbonation was at 650°C and 15 atm in 15% CO_2/N_2. The reactivity following high pressure calcination was slightly lower than that following low pressure calcination for both sorbents 7 and 9. As seen in Figure 7.6, the capacity following high pressure calcination appears to be more stable than that following low pressure calcination. Figure 7.7 shows similar behavior for sorbent 9. Figures 7.8 and 7.9 show the reactivity and capacity results versus cycle number using sorbents 7 and 9, respectively, using a carbonation temperature of 750°C. Otherwise, reaction conditions were the same as shown in Figures 7.6 and 7.7. Sorbent 7 experienced a gradual decrease in capacity with cycle number for both calcination pressures (Figure 7.8). The reactivity results are similar at 750 and 650°C carbonation temperatures. For sorbent 9, on the other hand, the capacity was essentially constant throughout the five cycles at both calcination pressures. Similarly, the reactivity of sorbent 9 was essentially constant over the five cycles at 750°C carbonation temperature.

High calcination pressure has shown no serious adverse effects on the carbonation reaction compared to low calcination pressure. Consequently, isobaric operation with

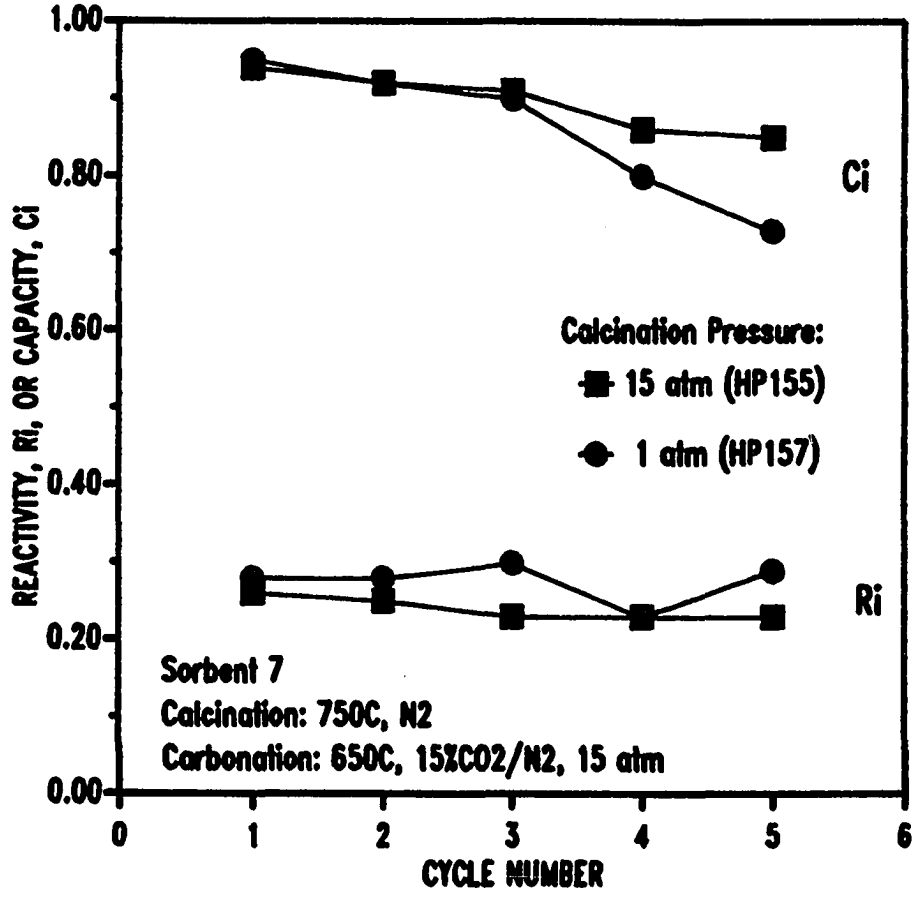

Figure 7.6 Five-Cycle Reactivity and Capacity of Sorbent 7 as a Function of Calcination Pressure; Carbonation at 650°C

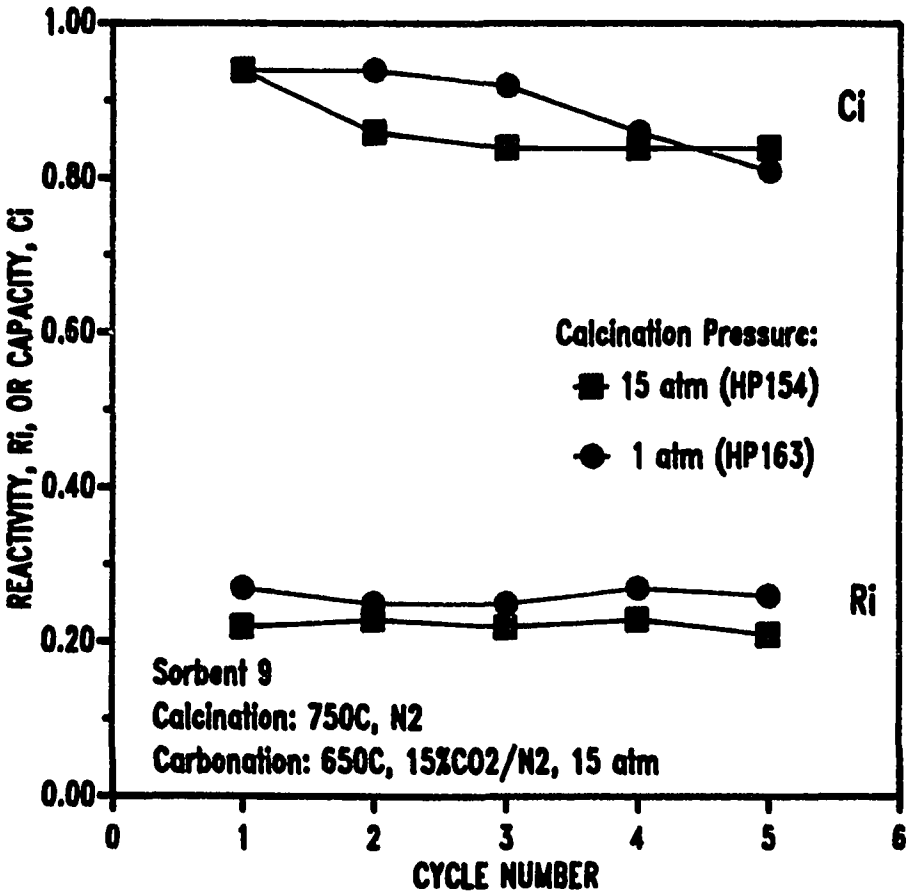

Figure 7.7 Five-Cycle Reactivity and Capacity of Sorbent 9 as a Function of Calcination Pressure: Carbonation at 650°C

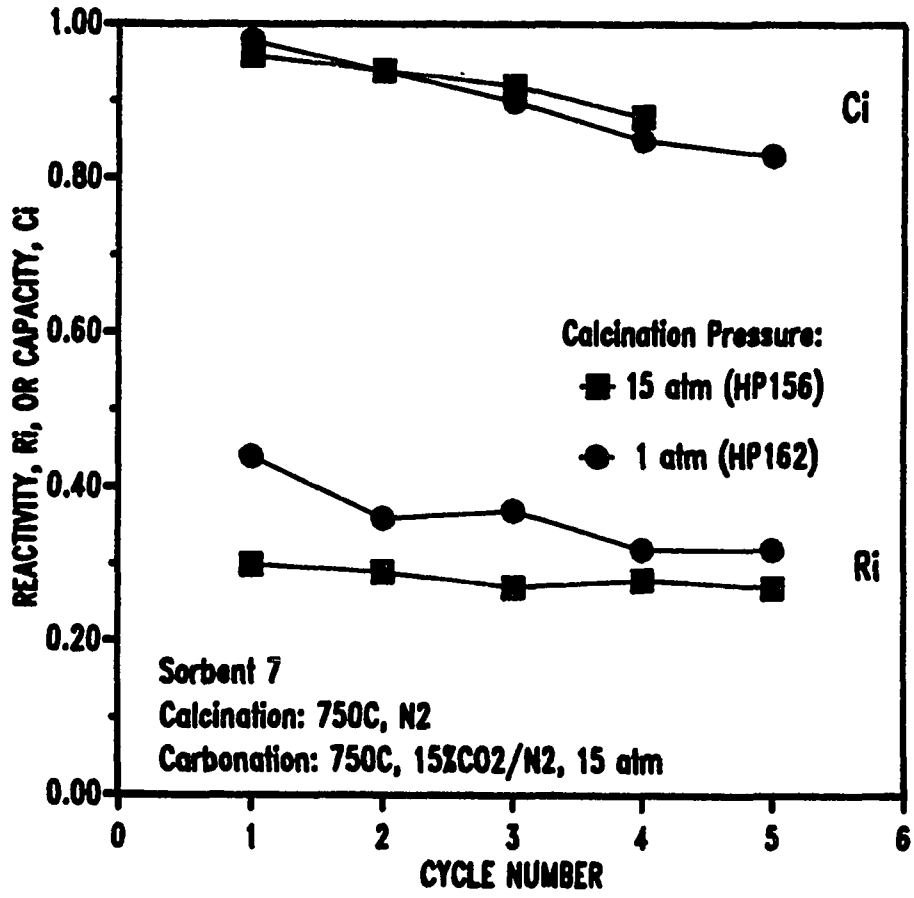

Figure 7.8 Five-Cycle Reactivity and Capacity of Sorbent 7 as a Function of Calcination Pressure; Carbonation at 750°C

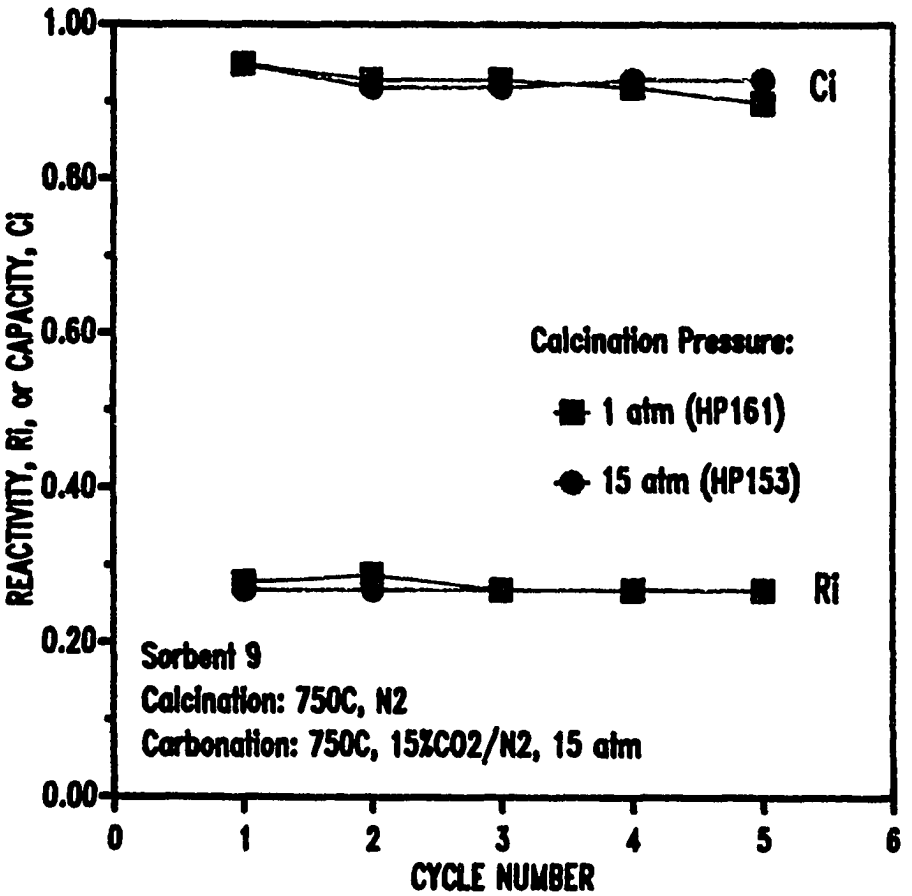

Figure 7.9 Five-Cycle Reactivity and Capacity of Sorbent 9 as a Function of Calcination Pressure; Carbonation at 750°C

sorbent regeneration accomplished via a change in temperature and/or CO_2 pressure is possible.

7.3 Effect of Carbonation Temperature

High carbonation temperature (750°C) produced higher capacity and capacity maintenance than low carbonationn temperature (650°C). As shown in Figures 7.6 and 7.7, 650°C carbonation temperature produced a gradual decrease in capacity with cycle number for both sorbents. At 750°C carbonation temperature, on the other hand, reasonably constant capacity maintenance was found for sorbent 9 (Figure 7.9) while sorbent 7 experienced a similar trend of capacity decrease as at 650°C (Figure 7.8).

The above results suggest that isothermal operation at 750°C through the calcination and carbonation phases would be better than operation with the temperature cycling between 750°C for calcination and 650°C for carbonation. However, high carbonation temperature will result in lower equilibrium CO_2 removal capability. If the inlet gas contains 15% CO_2 at 15 atm, for example, it is theoretically possible to remove about 99.6% of the CO_2 at 650°C compared to about 96.4% at 750°C.

7.4 Addition of H_2O to the Carbonation Gas

The addition of H_2O to the CO_2/N_2 mixture produced an increase in the rate of carbonation during the early rapid

reaction phase and had a small increase in capacity. This is illustrated in Figure 7.10 where first-cycle carbonation results are plotted versus time. Sorbent 9 was used and carbonation temperature and pressure were 750°C and 15 atm. The increased rate in the presence of 10% H_2O is particularly evident in the first 1½ minutes. After about 20 minutes, run HP205 achieved a fractional conversion of 0.95 compared to 0.93 for run HP153. The addition of H_2O to CO_2-N_2 gas produced a small but definite increase in capacity of the sorbent. Figure 7.11 shows the capacity though five cycles number for the same runs. Again, the capacity maintenance of sorbent 9 was quite good. Figure 7.12 shows the capacity versus cycle number for two tests using sorbent 7. The calcination was carried out at 750°C and 15 atm in N_2, and carbonation was at 650°C and 15 atm. Improved capacity and capacity maintenance were observed in the presence of H_2O.

7.5 CO_2 Removal from Simulated Coal Gas (H_2S-Free)

The addition of CO and H_2 to the previous gas composition (CO_2, H_2O, and N_2) provides all the major components of coal gas. In using the simulated coal gas, however, one must be aware of the possibility of carbon deposition during the operation. The gas composition of 15% CO_2, 10% H_2O, 20% CO, 10% H_2, and 45% N_2, for example, was unacceptable to the present TGA system because of excessive carbon deposition on the walls of the reactor and the

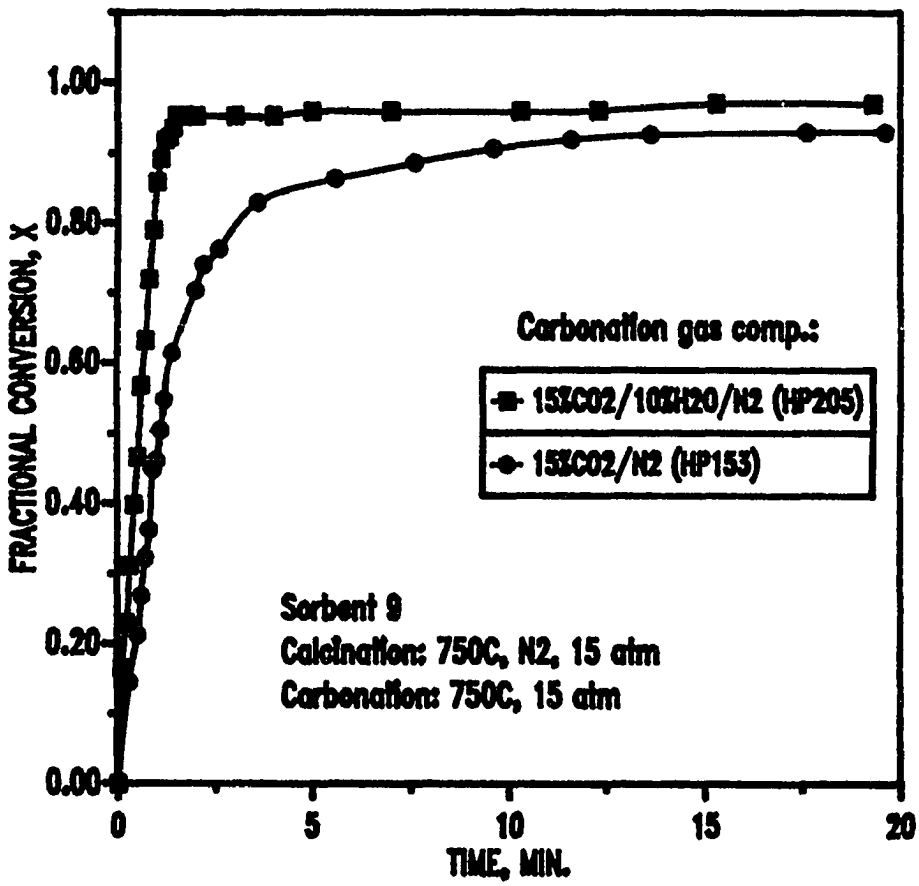

Figure 7.10 First-Cycle Carbonation Kinetics of Sorbent 9 in Different Gas Atmospheres

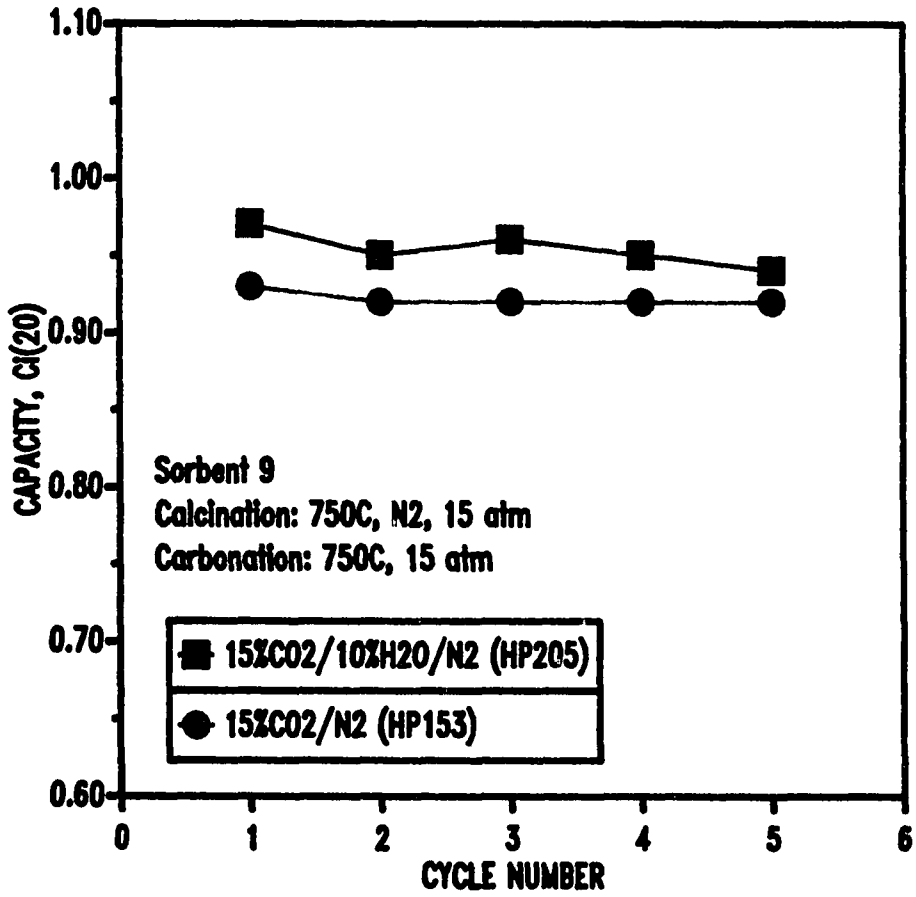

Figure 7.11 Five-Cycle Capacity of Sorbent 9 as a Function of Carbonation Gas Atmophere

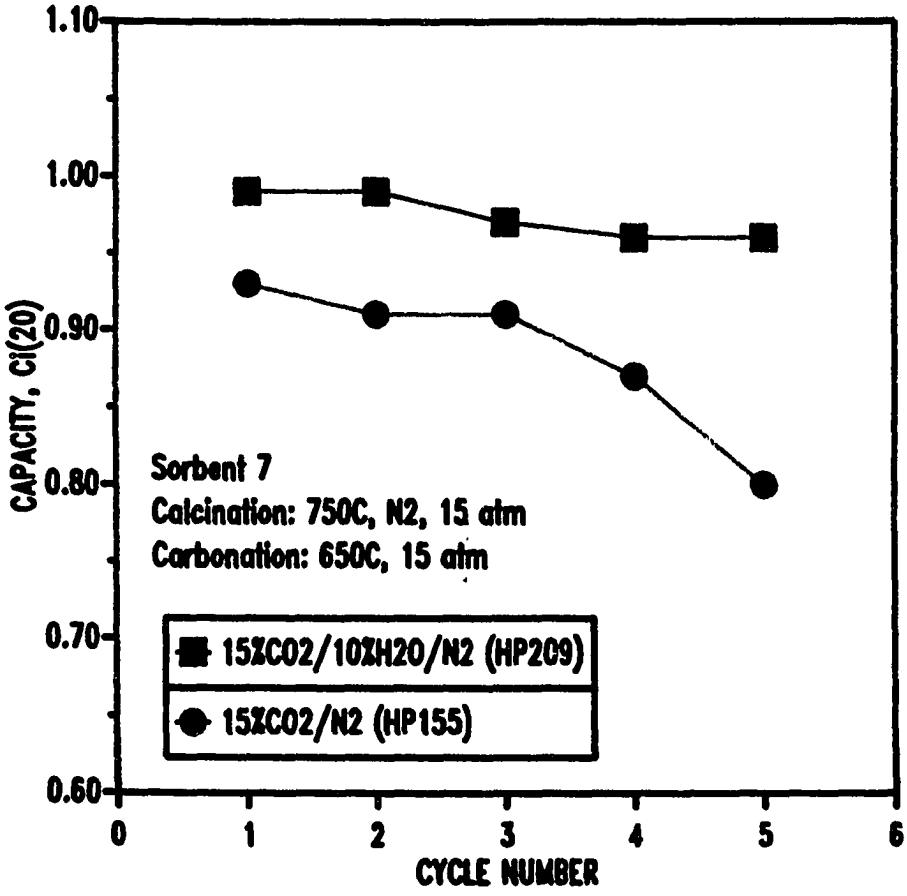

Figure 7.12 Five-Cycle Capacity of Sorbent 7 as a Function of Carbonation Gas Atmosphere

hangdown wire. The sorbent itself appeared to be free of carbon. Thermodynamic analysis of carbon deposition tendency (Lamoreaux *et al.*, 1986) predicted that the problem would be most severe as the reactive gas was heated to final reaction temperature, but less important once reaction temperature was reached. This is in agreement with the observed location of carbon deposited in the side stream heating line, the insert tube inside the reactor, and the upper hangdown wire.

The ratio of C/(O+H) for the above composition was 0.438 indicating a strong possibility of carbon deposition. Increasing the H_2O content to totally eliminate the possibility of carbon deposition was impossible for the current electrobalance system. A gas composition of 5% CO_2, 10% H_2O, 5% CO, 2.5% H_2, and 77.5% N_2 was selected as an alternate. Although this composition did not completely eliminate carbon deposition (C/(O+H) = 0.33), it reduced the quantity of carbon deposited on the hangdown wire to a level small enough that it did not confound the kinetic results.

The simulated coal gas created the possibility of the simultaneous occurrence of the water-gas shift and carbonation reactions:

$$CO_{(g)} + H_2O_{(g)} \rightleftharpoons CO_{2(g)} + H_{2(g)} \qquad (7\text{-}1)$$

and

$$CaO_{(s)} + CO_{2(g)} \rightleftharpoons CaCO_{3(s)} \qquad (7\text{-}2)$$

While no direct confirmation of the simultaneous reactions is possible using the electrobalance reactor, the previous atmospheric electrobalance tests (see Chapter 4) showed an increase in carbonation rate which would be consistent with higher concentration of CO_2 formed by water-gas shift. Figure 7.13 shows the fractional carbonation-time results for the first carbonation cycle for three runs with different feed gas compositions. All runs were subjected to calcination at 750°C and 15 atm in N_2 and carbonation at 750 and 15 atm. The results of run HP222 where the carbonation gas consisted of 5% CO_2/N_2 were taken as a base case for comparison. The addition of 10% H_2O in run HP224 produced a clear increase in carbonation rate. This is consistent with the previously discussed promotional effect of H_2O on carbonation rate. The highest overall carbonation rate was associated with run HP218 using feed gas composition of 5% CO_2, 10% H_2O, 5% CO, 2.5% H_2, and 77.5% N_2. The duration of the rapid initial reaction period was also longer for this run. Sorbent capacity, $C_1(20)$, was effectively the same in all runs.

The increased reactivity of HP218 compared to HP224 is taken as further evidence of the probable simultaneous occurrence of the carbonation and water-gas shift reactions. The presence of CO and H_2 in the HP218 carbonation gas provides all components necessary for the shift reaction to occur. This result is consistent with similar observations discussed in Chapter 4.

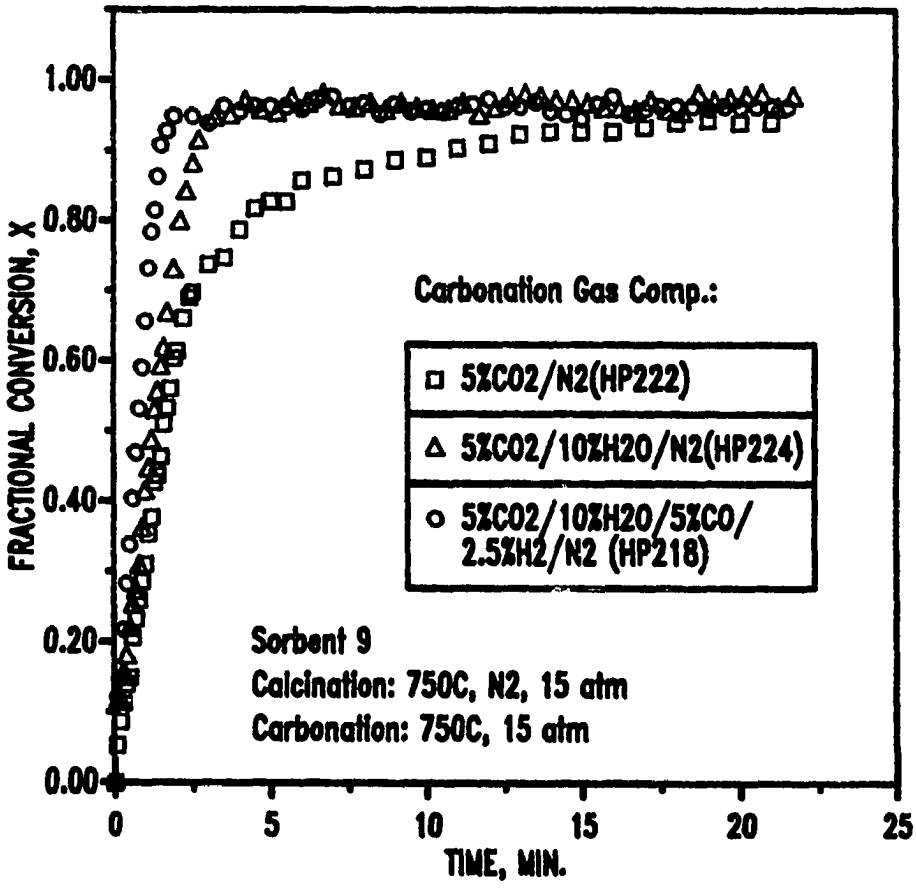

Figure 7.13 First-Cycle Carbonation Kinetics of Sorbent 9 using Three Different Gas Atmospheres

7.6 CO_2 Removal from Simulated Coal Gas (With H_2S)

H_2S present in the simulated coal gas reacted competitively with CO_2, thereby reducing the carbonation capacity. In addition, the sulfidation reaction was irreversible under the conditions of interest so that, in a relatively short time, the entire sorbent was converted to CaS and no CO_2 removal was possible.

Figure 7.14 shows the normalized sorbent weight, W/W_o, against time of run HP226 using the simulated coal gas with 0.22% H_2S in the carbonation cycles. Zero time corresponds to the beginning of the first carbonation cycle; the first calcination cycle is not included in this figure. During the early stages of the first carbonation cycle the sorbent weight increased rapidly due to the simultaneous reactions (7-2) and

$$CaO_{(s)} + H_2S_{(g)} \rightleftharpoons CaS_{(s)} + H_2O_{(g)} \qquad (7\text{-}3)$$

A maximum value of W/Wo ≈ 0.75 was achieved after about three minutes. Thereafter, W/W_o decreased due to the displacement of carbonate by the reaction

$$CaCO_{3(s)} + H_2S_{(g)} \rightleftharpoons CaS_{(s)} + H_2O_{(g)} + CO_{2(g)} \qquad (7\text{-}4)$$

This reaction and the resultant sorbent weight loss continued until the reactive gas flow was stopped after about 30 minutes. In the 40 to 55 minute time period the remaining

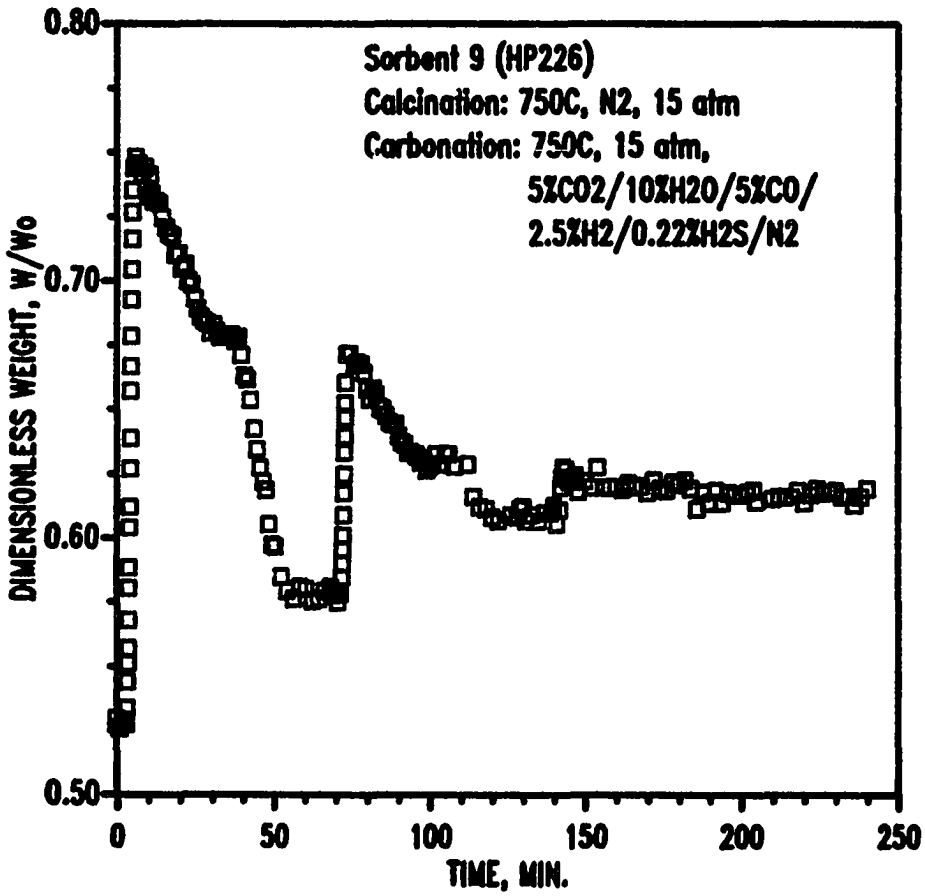

Figure 7.14 Weight-Time Response during Multicycle Carbonation of Sorbent 9 with H_2S in the Reacting Gas

$CaCO_3$ was decomposed by calcination in N_2. However, the final value of $W/W_o \approx 0.58$ suggests that more than 50% of the calcium had been irreversibly converted to CaS during the first reaction cycle. The second carbonation cycle was initiated at 70 minutes and the maximum value of W/W_o achieved was 0.68. The early weight increase was again due to the simultaneous sulfidation and carbonation reactions. After reaching the maximum, W/W_o decreased from 0.68 to 0.63, again due to the displacement of carbonate by sulfide. Third-cycle calcination in N_2 resulted in a reduction of W/W_o to 0.61, which suggested that approximately 90% of the calcium had been converted to CaS. Very little weight gain occurred in the third carbonation/calcination cycle since only a small fraction of calcium remained in the reactive CaO form. By the end of the third cycle, about 98% of the calcium had been irreversibly converted to CaS.

Much of the loss of carbonation capacity in run HP226 was due to the replacement of carbonate by sulfur after the maximum value of W/W_o was achieved. Similar runs were carried out using sorbents 7 (HP230) and 9 (HP229) in which the carbonation cycles were terminated just after the maximum weight was achieved. Although appreciable carbonation capacity was maintained throughout the four cycles, continuing capacity decrease with cycle number was evident due to the competitive formation of CaS. Figure 7.15 shows the increase in the estimated percent of calcium converted to

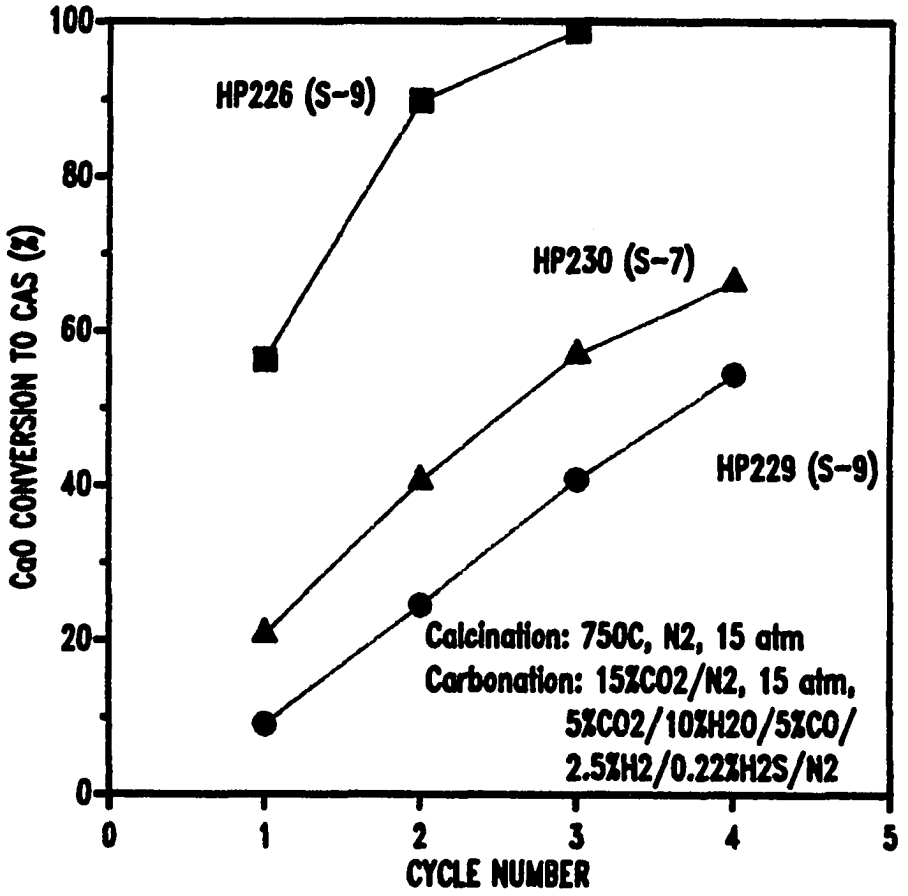

Figure 7.15 Build-Up of Calcium Sulfide during Carbonation Cycles

CaS following each cycle for runs HP229 and HP230. Results from HP226 are included for comparison. Sorbent 7 appeared to be even more susceptible to CaS formation than did sorbent 9. Even with the reduced carbonation cycle time, from 50 to 60% of the calcium was irreversibly converted to CaS after four cycles.

It appears, therefore, that prior desulfurization will be required if the CaO sorbent is to be used for many cycles of CO_2 removal.

7.7 Ten-Cycle Runs Using Simulated Coal Gas (H_2S-Free)

Figure 7.16 shows the fractional carbonation-time results for the first, fifth, and tenth carbonation cycles of sorbent 7 (HP232). Calcination was at 750°C and 15 atm in N_2, and carbonation was at 750°C and 15 atm in 5% CO_2, 10% H_2O, 5% CO, 2.5% H_2, and 77.5% N_2. The sorbent showed little change in initial reactivity, but the transition point between rapid and slow reaction phases occurred at successively lower values of fractional carbonation as the number of cycles increased. This shift in the transition level prompted a decrease in capacity with increased cycle number.

Figure 7.17 illustrates the carbonation capacity versus cycle number for four runs using sorbent 7. Results from earlier five-cycle runs, HP206 and HP221, at the same conditions as HP228 and HP232, respectively, are included for

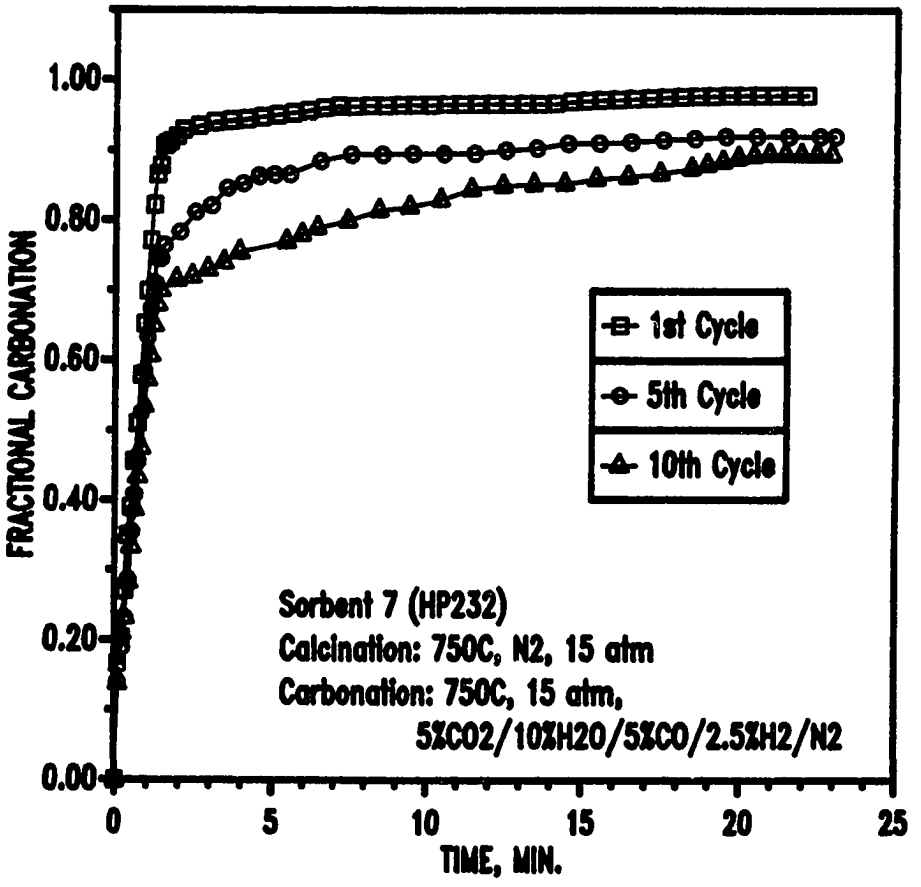

Figure 7.16 Carbonation Kinetics of Sorbent 7 in the First, Fifth, and Tenth Cycles

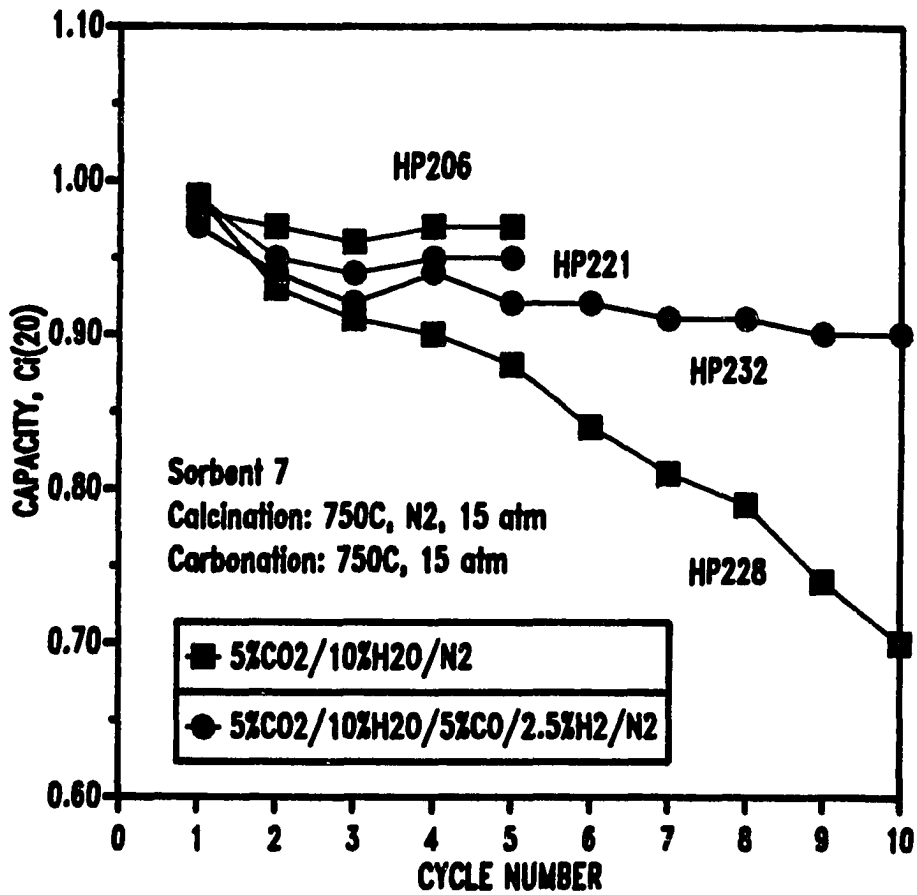

Figure 7.17 Carbonation Capacity Versus Cycle Number for Ten-Cycle Runs Using Sorbent 7

comparison. In the simulated coal-gas atmosphere (5% CO_2, 10% H_2O, 5% CO, 2.5% H_2, and 77.5% N_2) the five-cycle results from HP221 match the ten-cycle results from HP232 quite well. The capacity decrease over the ten-cycle test was less than 10%. In the simpler test gas containing no CO and H_2, performance during the ten-cycle run (HP228) was poorer than in the previous five cycle run (HP206). The first-cycle capacities were essentially indentical but HP228 sufferred significant capacity loss in each subsequent cycle; the capacity decreased by about 30% from the first to the tenth cycle. All other replicate tests produced much better agreement, and no reason for the lack of reproducibility in these two runs is known.

Sorbent 9 has shown better capacity maintenance than sorbent 7. Figure 7.18 shows the fractional carbonation-time results for the first, fifth, and the tenth cycles using sorbent 9 (HP231). The same operating conditions as those of sorbent 7 previously described were used. The curves for the three cycles were essentially identical suggesting that sorbent 9 maintains superior reactivity and capacity throughout ten cycles. Figure 7.19 illustrates the carbonation capacity versus cycle number for four runs using sorbent 9. The results from two five-cycle and two ten-cycle runs at the same conditions are shown. In this case, the results for all four tests are quite comparable, and the ten-cycle runs show good capacity maintenance, in contrast to

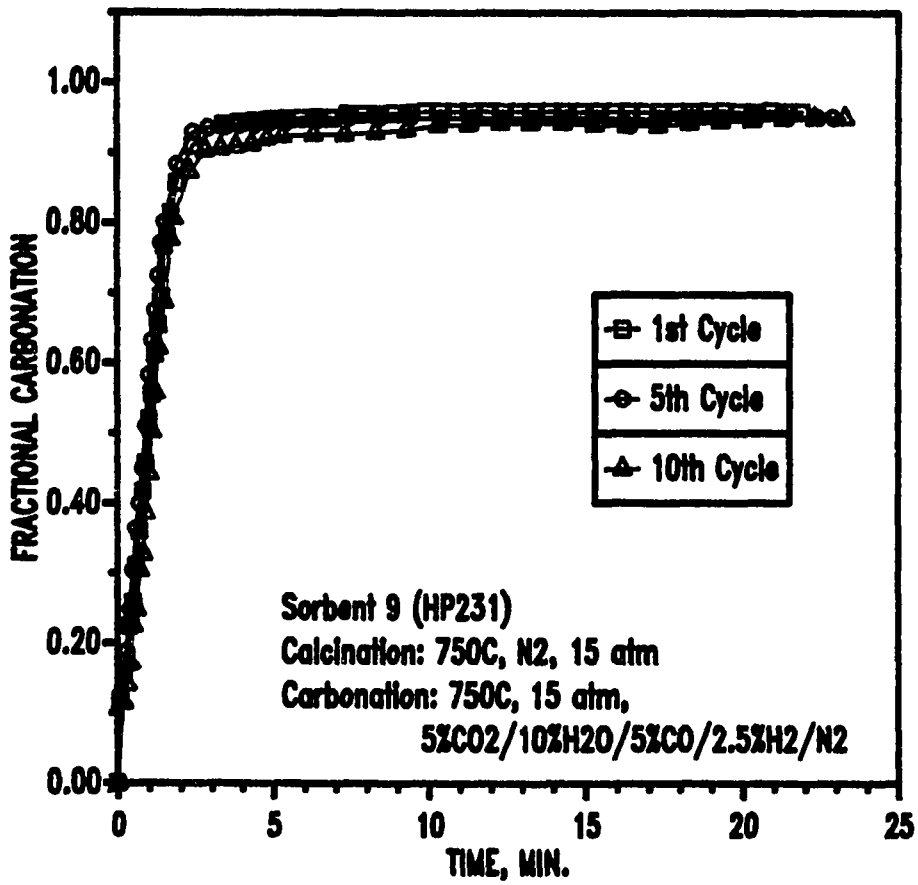

Figure 7.18 Carbonation Kinetics of Sorbent 9 in the First, Fifth, and Tenth Cycles

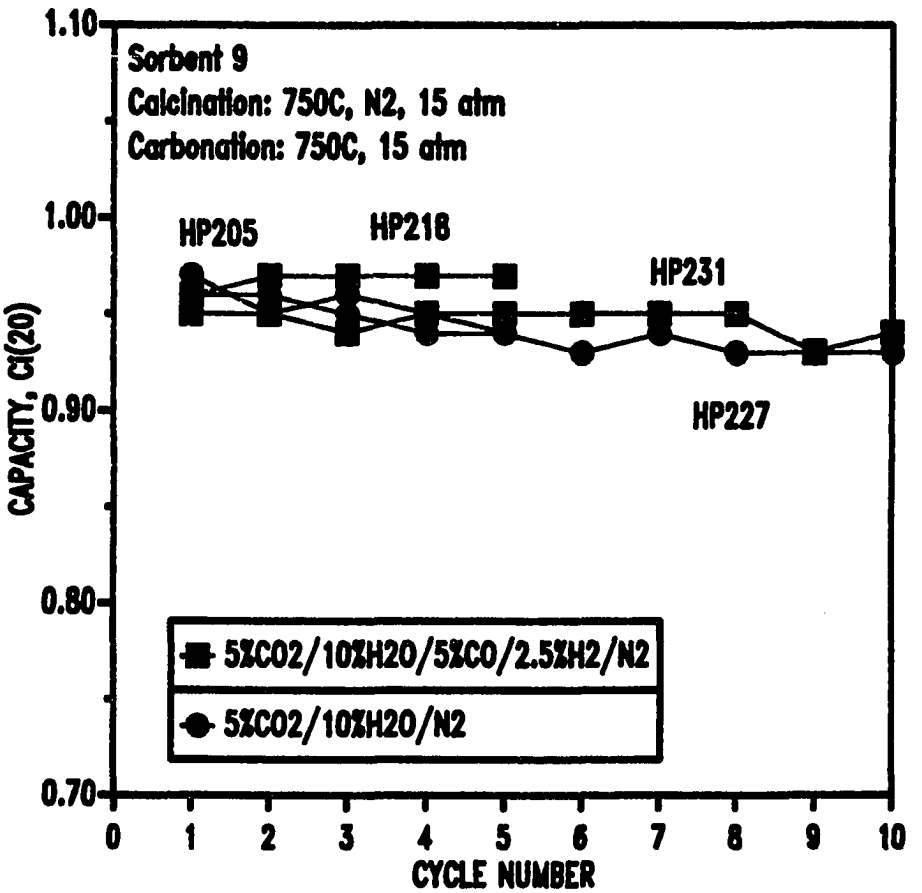

Figure 7.19 Carbonation Capacity Versus Cycle Number for Ten-Cycle Runs Using Sorbent 9

sorbent 7. In HP231 the capacity in the tenth cycle was only 1% lower than in the first cycle. In HP227 the capacity values for the first and the tenth cycles differed by approximately 3%.

7.8 Conclusions

Multicycle runs using sorbents 1, 7, and 9 have been carried out in order to extend the understanding of the durability of the sorbent. Sorbent 1 was found to posses the lowest reactivity maintenance and capacity maintenance after being subjected to five-cycle runs. Sorbent 7 had the highest calcium utilization in the first cycle, but experienced a gradual decrease in capacity with increasing number of cycles. Sorbent 9 was the best sorbent in term of reactivity maintenance and capacity maintenance.

The addition of steam to the carbonation background gas produced an improvement in sorbent reactivity, capacity, and durability. Further addition of CO and H_2 to produce a sulfur-free simulated coal-gas had no significant effect on the kinetics of the carbonation reaction. However, careful choice of gas composition was required in order to avoid carbon deposition in the reactor. Addition of H_2S caused a rapid and irreversible deterioration in carbonation capacity because of the irreversible reaction (7-3). In addition, H_2S was capable of displacing previously formed carbonate by reaction (7-4). Since CaS could not be reconverted to CaO, it

appears that a prior desulfurization step will be required before the calcium-based sorbent process can be used commercially for bulk removal of CO_2.

Chapter 8

Application of Pore Models with Structural Changes to the Carbonation Reaction

The reaction of interest is:

$$CaO_{(s)} + CO_{2(g)} \rightarrow CaCO_{3(s)}$$

The differences in molar volumes of reactant CaO (16.8 cm^3/mol) and product $CaCO_3$ (36.9 cm^3/mol) cause structural changes in the solid during the reaction. It has been shown from the TGA studies that the reaction occurred in two distinct phases: an early rapid reaction phase was followed by an abrupt transition to a slow reaction. During the slow phase, the reaction effectively stopped well before the theoretical maximum conversion was reached.

In order to describe the experimental results, a model which accounts for structural property changes during the reaction is required. The distributed pore size model developed by Christman and Edgar (1983) has been chosen for the modeling effort. The model provides for an evolution of pore size distribution in the solid as the reaction proceeds. The model accounts for four resistances: mass transfer of the reactive gas to the exterior of the particle, diffusion of gas in the pores, diffusion of gas through the product layer, and surface reaction.

This chapter begins with a brief derivation of the distributed pore size model which is adapted directly from Christman and Edgar (1983). The parameters required as input to the model are then discussed. Model predictions are then compared to the experimental data.

The model is only applied to the experimental data for sorbent 1 since the structural characteristics of that sorbent are better defined and the incomplete conversion was most noticeable for that sorbent. The model predictions are compared with the experimental data using sorbent structural properties determined from the mercury pore size distribution of Narcida (1992).

8.1 Distributed Pore Size Model

Consider the noncatalytic gas-solid reaction:

$$\beta_1 A_{(s)} + \beta_2 C_{(g)} \rightarrow \beta_3 B_{(s)} + \beta_4 D_{(g)}$$

The following assumptions are made:

(i) The solid reactant A is a porous spherical pellet having an initial radius of R_0 which remains constant throughout the reaction.

(ii) The porous medium is made up of a distribution of open, interconnecting, cylindrical pores with a random distribution of orientations and locations.

(iii) Isothermal conditions prevail.

(iv) The reactive gas concentration is a function of time and radial position in the pellet.

(v) The net mass flux of gas is neglected.

(vi) The pseudo steady state assumption for the gas concentration profile in the pellet is applicable.

Equations describing the diffusion of reactive gas through the product layer and the chemical reaction taking place on the product-reactant interface are first derived. The evolution of the pore size distribution is then discussed. Finally, by integrating the pore size distribution, the macroscopic properties necessary to obtain the pseudo steady state gas concentration in the pellet will be presented.

8.1.1 Chemical Reaction in a Single Pore

Consider a single pore with initial radius r_o. The reaction is assumed to obey the unreacted core model. During the reaction a product solid will accumulate on the walls between the pore and the product-reactant interface with a thickness of (r_2-r_1) as shown in Figure 8.1. It is assumed that the length of the cylindrical pore under consideration is small enough that the gas concentration C has the same value throughout the pore length, *l*.

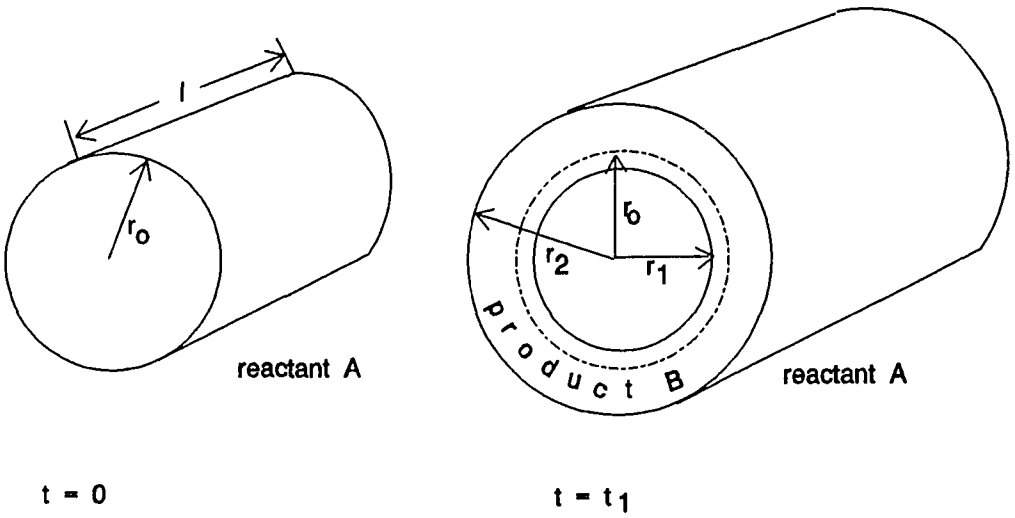

Figure 8.1 Geometric Changes During Reaction in a Single Pore (Christman and Edgar, 1983)

By assuming a first order reaction with respect to reactant gas, and performing a mass balance throughout the product layer, we obtain the gas concentration at the reaction interface, $C(r_2)$, as

$$C(r_2) = \frac{C}{1 + r_2(\frac{k}{D_s}) \ln(\frac{r_2}{r_1})} \qquad (8\text{-}1)$$

where C is the gas concentration in the pore in mol/cm^3, k is the surface reaction constant in cm/s, and D_s is the diffusivity of gas through the product layer in cm^2/s.

As the reaction proceeds, r_1 and r_2 will change. It is, therefore, necessary to express r_1 and r_2 as a function of time. The rate of change of r_2 is calculated from

$$[\frac{\partial r_2}{\partial t}]_{r_0} = (\frac{\beta_1}{\beta_2}) V_A k C(r_2) \qquad (8\text{-}2)$$

where V_A is the molar volume (cm^3/mol) of solid reactant A. Substituting Eq.(8-1) into Eq.(8-2) gives

$$[\frac{\partial r_2}{\partial t}]_{r_0} = \frac{(\frac{\beta_1}{\beta_2}) V_A k C}{1 + r_2 (\frac{k}{D_s}) \ln(\frac{r_2}{r_1})} \qquad (8\text{-}3)$$

The relationship between r_1 and r_2 is based upon the conservation of mass of solid A:

$$r_1^2 = \alpha r_0^2 + (1-\alpha) r_2^2 \qquad (8\text{-}4)$$

where

$$\alpha = \left(\frac{\beta_3}{\beta_1}\right)\left(\frac{V_B}{V_A}\right) \qquad (8\text{-}5)$$

α is the ratio of the molar volumes of the solid product and reactant, V_B/V_A, and the stoichiometric coefficients, β_3/β_1. Taking the derivative of Eq.(8-4) and applying Eq.(8-3) gives

$$\left[\frac{\partial r_1}{\partial t}\right]_{r_o} = \frac{\left(\frac{\beta_1}{\beta_2}\right) V_A k (1-\alpha) \left(\frac{r_2}{r_1}\right) C}{1 + r_2 \left(\frac{k}{D_s}\right) \ln\left(\frac{r_2}{r_1}\right)} \qquad (8\text{-}6)$$

$(\partial r_1/\partial t)$ in Eq.(8-6) depends on both r_1 and r_2, and gas concentration, C. Moreover, gas concentration C is a function of both time and radial position, R, within the pellet.

In order to eliminate the dependence of C on r_1 and r_2, a new parameter τ is introduced as

$$\tau = \int_0^t \frac{C(R,t)}{C_0}\, dt \qquad (8\text{-}7)$$

where C_0 is the gas concentration at the surface of the pellet ($R=R_0$). τ is called the cumulative gas concentration first introduced by Dudukovic (1976). Note that τ has the same value as time t if there is no pore diffusion resistance. By differentiating Eq.(8-7) with respect to time and using the chain rule for Eq.(8-6), we obtain

$$\left[\frac{\partial r_1}{\partial \tau}\right]_{t_0} = \frac{\left(\frac{\beta_1}{\beta_2}\right) V_A k (1-\alpha) \left(\frac{r_2}{r_1}\right) C_0}{1 + r_2 \left(\frac{k}{D_s}\right) \ln\left(\frac{r_2}{r_1}\right)} \qquad (8\text{-}8)$$

Eq.(8-8) can be combined with (8-4) to obtain an expression for $(\partial r_1/\partial t)$ that depends only on τ and r_1. Integrating this equation using the initial condition $r_1 = r_0$ at $\tau = 0$ yields

$$\tau = \frac{(1-\alpha) r_0}{\lambda k} \{ 1-[\frac{\alpha-(\frac{r_1}{r_0})^2}{\alpha-1}]\} + (\frac{r_0^2}{4\lambda D_s}) \{(\frac{r_1}{r_0})^2 \ln(\frac{r_1}{r_0})^2 - ((\frac{r_1}{r_0})^2 - \alpha)\ln[\frac{(\frac{r_1}{r_0})^2-\alpha}{1-\alpha}] \} \qquad (8\text{-}9)$$

where

$$\lambda = (\frac{\beta_1}{\beta_2}) V_A (\alpha-1) C_0 \qquad (8\text{-}10)$$

Eq.(8-9) is an analytical expression which relates τ to r_1 and r_0.

8.1.2 Evolution of Pore Size Distribution

In a spherical pellet, there exists a distribution of pores which intersect the surface of the sphere located at R. The distribution is defined by a distribution function $\eta_1(r_1,R,t)dr_1$, which is the number of pores per unit surface per unit radius of cyclindrical pore with sizes between r_1 and (r_1+dr_1). It is assumed that the pores are randomly oriented in the porous matrix independent of size r_1 and that the average length *l* of the pores is small with respect to the radius of the pellet.

The population balance over the pore size distribution generates the following equation (in term of τ)

$$\frac{\partial \eta_1(r_1,\tau)}{\partial \tau} + \frac{\partial}{\partial r_1}\left[\eta_1(r_1,\tau)\frac{\partial r_1}{\partial \tau}\right] = \eta_1(r_1,\tau)\frac{\partial \varphi(r_1,R,\tau)}{\partial \tau} \qquad (8\text{-}11)$$

where $(\partial\varphi/\partial\tau)$ is the net rate of the net fractional increase in the number of pores due to pore intersections. For simplicity, the model assumes that there are no pore intersections during the reaction. Eq.(8-11) is then simplified to

$$\frac{\partial \eta_1}{\partial \tau} + \frac{\partial}{\partial r_1}\left[\eta_1\frac{\partial r_1}{\partial \tau}\right] = 0 \qquad (8\text{-}12)$$

8.1.3 Chemical Reaction in Porous Medium

The macroscopic properties of the porous medium are obtained by relating the properties of individual pores to the pore size distribution. The void area per unit area ψ is

$$\psi = \int_0^\infty \pi\, r_1^2\, \eta_1\, dr_1 \qquad (8\text{-}13)$$

For randomly oriented pores, the void area per unit area is equal to the void volume per unit volume (Petersen, 1957; Schechter and Gidley, 1969), and, therefore, the porosity ϵ is

$$\varepsilon = \int_0^\infty \pi r_1^2 \eta_1 dr_1 \qquad (8\text{-}14)$$

Gas concentration profiles within the pellet are determined by performing a mass balance on reactant gas C undergoing diffusion and chemical reaction in a spherical porous pellet

$$\frac{1}{R^2}\frac{\partial}{\partial R}\left[R^2 D_e \frac{\partial C}{\partial R}\right] = K_e C \qquad (8\text{-}15)$$

where

$$D_e = \frac{1}{\zeta}\int_0^\infty (\pi r_1^2) D_c \eta_1 dr_1 \qquad (8\text{-}16)$$

$$K_e = 2k \int_0^\infty \frac{\pi r_2 \eta_1}{1 + r_2\left(\frac{k}{D_s}\right)\ln\left(\frac{r_2}{r_1}\right)} dr_1 \qquad (8\text{-}17)$$

$$D_c = \left(\frac{1}{D_{AB}} + \frac{1}{D_K(r_1)}\right)^{-1} \qquad (8\text{-}18)$$

ζ is a tortuosity factor (dimensionless), D_{AB} is the bulk diffusivity of the gas mixture, cm^2/s, D_K is the Knudsen diffusivity, cm^2/s, and D_c is the effective diffusion coefficient, cm^2/s. Note that D_c in Eq.(8-15) is a function of both time and location since it depends on the pore size distribution $\eta(R,t)$. Similarly, K_c depends on the pore size distribution $\eta(R,t)$. The boundary conditions required to solve Eq.(8-15) are

$$\frac{dC}{dR} = 0 \quad at\ R = 0 \tag{8-19}$$

$$D_e \frac{dC}{dR} = k_g (C_0 - C) \quad at \quad R = R_0 \tag{8-20}$$

where k_g is the mass transfer coefficient, cm/s.

The local conversion is expressed as

$$x(R,t) = \frac{\varepsilon_0 - \varepsilon(R,t)}{(1-\varepsilon_0)(\alpha-1)} \tag{8-21}$$

The rate of change of local conversion with time is obtained directly from the equivalent reactivity K_e as

$$\frac{dx}{dt} = \left(\frac{\beta_1}{\beta_2}\right) \frac{V_A K_e C}{(1-\varepsilon_0)} \tag{8-22}$$

The overall porosity, conversion, and reaction rate are determined using a volume-weighted integration over the local property of interest. The overall conversion, X(t), for example, is determined from the local conversion, x(R,t), as

$$X(t) = \frac{3}{4\pi R_0^3} \int_0^{R_0} 4\pi R^2\, x(R)\, dR \tag{8-23}$$

The overall conversion, X(t), may then be compared to the experimental data.

8.2 Numerical Solution Technique

The model must be solved numerically. Figure 8.2 shows a flow chart of the solution procedure taken from Christman (1981).

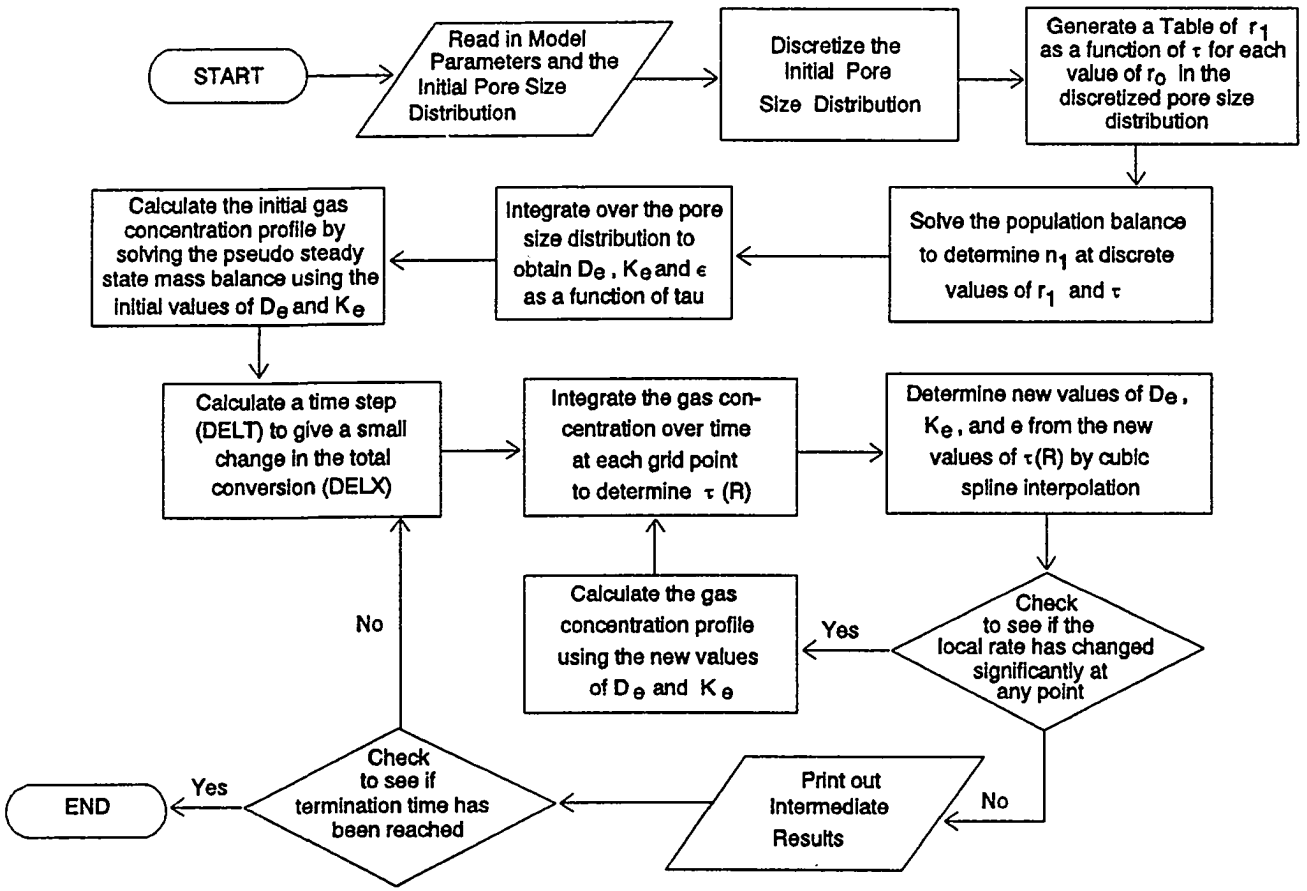

Figure 8.2 Flowchart for the Distributed Pore Size Model

(1) Initially, all model parameters and the initial pore size distribution are input.

(2) The pore size distribution is then internally discretized into approximately 50 divisions with a constant value of η_1 over each interval.

(3) Using Eq.(8-9) a table of r_1 as a function of τ, for each value of r_0, is generated.

(4) The population balance (Eq.(8-12)) is used to determine η_1 at discrete values of r_1 and τ.

(5) The macroscopic properties (D_e, K_e, and ϵ) are then tabulated at 100 values of τ by integrating over the pore size distribution using Eqs.(8-16), (8-17), and (8-14). Gauss-Legendre quadrature is used because τ is not a constant step size.

(6) A cubic spline is fit through all tabulated values for the purpose of interpolation later in the program.

(7) The initial gas concentration is obtained by solving Eq.(8-15) using a centered finite difference method giving a set of linear equations in local gas concentration which are solved using the tridiagonal matrix technique.

(8) Time is incremented by determining the time required to produce a specified small change in the total conversion. This is done by the following:

(8a) Integrate the gas concentration profile over time using the trapezoidal rule to determine a value of τ at each grid point (Eq.(8-7)).

(8b) From the new value of τ the new values of D_e, K_e, and ϵ are determined using a cubic spline interpolation.

(8c) The local rate of reaction (K_eC) is compared to its previous value at each point. If the local rate of reaction at any point has changed by more than a prespecified limit, the gas concentration is then calculated (Eq.8-15) using the new values of D_e and K_e (from step (8b)) and the procedure is repeated from step (8a) through step (8c).

(8d) If the change in the local rate of reaction at any point is less than the prespecified limit (i.e. convergence has been achieved), intermediate results are printed out. The results include the values of overall rate, conversion, and porosity which are calculated by integrating over the local values of these properties using Simpson's rule.

(9) A new time step is initiated and steps (8a) through (8d) are repeated until the desired total reaction time is reached or the pores at the outer shell of the pellet are plugged.

Before comparison with the experimental data, the program code was first validated by matching cases reported by Christman and Edgar (1983).

8.3 Model Parameters

The parameters required as input data for the distributed pore size model are summarized in Table 8-1, and are discussed below.

Table 8-1

Model Parameters Used for

Distributed Pore Size Model

Symbol	Parameter, Units
R_0	Particle Radius, cm
α	Ratio of Molar Volumes of Product (V_B) and Reactant (V_A)
k	Reaction Rate Constant, cm/s
D_{AB}	Bulk Diffusivity, cm^2/s
D_K	Knudsen Diffusion Coefficient, cm/s
D_s	Product Layer Diffusivity, cm^2/s
ζ	Tortuosity Factor
k_g	Mass Transfer Coefficient, cm/s
C_0	Effective Bulk Reactive Gas Concentration, mol/cm^3
β_i	Stoichiometric Coefficient of Component i
ρ	Mass Density of Solid Reactant, g/cm^3

(1) Physical Properties of Crystalline Solids

The molar volumes of CaO and $CaCO_3$ are 16.8 and 36.9 cm^3/mol, respectively, giving an expansion ratio, α, of 2.20. The true mass densities of CaO and $CaCO_3$ are 3.345 and 2.71 g/cm^3, respectively. These values are taken from Handbook of Chemistry and Physics (Weast, 1989).

(2) Particle Radius

The particle size of the initial solid CaO was determined from the SEM studies of Narcida (1992). The CaO particles were produced by calcination of $CaCO_3$ at 750°C and 1 atm in N_2 for 1 hr. The initial $CaCO_3$ particles were approximately cubical in shape with the particles ranging from 0.5 to 10 μm as determined from SEM photomicrographs. Using the BET surface area of 0.9 m^2/g (Narcida, 1992) and solid density of 2.71 g/cm^3, the average length of the cubical particles was calculated to be 2.5 μm. The mercury porosimetry tests of precursor $CaCO_3$ indicated effectively nonporous particles (see Chapter 2). From the SEM results, the particles remained cubical in shape after calcination, but a rough surface was observed suggesting that pores were created during calcination.

The particle radius used as a parameter in this model was determined using the equivalent radius of a sphere whose volume is equal to the volume of cubical CaO having length of

l. With the length of 2.5 μm the equivalent radius was calculated to be 1.55 μm.

(3) Pore Size Distribution

Pore size distribution is one of the very important parameters required in this model. This parameter plays an important role in describing the evolution of structural properties during the reaction. The sudden reaction "die-off" predicted by an average pore size (for example, Bhatia and Perlmutter, 1980, 1981) does not occur with a pore size distribution.

The mercury porosimetry results of Narcida (1992) summarized in Table 8-2 were used. Most of the pore volume corresponds to pore diameters ranging from 0.02 to 0.09 μm with a small additional pore volume in the pore diameter range of 0.003 to 0.01 μm. The total pore volume of 0.3629 cm^3/g corresponds to an initial porosity of 0.548. This is quite close to the theoretical porosity of 0.545 which would be produced by calcination of nonporous $CaCO_3$ at conditions where no sintering occurred. Note that the model will convert from the pore diameter, as shown in Table 8-2, into the pore radius for further calculations.

(4) CO_2 Gas Concentration

The carbonation reaction is assumed to be first order with respect to reactant gas concentration. At the

Table 8-2

Cumulative Pore Volume as a Function of Pore Diameter for Sorbent 1 (Narcida, 1992)

Pore Diameter (μm)	Cumulative Pore Volume (cm^3/g)
0.0907	0
0.0804	0.0029
0.0724	0.0109
0.0656	0.0292
0.0604	0.0498
0.0519	0.1070
0.0402	0.2100
0.0363	0.2357
0.0303	0.2601
0.0259	0.2674
0.0227	0.2711
0.0202	0.2731
0.0181	0.2753
0.0130	0.2780
0.0101	0.2839
0.0091	0.2879
0.0065	0.3001
0.005	0.3121
0.004	0.3247
0.003	0.3629

temperatures of interest, the equilibrium CO_2 pressure is significant at low total pressure. Therefore, the effective bulk reactant gas concentration, C_0, is taken to be the difference between the actual bulk CO_2 concentration, C_b, and the equilibrium CO_2 concentration, C_{eq}. Assuming ideal gas behavior, the "effective" gas concentration, C_0, is therefore

$$C_0 = \frac{p_{CO_2} - p_{eq}}{RT} = \frac{y_{CO_2}p - p_{eq}}{RT} \qquad (8\text{-}24)$$

At 650°C, for example, the equilibrium CO_2 pressure is 0.01 atm. With 0.15 mol fraction of CO_2 in the reactant gas at 1 atm total pressure, the effective CO_2 concentration is 1.85E-06 mol/cm^3.

(5) Surface Reaction Rate Constant

Bhatia and Perlmutter (1983) estimated the rate constant for the carbonation reaction by applying the random pore model (Bhatia and Perlmutter, 1980; 1981) to their experimental data during the rapid reaction phase. The intraparticle and transport resistances were reported to be negligible in that phase. The average value of the rate constant was found to be 0.0595 ± 0.0018 cm^4/(gmole)(s) in the temperature range of 550 to 725°C. The lack of temperature dependence suggests that the value is only approximate. No other literature values of the carbonation rate constant are known.

Note that the units of the rate constant reported by Bhatia and Perlmutter (1983) are different from the units used in this model. Bhatia and Perlmutter's value of 0.0595 $cm^4/(gmol)(s)$ may be converted to 0.00354 cm/s by dividing by the molar volume of CaO. This value will be used as a guide before being treated as a best-fit parameter.

(6) Molecular and Knudsen Diffusivity

Molecular diffusivity of CO_2 in N_2 was determined using the Chapman-Enskog equation (Bird, Stewart, and Lightfoot, 1960)

$$D_{AB} = 0.0018583 \frac{\sqrt{T^3 \left(\frac{1}{M_A} + \frac{1}{M_B}\right)}}{p\, \sigma_{AB}^2\, \Omega_{D,AB}} \qquad (8\text{-}25)$$

where D_{AB} is the molecular (or bulk) diffusivity in cm^2/s, T is the temperature in K, M_A and M_B are molecular weights of species A and B, respectively, p is the pressure in atm, σ_{AB} is the Lennard-Jones parameter in Å, and $\Omega_{D,AB}$ is a dimensionless function of temperature and of the intermolecular potential field for one molecule of A and one of B. Parameters needed to evaluate σ_{AB} and $\Omega_{D,AB}$ are tabulated (Bird, Stewart, and Lightfoot, 1960). For the CO_2-N_2 system at 650°C and 1 atm, for example, σ_{AB} is calculated to be 3.838, and $\Omega_{D,AB}$ to be 0.7896 giving the molecular diffusivity D_{AB} to be 1.08 cm^2/s.

The Knudsen diffusivity is a linear function of pore radius given by (Froment and Bischoff, 1990)

$$D_K = \frac{4}{3} r \left(\frac{2}{\pi} \frac{RT}{M_A}\right)^{\frac{1}{2}} \qquad (8\text{-}26)$$

where D_K is in cm^2/s, R is the gas constant in $kg.m^2/(s^2)(K)(mol)$, T is the temperature in K, r is the pore radius in cm, and M_A is the molecular weight of species A. For an average pore radius of 0.02 μm, for example, the Knudsen diffusivity of CO_2 at 650°C is 0.089 cm^2/s.

The effective diffusivity is the combination of molecular and Knudsen diffusivities according to Eq.(8-18). With an average pore radius of 0.02 μm the effective diffusivity at 650°C and 1 atm is 0.082 cm^2/s showing that Knudsen diffusion is the most important diffusion mechanism. At high pressure, however, both mechanisms are important. For example, at 650°C and 15 atm, D_{AB} = 1.08/15 = 0.072 cm^2/s while D_K = 0.089 cm^2/s, giving D_e = 0.040 cm^2/s.

(7) Tortuosity Factor

The tortuosity factor accounts for non-ideality in pore orientation, shape, and interconnectiveness. This value is expected to vary with pore size distribution in order to obtain the correct diffusional resistance through the porous matrix and the correct concentration profile in the pellet. If pore diffusion resistance is not important, however, the

model is not sensitive to the value. A tortuosity factor of 3, which is within the range reported by Satterfield (1970), has been chosen in all cases.

(7) Product Layer Diffusivity

Values of the product layer diffusivity reported in the literature vary significantly. Bhatia and Perlmutter (1983) applied the random pore model to estimate the "effective" product layer diffusivity (D_{pe}) for the carbonation reaction. D_{pe} was defined as $D_p C_s M_{CaO}/\rho_{CaO}$. D_p was the solid state diffusivity, C_s the diffusing species concentration (unknown), M_{CaO} the molecular weight of CaO, and ρ_{CaO} the mass density of CaO. The activation energy was found to be 21.2 ± 0.9 kcal/mol over the temperature range of 400 to 515°C and 42.8 ± 1.7 kcal/mol over 515 to 725°C. At 650°C, D_{pe} was found to be 1.0E-14 cm^2/s. Assuming that solid $CaCO_3$ was the diffusing species (C_s = 0.0271 mol/cm^3), the solid state diffusivity is, therefore, 2.2E-14 cm^2/s.

Anderson (1969) studied the diffusion of carbon and oxygen atoms in the calcite lattice. Calcite crystals were used in contact with a gas reservoir of isotopic CO_2. By measuring the change in the isotopic concentration in the gas reservoir, he concluded that over the temperature range of 550 to 850°C the self-diffusivity of the carbon atom was

$$D_{carbon} = 1.3E{+}03\exp(-88\,(kcal/mol)/RT) \qquad (8\text{-}27)$$

where D_{carbon} is in cm^2/s. At 650°C, D_{carbon} = 1.90E-18 cm^2/s. The oxygen self-diffusivity was found to be higher by a factor of four. Kronenberg *et al.* (1984) reported an activation energy of carbon self-diffusivity in the calcite crystals to be 87 ± 2 kcal/mol over the temperature range of 500 to 800°C. The carbon self-diffusivity at 650°C was 1.63E-18 cm^2/s, in agreement with Anderson (1969).

Mess (1989) reported the effective diffusion coefficient, D_{eff}, of the carbonation reaction at high temperatures (≥ 900°C) and longer times (≥ 600 minutes) as

$$D_{eff} = 0.65 \exp(-56.9(kcal/gmol)/RT) \qquad (8\text{-}28)$$

where D_{eff} is in cm^2/s. D_{eff} in Eq.(8-27) is, in principle, the same as the product layer diffusivity, D_s, discussed in this section except that D_{eff} was based on single crystal particles with no grain boundaries. At lower temperatures (≤ 850°) and short times, however, the D_{eff} values were not reported.

The product layer diffusivity is generally treated as an adjustable parameter in modeling gas-solid reactions. Lew *et al.* (1992b), for example, used the overlapping grain model (Sotirchos and Yu, 1988) and reported an activation energy of 26.4 kcal/mol for product layer diffusivity over the temperature range from 400 to 700°C for the ZnO + H_2S reaction. At 650°C, the product layer diffusivity was 5.50E-08 cm^2/s. In comparison, Ranade and Harrison (1981) applied the modified grain model to describe the ZnO + H_2S reaction

and an activation energy of 22 kcal/mol was reported. A product layer diffusivity of 3.0E-09 cm^2/s was calculated at 650°C, about an order of magnitude lower than the value reported by Lew *et al.* (1992b).

Variation in the values of product layer diffusivity are also found in the sulfation of solid CaO. Hartman and Coughlin (1976) reported the product layer diffusivity of 6.0E-09 cm^2/s at 850°C using the grain model. Georgakis *et al.* (1979) applied the changing grain model and estimated that the product layer diffusivity ranged from 8.0E-09 to 1.6E-07 cm^2/s at 850°C. Ramachandran and Smith (1977) reported the product diffusivity to be 7.5E-07 cm^2/s at 850°C using the single pore model. Christman and Edgar (1983) reported the product diffusivity to be 4.0E-08 cm^2/s at 850°C using the distributed pore size model.

In summary, values of $10^{-18} \leq D_s \leq 10^{-08}$ have been reported for various noncatalytic gas-solid reactions at the temperatures of interest. The product layer diffusivity, D_s, will be treated as an adjustable parameter in the modeling work which follows.

(8) Mass Transfer Coefficient

The external mass transfer coefficient can, in principle, be estimated using the Frossling correlation (Hughmark, 1967)

$$N_{Sh} = \frac{k_g L}{D_{AB}} = 2 + 0.6\, N_{Re}^{\frac{1}{2}}\, N_{Sc}^{\frac{1}{3}} \qquad (8\text{-}29)$$

where

N_{Sh} = Sherwood number, $(k_g)(L)/(D_{AB})$

N_{Re} = Reynolds number, $(L)(G)/(\mu_G)$

N_{Sc} = Schmidt number, $(\mu_G)/(\rho_G)(D_{AB})$

D_{AB} = molecular (bulk) diffusivity, cm^2/s

L = characteristic length, cm

G = mass flux of gas, $g/(cm^2)(min)$

μ_G = bulk gas viscosity, $g/(cm^2)(s)$

ρ_G = bulk gas density, g/cm^3.

In calculating the Reynolds number, N_{Re}, the mass flux of gas was determined using the reactor tube diameter of 2.54 cm and the total flow rate of 500 cm^3/min (STP). At 650°C and 1 atm, the total mass flux was 0.135 $g/(cm^2)(min)$ while the average gas viscosity was 3.8E-04 g/(cm)(sec). In the reactor tube, the gas flowed downward and passed over the particles which were contained in a sample pan having a diameter of about 1 cm. If the pan diameter is considered as the characteristic length, L, the Reynolds number (GL/μ_G) is 5.92. Using Eq.(8-29) with the Schmidt number of 0.87 at 650°C and 1 atm, the Sherwood number was estimated to be 3.4, corresponding to a mass transfer coefficient, k_g, of 3.67 cm/s. If the equivalent diameter of the particle (3.1 μm) is taken as the characteristic length, the resultant mass

transfer coefficient is about 1.2E+04 cm/s. In this latter case the mass transfer resistance would be negligible under all experimental conditions. At 650°C and 1 atm, a value of k_g = 0.5 cm/s has been used in most of the modeling effort. In this case the mass transfer resistance is negligible at 1 atm but becomes significant at high pressure.

8.4 General Discussion of the Solution Characteristics

In this section the general characteristics of the solution of the distributed pore size model are discussed. The model parameters used are summarized in Table 8-3. In order to determine the effect of intraparticle diffusion resistance on the overall reaction, two different particle radii are used. The initial pore size distribution as a function of pore diameter illustrated in Figure 8.3 is also used.

Figure 8.4 compares the conversion-time results predicted using the distributed pore size model for two cases. Curve A, using a particle radius of 2.5×10^{-03} cm, illustrates the results when pore diffusion resistance within the particle is negligible. Complete conversion is predicted after 3.5 min. The initial pore volume of the solid reactant is 0.360 cm^3/g (see Figure 8.3) which corresponds to a porosity of 0.546. Since there is no pore diffusion resistance within the particle, the pores fill uniformly.

Table 8-3
Model Parameters Used for
General Solution of Distributed Pore Size Model

Symbol	Parameter, units	Value
R_0	Particle Radius, cm	2.5×10^{-03} (Curve A) 2.5×10^{-02} (Curve B)
α	Ratio of Molar Volumes of Product and Solid Reactant	2.2
C_0	Effective Reactive Gas Concentration, mol/cm^3	1.85×10^{-06}
k	Surface Reaction Rate Constant, cm/s	1×10^{-03}
D_s	Product Layer Diffusivity, cm^2/s	1×10^{-09}
D_{AB}	Molecular Diffusivity, cm^2/s	1.00
k_g	Mass Transfer Coefficient, cm/s	10.0
V_R	Molar Volume of Solid Reactant, cm^3/mol	16.8

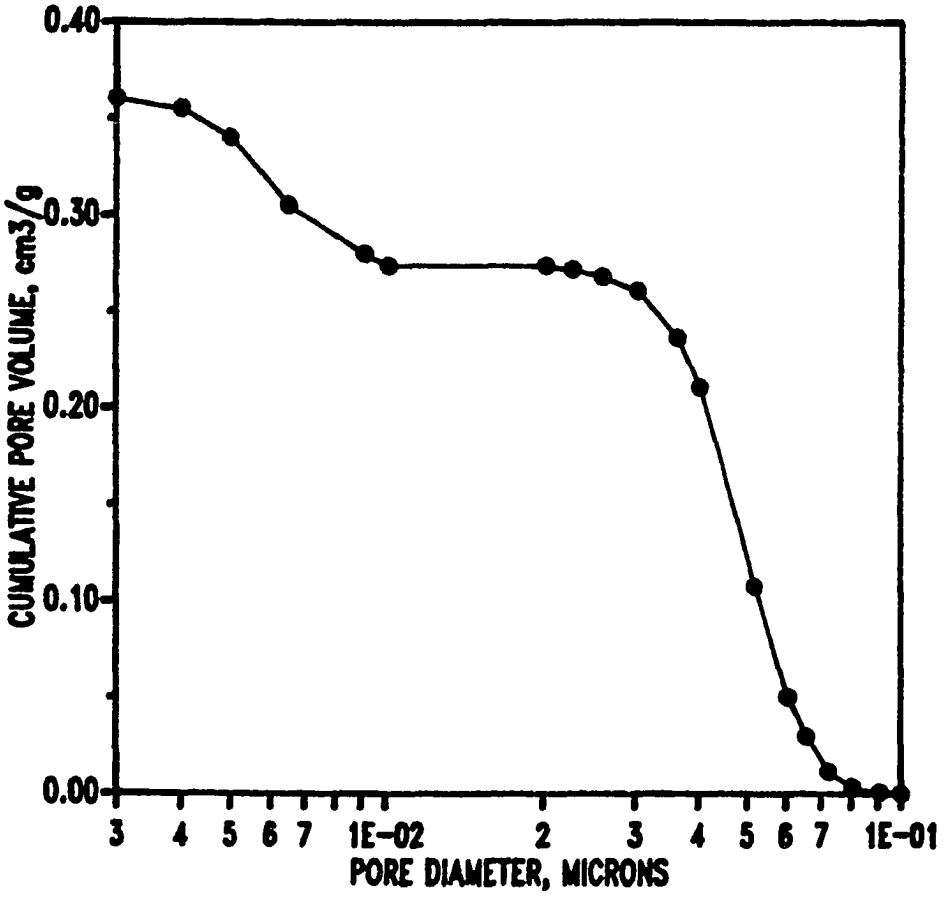

Figure 8.3 Cumulative Pore Volume as a Function of Pore Diameter Used for General Discussion of the Solution Characteristics

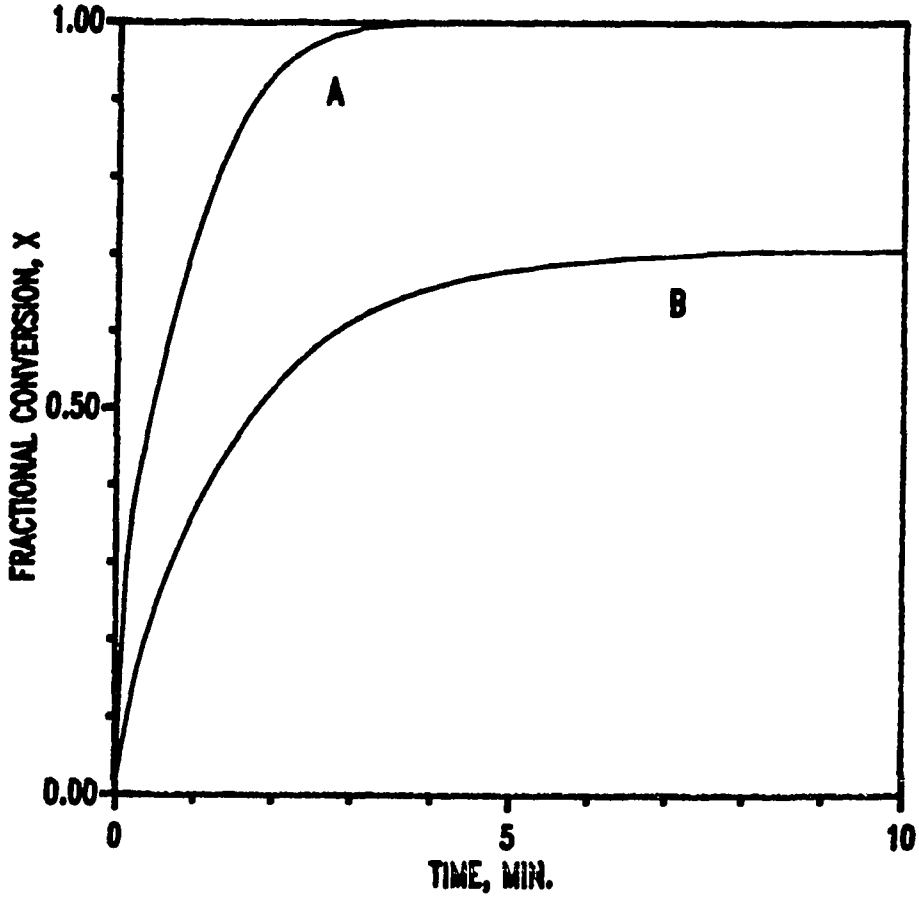

Figure 8.4 Model Prediction of Conversion-Time Results Using Parameters in Table 8-3 and Initial Pore Size Distribution in Figure 8.3

Further, the initial porosity is sufficiently large to allow complete conversion to occur.

When the particle radius is increased by a factor of 10 to 2.5×10^{-02} cm, the pore diffusion resistance becomes significant and the time-conversion results shown by curve B are predicted. The reaction stops after 8 minutes as a result of pore plugging at the outer shell of the particle, leaving a significant amount of inaccessible unreacted solid inside the particle. The overall conversion reached when pore plugging occurs is 0.69.

Figure 8.5 illustrates the local porosity as a function of radial position within the particle with the reaction time as a parameter. Curve B parameters were used in this calculation. Initially, the particle porosity was 0.546 at all radial positions. After 0.5 min the local porosity at the particle exterior surface decreased to 0.29 while the local porosity at the center of the particle was near the original value. The reaction stopped after 8 min when pores at the outer shell of the particle became plugged as shown by the zero local porosity value.

When pore diffusion resistance is negligible, the maximum achievable conversion becomes a function only of the initial porosity as shown in Figure 8.6. The rate of reaction is determined by parameter values such as k, D_s, D_e, and k_g. However, given sufficient time, the conversion will always approach the values shown in Figure 8.6. It also follows that

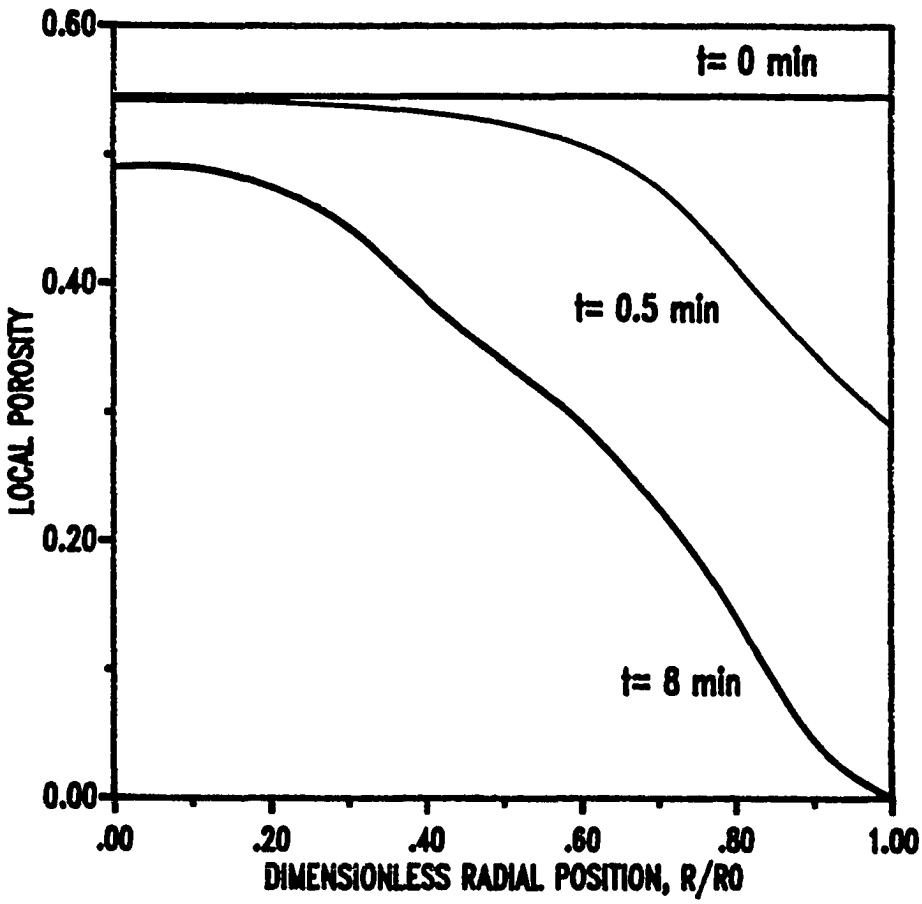

Figure 8.5 Local Porosity as a Function of Radial Position within the Particle with the Reaction Time as a Parameter; Significant Pore Diffusion Resistance within the Particle

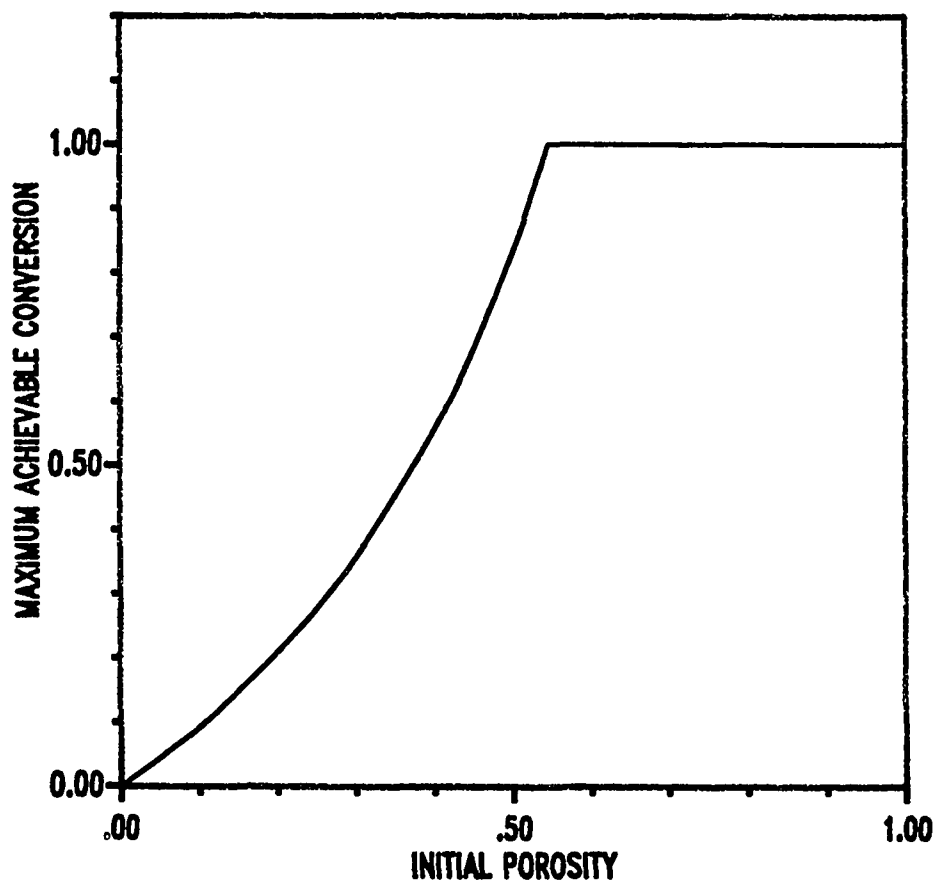

Figure 8.6 Effect of Initial Particle Porosity on Maximum Achievable Conversion with Negligible Pore Diffusion Resistance; $\alpha = 2.20$

the only way in which incomplete conversion can be predicted in a particle whose initial porosity is 0.54 or greater is by the inclusion of significant pore diffusion resistance.

8.5 Comparison between Model Prediction and Experimental Data

In this section the distributed pore size model predictions are compared to experimental results using the pore size distribution shown in Table 8-2. Run HP046 (see Table 5-2) in which calcination was carried out at 750°C and 1 atm in N_2 followed by carbonation at 650°C and 1 atm in 15% CO_2/N_2 has been selected for the initial or base case comparison. Certain parameter values are selected more or less arbitrarily to fit the experimental data for this base case.

Thereafter, experimental runs representing the effects of CO_2 mol fraction, reaction pressure, and temperature are considered. Adjustments in the parameter values which are consistent with theory are made and model predictions are again compared to the experimental data.

8.5.1 Base Case Comparison

Figure 8.7 compares three cases of model predictions with the experimental results from the base run. Table 8-4 summarizes the values of the model parameters which were fixed at the beginning and were not varied thereafter.

Table 8-4
Model Parameters Whose Values Were Not Changed in Modeling Test HP046

Symbol	Parameter	Value
R_0	Particle Radius, cm	1.55×10^{-4}
α	Ratio of Molar Volumes of Product and Reactant,	2.20
y	CO_2 Mol Fraction	0.15
ζ	Tortuosity Factor	3.0
ρ	Mass Density of CaO, g/cm^3	3.345
k	Reaction Rate Constant, cm/s	3.54×10^{-03}
k_g	Mass Transfer Coefficient, cm/s	0.5
T	Reaction Temperature, C	650
p	Total Pressure, atm	1
p_{eq}	CO_2 Equilibrium Pressure, atm	0.01

Table 8-5
Model Parameters Whose Values Were Adjusted in Modeling Test HP046

Case	D_s, cm^2/s	D_{c0}, cm^2/s
A	2.2×10^{-14}	1.4×10^{-02}
B	1.7×10^{-09}	1.4×10^{-02}
C	1.7×10^{-09}	1.3×10^{-06}

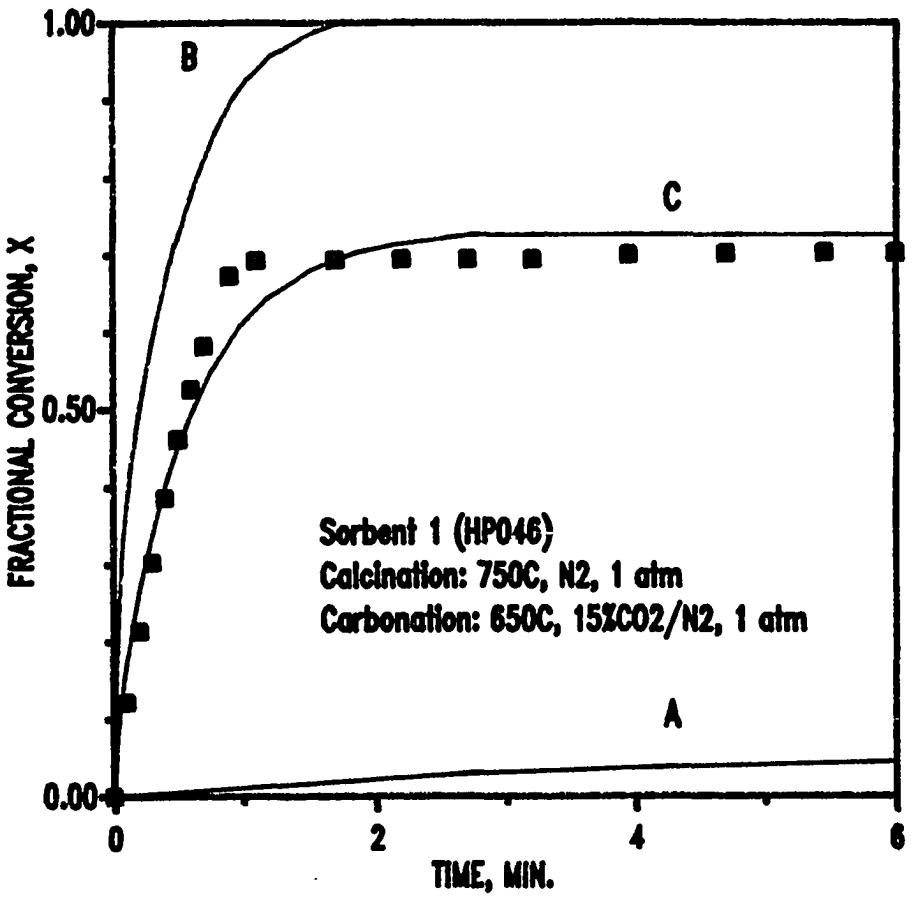

Figure 8.7 Comparison between Model Predictions and Experimental Data of Run HP046

Parameter values which were varied in the three model cases are shown in Table 8-5.

Curve A in Figure 8.7 represents the model prediction using Case A. After 6 minutes the predicted overall conversion was only 0.05 while the experimental overall conversion was about 0.70 after 1 minute. The product layer diffusion resistance associated with $D_s = 2.2 \times 10^{-14}$ cm^2/s was the dominant resistance. Although the rate of reaction is quite small, pores fill uniformly and complete reaction would be predicted if the reaction time was sufficiently large.

Increasing the value of D_s to 1.7×10^{-09} cm^2/s while the other parameters were unchanged (Case B) produced the time-conversion result shown by curve B. The model predicted complete carbonation in approximately 2 minutes. Both surface reaction and product layer diffusion resistances were important. Since the pore diffusion resistance within the particle was negligible and the initial solid porosity was 0.548, all pores were filled uniformly and complete carbonation was predicted.

The only way to predict incomplete conversion with $\epsilon_0 = 0.548$ is to force pore diffusion resistance within the particle to become important. Curve C shows the effect of decreasing the initial effective diffusivity to 1.3×10^{-06} cm^2/s. This unreasonably small value of D_{e0} produced significant pore diffusion resistance and caused the reaction to stop after 2.5 minutes due to pore plugging at the outer

shell of the particle, leaving inaccessible pores inside the particle. The final overall fractional carbonation predicted was 0.726 compared to the experimental value of 0.70. The agreement between model and experiment was quite good throughout.

8.5.2 Effect of CO_2 Mol Fraction at Constant Temperature and Pressure

The effect of CO_2 mol fraction was examined using the experimental data of run HP043 (Table 5-2). Calcination was at 750°C and 1 atm in N_2 followed by carbonation at 650 and 1 atm in 5% CO_2/N_2. The only parameter to change was the CO_2 mol fraction; other parameter values were the same as shown in Tables 8-4 and 8-5, Case C. Figure 8-8 compares the model prediction to the experimental data. Good agreement between model and experiment was achieved for the first two minutes. Thereafter, the predicted conversion was slightly less than the experimental. According to the model, pore plugging at the particle exterior would occur after 9 minutes with an overall fractional conversion of 0.726. The experimental fractional conversion after 9 minutes was 0.732.

8.5.3 Effect of Pressure with Constant CO_2 Concentration

The experimental data for run HP137 (Table 5-2), with calcination at 750°C and 1 atm in N_2 and carbonation at 15 atm and 650°C in 1% CO_2/N_2, was selected to evaluate the

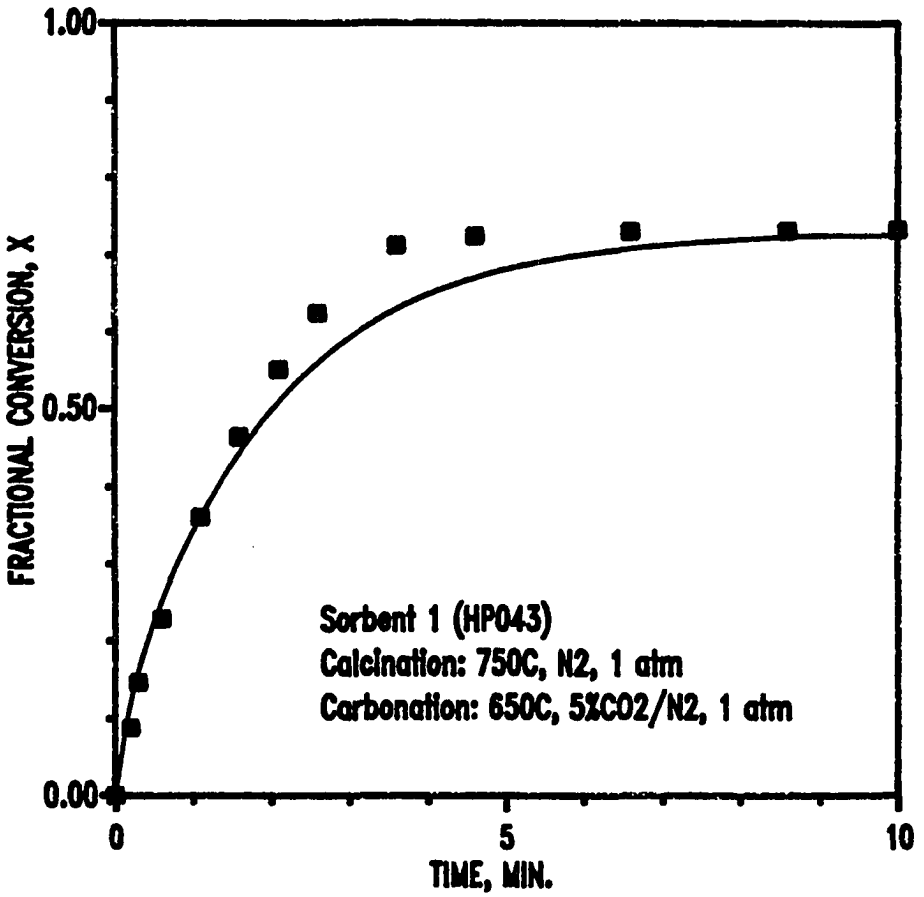

Figure 8.8 Comparison between Model Prediction and the Experimental Data of Run HP043; Effect of CO_2 Mol Fraction

effect of pressure. Bulk CO_2 concentration for this run using 1% CO_2 at 15 atm was the same as the base case run using 15% CO_2 at 1 atm. The values of D_s and k were maintained at $1.7x10^{-09}$ cm^2/s and $3.54x10^{-03}$ cm/s, respectively, since the reaction temperature did not change. The effect of pressure on the effective diffusivity was negligible because the value of D_{e0} = $1.3x10^{-06}$ cm^2/s was within the region where Knudsen diffusion would dominate. Figure 8.9 compares the model predictions with experimental data using two different values of mass transfer coefficient, k_g. The value of k_g = 0.033 cm/s (0.5/15) was selected because k_g should be approximately inversely proportional to the reaction pressure. With k_g = 0.033 cm^2/s, the ratio of the initial particle surface concentration to the effective bulk CO_2 concentration ($C(R=R_0)/C_0$) was 0.31, indicating that mass transfer provided the most important resistance initially. However, as the reaction progressed and pore plugging was approached the pore diffusion resistance began to dominate. As seen in the figure, the predicted overall conversion was significantly larger than the experimental result during the early portions of the run. Pore closure was predicted after 8 minutes at a fractional conversion of 0.726 compared to the experimental value of 0.68 at that time. Decreasing the value of k_g to 0.01 cm/s increased the importance of the mass transfer resistance, and decreased the ratio of initial surface concentration to the effective bulk CO_2 concentration to

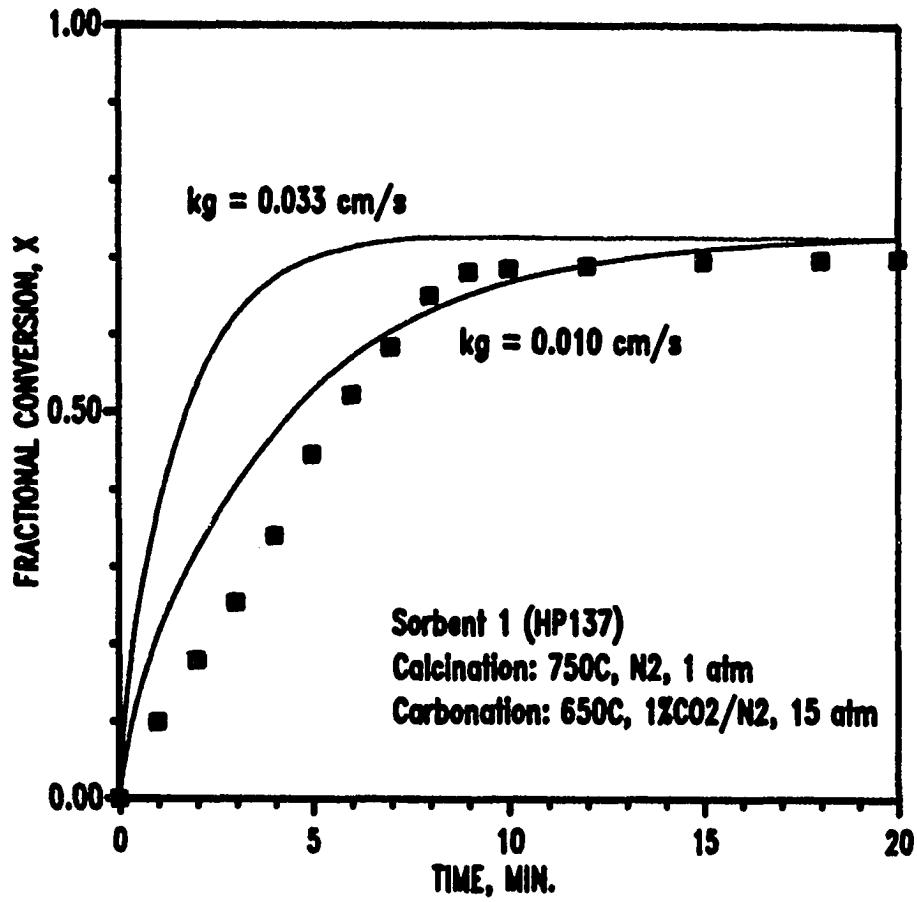

Figure 8.9 Comparison between Model Prediction and Experimental Data of Run HP137; Effect of Carbonation Pressure

0.12. With this value of k_g the agreement between prediction and experiment improved significantly as shown in Figure 8.9. Pore closure was predicted after 20 minutes when the overall conversion was 0.726. The experimental conversion after 20 minutes was 0.70.

8.5.4 Effect of Temperature

Carbonation temperature should affect the model parameter values k, D_s, D_e, k_g, and C_0. The intrinsic reaction rate constant, k, is expected to increase with temperature according to the Arrhenius relationship. However, Bhatia and Perlmutter (1983) reported an activation energy of zero for the intrinsic rate constant. The product layer diffusivity, D_s, is expected to be strongly temperature dependent. The temperature relationship should also be given by the Arrhenius equation with a large activation energy. The value of the effective diffusivity, D_e, should increase slightly since D_e is controlled by Knudsen diffusion which is proportional to $T^{1/2}$. The mass transfer coefficient k_g should also increase slightly with temperature. The effective bulk CO_2 concentration, C_0, decreases with increasing temperature while the equilibrium CO_2 pressure increases with temperature.

Figure 8.10 compares three model predictions with the experimental data for run HP066 (Table 5-2). Calcination was carried out at 750°C and 1 atm in N_2, and carbonation was at

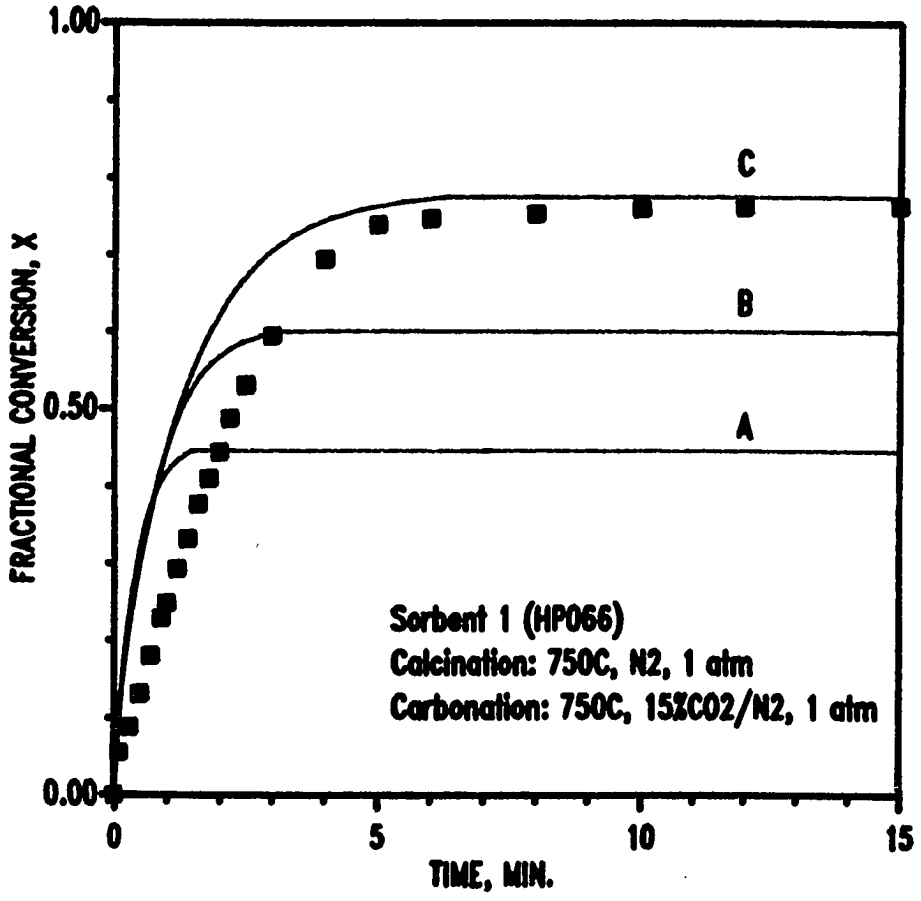

Figure 8.10 Comparison between Model Predictions and Experimental Data for Run HP066; Carbonation at 750°C and 1 atm in 15% CO_2/N_2

Table 8-6
Model Parameters Used for Carbonation Reaction for Run HP066

Symbol	Parameter, units	Value
T	Reaction Temperature, °C	750
p_{eq}	CO_2 Equilibrium Pressure, atm	0.082
k_g	Mass Transfer Coefficient, cm/s	0.53
D_{c0}	Initial Effective Diffusivity, cm^2/s	1.4×10^{-06}
k	Reaction Rate Constant, cm/s	
	Curve A: (E_a = 10 kcal/mol)	6.0×10^{-03}
	Curve B: (E_a = 0 kcal/mol)	3.54×10^{-03}
	Curve C: (E_a = 0 kcal/mol)	3.54×10^{-03}
D_s	Product Layer Diffusivity, cm^2/s	
	Curve A: (E_a = 42 kcal/mol)	1.6×10^{-08}
	Curve B: (E_a = 21 kcal/mol)	5.2×10^{-09}
	Curve C: (E_a = 0 kcal/mol)	1.7×10^{-09}

750°C and 1 atm in 15% CO_2/N_2. Table 8-6 summarizes the model parameters used for the three model predictions. Three values of reaction rate constant, k, and product layer diffusivity, D_s, were calculated based upon the activation energies shown in the table. Curve A represents the values k and D_s, using the highest activation energies of 10 and 42 kcal/mol, respectively, while curve B represents the values of zero activation energy for the reaction rate constant and 21 kcal/mol for the product layer diffusivity. Zero activation energies for both k and D_s were assumed in curve C. As seen in Figure 8.10, none of the predicted conversion-time results were in good agreement with the experimental results during the rapid reaction phase. For curve A, pore plugging was predicted after about 1.5 min with an overall conversion of 0.45. For curve B, pore plugging was predicted after 3 min with an overall conversion of 0.60. For curve C, using zero activation energies for both k and D_s, pore plugging was predicted after 6 min with an overall conversion of 0.77, compared to the experimental conversion of 0.75 at that time.

A similar approach was used to compare the model prediction to the experimental data at the lower carbonation temperature of 550°C. Figure 8.11 compares the model predictions to the experimental data for run HP049 (Table 5-2). Calcination was at 750°C and 1 atm in N_2, and carbonation was at 550°C and 1 atm in 15% CO_2/N_2. Table 8-7 summarizes the model parameters used for the three model predictions. Curve

Table 8-7
Model Parameters Used for Carbonation Reaction for Run HP049

Symbol	Parameter, units	Value
T	Reaction Temperature, °C	550
p_{eq}	CO_2 Equilibrium Pressure, atm	0.0007
k_g	Mass Transfer Coefficient, cm/s	0.47
D_{e0}	Initial Effective Diffusivity, cm^2/s	1.23×10^{-06}
k	Reaction Rate Constant, cm/s	
	Curve A: (E_a = 10 kcal/mol)	1.82×10^{-03}
	Curve B: (E_a = 0 kcal/mol)	3.54×10^{-03}
	Curve C: (E_a = 0 kcal/mol)	3.54×10^{-03}
D_s	Product Layer Diffusivity, cm^2/s	
	Curve A: (E_a = 42 kcal/mol)	1.05×10^{-10}
	Curve B: (E_a = 21 kcal/mol)	4.2×10^{-10}
	Curve C: (E_a = 0 kcal/mol)	1.7×10^{-09}

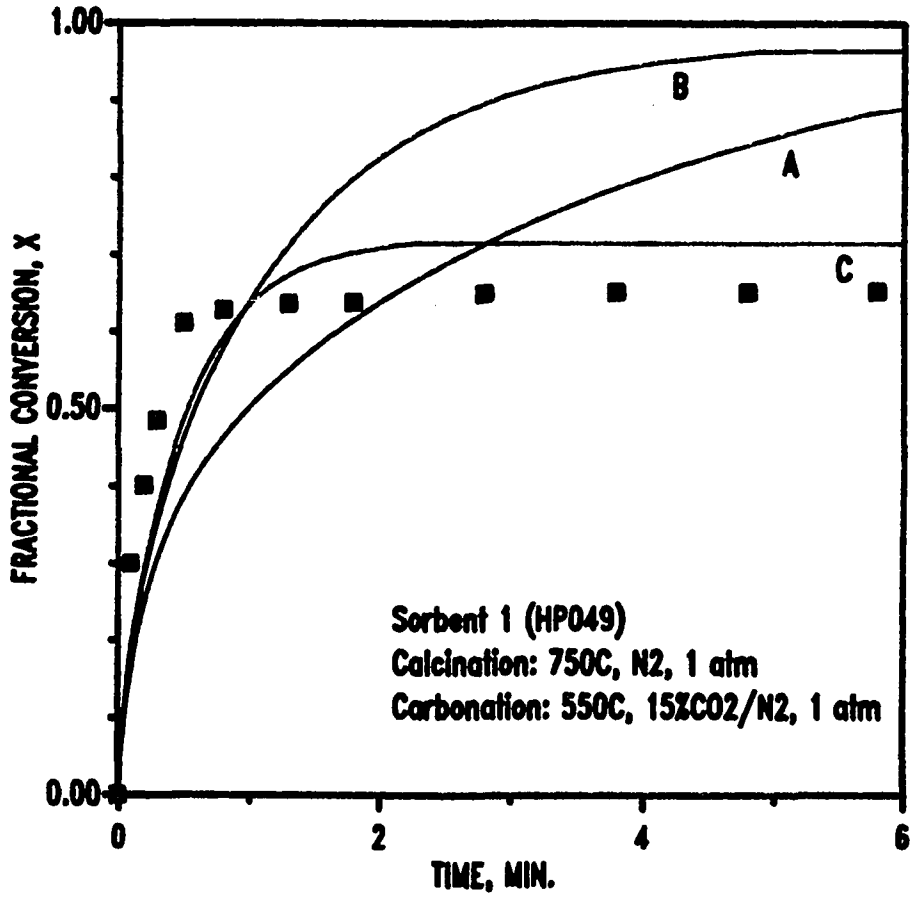

Figure 8.11 Comparison between Model Predictions and Experimental Data for Run HP049; Carbonation at 550°C and 1 atm in 15% CO_2/N_2

A, using the highest activation energies to calculate k and D_s, shows the predicted rate to be slower than the experimental result during early stages of the reaction. However, complete conversion after 16 minutes (not shown) was predicted, in contrast with the experimental data where the final conversion was 0.67 after 55 minutes. When the lower activation energy for product layer diffusivity (21 kcal/mol) and zero activation energy for the reaction rate constant were used (curve B), improved agreement during the early reaction phase was achieved, but complete conversion was predicted after 8 minutes (not shown). Curve C, in which zero activation energies were used to calculate k and D_s provided reasonable agreement throughout the reaction. Pore plugging was predicted after 2.3 min with an overall conversion of 0.72, compared to an experimental conversion of 0.64 at that time.

Figure 8.12 compares predicted maximum conversions from Figures 8.10 and 8.11 with the experimental "maximum" conversion at the three carbonation temperatures. The experimental "maximum" increased with temperature while the predicted maximum decreased with temperature except when zero activation energies were used for both reaction rate constant and product layer diffusivity.

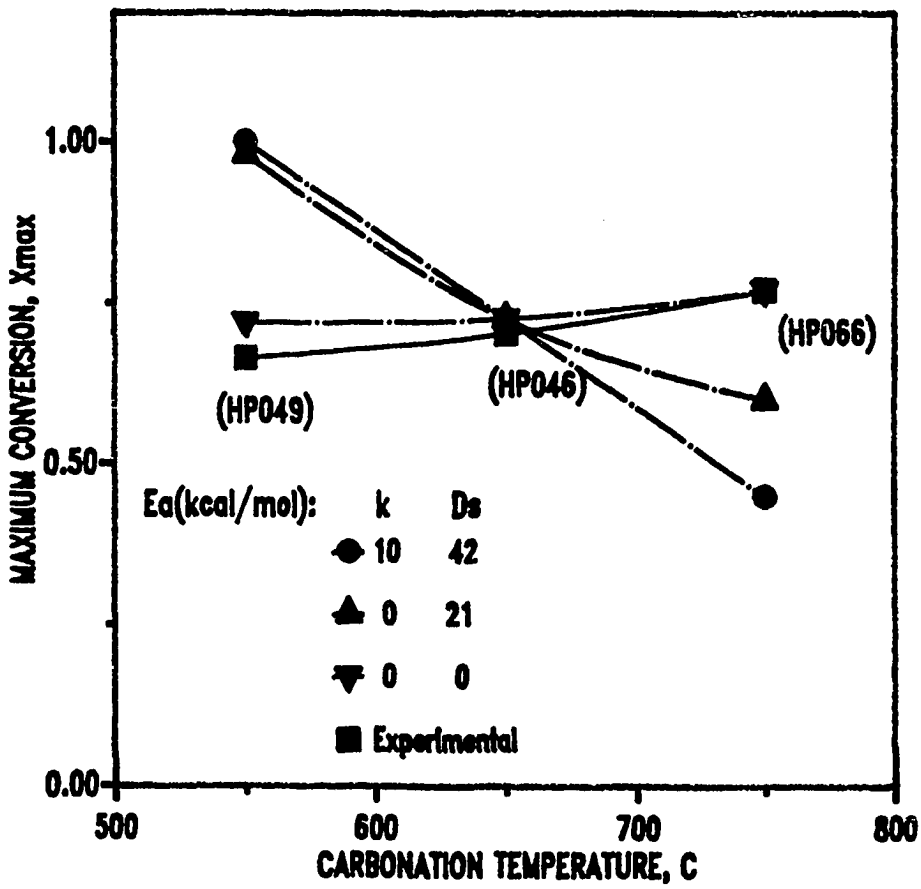

Figure 8.12 Comparison between Predicted Maximum Conversions and Experimental "Maximum" Conversion at Different Carbonation Temperatures

8.6 Model Predictions with No Pore Diffusion Resistance Using a Modified Pore Size Distribution

As discussed previously, the model predicts complete carbonation given sufficient time when the initial porosity is equal to or greater than 0.54 and when pore diffusion resistance is negligible. In the previous section, incomplete conversion due to pore plugging was achieved by arbitrarily reducing D_{c0} to a value several orders of magnitude than expected.

Mercury porosimetry results for calcined CaO from Table 8-2 (Narcida, 1992) showed that the pore volume was primarily associated with pore diameters in the 0.026 - 0.08 μm range, with additional pore volume contributed by pore diameters $\leq$ 0.01 μm. The surface area of the calcined CaO reported by the mercury porosimeter, including the smallest pores with $\leq$ 0.01 μm diameter was 99 m^2/g, well above the measured BET surface area of 18.5 m^2/g (Narcida, 1992). However, if the smaller pores in the $\leq$ 0.026 μm diameter range are ignored, the mercury porosimeter surface area was 22.7 m^2/g, reasonably close to the measured BET surface area.

The reliability of mercury porosimeter results at the high pressure range corresponding to pore diameters less than 0.01 μm is suspect. Sample compression and instrument blank error are known to occur at the highest porosimeter pressures (Micromeritics, 1990). By ignoring the pores in the 0.003 - 0.026 μm diameter range in Table 8-2, the initial pore volume

of CaO is reduced to 0.26 cm^3/g, corresponding to an initial porosity of 0.47. The theoretical maximum conversion is, therefore, limited to 0.74 which is close to the experimentally determined maximum conversion. This modified pore size distribution has been used the following modeling cases.

8.6.1 Base Case Comparison

Figure 8.13 compares the model prediction with the experimental results from the base run (HP046). The model parameters shown in Table 8-4 were used with the exception of the reaction rate constant, k. D_{AB} was estimated from Eq.(8-25) to be 1.08 cm^2/s giving the initial effective diffusivity, D_{e0}, of $1.6x10^{-02}$ cm^2/s. The values of k and D_s were $2x10^{-03}$ cm/s and $2x10^{-09}$ cm^2/s, respectively, chosen to match the experimental data. As seen in Figure 8.13, the predicted conversion-time matched the experimental data quite well during the rapid reaction phase. Both surface reaction and product layer diffusion resistances were important. Due to the fact that pore diffusion resistance within the particle was negligible, the pores filled uniformly leading to the predicted maximum conversion was 0.74 which would be reached in about 2 minutes. At that time the experimental conversion was 0.69. The actual reaction continued at a slow rate and the conversion increased to 0.73 after 40 minutes.

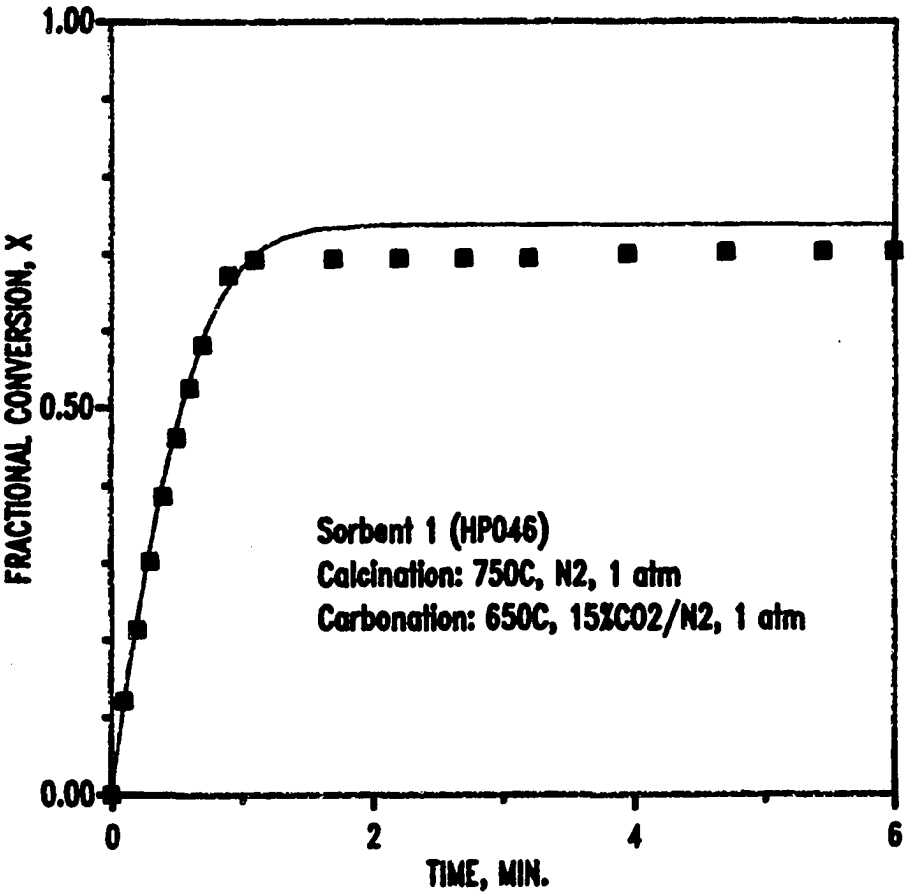

Figure 8.13 Comparison between Model Prediction and Experimental Data of Run HP046 Using Modified Pore Size Distribution

8.6.2 Effect of CO_2 Mol Fraction at Constant Temperature and Pressure

Figure 8.14 compares the model prediction with the experimental data from run HP043 in which the CO_2 mol fraction was reduced to 0.05 at constant carbonation temperature and pressure. The only model parameter to change was the CO_2 mol fraction; other parameter values were the same as shown in Table 8-4 coupled with the values of k, D_{c0}, and D_s used in the previous section. Good agreement between the model and the experiment was achieved for both rapid reaction and slow reaction phases. The predicted pore filling occurred after about 8 minutes. The experimental conversion of 0.73 at 8 minutes was effectively identical to the value of 0.74 predicted by the model.

8.6.3 Effect of Pressure with Constant CO_2 Concentration

Figure 8.15 compares the experimental data of run HP137 with model predictions using three different values of k_g. Calcination was at 750°C and 1 atm in N_2 and carbonation at 650°C and 15 atm in 1% CO_2/N_2. The CO_2 concentration at these conditions was the same the base run using 15% CO_2 and 1 atm (HP046). The value of D_{AB} was reduced to 0.072 cm^2/s (1.08/15) according to Eq.(8-25) which produced a value of D_{c0} = $6.7x10^{-03}$ cm^2/s. Three values of k_g were used in order to match the experimental data. The other model parameters were the same as previously used.

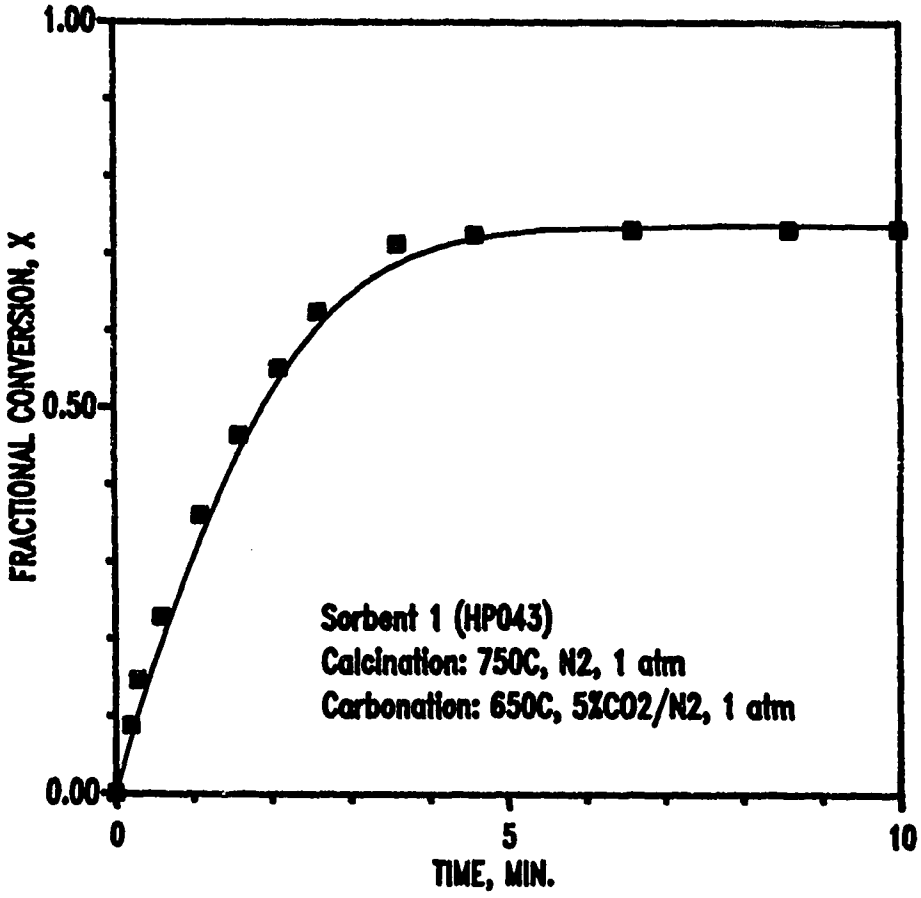

Figure 8.14 Comparison between Model Prediction and the Experimental Data of Run HP043; Effect of CO_2 Mol Fraction, Using Modified Pore Size Distribution

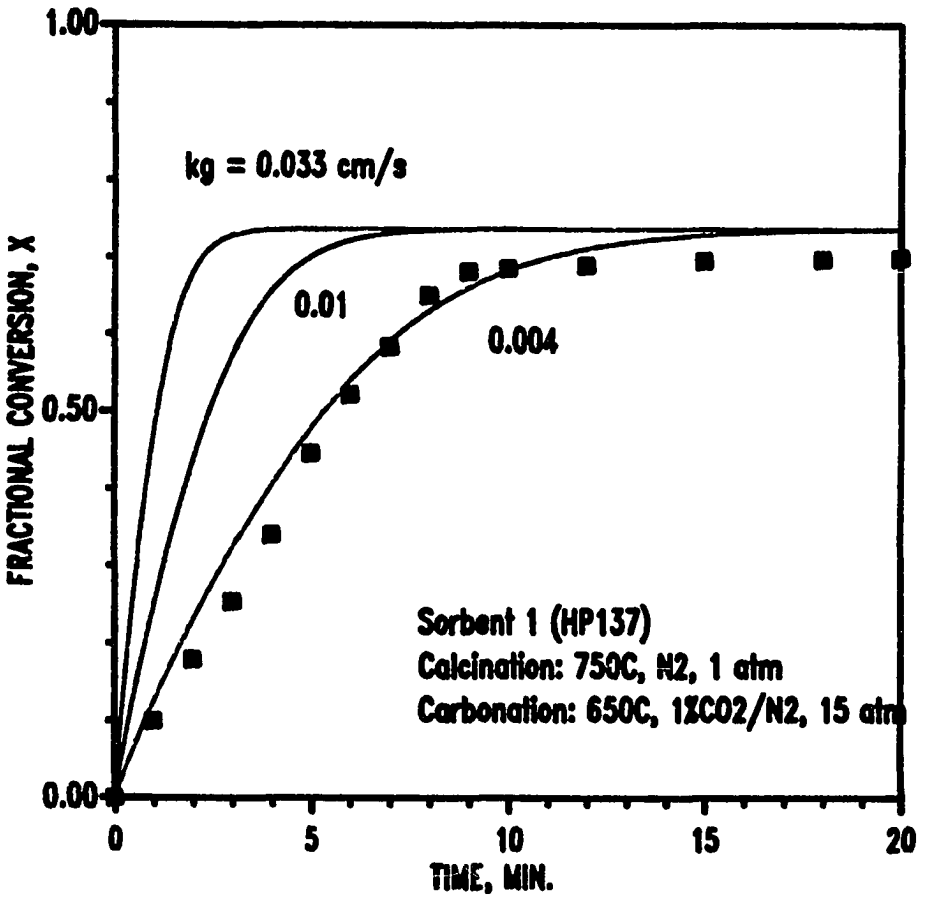

Figure 8.15 Comparison between Model Prediction and Experimental Data of Run HP137; Effect of Carbonation Pressure, Using Modified Pore Size Distribution

As seen in Figure 8.15, the k_g values of 0.033 and 0.01 cm/s used in the previous modeling resulted in a significant difference between the model and experiment during the rapid reaction phase. However, if k_g = 0.004 cm/s was used, quite good agreement between experiment and prediction was achieved. The ratio of initial CO_2 concentration at the particle surface to the effective bulk CO_2 concentration was 0.10, very close to the value of 0.12 associated with k_g = 0.01 cm/s used in the previous section.

8.6.4 Effect of Temperature

The effect of carbonation temperature was examined, as before, using runs HP066 (750°C) and HP049 (550°C). Since pore diffusion resistance was negligible, the theoretical maximum conversion of 0.74 was always achieved given sufficient time regardless the carbonation temperature was used.

Figure 8.16 compares the experimental data to the model predictions using three cases of k and D_s for run HP066, in which carbonation was at 750°C and 1 atm in 15% CO_2/N_2. The model parameters, summarized in Table 8.8, were based upon the same values of activation energy for k and D_s as used in the previous section. For all three cases, the model predicted a faster rate during the early reaction phase than measured experimentally. Curve A, whose k and D_s values were based upon the highest activation energies, exhibited

Table 8-8
Model Parameters Used for Carbonation Reaction
for Run HP066 Using Modified Pore Size Distribution

Symbol	Parameter, units	Value
T	Temperature, °C	750
p_{eq}	CO_2 Equilibrium Pressure, atm	0.082
k_g	Mass Transfer Coefficient, cm/s	0.53
D_{AB}	Bulk Diffusivity, cm^2/s	1.26
D_{c0}	Initial Effective Diffusivity, cm^2/s	$1.7x10^{-02}$
k	Reaction Rate Constant, cm/s	
	Curve A : (E_a = 10 kcal/mol)	$3.4x10^{-03}$
	Curve B : (E_a = 0 kcal/mol)	$2.0x10^{-03}$
	Curve C : (E_a = 0 kcal/mol)	$2.0x10^{-03}$
D_s	Product Layer Diffusivity, cm^2/s	
	Curve A : (E_a = 42 kcal/mol)	$2.1x10^{-08}$
	Curve B : (E_a = 21 kcal/mol)	$6.1x10^{-09}$
	Curve C : (E_a = 0 kcal/mol)	$2.0x10^{-09}$

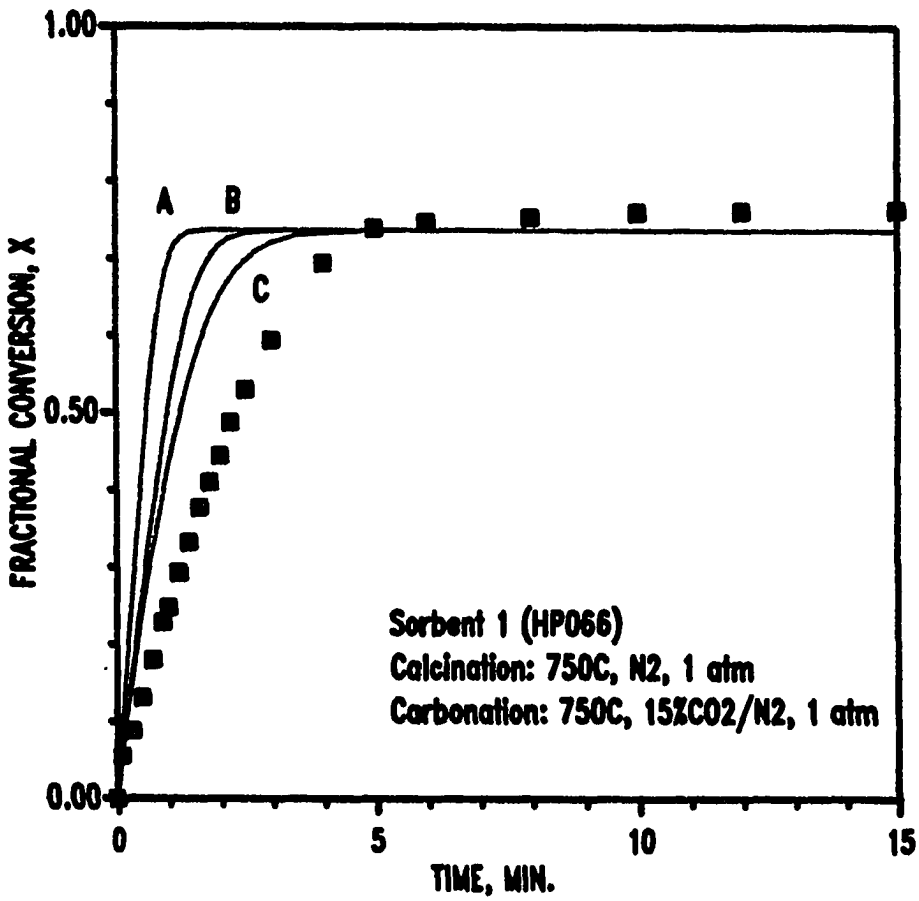

Figure 8.16 Comparison between Model Predictions and Experimental Data for Run HP066; Carbonation at 750°C and 1 atm in 15% CO_2/N_2, Using Modified Pore Size Distribution

the highest initial reaction rate. The maximum conversion of 0.74 associated with complete pore filling was predicted after 1.7 min; the experimental conversion at that time was only 0.4. The maximum conversion from curve B, using zero activation energy for k and an activation energy of 21 kcal/mol for D_s, was predicted after 3 min. The experimental conversion at that time was 0.6. When zero activation energies for both k and D_s were applied, the result is shown in curve C. The theoretical maximum conversion was predicted after 5 minutes, and the experimental conversion at that time was also 0.74.

Comparison between the model predictions and the experimental data for run HP049 using a carbonation temperature of 550°C is shown in Figure 8.17. The model parameters used are summarized in Table 8.9. Curve A, using the highest activation energies to calculate k and D_s values, shows a significantly slower rate than measured experimentally during the early portions of reaction. The maximum conversion of 0.74 was predicted after 19 minutes (not shown) compared to the experimental conversion of 0.66 at that time. Curve B, using zero and 21 kcal/mol activation energies to calculate k and D_s, respectively, predict complete pore filling associated with the maximum conversion of 0.74 after 5 minutes compared to the experimental conversion of 0.65 at that time. Curve C, in which zero activation energies were used to calculate k and D_s, was in

Table 8-9
Model Parameters Used for Carbonation Reaction for Run HP049 Using Modified Pore Size Distribution

Symbol	Parameter, units	Value
T	Temperature, °C	550
p_{eq}	CO_2 Equilibrium Pressure, atm	0.0007
k_g	Mass Transfer Coefficient, cm/s	0.47
D_{AB}	Bulk Diffusivity, cm^2/s	0.91
D_{e0}	Initial Effective Diffusivity, cm^2/s	$1.5x10^{-02}$
k	Reaction Rate Constant, cm/s	
	Curve A : (E_a = 10 kcal/mol)	$1.0x10^{-03}$
	Curve B : (E_a = 0 kcal/mol)	$2.0x10^{-03}$
	Curve C :	$2.0x10^{-03}$
D_s	Product Layer Diffusivity, cm^2/s	
	Curve A : (E_a = 42 kcal/mol)	$1.24x10^{-10}$
	Curve B : (E_a = 21 kcal/mol)	$5.00x10^{-10}$
	Curve C : (E_a = 0 kcal/mol)	$2.0x10^{-09}$

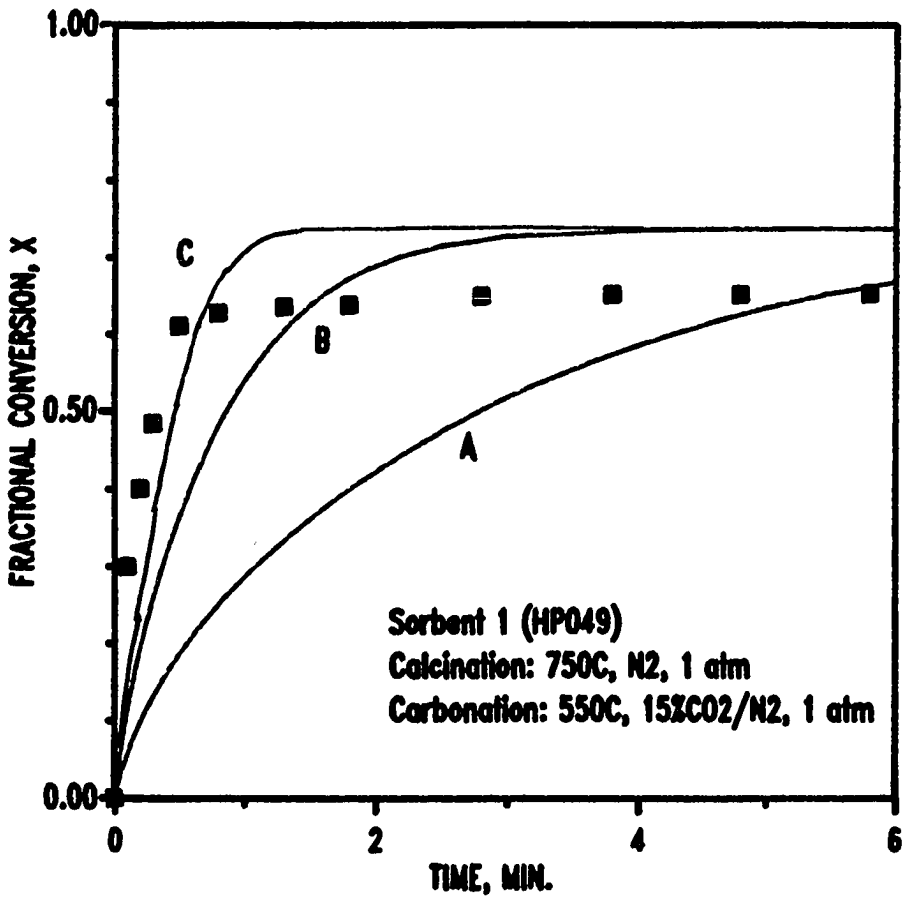

Figure 8.17 Comparison between Model Predictions and Experimental Data for Run HP049; Carbonation at 550°C and 1 atm in 15% CO_2/N_2, Using Modified Pore Size Distribution

reasonably good agreement with the experiment during the early reaction phase. The maximum conversion of 0.74 was predicted after about 2 minutes, compared to the experimental conversion of 0.64 at that time.

8.7 Summary

The distributed pore size model has been used to describe the experimental data for the carbonation reaction of sorbent 1. This sorbent was chosen because of its well defined structural properties and noticeably incomplete conversion during the reaction.

The initial pore size distribution of calcined CaO reported by Narcida (1992) produced an initial porosity of 0.548. The pore volume was primarily associated with pore diameters of 0.02 - 0.08 μm with a small additional pore volume in the $\leq$ 0.01 μm diameter range.

The model parameters were first estimated using literature values, diffusion theory, and literature correlations. With this approach, it was found that pore diffusion resistance within the particle was negligible. As a result, based upon the initial porosity of 0.548, complete carbonation was always predicted given sufficient time. The only way to predict incomplete conversion was to force the pore diffusion resistance to become important by using a very small value of the initial effective diffusivity, D_{c0}.

Incomplete conversion was predicted using the "new" D_{e0} and "reasonable" model parameters were found which resulted in good agreement between model and experiment for a base run in which carbonation was carried out at 650°C and 1 atm in 15% CO_2/N_2. When these model parameters were used to examine the effect of CO_2 mol fraction at constant temperature and pressure, the agreement between the model and experiment was quite good. Qualitative agreement between the model and experiment was also found when the effect of pressure at constant temperature and CO_2 concentration was modelled using a "best-fit" mass transfer coefficient. The effect of carbonation temperature was modelled reasonably well when both intrinsic rate constant and product diffusion coefficient were taken to be independent of temperature.

An alternative approach in which the initial pore size distribution was modified by neglecting pore volume associated with pore diameters less than 0.026 μm was also used to model the data. The initial porosity of the CaO was reduced to 0.47. Based on this value, the theoretical maximum conversion of 0.74 was close to the experimentally determined maximum conversion. This maximum conversion was associated with uniform filling of the pores along their length and was achieved when pore diffusion resistance was negligible. The modification of the initial pore size distribution was justified on the basis of sample compression and instrument blank error which occur at the highest porosimeter pressures.

The model predictions using the modified pore size distribution showed good agreement with the experimental results of the base case. "Best-fit" values of k and D_s were practically the same as those using the original pore size distribution. Also good agreement between prediction and experiment was found in examining the effect of CO_2 mol fraction at constant temperature and pressure. Using the "best-fit" mass transfer coefficient, k_g, agreement was also obtained between model experiment when the carbonation pressure was increased. In order to model the effect of carbonation temperature, it was again necessary to assign zero activation energies to the intrinsic rate constant and product layer diffusion coefficient.

In summary, neither approach was completely satisfactory in modeling the experimental results. Good agreement between the model prediction and experiment was achieved for runs at 650°C. However, the absence of a strong temperature effect could only be matched by assigning zero activation energies to k and D_s, both of which should have quite large activation energies.

Chapter 9

Conclusions and Recommendations for Future Work

Advantages associated with the high temperature removal of CO_2 from coal gas before further processing include increased heating value of the fuel gas, increased efficiency of the shift conversion process for production of hydrogen or methanol and ammonia synthesis gas, and improved efficiency of molten carbonate fuel cells.

A potential application of particular interest is a combination of the water-gas shift reaction with CO_2 removal in one reactor, thereby providing for the direct production of hydrogen in a single-step process. Such a process would be much simpler and potentially less expensive than the current multi-step catalytic processes for hydrogen production.

The removal of CO_2 using regenerable calcium-based sorbents at high temperature and high pressure has been investigated in this study. CO_2 removal is based upon the noncatalytic gas-solid reaction between CO_2 from the coal gas and CaO-based sorbents to produce $CaCO_3$ according to

$$CaO_{(s)} + CO_{2(g)} \leftrightarrow CaCO_{3(s)}$$

The forward (carbonation) reaction is favored by high pressure and is feasible in the temperature range of 550-750°C. Approximately 99.6% CO_2 removal from a coal gas

containing 15%(vol) CO_2 at 15 atm and 650°C is theoretically possible. Accordingly, the reverse (calcination) reaction is favored by lower pressure, higher temperature, and/or lower CO_2 pressure.

A high-pressure thermobalance reactor was used to study the kinetics of the calcination and carbonation reactions as a function of temperature, pressure, CO_2 concentration, and background gas composition. A number of CaO-based sorbent precursors were studied and multicycle calcination and carbonation runs were carried out in order to have a better understanding of sorbent durability, a very important property in a commercial process.

Three out of nine sorbent precursors were selected for detailed kinetic studies. They were (i) reagent grade calcium carbonate (sorbent 1) considered as the standard or reference sorbent, (ii) reagent grade calcium acetate (sorbent 7), and (iii) commercial grade dolomite (sorbent 9) having essentially equimolar quantities of $MgCO_3$ and $CaCO_3$. The three sorbent precursors produced a wide range of structural properties following calcination (Narcida, 1992).

In particular, calcination of the three sorbents produced different pore volumes and pore size distributions. In sorbent 7, the pore volume was created first by driving off the water of hydration, then decomposing the calcium acetate to calcium carbonate, and finally decomposing calcium carbonate to calcium oxide. The pore volume in sorbent 9 was

created by decomposing both $MgCO_3$ and $CaCO_3$. Since MgO, at the carbonation conditions of interest, was inert, "excess" pore volume created by $MgCO_3$ decomposition allowed the complete carbonation of CaO. The pore volume in sorbent 1, on the other hand, was created only by decomposing $CaCO_3$; therefore, no "excess" pore volume was available.

Carbonation of sorbent 1 was characterized by an initial rapid reaction followed by an abrupt transition to a slow reaction well before complete carbonation. The maximum fractional conversion which could be achieved was only about 0.75. In contrast, almost complete carbonation of CaO to $CaCO_3$ was possible using both sorbents 7 and 9. These reactivity differences may be attributed directly to the different structural properties of the calcined sorbents.

Two-cycle calcination-carbonation kinetics of the three sorbent precursors as a function of temperature, pressure, and CO_2 mol fraction in N_2 were investigated. Calcination temperatures of 750, 825, and 900°C, carbonation temperatures of 550, 650, and 750°C, calcination pressure of 1 atm, carbonation pressures of 1, 5, and 15 atm, and CO_2 mol fractions of 0.01, 0.05, and 0.15 were used. Reactivity and capacity indices were defined in order to permit direct comparison of the experimental results. The following conclusions were reached:

(1) Calcination at 900°C produced a significant adverse effect on carbonation performance for all three sorbents. In

particular, the second-cycle carbonation performance deteriorated due to sintering at the high calcination temperature. Calcination at 750°C resulted in better carbonation capacity maintenance for all sorbents.

(2) Carbonation at 650 to 750°C was found to be favorable in term of reactivity, capacity, and capacity maintenance. Carbonation at 550°C unexpectedly showed a significant drop in capacity maintenance compared to the higher temperatures. This adverse behavior may be due to the different structure of the product carbonate formed at high and low temperature (Bhatia and Perlmutter, 1983; Mess, 1989).

(3) Sorbent reactivity decreased with increasing carbonation pressure. Transport resistances were important in establishing reactivity, particularly at high pressure. Carbonation pressure had little effect on sorbent capacity in either cycle, or on capacity maintenance.

(4) CO_2 mol fraction had an effect only on reactivity. As expected, the reactivity increased with increasing CO_2 mol fraction. Sorbent capacity, on the other hand, was independent of CO_2 mol fraction.

(5) Sorbents 7 and 9 had a clear advantage over sorbent 1 in terms of both capacity and capacity maintenance. Sorbents 7 and 9 were somewhat more reactive in both cycles than sorbent 1. There were no significant reactivity

differences between sorbents 7 and 9, although the reactivity maintenance of sorbent 7 was slightly higher than sorbent 9.

The experimental study was then extended to multicycle runs in which the effects of calcination pressure, carbonation temperature, and background gas composition were investigated using the three sorbent precursors. The following conclusions were reached:

(1) Sorbent 1 exhibited the lowest reactivity maintenance and capacity maintenance after being subjected to five-cycle runs. Sorbent 7 had the highest calcium utilization in the first cycle, but experienced a gradual decrease in capacity with increasing number of cycles. Sorbent 9 was the best sorbent in terms of reactivity maintenance and capacity maintenance.

(2) Calcination at 15 atm was feasible at a temperature of 750°C. Moreover, reactivity, capacity, and capacity maintenance for the subsequent carbonation reaction showed no adverse effect of high calcination pressure.

(3) The addition of H_2O, CO, and H_2 to simulate a sulfur-free coal-gas resulted in improved sorbent reactivity, capacity, and durability. Importantly, the increase in carbonation reactivity was consistent with a higher concentration of CO_2 formed by the water-gas shift reaction.

(4) The addition of H_2S to the simulated coal gas caused a rapid and irreversible deterioration in carbonation capacity because of the irreversible $CaO + H_2S$ reaction to

form CaS. In addition, H_2S was capable of displacing previously formed carbonate ($CaCO_3$) to form CaS. A prior desulfurization step would be required before the regenerable calcium-based sorbent process could be used commercially for CO_2 removal. Simultaneous CO_2 - H_2S removal could be carried out if the sorbent was used on a once-through basis or for a small number of cycles.

A few ten-cycle runs using sorbents 7 and 9 were also carried out. Sorbent 7 suffered a small capacity loss in each cycle with the capacity decrease over ten cycles less than 10%. Sorbent 9 possessed superior durability. The capacity in the tenth cycle was only about 3% lower than in the first cycle.

The distributed pore size distribution model developed by Christman and Edgar (1983) was chosen to model the carbonation reaction for sorbent 1. The initial pore size distribution reported by Narcida (1992) was used. When a priori best estimates of the model parameters were used, complete conversion was predicted given sufficient time since pore diffusion resistance within the particle was negligible. By forcing the initial effective diffusivity, D_{e0}, to a very small value (i.e. forcing pore diffusion resistance to become important), pore plugging was predicted at the outer surface, leaving inaccessible unreacted solid inside the particle. Using this approach, good agreement between the model and

experiment was achieved for runs at 650°C and varying pressure and CO_2 concentration.

The pore size distribution was then modified by neglecting pores whose diameters were less than 0.026 μm and the modeling was repeated. This reduced the initial porosity of the sorbent from 0.548 to 0.47, which limited the maximum fractional conversion to 0.74. With a negligible pore diffusion resistance, this maximum fractional conversion, which was always predicted, was in reasonably good agreement with the experimental data.

Neither approach was completely satisfactory when the model was applied at different carbonation temperatures. The absence of strong temperature effect, which was observed experimentally, could only be matched by assigning zero activation energies to the intrinsic rate constant and the product layer diffusion coefficient, both of which should have quite large activation energies.

Based on the above conclusions, the following recommendations for future work are offered.

(1) One of interesting results from this study was the indirect evidence of the simultaneous water-gas shift reaction and CO_2 removal taking place at high temperature. This should be confirmed by performing studies using a small fixed-bed reactor having capability for inlet and outlet gas analysis. Simultaneous occurrence of the two reactions could

provide an alternate method for H_2 synthesis in which H_2 could be produced at high temperature in a simple one-step process.

(2) Dolomite with equimolar quantities of $MgCO_3$ and $CaCO_3$ showed superior carbonation capacity maintenance after multicycle runs. However, MgO present in the sorbent lowered the CO_2 capacity per gram of sorbent. Studies on the effect of MgO concentration would be beneficial in a number of areas. Reducing the MgO content would be desirable from the capacity standpoint but less "excess" pore volume would be created. Another important question is whether the sole function of $MgCO_3$ is simply to create excess pore volume or does it also stabilize the sorbent for multicycle runs. In addition, this work would be help to answer the question of whether MgO serves as a catalyst for the water-gas shift reaction.

(3) One particular dolomite from National Lime, Co., Findley, Ohio, was used in this study. Since dolomites having different properties are available throughout the country, a screening study should be conducted to determine if favorable reaction characteristics are a general property of all dolomites, or if careful selection of particular dolomites will be required.

(4) A preliminary design study and economic analysis should be conducted to determine the commercial potential of hydrogen production via the simultaneous water-gas shift reaction and CO_2 separation at high temperature and high

pressure. Results should be compared to a conventional hydrogen production process using two stages of water-gas shift reactors with either pressure swing adsorption or CO_2 scrubbing for hydrogen purification.

References

Anderson, T.F., Self-Diffusion of Carbon and Oxygen in Calcite by Isotope Exhange with Carbon Dioxide, *Journal of Geophysical Research,* **74,** 3918 (1969)

Ausman, J. M. and C. C. Watson, Mass Transfer in a Catalyst Pellet during Regeneration, *Chem. Engng Sci.,* **17,** 323 (1962)

Barin, I. and O. Knacke, **Thermochemical Properties of Inorganic Substances,** Springer-Verlag, New York (1973)

Barker, R., The Reversibility of the Reaction $CaCO_3$ = CaO + CO_2, *J. Appl. Chem. Biotechnol.,* **23,** 733 (1973)

Barker, R., The Reactivity of Calcium Oxide Towards Carbon Dioxide and Its Use for Energy Storage, *J. Appl. Chem. Biotechnol.,* **24,** 221 (1974)

Beruto, D., M. Kim, and A. Searcy, Microstructure and Reactivity of Porous and Ultrafine CaO Particles with CO_2, *High Temperature - High Pressures,* **20,** 25 (1988)

Bethea, R. M., B. S. Duran, and T. L. Boullion, **Statistical Methods for Engineers and Scientists,** Marcel Dekker, Inc., New York (1979)

Bhatia, S. K. and D. D. Perlmutter, A random Pore Model for Fluid-Solid Reactions: I. Isothermal, Kinetic Control, *AIChE J.,* **26,** 379 (1980)

Bhatia, S. K. and D. D. Perlmutter, A random Pore Model for Fluid-Solid Reactions: I. Diffusion and Transport Effects, *AIChE J.,* **27,** 247 (1981)

Bhatia, S. K. and D. D. Perlmutter, Effect of the Product Layer on the Kinetics of CO_2 - Lime Reaction, *AIChE J.,* **29,** 79 (1983)

Bird, R. B., W. E. Stewart, and E.N. Lighfoot, **Transport Phenomena,** John Wiley and Sons, Unc., New York (1960)

Borgwardt, R. H., Sintering of Nascent Calcium Oxide, *Chem. Engng Sci.,* **44,** 53 (1989)

Buckman, J.W., E.C. Perko, E. Castorina, R.L. Hails, and A.E. Cover, Proceedings of the Eighth Annual Gasification and Gas Stream Cleanup Systems Contractors Review Meeting, Vol. 1, DOE/METC-88/6092, p. 1. (1988)

Cook, C.S., E. Gal, A.H. Furman, and R. Ayala, Proceedings of the Eighth Annual Gasification and Gas Stream Cleanup Systems Contractors Review Meeting, Vol. 1, DOE/METC-88/6092, p. 11. (1988)

Christman, P. G., Analysis of Simultaneous Diffusion and Chemical Reaction in the Calcium Oxide/Sulfur Dioxide System, Ph.D. Dissertation, The University of Texas, Austin (1981)

Christman, P. G. and T. F. Edgar, Distributed Pore-Size Model for Sulphation of Limestone, *AIChE J.*, **29,** 388 (1983)

Chrostowski, J. W. and C. Georgakis, Pore Plugging Model for Gas-Solid Reactions, **Proc. 5th Int. Symp. Chem. Reaction Engng, Houston, Texas,** p. 225 (1978)

Curran, G. P., C. E. Fink, and E. Gorin, CO_2 Acceptor Gasification Process: Studies of Acceptor Properties, in **Advances in Chemistry, 69,** Fuel Gasification, edited by F. C. Schora, p. 141, American Chemical Society, Washington, D. C. (1967)

Dedman, A. J. and A. J. Owen, Calcium Cyanide Synthesis. Part 4 - The Reaction $CaO + CO_2 <==> CaCO_3$, *Trans. Farad. Soc.*, **58,** 2027 (1962)

DeLucia, D. E., The Cyclic Use of Limestone to Capture CO_2, M.Sc. Thesis, Massachusetts Institute of Technology (1985)

Dhupe, A. P., V. K. Jayaraman, A. N. Gokarn, and L. K. Doraiswamy, Effect of Inert in Gas-Solid Reactions, *Chem. Engng Sci.*, **42,** 2285 (1987)

Dhupe, A. P. and A. N. Gokarn, Use of Inert Solids in Some Industrially Important Gas-Solid Reactions, *Ind. Eng. Chem. Res.*, **29,** 784 (1990)

Dogu, T., The Importance of Pore Structure and Diffusion in the Kinetics of Gas-Solid Non-Catalytic Reactions: Reaction of Calcined Limestone with SO_2, *Chem. Eng. Journ.*, **21,** 213 (1981)

Dudukovic, M. P., A note on Gas-Solid Noncatalytic Reactions, *AIChE J,* **22,** 945 (1976)

Focht, G.D., P.V. Ranade, and D.P. Harrison, High Temperature Desulfurization Using Zinc Ferrite: Reduction and Sulfidation Kinetics, *Chem. Engng Sci.*, **43,** 3005 (1988)

Focht, G.D., P.V. Ranade, and D.P. Harrison, High Temperature Desulfurization Using Zinc Ferrite: Regeneration Kinetics and Multicycle Testing, *Chem. Engng Sci.*, **44,** 2919 (1989)

Froment, G. F. and K. B. Bischoff, **Chemical Reactor Analysis and Design,** John Wiley and Sons, Inc., Second Edition, New York (1990)

Fuertes, A. B., D. Alvarez, F. Rubiera, J. J. Pis, and J. M. Palacios, Surface Area and Pore Size Changes During

Sintering of Calcium Oxide Particles, *Chem. Eng. Comm.*, **109,** 73 (1991)

Gangwal, S.K., S.M. Harkin, J.M. Stogner, and M.C. Woods, Multicycle Testing of Zinc Ferrite, Final Report DOE/MC/23162-2662 (1988)

Gangwal S.K., S.M. Harkin, M.C. Woods, S.C. Jain, S.J. Bossart, Bench-Scale Testing of High-Temperature Desulfurization Sorbents, *Environ. Prog.*, **8,** 265 (1989)

Gauthier, A., *Bull. Soc. Chim.*, **35, 929,** from **Chemical Abstract, 1,** 274 (1909)

Gavalas, G. R., A Random Capillary Model with Application to Char Gasification at Chemically Controlled Rates, *AIChE J.*, **26,** 577 (1980)

Georgakis, C., W. Chang, and J. Szekely, A Changing Grain Size Model for Gas-Solid Reactions, *Chem. Engng Sci.*, **34,** 1072 (1979)

Gibson, J.B. and D.P. Harrison, The Reaction Between Hydrogen Sulfide and Spherical Pellets of Zinc Oxide, *Ind. Eng. Chem. Proc. Des. Dev.*, **19,** 231 (1980)

Gluud, W., K. Keller, R. Schonfelder, and W. Klempt, Production of Hydrogen, *U.S. Patent 1,816,523* (1931)

Grindley, and Steinfeld, Development and Testing of Regenerable Hot Coal Gas Desulfurization Sorbents, Final Report, DOE/METC/16545-1125 (1981)

Hartman, M. and R. W. Coughlin, Reaction of Sulfur Dioxide with Limestone and Influence of Pore Structure, *Ind. Eng. Chem. Proc. Des. Dev.*, **13,** 248 (1974)

Hartman, M. and R. W. Coughlin, Reaction of Sulfur Dioxide with Limestone and the Grain Model, *AIChE J.*, **22,** 490 (1976)

Hartman, M., J. Pata, and R. W. Coughlin, Influence of Property of Calcium Carbonates on Their Reactivity with Sulfur Dioxide, *Ind. Eng. Chem. Proc. Des. Dev.*, **17**, 411 (1978)

Hauserman, W.B., A. Lee, S.J. Meyer, and G. Steinfield, Proceedings of the Eleventh Annual Gasification and Gas Stream Cleanup Systems Contractors Review Meeting, DOE/METC-91/6123, Vol.1, 323-331 (1991)

Holt, N., Gasification Power Plants: Highly Efficient Advanced Cycles, *EPRI Journal*, April/May , 40 (1991)

Hougen, O. A., K. M. Watson, and R. A. Ragatz, **Chemical Process Principles, Part II: Thermodynamics**, Second Edition, John Wiley and Sons, New York (1959)

Hughmark, G. A., Mass and Heat Transfer from Rigid Sphere, *AIChE J*, **13**, 1219 (1967)

Kronenberg, A. K., R. A. Yund, and B. J. Gilleti, Carbon and Oxygen Diffusion in Calcite; Effects of Mn Content and P_{H2O}, *Physics and Chemistry of Mineral*, **11**, 102 (1984)

Lamoreaux, R. H., R. Brittain, S. Leach, and G. Tong, Determination of Solid Phase Boundaries in Coal Gas Desulfurization by Zinc Ferrite, Final Report, DE-AC21-84MC21096 (1986)

Lee, H. H., Simple Conversion Relationships for Noncatalytic Gas-Solid REactions, *Ind. Eng. Chem. Proc. Des. Dev.*, **19**, 242 (1980)

Lew, S., High-Temperature Sulfidation and Reduction of Zinc Titanate and Zinc Oxide Sorbents, Ph.D. Dissertation, Massachussetts Institute of Technology, Cambridge, MA (1990)

Lew, S., A.F. Sarofim, and M. Flytzani-Stephanopoulos, The Reduction of Zinc Titanate and Zinc Oxide Solids, *Chem. Engng Sci.*, **47**, 1421 (1992a)

Lew, S., A.F. Sarofim, and M. Flytzani-Stephanopoulos, Modeling of the Sulfidation of Zinc-Titanium Oxide Sorbents with Hydrogen Sulfide, *AIChE J.*, **38**, 1161 (1992b)

Mess, D., Product Layer Diffusion in the Carbonation of Calcium Oxide, Ph. D. Thesis, Massachusetts Institute of Technology, Cambridge, MA (1989)

Micromeritics, Operator's Manual - Autopore II 9220, Norcross, Ga (1990)

Narcida, M. V., Structural Properties of Calcium-Based Sorbents Used for High Temperature CO_2 Separation, M.S. Thesis, Louisiana State University, Baton Rouge (1992)

Oakeson, W. G. and I. B. Cutler, Effect of CO_2 Pressure on the Reaction with CaO, *J. Am. Ceram. Soc.*, **62**, 556 (1979)

Petersen, E. E., Reactions in Porous Solids, *AIChE J.*, **3**, 443 (1957)

Ramachandran, P. A. and J. M. Smith, A Single-Pore Model for Gas-Solid Noncatalytic Reactions, *AIChE J.*, **23**, 353 (1977)

Ranade, P.V. and D.P. Harrison, The Grain Model Applied to Porous Solids with Varying Structural Properties, *Chem. Engng Sci.*, **34**, 427 (1979)

Ranade, P.V. and D.P. Harrison, The Variable Property Grain Model Applied to the ZnO-H_2S Reaction, *Chem. Engng Sci.*, **36**, 1079 (1981)

Reyes, S. and K. F. Jensen, Percolation Concept in Modeling of Gas-Solid Reactions - III: Application to Sulphation of Calcined Limestone, *Chem. Engng Sci.*, **42**, 565 (1987)

Robin, A.M., J. C. Wu, and M. S. Najjar, Proceedings of the Eighth Annual Gasification and Gas Stream Cleanup Systems Contractors Review Meeting, Vol. 1, DOE/METC-88/6092, p. 21. (1988)

Rofer-Depoorter, C., Untangling the Water Gas Shift from Fischer-Tropsch, in **Catalytic Conversions of Synthesis Gas and Alcohols to Chemicals,** R.G. Herman, ed., Plenum Press, New York, p. 97 (1984)

Sahimi, M., G. R. Gavalas, and T. T. Tsotsis, Review Article Number 32: Statistical and Continuum Models of Fluid-Solid Reactions in Porous Media, *Chem. Engng Sci.*, **45**, 1443 (1990)

Satterfield, C. N., **Mass Transfer in Heterogneous Catalysis,** MIT Press, Cambridge, Mass. (1970)

Schechter, R. S. and J. L. Giley, The Change in Pore Size Distribution from Surface Reactions in Porous Media, *AIChE J,* **15,** 339 (1969)

Schmidt, D.K., G.B. Haldipur, K.J. Smith, S. Datta, and P. Cherish, Proceedings of the Eighth Annual Gasification and Gas Stream Cleanup Systems Contractors Review Meeting, Vol. 1, DOE/METC-88/6092, p.32 (1988)

Shankar, K. and Y. C. Yortsos, Asymptotic Analysis of Single Pore Gas-Solid Reactions, *Chem. Engng Sci.*, **38,** 1159 (1983)

Silaban, A., D.P. Harrison, M.H. Berggren, and M.C. Jha, The Reactivity and Durability of Zinc Ferrite High Temperature Desulfurization Sorbents, *Chem. Eng. Comm.*, **107,** 55-71 (1991)

Sohn, H. Y. and J. Szekely, A Structural Model for Gas-Solid Reactions with a Moving Boundary. III: A General Dimensionless Representation of the Irreversible Reaction between a Porous Solid and a Reactant Gas, *Chem. Engng Sci.*, **27,** 763 (1972)

Sotirchos, S. V. and H. C. Yu, Mathematical Modelling of Gas-Solid Reactions with Solid Products, *Chem. Engng Sci.*, **40,** 2039 (1985)

Sotirchos, S. V. and H. C. Yu, Overlapping Grain Models for Gas-Solid Reactions with Solid Product, *Ind. Eng. Chem. Res.*, **27,** 836 (1988)

Squires, A.M., Cyclic Use of Calcined Dolomite to Desulfurize Fuels Undergoing Gasification, in Advances in Chemistry, **69,** Fuel Gasification, F.C. Schora, ed., American Chemical Society, Washington, D.C., p.205 (1967)

Szekely, J., C. I. Lin, and H. Y. Sohn, A Structural Model for Gas-Solid Reactions with a Moving Boundary. V. An Experimental Study of the Reduction of Porous Nickel-Oxide Pellets with Hydrogen, *Chem. Engng Sci.*, **28,** 1975 (1973)

Szekely, J. and J. W. Evans, A Structural Model for Gas-Solid Reactions with a Moving Boundary, *Chem. Engng Sci.*, **25,** 1091 (1970)

Szekely, J. and J. W. Evans, A Structural Model for Gas-Solid Reactions with a Moving Boundary. II. The Effect of Grain Size, Porosity, and Temperature in the Reaction of Porous Pellets, *Chem. Engng Sci.*, **26,** 1901 (1970)

Ulerich, N. H., E. P. O'Neill, and D. L. Keairns, A Thermogravimetric Study of the Effect of Pore Volume-Pore Size Distribution on the Sulfation of Calcined Limestone, *Thermochimica Acta,* **26,** 269 (1978)

Weast, Handbook of Chemistry and Physics, 70th Ed., CRC Press, Boca Raton, Fl (1989)

Wen, C. Y., Noncatalytic Heterogeneous Solid Fluid Reaction Models, *Ind. Engng. Chem.*, **60,** 34 (1968)

Westmoreland, P.R. and D.P. Harrison, Evaluation of Candidate Solids for High-Temperature Desulfurization of Low Btu Gases, *Environ.Sci.Technol.*, **10,** 659-660 (1976)

Westmoreland, P.R., J.B. Gibson, and D.P. Harrison, Comparative Kinetics of High-Temperature Desulfurization of Low-Btu Gases, *Environ.Sci.Technol.*, **11,** 488 (1977)

Woods, M. C., S.K. Gangwal, D.P. Harrison, and K. Jothimurugesan, Kinetics of the Reactions of Zinc Ferrite Sorbent in High-Temperature Coal Gas Desulfurization, *Ind.Eng.Chem.Res.*, **30,** 100 (1991)

Woods, M.C., S.K. Gangwal, K. Jothimurugesan, and D.P. Harrison, Reaction between H_2S and Zinc Oxide-Titanium Oxide Sorbents. 1. Single-Pellet Kinetics Studies, *Ind.Eng.Chem.Res.*, **29,** 1160 (1990)

Yagi, S. and D. Kunii, Fifth International Symposium on Combustion, Reinhold, New York, p.231 (1955)

Yortsos, Y. C. and M. M. Sharma, Application of Percolation Theory to Non-catalytic Gas-Solid Reactions, *AIChE J.*, **32,** 46 (1986)

Yu, H. C. and S. V. Sotirchos, A Generalized Pore Model for Gas-Solid Reactions Exhibiting Pore Closure, *AIChE J.*, **33,** 382 (1987)

Nomenclature

C_b	bulk reactive gas concentration, mol/cm^3
C_{eq}	equilibrium reactive gas concentration, mol/cm^3
C_0	effective gas concentration, mol/cm^3
$C(r_2)$	gas concentration at the reaction interface, mol/cm^3
D_{AB}	bulk diffusivity of gas mixture, cm^2/s
D_c	combined bulk and Knudsen diffusivity, cm^2/s
D_e	effective diffusivity, cm^2/s
D_K	Knudsen diffusivity, cm^2/s
D_S	product layer diffusivity, cm^2/s
E_a	activation energy, kcal/mol
k	surface reaction rate constant, cm/s
K_a	overall equilibrium for combined reactions as defined in Eq.(1-5)
K_e	effective reactivity, 1/s
k_g	mass transfer coefficient, cm/s
K_{pi}	equilibrium constant for reaction i
l	cylindrical pore length between R and (R+dR), cm
M_A	molecular weight of species A, g/gmol
p	total pressure, atm
p_i	partial pressure of component i, atm
p_{eq}	equilibrium pressure of reractive gas, atm
r_0	initial pore radius, cm
r_1	pore radius, cm
r_2	radius of product-reactant interface, cm

R	radial position of in particle, cm
R_0	initial radius of particle, cm
T	temperature, K
t	time, s
V_A, V_B	molar volumes of solid reactant A and solid product B, cm^3/mol
y_i	mol fraction of reactive gas i
α	ratio of molar volume of solid product and solid reactant
β_i	stoichiometric coefficient of component i
δ_1	distance between the original pore wall (at time = 0) and the current pore wall (at time = t) in the Single Pore Model
δ_2	distance between the original pore wall (at time = 0) and the current reaction interface in the Single Pore Model
ϵ	porosity of porous matrix
ϵ_0	initial porosity of solid reactant
ζ	tortuosity
λ	dimensionless constant defined in Eq.(8-10)
η_1	number of pores intersecting a unit area per unit radius (r_1) of cylindrical pore
μ_G	bulk gas viscosity, $g/cm^2.s$
ρ	mass density of solid reactant, g/cm^3
ρ_G	bulk gas density, g/cm^3
σ_{AB}	Lennard-Jones parameter, Å
τ	cummulative gas concentration defined in Eq.(8-7), s
φ	net function of pores gained via birth and death

ψ void area per unit area defined in Eq.(8-13)

$\Omega_{D,AB}$ dimensionless function of temperature and of the intermolecular potential field for one molecule of A and one of B

Appendix A

Master List of Runs

Run	Sorbent	Initial Weight (mg)	Calcination			Carbonation			Number of Cycle
			Temp. (°C)	Gas	Press. (atm)	Temp. (°C)	Gas	Press. (atm)	
HP146	9	12.57	750	N	1	750	A	1	5
HP147	7	12.66	750	N	1	650	A	1	5
HP148	1	11.29	750	N	1	750	A	1	5
HP149	7	12.36	750	N	1	750	A	1	5
HP150	CMA	19.44	750	N	1	750	A	1	2
HP151	CMA	12.50	750	N	1	750	A	1	5
HP152	CMA	12.54	750	N	1	750	A	1	2
HP153	9	12.67	750	N	15	750	A	15	5
HP154	9	12.42	750	N	15	650	A	15	5
HP155	7	12.90	750	N	15	650	A	15	5
HP156	7	12.35	750	N	15	750	A	15	5
HP157	7	12.32	750	N	1	650	A	15	5
HP158	7	12.48	750	N	1	750	B	1	2
HP159	7	12.38	750	N	1	750	B	1	2
HP161	9	12.63	750	N	1	750	A	15	5
HP162	7	12.53	750	N	1	750	A	15	5
HP163	9	12.72	750	N	1	650	A	15	5
HP168	9	12.71	750	N	1	750	A	1	5
HP169	9	12.87	750	N	1	750	A	1	2
HP170	9	12.75	750	N	1	750	B	1	5
HP172	9	12.72	750	N	1	650	A	1	2
HP199	7	12.68	650	N	1	650	A	15	2
HP200	7	12.16	750	N	5	750	A	15	2
HP205	9	12.53	750	N	15	750	B	15	5
HP206	7	12.64	750	N	15	750	B	15	5
HP207	9	12.20	750	N	1	750	B	15	5
HP208	9	12.60	750	N	15	650	B	15	5
HP209	7	12.32	750	N	15	650	B	15	5
HP210	9	12.30	750	N	1	750	A	1	5

HP211	9	12.38	750	N	1	750	E	1	5
HP212	9	12.60	750	N	1	750	A	1	2
HP218	9	12.08	750	N	15	750	C	15	5
HP219	9	12.65	750	N	15	650	C	15	5
HP220	7	12.26	750	N	15	650	C	15	5
HP221	7	12.70	750	N	15	750	C	15	5
HP222	9	12.50	750	N	15	750	A	15	5
HP224	9	12.67	750	N	15	750	B	15	5
HP225	9	12.44	750	N	15	750	C	15	5
HP226	9	12.65	750	N	15	750	D	15	5
HP227	9	12.60	750	N	15	750	B	15	10
HP228	7	12.55	750	N	15	750	B	15	10
HP229	9	12.66	750	N	15	750	D	15	5
HP230	7	12.50	750	N	15	750	D	15	5
HP231	9	12.60	750	N	15	750	C	15	10
HP232	7	12.45	750	N	15	750	C	15	10
HP233	7	12.42	750	N	1	750	A	1	2
HP235	7	12.42	750	N	1	450	A	1	2
HP236	7	12.75	750	N	1	650	A	1	2
HP237	7	12.68	750	N	1	550	A	1	2
HP238	7	12.73	750	N	1	750	F	1	2
HP240	7	12.47	750	N	15	750	A	15	2

Note:

Calcination :

N - 100% N_2

Carbonation :

A - 15% CO_2 / N_2
B - 15% CO_2 / 10% H_2O / N_2
C - 15% CO_2 / 10% H_2O / 5% CO / 2.5% H_2 / N_2
D - 15% CO_2 / 10% H_2O / 5% CO / 2.5% H_2 / 0.22% H_2S
E - 15% CO_2 / 10% H_2O / 20% CO / 10% H_2 / N_2
F - 25% CO_2 / N_2

Appendix B

Computer Program of Distributed Pore Size Model

```
      PROGRAM MPORE
C
C   FROM P.G. CHRISTMAN (1981)
C      "DISTRIBUTED PORE SIZE MODEL"
C
      REAL DIA(50),CUMVOL(50),ETA(50),RZERO(50),R1(50)
      REAL KRATE,MW,KG
      REAL CONC(50),LRATE2(50),LCONV(50),LPRSTY(50)
      REAL RZSQ(50,2)
      REAL LRATE(50)
      REAL   XDATA(600), YDATA(600)
      INTEGER*4    NSET, NXDATA, IFREE, NXVCTR(20)
      CHARACTER*20 KEYS(20) ,HEAD
      COMMON/TABLE/TTABLE(100,50),RTABLE(100,50),PTABLE(100,50)
      COMMON/PARAM/KRATE,ALPHA,DB,DK,DS,VR,CZERO,CBULK
      COMMON/COEFF/DEFF(50),RK(50)
      COMMON/VALUES/TVALUE(100),DVALUE(100),RVALUE(100),PVALUE(100)
      COMMON/PVAL/DPVAL(100),RPVAL(100),PPVAL(100)
      COMMON/PELLET/RPEL(50),RPSQ(50),DELRP,DELRSQ
      COMMON/PROP/RZERO,RZSQ
      COMMON/FACTOR/TRTSTY
      COMMON/TIME/NTIME
      COMMON/WORK/TAUFTR,CNVFTR,RTEFTR,RADFTR,EPSLN,FINFTR,FCORR
      COMMON/LENGTH/ NDIV
      DATA R1(1)/0.0/
      DATA NPTR,NUM/50,50/
      DATA MW/56./
C     650C, 15%CO2, 1 ATM (HP046)
      DATA (XDATA(I),I=1,15)/0.,0.1,0.2,0.3,0.4,0.5,0.6,
     &      0.7,0.9,1.1,1.7,2.2,2.7,3.2,4.7/
      DATA (YDATA(I),I=1,15)/0.,0.121,0.213,0.302,0.386,
     &    0.461,0.525,0.581,0.672,0.684,0.692,0.693,0.694,0.694,0.702/
      IDATA = 15
C     650C, 1%CO2, 15 ATM  (HP137)
C     DATA (XDATA(I),I=1,15)/0.,1.,2.,3.,4.,5.,6.,7.,8.,9.,10.,12.
C    $  ,15.,18.,20./
C     DATA (YDATA(I),I=1,15)/0.,.1,.18,.254,.341,.446,.522,.584,
C    $           .651,.682,.686,.69,.696,.698,.7/
C     IDATA= 15
C     BHATIA, 655, 1 ATM, 10%CO2/N2, RUN 10-12
C     DATA (XDATA(I),I=1,8 )/0.,2.5,5.,7.5,10.,15.,20.,30./
C     DATA (YDATA(I),I=1,8 )/0.,.5,.58,.62,.65,.68,.685,.7/
C     IDATA=  8
C     750C,15%CO2, 1 ATM (HP066)
      DATA (XDATA(I),I=1,23)/0.,.1,.3,.5,.7,.9,1.,1.2,1.4,1.6,1.8,
     $   2.0,2.2,2.5,3.,4.,5.,6.,8.,10.,12.,15.,20./
      DATA (YDATA(I),I=1,23)/0.,.055,.088,.131,.180,.229,.248,.293,
     $  .332,.377,.41,.444,.487,.530,.594,.694,.739,.747,.753,.76,.762,
     $   .764, .77/
      IDATA= 23
C     650C, 5%CO2, 1 ATM (HP043)
C     DATA (XDATA(I),I=1,13)/0.,.2,.3,.6,1.1,1.6,2.1,2.6,3.6,4.6,6.6,
C    $     8.6,10./
C     DATA (YDATA(I),I=1,13)/0.,.088,.147,.229,.361,.464,.551,.625,
C    $           .713,.725,.731,.732,.733/
C     IDATA= 13
C     550C,15%CO2, 1 ATM (HP049)
C     DATA (XDATA(I),I=1,14)/0.,.1,.2,.3,.5,.8,1.3,1.8,2.8,3.8,
C    $            4.8,6.8,9.8,11.8/
C     DATA (YDATA(I),I=1,14)/0.,.3,.401,.484,.611,.628,.636,.638,.650
C    $    ,.652,.652,.654,.660,.662/
```

```
C      IDATA= 14
C      650C,15%CO2, 15ATM (HP141)
C      DATA (XDATA(I),I=1,17)/0.,.2,.3,.4,.5,.6,.7,.8,.9,1.,
C     $       1.1,1.2,1.4,1.6,1.8,2.,3./
C      DATA (YDATA(I),I=1,17)/0.,.093,.129,.169,.22,.256,.30 ,.34 ,
C     $     .393,.43 ,.472,.526,.603,.645,.655,.655,.655/
C      IDATA= 17
C      DATA (XDATA(I),I=1,15)/0.,0.1,0.2,0.3,0.4,0.5,0.6,
C     &      0.7,0.9,1.1,1.7,2.2,2.7,3.2,4.7/
C      DATA (YDATA(I),I=1,15)/0.,0.121,0.213,0.302,0.386,
C     &    0.461,0.525,0.581,0.672,0.684,0.692,0.693,0.694,0.694,0.702/
C      IDATA = 15
C      DATA (XDATA(I),I=1,12)/0.,1.,2.,3.,4.,5.,6.,7.,8.,9.,10.,12./
C      DATA (YDATA(I),I=1,12)/0.,.1,.18,.254,.341,.446,.522,.584,
C     $            .651,.682,.686,.69/
C      IDATA= 12
       NDATA= IDATA+1
C
       NTIME = 25
       NDIV = 100
C
C      READ IN THE MODEL PARAMETERS
C
       CALL READIN(PELLET,ALPHA,CZERO,KRATE,DS,TRTSTY,DB,KG,
      1            DK,VR,VG,DIA,CUMVOL,RXNHRS,NPTS,DELX)
C
       CBULK=CZERO
C
C
C      CALCULATE SECONDARY PARAMETERS
C
C      TAUFTR= VR*(ALPHA-1.)*KRATE*CZERO
       EPSLN= CUMVOL(NPTS)
       TEMP1= 1.-EPSLN
       RTEFTR= VG*MW/TEMP1
       CNVFTR=TEMP1*(ALPHA-1.)
       TEMP2=PELLET*PELLET*PELLET
       RADFTR=3./TEMP2
       RHO=MW*TEMP1/VR
       RXNSEC=RXNHRS*3600.
       DELRP=PELLET/FLOAT(NPTR-1)
       FINFTR=KG*DELRP
       FCORR= -(1.- 2.*DELRP/PELLET)
C
C      CALCULATE INITIAL VALUES OF CONSTANT FOR PDE
C
       TIME= 0.0
       NITER= 1
       CALL DIST(DIA,CUMVOL,NPTS,ETA,NTOT,NUM)
       CALL EVOLVE(RZERO,NTOT,RXNSEC)
       CALL REACT(NTOT,RXNSEC)
       CALL START(NTOT,NPTR,TPLUG,RTEMAX,PELLET,LCONV,LPRSTY)
       AREA= RK(1)/KRATE/RHO
C
C      CALCULATE INITIAL PROFILES
C
       CALL DIFFEQ(CONC,CBULK,NPTR)
C
       CZERO = CONC(NPTR)
C
       CALL EVOLVE(RZERO,NTOT,RXNSEC)
       CALL REACT(NTOT,RXNSEC)
```

```
      CALL START(NTOT,NPTR,TPLUG,RTEMAX,PELLET,LCONV,LPRSTY)
C
C     CALCULATE INITIAL PROFILES
C
      CALL DIFFEQ(CONC,CBULK,NPTR)
C
      AREA= RK(1)/KRATE/RHO
      DO 16 I=1,NPTR
        LRATE(I) = CONC(I)*RK(I)*RTEFTR
16    CONTINUE
      CALL FINISH(CONV,LCONV,RATE,LRATE,PRSTY,LPRSTY,RTEMAX,EFF,NPTR)
      WRITE(6,500) TPLUG,RXNSEC,AREA
      IF (TPLUG.LT.RXNSEC) RXNSEC=TPLUG
      CALL SHOW(TIME,CONV,RATE,EFF,PRSTY,CONC,DEFF,
     1          LCONV,LRATE,LPRSTY,NPTR,NITER)
      XDATA(NDATA  ) = 0.
      YDATA(NDATA  )= 0.
C
      NITER= 0
 18   DELTM= DELX/RATE
      NDATA= NDATA+1
      TEMP= TIME+DELTM
      IF(TEMP.LT.RXNSEC) GOTO 19
      TEMP=RXNSEC
      DELTM=TEMP-TIME
19    CONTINUE
      TIME=TEMP
20    CALL DIFFEQ(CONC,CBULK,NPTR)
C
      CZERO = CONC(NPTR)
C     WRITE(6,*) 'CONC(50) = ', CONC(NPTR)
C
      DO 30 J=1,NPTR
        LRATE2(J) = LRATE(J)
30    CONTINUE
      CALL RESET(CONC,TIME,NPTR,DELTM,LCONV,LPRSTY,LRATE)
      NITER=NITER + 1
      IF(NITER.GE.50) GO TO 50
      DO 40 I=1,NPTR
         J=NPTR+1-I
         IF(LRATE(J).LE.0.0) GOTO 50
         DRATE= ABS(LRATE2(J)-LRATE(J))
         DFRAC= DRATE/LRATE(J)
         IF(DFRAC.GE.0.01 ) GOTO 20
40    CONTINUE
50    CALL FINISH(CONV,LCONV,RATE,LRATE,PRSTY,LPRSTY,
     1            RTEMAX,EFF,NPTR)
      CALL SHOW(TIME,CONV,RATE,EFF,PRSTY,CONC,DEFF,
     1          LCONV,LRATE,LPRSTY,NPTR,NITER)
      XDATA(NDATA) = TIME/60.
      YDATA(NDATA) = CONV
C      ADATA(NDATA)  = CONC(1)
C      BDATA(NDATA) = CONC(NPTR)
      IF(TIME.LT.RXNSEC) GOTO 18
      DUMMY  = NDATA-IDATA
      IF(DUMMY.GE.MAX)  MAX= DUMMY
      NXDATA= MAX
C     XDATA(NDATA+DUMMY*1) =0.
C     YDATA(NDATA+1) = 0.
      NXVCTR(1) = IDATA
      NXVCTR(2) = DUMMY
C     NXVCTR(3) = 1
```

```
      NSET= 2
       IFREE = 1
      CALL GRAPHF( XDATA, YDATA, KEYS, HEAD, NSET, NXDATA, IFREE,
     &             NXVCTR )
C
500   FORMAT(1H1,9X,'TPLUG=',E12.5,1X,'RXNSEC=',E12.5,2X,
     1       'AREA(CM2/G)= ',E12.5)
      STOP
      END
C

C
      SUBROUTINE READIN(PELLET,ALPHA,CZERO,KRATE,DS,TRTSTY,DB,KG,
     1            DK,VR,VG,DIA,CUMVOL,RXNHRS,NPTS,DELX)
C
C     THIS SUBROUTINE READS THE MODEL PARAMETERS INTO THE COMPUTER
C     AND GENERATES AN ECHO PRINT
C
      REAL KRATE,KG,MWCO2,MWN2,MWGAS,MWAIR,MW
      REAL DIA(50), CUMVOL(50), DATA(17)
      INTEGER GAS, AIR
      COMMON/PRINT/IPRINT
      DATA NUM/50/
C     DATA PRESS/1./
      DATA MWCO2,TCO2,MWN2,TN2,MWAIR,TAIR/44.,3.996,28.,3.681,
     1     29.,3.617/
C     DATA PRESS/1./
C     DATA MWSO2,TSO2,MWN2,DVN2,MWAIR,DVAIR/64.,41.1,28.,17.9,
C    1     29.,20./
      DATA AIR/3    /
      DATA RG/82.057/
      DATA MW/56.0/
C
C     PELLET= RADIUS OF PELLET (CM)
C     ALPHA= RATIO OF THE MOLAR VOLUMES OF THE PRODUCT
C            AND THE REACTANT
C     CZERO= CONC. OF GAS REACTANT (MOLES/CM3)
C     KRATE= SURFACE REACTION RATE CONSTANT (CM/SEC)
C     DS = DIFF. OF THE GAS REACTANT THROUGH THE PRODUCT
C          LAYER (CM2/SEC)
C     TRTSTY = TORTUOSITY THROUGH THE POROUS MEDIUM
C     DB  = BULK DIFF. OF THE GAS REACTANT (CM2/SEC)
C     DK = KNUDSEN DIFFUSIVITY/PORE RADIUS (CM/SEC)
C     VR= MOLAR VOLUME OF THE REACTANT(CM3/MOLE)
C     DIA  = VECTOR CONTAINING THE DIAMETER OF THE PORES FROM THE
C            MEASURED PORE SIZE DISTRIBUTION (MICRONS), (CM)
C     CUMVOL = VECTOR CONTAINING THE CUMULATIVE VOLUME OF ALL
C              PORES LARGER THAN THE CORRESPONDING VALUE OF DIA
C     (CM3/GM), (CM3/CM3)
C     RXNHRS= REACTION TIME OF INTEREST (HRS)
C     NPTS=  NUMBER OF VALUES IN THE VECTORS DIA, AND CUMVOL
C     DELX = THE DESIRED INCREMENT IN CONVERSION FOR EACH TIME
C             STEP, IN GENERAL THE ACTUAL CHANGE IN CONVERSION
C            WILL BE LESS THAN THIS VALUE
C     VG=  VOLUME OF PURE REACTANT PER GRAM
C     KG=  MASS TRANSFER COEFF. OUTSIDE THE PELLET (MOLES/CM2/SEC)
C
C     IPRINT DETERMINES THE LEVEL OF OUTPUT ON FILE OUTPUT
C     IF(IPRINT.EQ.0) OUTPUT CONTAINS THE MACROSCOPIC PROPERTIES
C                     OF THE PELLET AS A FUNTION OF TIME
C     IF(IPRINT.EQ.1) OUTPUT CONTAINS THE NORMAL OUTPUT
C     IF(IPRINT.EQ.2) OUTPUT CONTAINS THE MACROSCOPIC PROPERTIES
```

```
C                    AT EVERY GRID POINT IN THE FINITE DIFFERENCE
C                    APPROXIMATION OF THE PELLET
C     IF(IPRINT.NE.1) THERE IS NO ECHO PRINT
C
      DO 1 I=1,7
          READ(5,*) DATA(I)
1     CONTINUE
      DO 2 I=9,17
         READ(5,*) DATA(I)
2     CONTINUE
      READ(5,*) IPRINT
      MWGAS=MWN2
      TGAS=TN2
      READ(5,*) GAS
C     IF(GAS.EQ.AIR) MWGAS=MWAIR
C     IF(GAS.EQ.AIR) TGAS=TAIR
      TEMP=DATA(13) +273.16
      PRESS= DATA(16)
      DATA(3) = (DATA(3)*PRESS - DATA(17))/TEMP/RG
      DATA(8)= 9700.*SQRT(TEMP/MWCO2)
C     DTEMP1=SQRT((MWCO2+MWGAS)/(MWCO2*MWGAS))
C     DTEMP1= DTEMP1*SQRT(TEMP**3)
C     TAUAB= (TCO2+TGAS)/2.
C     TAUSQR= TAUAB*TAUAB
C     XOMEGA=0.7896
C     DTEMP2= PRESS*TAUSQR*XOMEGA
C     DATA(7)= 0.00158583*DTEMP1/DTEMP2
C     DATA(7)= 1.08/15.
C     DATA(7)= 1.08
C     DATA(7)= 0.00002
C     KG=DATA(12)*DATA(7)*DATA(3)/DATA(1)/2.
      KG = DATA(12) * DATA(3)
      PELLET=DATA(1)
      ALPHA= DATA(2)
      CZERO=DATA(3)
      KRATE= DATA(4)
      DS= DATA(5)
      TRTSTY= DATA(6)
      DB=DATA(7)
      DK= DATA(8)
      VR=DATA(9)
      RXNHRS=DATA(10)
      VG=1./DATA(11)
      DATA(11)= VG
      DMAX=DATA(14)
      DELX=DATA(15)
      READ(5,*) LNPTS
      IFLAG=0
      NSAVE=LNPTS-1
      ISTOP=LNPTS
      READ(5,*) DIA(1),CUMVOL(1)
      DO 7 I=2,ISTOP
3     READ(5,*) DIA(I),CUMVOL(I)
      IF(IFLAG.GT.0) GOTO 5
      IF(DIA(I).LE.DMAX) GOTO 4
      LNPTS=LNPTS-1
      DIA(1)= DIA(2)
      CUMVOL(1) = CUMVOL(2)
      GOTO 3
4     IFLAG= 1
      SLOPE=(CUMVOL(2)-CUMVOL(1))/ALOG(DIA(2)/DIA(1))
      CUMVOL(1)=SLOPE*ALOG(DMAX/DIA(1))+CUMVOL(1)
```

```
      CSAVE= CUMVOL(1)
      CUMVOL(1)= 0.0
      DIA(1)= DMAX
5     CUMVOL(I)=CUMVOL(I)- CSAVE
7     CONTINUE
      NPTS= LNPTS
C
C     ECHO PRINT
C
      IF(IPRINT.NE.1) GOTO 9
      WRITE(6,200) DATA(13)
      WRITE(6,205) (DATA(I), I=1,12)
      WRITE(6,210) LNPTS,NUM,DELX
      WRITE(6,215)
9     CONTINUE
C
C     CONVERT FROM MICRONS TO CM
C
      XSOLV= CUMVOL(1)
      FTR= VG+ (CUMVOL(LNPTS) -XSOLV)
      DO 10 I=1,LNPTS
           DIA(I)= DIA(I)*0.0001
           CUMVOL(I) =(CUMVOL(I)-XSOLV)/FTR
10    CONTINUE
      IF(IPRINT.EQ.1) WRITE(6,230)
      IF(IPRINT.EQ.1) WRITE(6,240) (DIA(I),CUMVOL(I),I=1,LNPTS)
200   FORMAT(30X,'MULTIPLE PORE MODEL'//,30X,
     1  'TEMPERATURE(DEG C)=',F8.1,18X,//18X,'INPUT DATA')
205   FORMAT(/10X,'PELLET RADIUS(CM)= ',E12.5/10X,
     A 'RATIO OF MOLAR VOLUMES= ',F12.4/10X,
     1 'BULK CO2 CONCENTRATION(MOLES/CC)= ',E12.5/
     B 10X,'REACTION RATE CONCTANT(CM/SEC)= ',E12.5/
     C 10X,'PRODUCT LAYER DIFFUSIVITY(CM2/SEC)= ',E12.5/
     D 10X,'PELLET TURTUOSITY FACTOR= ',F12.2/
     E 10X,'BULK DIFFUSIVITY (CM2/SEC)= ',E12.5/
     F 10X,'KNUDSEN DIFFUSION COEFF. (CM/SEC)= ',E12.5/
     G 10X,'REACTANT MOLAR VOLUME= ',F12.4/
     H 10X,'REACTION TIME(HRS)= ',F12.4/
     I 10X,'VOLUME PER GRAM OF SOLID(CM3/GM)= ',F12.4/
     J 10X,'MASS TRANSFER COEFF.= ',F10.5)
210   FORMAT(/10X,'TOTAL NUMBER OF DATA POINTS= ',I5/
     A 10X,'MAXIMUM NUMBER OF DIVISION= ',I5/
     B 10X,'CONVERSION INCREMENT= ',F5.3)
215   FORMAT(//10X,5(A6)//10X,'DIAMETER(MICRON)= ',3X,
     1 'CUMULATIVE VOLUME(CM3/GM)= '/)
230   FORMAT(//10X,'DIAMETER(CM)=',7X,'CUMVOLUME(CM3/CM3)'/)
240   FORMAT(10X,E12.5,10X,F10.4)
      RETURN
      END
C
C
      SUBROUTINE DIST(DIA,CUMVOL,NPTS,ETA,NTOT,NUM)
C
C     THIS SUBROUTINE GENERATES RZERO AND ETA FROM THE MEASURED PORE
C     SIZE DISTRIBUTION. IT INTERPOLATE BETWEEN DATA POINTS
C     REPRESENTED BY DIA AND CUMVOL BY ASSUMING THAT CUMVOL IS
C     A LINEAR FUNCTION OF LOG(DIA).
C     NTOT IS DETERMINED BY DIVIDING EACH SECTION INTO AN EQUAL
CC         NUMBER OF SMALLER INTERVALS DETERMINED SUCH THAT
C     (NTOT.LE.NUM).
C     ETA IS ASSUMED TO BE A CONSTANT OVER EACH INTERVAL (R-DELTA R)
C     TO R.
```

```
C
      REAL DIA(50),CUMVOL(50), ETA(50)
      REAL RTEMP(50), VTEMP(50)
      REAL FRACV(50), LOGRT(50),LSLOPE(50)
      COMMON/FACTOR/TRTSTY
      COMMON/TOTAL/ETASUM(50),EZERO(50),ETATOT
      COMMON/PROP/RZERO(50),RZSQ(50,2)
      COMMON/PRINT/IPRINT
      DATA Z/0.5773503/
C
C     DIA  = VECTOR CONTAINING THE DIAMETER OF THE PORES FROM THE
C            MEASURED PORE SIZE DISTRIBUTION (MICRONS), (CM)
C     CUMVOL = VECTOR CONTAINING THE CUMULATIVE VOLUME OF ALL
C              PORES LARGER THAN THE CORRESPONDING VALUE OF DIA
C     (CM3/GM), (CM3/CM3)
C     ETA = VECTOR CONTAINING NUMBER OF PORES WITH RADIUS BEWEEN
C           (R-DELTA R) AND R PER UNIT RADIUS, PER UNIT AREA
C     NTOT = DIMENSION OF ETA
C     NUM = MAXIMUM VALUE OF NTOT
C
      LOCNPT= NPTS
      NACT=(NUM-1)/(LOCNPT-1)
      FACT=FLOAT(NACT)
      NTOT=NACT*(LOCNPT-1) +1
      LCNTOT=NTOT
      DO 5 I=1,LOCNPT
         INV=LOCNPT+1 - I
         RTEMP(I)= DIA(INV)/2.
         LOGRT(I)= ALOG(RTEMP(I))
      VTEMP(I) = CUMVOL(LOCNPT)-CUMVOL(INV)
5     CONTINUE
      FRACV(1)= 0.
      DO 7 I=2,LOCNPT
         LSLOPE(I)= (VTEMP(I)-VTEMP(I-1))/(LOGRT(I)-LOGRT(I-1))
7     CONTINUE
      RZERO(1)=RTEMP(1)
      ETA(1)=0.
      DO 20 I=2,LOCNPT
           IKOUNT=1+(I-1)*NACT
           RZERO(IKOUNT)=RTEMP(I)
           JSTART=(IKOUNT-NACT)+1
           JSTOP=IKOUNT
           JKOUNT=NACT-1
           STEP=(RTEMP(I)-RTEMP(I-1))/FACT
        DO 10 J=JSTART,JSTOP
          RZERO(J)=RTEMP(I)-(FLOAT(JKOUNT)*STEP)
          CALL EFUN(RZERO(J-1),RZERO(J),FRACV(J),LSLOPE(I),ETA(J))
          JKOUNT=JKOUNT-1
10        CONTINUE
20        CONTINUE
      ETASUM(1)=0.
      ETATOT = 0.
      EZERO(1)=ETA(1)
C
C  ETA(I)*DEL(RZERO) = # OF PORES WITH SIZES BETWEEN
C                      RZERO AND (RZERO+DRZERO)
      DO 30 I=2,LCNTOT
         DELRZ=RZERO(I)-RZERO(I-1)
         ETASUM(I)=ETA(I)*DELRZ
         EZERO(I)=ETA(I)
         ETATOT=ETATOT+ETASUM(I)
30    CONTINUE
```

```
      DO 40 I=2,LCNTOT
      ZTEMP1=Z*(RZERO(I)-RZERO(I-1))
      ZTEMP2=RZERO(I-1)+RZERO(I)
      RZT1=(ZTEMP2-ZTEMP1)/2.
      RZT2=(ZTEMP2+ZTEMP1)/2.
      RZSQ(I,1)=RZT1*RZT1
      RZSQ(I,2)=RZT2*RZT2
40    CONTINUE
      IF(IPRINT.EQ.1) WRITE(6,499)
      IF(IPRINT.EQ.1) WRITE(6,500) (RZERO(I),ETASUM(I),ETA(I),
     1                I=1,LCNTOT)
499   FORMAT(1H1,13X,'RZERO',12X,'ETASUM',14X,'EZERO'/)
500   FORMAT(3(8X,E12.5))
      RETURN
      END
C  ****************************************
      SUBROUTINE EVOLVE(RZERO,NTOT,TAUMAX)
C  ****************************************
C
C  THIS SUBROUTINE GENERATES THE VALUES STORED IN COMMON BLOCK
C  /TABLE/. FROM THE VALUES STORED IN RTABLE A CUBIC SPLINE IS
C  FIT TO INTERPOLATE R1 AS A FUNCTION OF TAU
C
      REAL RZERO(50)
      COMMON/TABLE/TTABLE(100,50),RTABLE(100,50),PTABLE(100,50)
      COMMON/TIME/NTIME
      COMMON/LENGTH/NDIV
      DATA EXPNT/3./
      DATA IOPT/0/
C
C     RZERO= VECTOR CONTAINING THE INITIAL VALUES OF THE PORE RADII
C     NTOT= DIMENSION OF VECTOR RZERO
C     TAUMAX=MAXIMUM VALUE OF TAU THAT IS OF INTEREST IN THIS
C            SIMULATION
C
      TAULO=TAUMAX*1.05
      TAUHI=TAULO*1.01
      TAUMED=TAULO*1.005
      LNTOT=NTOT
      NDIVL1=NDIV-1
      DO 20 I=1,LNTOT
           RTABLE(1,I)=RZERO(I)
           TTABLE(1,I)=0.
           DO 10 J=2,NDIV
           FACTOR=FLOAT(NDIV-J)/FLOAT(NDIVL1)
           RTABLE(J,I)=RZERO(I)*(FACTOR**(1./EXPNT))
           TTABLE(J,I)=FTAU(RTABLE(J,I),RZERO(I))
10    CONTINUE
        CALL SPLINE(TTABLE(1,I),RTABLE(1,I),PTABLE(1,I),NDIV,IOPT)
        IF(TTABLE(NDIV,I).GT.TAULO) GO TO 30
20    CONTINUE
      RETURN
30    CONTINUE
      ISTART=I+1
      IF(ISTART.GT.LNTOT) RETURN
      DO 50 II=ISTART,LNTOT
      RGUES1 =0.
      TGUES1=FTAU(0.0,RZERO(II))
      RGUES2=RZERO(II)
      TGUES2=0.
35    CONTINUE
      SLOPE=(RGUES1-RGUES2)/(TGUES1-TGUES2)
```

```
      RGUES3=SLOPE*(TAUMED-TGUES2)+RGUES2
      TGUES3=FTAU(RGUES3,RZERO(II))
      IF(TGUES3.GT.TAULO) GOTO 36
      RGUES2=RGUES3
      TGUES2=TGUES3
      GOTO 35
 36   CONTINUE
      IF(TGUES3.LE.TAUHI) GO TO 37
      RGUES1=RGUES3
      TGUES1=TGUES3
      GO TO 35
 37   CONTINUE
      RMINSQ=RGUES3**EXPNT
      RZSQ=RZERO(II)**EXPNT
      DIFFSQ=RZSQ-RMINSQ
      RTABLE(1,II)=RZERO(II)
      TTABLE(1,II)=0.0
      DO 40 J=2,NDIV
      FACTOR=FLOAT(NDIV-J)/FLOAT(NDIVL1)
      RTABLE(J,II)=((DIFFSQ*FACTOR)+RMINSQ)**(1./EXPNT)
      TTABLE(J,II)=FTAU(RTABLE(J,II),RZERO(II))
 40   CONTINUE
      CALL SPLINE(TTABLE(1,II),RTABLE(1,II),PTABLE(1,II),NDIV,IOPT)
 50   CONTINUE
      RETURN
      END
C
C
      SUBROUTINE SPLINE(XV,YV,PV,NDIV,IOPT)
C
C   THIS SUBROUTINE CALCULATES AN INTERPOLATING CUBIC SPLINE
C   FOR DATA STORED IN THE VECTORS XV, YV
C
      REAL A(100),B(100),C(100),D(100),H(100)
      REAL XV(100),YV(100),PV(100)
      DATA C/100*1.0/
      DATA IFIRST/2/
C
C    XV=VECTOR CONTAINING THE X VALUES
C    YV=VECTOR CONTAINING THE Y VALUES
C    PV=VECTOR CONTAINING THE VALUES OF THE 2ND DERIVATIVE OF THE
C       INTERPOLATING CUBIC SPLINE
C    NDIV= DIMENSION OF THE VECTORS
C
C    IF(IOPT.EQ.1) THE 2ND DERIVATIVES AT THE END POINTS ARE SET
C          EQUAL TO ZERO
C    IF (IOPT.EQ.0) THE 2ND DERIVATIVES AT THE END POINTS ARE SET
C          EQUAL TO THE VALUE AT THEIR NEAREST NEIGHBOR
C
C
      LIM=NDIV-1
      DO 10 I=1,LIM
        H(I)=XV(I+1) - XV(I)
10    CONTINUE
      DO 20 I=2,LIM
       A(I)=H(I-1)/H(I)
       B(I)=2.*(H(I)+H(I-1))/H(I)
       DTEMP1=(YV(I+1)-YV(I))/H(I)
       DTEMP2=(YV(I)-YV(I-1))/H(I-1)
       D(I) = 6.*(DTEMP1-DTEMP2)/H(I)
20     CONTINUE
       IF(IOPT.EQ.0) GO TO 30
```

```
        B(2)=(3.*H(1)+2.*H(2))/H(2)
        B(LIM)= (2.*H(LIM-1)*3.*H(LIM))/H(LIM)
          CALL TRIDAG(IFIRST,LIM,A,B,C,D,PV)
        PV(1)=PV(2)
        PV(NDIV)=PV(LIM)
        RETURN
30      CONTINUE
          CALL TRIDAG(IFIRST,LIM,A,B,C,D,PV)
          PV(1)=0.
          PV(NDIV)=0.
          RETURN
          END
C ****************************************
        SUBROUTINE REACT(NTOT,RXNSEC)
C ****************************************
C
C    THIS SUBROUTINE CALCULATES THE VALUES OF THE DIFFUSIVITY,
C     REACTIVITY, AND POROSITY AS A FUNCTION OF TAU AND STORES
C     THE RESULTS IN THE COMMON BLOCK/VALUES/. IT CALCULATES
C     AN INTERPOLATING CUBIC SPLINE FOR EACH PROPERTY AND STORES
C     THE 2ND DERIVATIVERS IN /PVAL/.
C
       REAL R1(50), ETA(50)
       COMMON/TABLE/TTABLE(100,50),RTABLE(100,50),PTABLE(100,50)
       COMMON/VALUES/TVALUE(100),DVALUE(100),RVALUE(100),PVALUE(100)
       COMMON/PVAL/DPVAL(100),RPVAL(100),PPVAL(100)
       COMMON/PARAM/KRATE,ALPHA,DB,DK,DS,VR,CZERO,CBULK
       COMMON/WORK/TAUFTR,CNVFTR,RTEFTR,RADFTR,EPSLN,FINFTR,FCORR
       COMMON/LENGTH/NDIV
       COMMON/PRINT/IPRINT
       DATA IOPT1/0/
C
C
C
       LNTOT=NTOT
       AFTR=ALPHA-1.
       EFTR=1.-EPSLN
       NCHECK=NDIV/LNTOT
       IF(NCHECK.EQ.2) GOTO 5
      WRITE(6,200) NDIV, LNTOT
       STOP
 5     CONTINUE
       DO 10 I=1,LNTOT
         INC=I*2
         INCL1=INC-1
         TVALUE(INCL1)=TTABLE(INCL1,I)
         TVALUE(INC)=TTABLE(INC,I)
 10    CONTINUE
         IF(TVALUE(LNTOT-1).GT.RXNSEC) TVALUE(LNTOT-1)=RXNSEC*1.01
         IF(TVALUE(LNTOT).GT.RXNSEC) TVALUE(LNTOT)=RXNSEC*1.02
         ISTART=(2*LNTOT)+1
         IF(ISTART.GT.NDIV) GO TO 25
         DO 20 I=ISTART, NDIV
            TVALUE(I)= TTABLE(I,LNTOT)
 20      CONTINUE
 25      CONTINUE
      DO 30 I=1,NDIV
            CALL LOOK(TVALUE(I),R1,ETA,LNTOT)
C     WRITE(6,*) I, TVALUE(I)
            CALL INTE(R1,ETA,DVALUE(I),RVALUE(I),PVALUE(I),LNTOT)
 30      CONTINUE
         CALL SPLINE(TVALUE,DVALUE,DPVAL,NDIV,IOPT1)
```

```
            CALL SPLINE(TVALUE,RVALUE,RPVAL,NDIV,IOPT1)
            CALL SPLINE(TVALUE,PVALUE,PPVAL,NDIV,IOPT1)
            IF(IPRINT.NE.1) GO TO 40
          WRITE(6,100)
       WRITE(6,105) (TVALUE(I),DVALUE(I),RVALUE(I),PVALUE(I),I=1,NDIV)
 40    CONTINUE
 100   FORMAT(10X,'TAU',10X,'DIFFUSIVITY',10X,'RATE CONST.',
     1       10X,'POROSITY'/)
 105   FORMAT(4(5X,E12.5))
 200   FORMAT(///15X,'THE TOTAL NUMBER OF PORE RADII CAN BE DIVIDED'/
     1    15X,'INTO THE NUMBER OF TAU VALUES BY A VALUE OTHER',
     2    15X,'THAN TWO.'/15X,'NTOT',I4/)
          RETURN
          END
C  ****************************************************************
      SUBROUTINE START(NTOT,NPTR,TPLUG,RMAX,PELLET,LCONV,LPRSTY)
C  ****************************************************************
C
C   THIS SUBROUTINE INITIALIZE ALL THE VALUES OF THE MACROSCOPIC
C   PROPERTIES OF THE POROUS MEDIUM ASSUMING THAT THE PELLET IS
C   INITIALLY ISOTROPIC.
C
       REAL LCONV(50),ETA(50),LPRSTY(50)
       REAL KRATE
       COMMON/PELLET/RPEL(50),RPSQ(50),DELRP,DELRSQ
       COMMON/PARAM/KRATE,ALPHA,DB,DK,DS,VR,CZERO,CBULK
       COMMON/PROP/RZERO(50),RZSQ(50,2)
       COMMON/COEFF/DEFF(50),RK(50)
       COMMON/WORK/TAUFTR,CNVFTR,RTEFTR,RADFTR,EPSLN,FINFTR,FCORR
       COMMON/VALUES/TVALUE(100),DVALUE(100),RVALUE(100),PVALUE(100)
       DATA RANGE/.999/
C
C  ETA = VECTOR CONTAINING THE NUMBER OF PORES WITH RADII BETWEEN
C        (R1-DELTA R1) AND R1 PER UNIT RADIUS PER UNTI AREA
C  NTOT= SIZE OF THE VECTOR ETA
C  NPTR= THE NUMBER OF GRID POINTS IN FINITE DIFFERENCE
C        REPRESENTATION OF P\THE PELLET
C  TPLUG= THE TIME IT TAKES FOR ALL THE PORES AT THE OUTSIDE
C         OF THE PELLET TO PLUG
C  RMAX= THE MAXIMUM REACTION RATE, AT ZERO CONVERSION, IN THE
C        ABSENCE OF DIFFUSIONAL RESISTANCE
C  PELLET = RADIUS OF THE PELLET
C  LCONV= VECTOR CONTAINING THE VALUE OF THE LOCAL CONVERSION
C  LPRSTY= VECTOR CONTAINING THE VALUE OF THE LOCAL POROSITY
C
       A1=DVALUE(1)
       A3=RVALUE(1)
       LPRSTY(1)=PVALUE(1)
       LCONV(1)=(EPSLN-LPRSTY(1))/CNVFTR
       IF(LCONV(1).LE.1.E-12) LCONV(1)= 0.
       RPEL(1)= 0.
       RPSQ(1)= 0.
       DELRSQ=DELRP*DELRP
      DEFF(1)= A1
      RK(1) = A3
       RMAX=A3*CZERO*RTEFTR
      WRITE(6,*) 'RTEMAX= ',RMAX
       DO 20 I=2,NPTR
         RPEL(I)=PELLET*FLOAT(I-1)/FLOAT(NPTR-1)
         DEFF(I)= A1
         RK(I) = A3
         LCONV(I)= LCONV(1)
```

```
          LPRSTY(I)=LPRSTY(1)
          RPSQ(I)=RPEL(I)*RPEL(I)
 20     CONTINUE
C
C       CALCULATE THE PORE PLUGGING TIME FOR THE LARGEST PORES
C
       TPLUG=FTAU(0.0,RZERO(NTOT))*RANGE
       RETURN
       END
C
        FUNCTION FTAU(R1,RZERO)
C
C    THIS FUNCTION CALCULATES THE VALUE OF TAU FROM THE INITIAL
C    (RZERO) AND INNER (R1) RADII OF A PORE.
C
        COMMON/PARAM/KRATE,ALPHA,DB,DK,DS,VR,CZERO,CBULK
        COMMON/WORK/TAUFTR,CMVFTR,RTEFTR,RADFTR,EPSLN,FINFTR,FCORR
        REAL KRATE
C
C    R1 = VALUE OF THE INNER RADIUS OF THE PORE
C    RZERO= VALUE OF THE INITIAL PORE RADIUS
C
       BETA1=1.
       BETA2=1.
       XLAMBDA= (BETA1/BETA2)*VR*CZERO*(ALPHA-1.)
       DUM1=(R1/RZERO)
       DUM2=DUM1*DUM1
       DUM3=(1.-ALPHA)*RZERO*(1.- (ALPHA-DUM2)/(ALPHA-1.))
      1     /XLAMBDA/KRATE
       DUM4=RZERO*RZERO/4./XLAMBDA/DS
       IF(DUM1.LE.0.0) GO TO 10
       DUM5=DUM2*ALOG(DUM2)
       DUM6=(DUM2-ALPHA)*ALOG((DUM2-ALPHA)/(1.-ALPHA))
       FTAU=DUM3+DUM4*(DUM5-DUM6)
       RETURN
10     FTAU=RZERO/XLAMBDA/KRATE
       DUM= RZERO*RZERO*ALPHA/4./XLAMBDA/DS
       FTAU=FTAU + DUM*ALOG(ALPHA/(ALPHA-1.))
       RETURN
        END
C
       SUBROUTINE LOOK(TAU,R1,ETA,NDIM)
C
C    THIS SUBROUTINE USES SPLFUN TO INTERPOLATE VALUES OF R1 AS
C    A FUNCTION OF TAU. GIVEN A VALUE OF R1, ETA IS CALCULATED
C    SUCH THAT THE POPULATION BALANCE IS OBEYED
C
       REAL ETA(50),R1(50)
       COMMON/TABLE/TTABLE(100,50),RTABLE(100,50),PTABLE(100,50)
       COMMON/TOTAL/ETASUM(50),EZERO(50),ETATOT
       COMMON/LENGTH/NDIV
C
C    TAU = INTEGRAL OF (C/CZERO) WITH RESPECT TO TIME
C    R1 = VECTOR WHICH CONTAINS THE VALUES OF THE INNER RADII
C    ETA = VECTOR WHICH CONTAINS THE NUMBER OF PORES WITH RADII
C          BETWEEN (R1-DELTA R1) AND R1, PER UNIT RADIUS,PER UNIT AREA
C    NDIM = SIZE OF VECTORS R1 AND ETA
C
        TLOC=TAU
        LCNDIM=NDIM
        NDIVL1=NDIV-1
        DO 10 I=1,LCNDIM
```

```
          IF(TLOC.LT.TTABLE(NDIV,I)) GO TO 20
          R1(I) = 0.
          ETA(I) = 0.
10       CONTINUE
         RETURN
20       CONTINUE
        DO 50 J=I,LCNDIM
        DO 30 K=2,NDIV
          IF(TLOC.LE.TTABLE(K,J)) GO TO 40
30      CONTINUE
         WRITE(6,910) TLOC,NDIV,J,TTABLE(NDIV,J)
         R1(J) = RTABLE(NDIV,J)
         GO TO 50
40      CONTINUE
         KK=K-1
         R1(J) =SPLFUN(TLOC,TTABLE(KK,J),TTABLE(KK+1,J),
     1   RTABLE(KK,J),RTABLE(KK+1,J),PTABLE(KK,J),PTABLE(KK+1,J))
50       CONTINUE
         IF(TLOC.GE.TTABLE(NDIV,1)) GO TO 51
         ETA(I) = 0.
         GO TO 59
51       EPSLN= TTABLE(NDIV,I)*0.001
         TAU1=TTABLE(NDIV,I)
         TAU2= TTABLE(NDIV,I-1)
         RZERO1=RTABLE(1,I)
         RZERO2=RTABLE(1,I-1)
52       TEMP1=TAU1-TAU2
         TEMP2= TAU1-TLOC
         TEMP3=RZERO1-RZERO2
         RPLUG=RZERO1-(TEMP3*TEMP2/TEMP1)
         TGUESS=FTAU(0.0,RPLUG)
         ERROR= TGUESS-TLOC
         AERROR=ABS(ERROR)
         IF(AERROR.LE.EPSLN) GO TO 58
         IF(ERROR.LT.0.0) GO TO 56
         RZERO1=RPLUG
         TAU1=TGUESS
         GO TO 52
56       RZERO2=RPLUG
         TAU2=TGUESS
         GO TO 52
58       WT=(RTABLE(1,I)-RPLUG)/(RTABLE(1,I)-RTABLE(1,I-1))
         ETSMTP=ETASUM(I)*WT
         ETA(I)= ETSMTP/R1(I)
         IF(I.EQ.LCNDIM) GO TO 70
59       IPLUS=I + 1
         DO 60 L=IPLUS,LCNDIM
              DELR=R1(L) -R1(L-1)
              ETA(L)=ETASUM(L)/DELR
60       CONTINUE
70       CONTINUE
910      FORMAT(///20X,'TAU  IS TOO LARGE'/20X,'TAU= ',E12.5/
     1          20X,'TABLE(',I3,',',I3,')= ',E12.5)
         RETURN
         END
C
         FUNCTION SPLFUN(XVAL,XI,XIP1,YI,YIP1,PI,PIP1)
C
C    THIS FUNCTION INTERPOLATES A VALUE GIVEN AN X VALUE AND THE
C    APPROXIMATE CONSTANTS NECESSARY TO EVALUATE A CUBIC SPLINE.
C
C     XVAL= ARGUMENT OF THE SPLINE FUNCTION
```

```
C     XI= LOWER VALUE OF X
C     XIP1= UPPER VALUE OF X
C     YI= VALUE OF THE FUNCTION EVALUATED AT XI
C     YIP1= VALUE OF THE FUNCTION EVALUATED AT XIP1
C     PI = 2ND DERIVATIVE OF THE FUNCTION EVALUATED AT XI
C     PIP1= 2ND DERIVATIVE OF THE FUNCTION EVALUATED AT XIP1
C
          DELX1= XVAL-XI
       IF(DELX1.LE.1.E-12) DELX1=0.
          DELX13=DELX1*DELX1*DELX1
          DELX2=XIP1-XVAL
       IF(DELX2.LE.1.E-12) DELX2=0.
          DELX23=DELX2*DELX2*DELX2
          HI=XIP1-XI
          P1=PI/6.
          P2=PIP1/6.
          Y1=YI/HI
          Y2=YIP1/HI
          TEMP1=P1*DELX23/HI
          TEMP2=P2*DELX13/HI
          TEMP3=(Y2-(P2*HI))*DELX1
          TEMP4=(Y1-(P1*HI))*DELX2
          TEMP5=TEMP1+TEMP2+TEMP3+TEMP4
          SPLFUN=ABS(TEMP5)
          RETURN
          END
C
          SUBROUTINE EFUN(XLO,XHI,FRAVOL,B1,ETA)
C
C  THIS SUBROUTINE CALCULATES ETA GIVEN THE VOID VOLUME OF ALL
C  PORES WITH RADII BETWEEN XLO AND XHI
C
          DATA PI/3.14159/
C
C     XLO= LOWER VALUE OF THE PORE RADIUS
C     XHI= UPPER VALUE OF THE PORE RADIUS
C     FRAVOL= FRACTION OF THE VOID VOLUME CONTAINED IN PORES WITH
C             RADII BETWEEN THE LOWER AND THE UPPER
C     B1= SLOPE OF THE LINE ON A PLOT OF CUMULATIVE VOLUME VS.
C         LOG(PORE RADIUS)
C     ETA= NUMBER OF PORES WITH RADII BETWEEN XLO AND XHI PER UNIT
C          RADIUS, PER UNIT AREA
C
          FRAVOL=B1*ALOG(XHI/XLO)
          XLO2=XLO*XLO
          XLO3=XLO2*XLO
          XHI2=XHI*XHI
          XHI3=XHI2*XHI
          DELX=XHI-XLO
          ETEMP=XHI3-XLO3
          ETA2=3.*FRAVOL/PI/ETEMP
          ETA=ETA2
          RETURN
          END
C
          SUBROUTINE RESET(CONC,TIME,NPT,DELTM,LCONV,LPRSTY,LRATE)
C
C   THIS SUBROUTINE CALCULATES THE VALUE OF TAU AT
C   EACH POINT IN THE PELLET BASED ON THE CONCENTRATION
C   HISTORY OF THE GAS REACTANT. THEN OBTAINS THE VALUES
C   OF CONVERSION, DIFFUSIVITY, POROSITY AND REACTIVITY USING
C   NEWVAL
```

```
C
      REAL KRATE
      REAL R1(50)
      REAL ETA(50),LCONV(50),LPRSTY(50)
      REAL CONC(50),LRATE(50)
      REAL OLDTAU(50),NEWTAU(50),OLDCNC(50),NEWCNC(50)
      COMMON/WORK/TAUFTR,CNVFTR,RTEFTR,RADFTR,EPLSN,FINFTR,FCORR
      COMMON/PARAM/KRATE,ALPHA,DB,DK,DS,VR,CZERO,CBULK
      COMMON/TABLE/TTABLE(100,50),RTABLE(100,50),PTABLE(100,50)
      COMMON/PELLET/RADIUS(50),RSQRD(50),DELRP,DELRSQ
      COMMON/COEFF/A1(50),A3(50)
      DATA NEWCNC/50*0.0/
      DATA OLDTAU,NEWTAU/100*0.0/
      DATA OLDTM,NCALL/0.,0/
C
C   CONC=VECTOR CONTAINING THE LOCAL GAS CONCENTRATION CALCULATED
C        FROM A PSEUDO STEADY STATE MASS BALANCE
C   TIME=TIME SINCE THE BEGINNING OF REACTION
C   NPT=NUMBER OF GRID POINTS IN THE PELLET DIFFERENCE
C       REPRESENTATION OF THE PELLET
C   DELTM= TIME INCREMENT
C   LCONV=VECTOR CONTAINING THE VALUE OF THE LOCAL CONVERSION
C   LPRSTY=VECTOR CONTAINING THE VALUE OF LOCAL POROSITY
C   LRATE=VECTOR CONTAINING THE VALUE OF THE LOCAL RATE
C
      LOCNPT=NPT
      NCALL=NCALL+1
      IF(TIME.LE.OLDTM) GO TO 20
      OLDTM=TIME
      IF(NCALL.GT.1) GO TO 5
      DO 4  I=1,LOCNPT
         OLDCNC(I)=CONC(I)
4     CONTINUE
      GO TO 20
5     CONTINUE
      DO 10 I=1,LOCNPT
         OLDTAU(I)= NEWTAU(I)
         OLDCNC(I)= NEWCNC(I)
10    CONTINUE
20    CONTINUE
      DO 30 I=1,LOCNPT
         NEWCNC(I) = CONC(I)
         AVECNC   =(NEWCNC(I)+OLDCNC(I))/2.
         NEWTAU(I)= OLDTAU(I) + AVECNC*DELTM/CZERO
30    CONTINUE
      DO 50 I=1,LOCNPT
       CALL NEWVAL(NEWTAU(I),A1(I),A3(I),LCONV(I),LPRSTY(I))
       LRATE(I)=A3(I)*CONC(I)*RTEFTR
C     WRITE(6,*) I, 'RTABLE(1,I)= ',RTABLE(1,I)
50    CONTINUE
      RETURN
      END
C
      SUBROUTINE NEWVAL(TAU,DIFF,RTE,CONV,PRSTY)
C
C   THIS SUBROUTINE CALCULATES VALUES OF THE MACROSCOPIC
C    PROPERTIES OF THE POROUS MEDIUM FOR A GIVEN VALUE OF TAU.
C    IT INTERPOLATES OVER A CUBIC SPLINE USING SPLFUN.
C
      COMMON/VALUES/TVALUE(100),DVALUE(100),RVALUE(100),PVALUE(100)
      COMMON/PVAL/DPVAL(100),RPVAL(100),PPVAL(100)
      COMMON/WORK/TAUFTR,CNVFTR,RTEFTR,RADFTR,EPSLN,FINFTR,FCORR
```

```
       COMMON/LENGTH/NDIV
C
C      TAU= INTEGRAL OF (C/CZERO) W.R.T TIME
C      DIFF= EFFECTIVE DIFFUSIVITY OF THE POROUS MEDIUM
C      RTE= EFFECTIVE REACTIVITY OF POROUS MEDIUM
C      CONV=CONVERSION OF THE SOLID REACTANT
C      PRSTY= POROSITY OF THE POROUS MEDIUM
C
       LNDIV=NDIV
       TLOC=TAU
       DO 10 J=1,LNDIV
         IF(TLOC.LT.TVALUE(J)) GO TO 20
10     CONTINUE
       WRITE(6,100) TLOC
       STOP
20     CONTINUE
       I=J-1
       DIFF = SPLFUN(TLOC,TVALUE(I),TVALUE(I+1),DVALUE(I),DVALUE(I+1),
      1              DPVAL(I),DPVAL(I+1))
       RTE=SPLFUN(TLOC,TVALUE(I),TVALUE(I+1),RVALUE(I),RVALUE(I+1),
      1          RPVAL(I),RPVAL(I+1))
       PRSTY=SPLFUN(TLOC,TVALUE(I),TVALUE(I+1),PVALUE(I),PVALUE(I+1),
      1        PPVAL(I),PPVAL(I+1))
       CONV=(EPSLN-PRSTY)/CNVFTR
       IF(CONV.LE.1.E-12) CONV= 0.
100    FORMAT(///20X,'TAU IS OUT OF BOUNDS'/20X,'TAU =',E12.5)
       RETURN
       END
C
       SUBROUTINE FINISH(CONV,LCONV,RATE,LRATE,PRSTY,LPRSTY,
      1 RTEMAX,EFF,NPT)
C
C    THIS SUBROUTINE INTEGRATES OVER THE ENTIRE PELLET TO
C    DETERMINE THE OVERALL VALUES OF THE MACROSCOPIC
C    PROPERTIES OF INTEREST
C
         REAL LCONV(50),LRATE(50),LPRSTY(50)
         REAL RLRATE(50),RLCONV(50), RLPR(50)
         COMMON/COEFF/A1(50),A3(50)
         COMMON/PELLET/RADIUS(50),RSQRD(50),DELRP,DELRSQ
         COMMON/WORK/TAUFTR,CNVFTR,RTEFTR,RADFTR,EPSLN,FINFTR,FCORR
C
C     CONV= OVERALL CONVERSION OF SOLID REACTANT
C     LCONV=VECTOR CONTAINING THE LOCAL CONVERSION
C     RATE= OVERALL RATE OF CHANGE OF CONVERSION
C     LRATE=VECTOR CONTAINING THE VALUE OF THE LOCAL RATE
C     PRSTY=OVERALL POROSITY
C     LPRSTY=VECTOR CONTAINING LOCAL POROSITY
C     RTEMAX= RATE AT THE OUTSIDE THE PELLET WHEN T= 0.
C     EFF= EFFECTIVENESS FACTOR (RATE/RTFMAX)
C     NPT= NUMBER OF GRID POINTS IN THE FINITE DIFFERENCE
C          REPRESENTATION OF THE PELLET
C
         LNPT=NPT
         DO 10 I=1,NPT
           RLRATE(I) = RSQRD(I)*LRATE(I)
           RLCONV(I)= RSQRD(I)*LCONV(I)
           RLPR(I) = RSQRD(I)*LPRSTY(I)
10       CONTINUE
         CALL SIMPSN(RLRATE,RTEMP,DELRP,LNPT)
         CALL SIMPSN(RLCONV,COTEMP,DELRP,LNPT)
         CALL SIMPSN(RLPR,PTEMP,DELRP,LNPT)
```

```
      RATE=RTEMP*RADFTR
      CONV=COTEMP*RADFTR
      PRSTY=PTEMP*RADFTR
      EFF=RATE/RTEMAX
      RETURN
      END
C
      SUBROUTINE SIMPSN(F,FSUM,DELX,NPT)
C
C     THIS SUBROUTINE EMPLOYS SIMPSON'S 2ND RULE OVER THE
C     FIRST FOUR POINTS AND THE COMPOSITE OF SIMPSON'S 1ST
C     RULE OVER THE REMAINING POINTS TO INTEGRATE THE FUNCTION
C     F. THIS SUBROUTINE REQUIRES THAT NPT BE AN EVEN VALUE.
C
      REAL F(50),WT(6)
      DATA WT/9.,27.,27.,17.,4.,2./
C
C    F=VECTOR CONTAINING VALUES OF THE FUNCTION TO BE INTEGRATED
C    FSUM=INTEGRATED VALUE OF THE FUNCTION F.
C    DELX=THE STEP SIZE IN THE INDEPENDENT VARIABLE X
C    NPT=EVEN NUMBER, WHICH REPRESENTS THE NUMBER OF POINTS AT
C        WHICH F IS EVALUATED
C
      LNPT=NPT
      FTOT=F(LNPT)
      DO 10 I=1,4
        FTOT=FTOT+(WT(I)*F(I)/8.)
10    CONTINUE
      FTOT=FTOT+(WT(5)*F(5))
      LIM=LNPT-2
      DO 20 I=6,LIM,2
      SUM=(WT(6)*F(I))+(WT(5)*F(I+1))
      FTOT=FTOT+SUM
20    CONTINUE
      FSUM=FTOT*DELX/3.
      RETURN
      END
C
      FUNCTION COMB(R1)
      COMMON/PARAM/KRATE,ALPHA,DB,DK,DS,VR,CZERO,CBULK
C
C   THIS FUNCTION CALCULATES THE DIFFUSIVITY THROUGH A SINGLE
C   PORE OF RADIUS R1, TAKING INTO ACCOUNT THE COMBINATION OF
C   BULK AND KNUDSEN DIFFUSION
C
      IF(R1.GT.0.) GO TO 10
      COMB=0.
      RETURN
10    COMB=1./((1./DB)+(1./DK/R1))
      RETURN
      END
C
      SUBROUTINE INTE(R1,ETA,A1,A3,LPRSTY,NTOT)
C
C   THIS SUBROUTINE EMPLOYS TWO POINT GAUSS-LEGENDRE
C   QUADRATURE TO INTEGRATE OVER ALL VALUES OF R1 AND
C   ETA TO OBTAIN MACROSCOPIC PROPERTIES OF THE POROUS
C   MEDIUM
C
      EXTERNAL COMB
      REAL R1(50),ETA(50),R1CUBE(50)
      REAL A1TEMP(50),A3TEMP(50)
```

```
      REAL R1TSQ(2),R1TEMP(2),F1TEMP(2),R2TSQ(2),R2TEMP(2),F3TEMP(2)
      REAL KRATE,LCFTR,LCONV,LPRSTY
      COMMON/PROP/RZERO(50),RZSQ(50,2)
      COMMON/PARAM/KRATE,ALPHA,DB,DK,DS,VR,CZERO,CBULK
      COMMON/FACTOR/TRTSTY
      COMMON/TOTAL/ETASUM(50),EZERO(50),ETATOT
      DATA PI/3.14159/
      DATA Z/0.5773503/
C
C   R1=  VECTOR CONTAINING THE VALUES OF THE INNER RADII
C   ETA=VECTOR CONTAINING THE NUMBER OF PORES WITH RADII
C        BETWEEN (R1-DELTA R1) AND R1 PER UNIT RADIUS,
C        PER UNIT AREA
C   A1= EFFECTIVE DIFFUSIVITY OF THE POROUS MEDIUM
C   A3= EFFECTIVE REACTIVITY OF THE POROUS MEDIUM
C   LPRSTY=LOCAL POROSITY OF THE POROUS MEDIUM
C   NTOT=SIZE OF VECTORS R1 AND ETA
C
      LOCN=NTOT
      DO 10 I=1,LOCN
        IF(ETA(I).GT.0.) GO TO 20
10    CONTINUE
      A1=0.
      A3=0.
      LPRSTY=0.
      RETURN
20    CONTINUE
      DO 30 J=I,LOCN
        ZTEMP1=Z*(R1(J)-R1(J-1))
        ZTEMP2=R1(J-1)+R1(J)
        R1TEMP(1)=(ZTEMP2-ZTEMP1)/2.
        R1TEMP(2)=(ZTEMP2+ZTEMP1)/2.
        DO 25 K=1,2
          R1TSQ(K)=R1TEMP(K)*R1TEMP(K)
          F1TEMP(K)=R1TSQ(K)*COMB(R1TEMP(K))
          TEMP1=R1TSQ(K)-(ALPHA*RZSQ(J,K))
          R2TSQ(K)=TEMP1/(1.-ALPHA)
          R2TEMP(K)=SQRT(R2TSQ(K))
          TEMP2=(R2TEMP(K)/DS)*ALOG(R2TEMP(K)/R1TEMP(K))
          TEMP3=(1./KRATE)+TEMP2
          F3TEMP(K)=R2TEMP(K)/TEMP3
25      CONTINUE
        A1TEMP(J)=F1TEMP(1)+F1TEMP(2)
        A3TEMP(J)=F3TEMP(1)+F3TEMP(2)
C     WRITE(6,*) J, 1./KRATE, TEMP2
30      CONTINUE
        A1LOC=0.
        A3LOC=0.
        PLOC=0.0
        R1CUBE(I-1)=R1(I-1)*R1(I-1)*R1(I-1)
        DO 40 J=I,LOCN
          A1R1= A1TEMP(J)*ETA(J)
          A3R1=A3TEMP(J)*ETA(J)
          DELR=R1(J)-R1(J-1)
          A1LOC=A1LOC+(A1R1*DELR)
          A3LOC=A3LOC+(A3R1*DELR)
          R1CUBE(J)=R1(J)*R1(J)*R1(J)
          PTEMP1=R1CUBE(J)-R1CUBE(J-1)
          PTEMP2=PTEMP1*ETA(J)
          PLOC=PLOC+PTEMP2
40      CONTINUE
        A1=PI*A1LOC/TRTSTY/2.
```

```
        A3=PI*A3LOC
        LPRSTY=PLOC*PI/3.
        RETURN
        END
C
      SUBROUTINE SHOW(TIME,CONV,RATE,EFF,PRSTY,CONC,DEFF,
     1     LCONV,LRATE,LPRSTY,NPTR,NITER)
C
C   THIS SUBROUTINE PRINTS THE IMPORTANT VALUES CALCULATED
C   AT EACH TIME STEP
C
      REAL DEFF(50),LCONV(50),LRATE(50),LPRSTY(50),CONC(50)
C     CHARACTER*20 LABEL(6)
      COMMON/PELLET/RADIUS(50),RSQRD(50),DELPR,DELRSQ
       COMMON/PARAM/KRATE,ALPHA,DB,DK,DS,VR,CZERO,CBULK
      COMMON/PRINT/IPRINT
C     DATA LABEL/  RADIUS,  CONC,  D(EFF),  LCONV,
C    1    LRATE,  LPRSTY/
C
C  TIME= TIME SINCE THE REACTION BEGAN (SEC)
C  CONV= OVERALL CONVERSION IN THE PELLET
C  RATE=  OVERALL RATE OF CHANGE OF CONVERSION (SEC-1)
C  EFF= EFFECTIVENESS FACTOR(RATE/RTEMAX)
C  PRSTY=OVERALL POROSITY (CM3/CM3)
C  CONC=VECTOR CONTAINING THE REACTANT GAS CONCENTRATION (MOLE/CM3)
C  DEFF= VECTOR CONTAINING THE EFFFECTIVE DIFFUSIVITY (CM2/SEC)
C  LCONV= VECTOR CONTAINING THE LOCAL CANVERSION
C  LRATE= VECTOR CONTAINING THE LOCAL REACTION RATE (SEC-1)
C  LPRSTY= ========================= POROSITY (CM3/CM3)
C  NPTR=NUMBER OF GRID POINTS IN THE FINITE DIFFERENCE AT THIS
C       TIME STEP
C
C   IF (IPRINT.EQ.0) ONLY THE INTEGRATED VALUES ARE PRINTED OUT
C   IF (IPRINT.EQ.1) LOCAL VALUES ARE PRINTED OUT AT EVERY
C                    (NPTR/10) GRID POINTS
C   IF (IPRINT.EQ.2) LOCAL VALUES ARE PRINTED OUT AT EVERY POINT
C
       INC=NPTR/10
       IF(IPRINT.EQ.2) INC=1
       NPT=NPTR
       WRITE(6,510) TIME/60.,CONV,RATE,EFF,PRSTY
       IF(IPRINT.EQ.0) GO TO 10
       WRITE(6,*) '(1)R(I) (2)C(I) (3)DE(I)(4)X(I)  (5) KE(I)(6)E(I)'
       WRITE(6,520)   (RADIUS(J)/RADIUS(NPT),J=INC,NPT,INC)
       WRITE(6,525)   (CONC(J)/CBULK,J=INC,NPT,INC)
       WRITE(6,520)          (DEFF(J),J=INC,NPT,INC)
       WRITE(6,520)          (LCONV(J),J=INC,NPT,INC)
       WRITE(6,520)          (LRATE(J),J=INC,NPT,INC)
       WRITE(6,520)          (LPRSTY(J),J=INC,NPT,INC)
       WRITE(6,530) NITER
10     CONTINUE
       NITER=0
510   FORMAT(5X,'TIME (MIN.)= ',E12.5,9X,'CONV= ',E12.5,
     1 /9X,'RATE= ',E12.5,9X,'EFF= ',E12.5,/9X,'POROSITY= ',E12.5)
520    FORMAT(5X, 2(5E12.5/))
525    FORMAT(5X, 2(5E12.5/))
530    FORMAT(5X,'NUMBER OF ITERATIONS= ',I3//)
       RETURN
       END
C
       SUBROUTINE TRIDAG(IF,L,A,B,C,D,Y)
C
```

```
C   THIS SUBROUTINE SOLVES ANY SET OF LINEAR EQUATIONS
C   THAT CAN BE PUT INTO A TRIDIAGONAL MATRIX (FINITE
C   DIFFERENCE AND CUBIC SPLINE)
C
      DIMENSION A(L),B(L),C(L),D(L),Y(L),BETA(301),GAMMA(301)
C
C    IF = INDEX OF THE FIRST VALUE
C    L = INDEX OF THE LAST VALUE
C    A,B,C = VECTORS SPECIFYING THE COEFFICIENTS IN THE TRIDIAGONAL
C            MATRIX
C    D = VECTOR SPECIFYING THE CONSTANT TERM
C    Y = RESULTANT VECTOR FROM SOLVING THE (L-IF) LINEAR EQNS.
C
      BETA(IF)= B(IF)
      GAMMA(IF)=D(IF)/BETA(IF)
      IFP1= IF+1
      DO 1 I=IFP1,L
      BETA(I)=B(I)-A(I)*C(I-1)/BETA(I-1)
 1    GAMMA(I)=(D(I)-A(I)*GAMMA(I-1))/BETA(I)
      Y(L)=GAMMA(L)
      LAST=L-IF
      DO 2 K=1,LAST
      I=L-K
 2    Y(I)=GAMMA(I)-C(I)*Y(I+1)/BETA(I)
      RETURN
      END
C
      SUBROUTINE DIFFEQ(CONC,CBULK,NPTR)
C
C   THIS SUBROUTINE GENERATES A SET OF LINEAR EQUATIONS GENERATED
C   BY THE FINITE DIFFERENCE APPROXIMATION OF THE MASS BALANCE OF
C   A GAS DIFFUSING INTO A SPHERICAL PELLET WITH CHEMICAL REACTION.
C
C   IT THEN SOLVES THESE EQUATIONS TO OBTAIN THE PSEUDO STEADY
C   STATE GAS CONCENTRATION PROFILE
C
      REAL CONC(50)
      REAL A(50),B(50),C(50),D(50)
      COMMON/COEFF/DEFF(50),RK(50)
      COMMON/PELLET/RPEL(50),RPSQ(50),DELR,DELRSQ
      COMMON/WORK/TAUFTR,CNVFTR,RTEFTR,RADFTR,EPSLN,FINFTR,FCORR
      DATA A,B,C,D/49*0.0,1.0,150*0.0/
      DATA IFIRST/1/
CC
CC    CONC=VECTOR CONTAINING THE CONCENTRATION OF THE REACTANT GAS
CC    CZERO= REACTANT GAS CONC. AT R=RZERO (OUTSIDE OR THE PELLET)
CC    NPTR = NUMBER OF GRID POINTS IN THE FINITE DIFFERENCE
CC           APPROXIMATION OF THE PELLET
CC
       LNPT=NPTR-1
       C(1)=-6.*DEFF(1)/DELRSQ
       B(1)=RK(1)-C(1)
       A(2)=-(RPSQ(2)*DEFF(2))/2.
       TEMP2=RPSQ(3)*DEFF(3)
       C(2)=(A(2)-TEMP2)/2.
       TEMP3=RPSQ(2)*RK(2)*DELRSQ
       B(2)=TEMP3-C(2)-A(2)
       DO 10 I=3,LNPT
          TEMP1=TEMP2
          TEMP2=RPSQ(I+1)*DEFF(I+1)
          C(I)=-(TEMP1+TEMP2)/2.
          A(I)=C(I-1)
```

```
         TEMP3=RPSQ(I)*RK(I)*DELRSQ
         B(I)=TEMP3-C(I)-C(I-1)
10    CONTINUE
      LNPT= LNPT+1
      FTR=FINFTR/DEFF(LNPT)
      A(LNPT)=FCORR
      B(LNPT)=(FTR/CBULK)-A(LNPT)+(DELRSQ*RK(LNPT)/DEFF(LNPT)/2.)
      D(LNPT)=FTR
      CALL TRIDAG(IFIRST,LNPT,A,B,C,D,CONC)
      RETURN
      END
```

Data Input for Sorbent 1

INPUT VALUE	COMMENT
2.5E-02	particle radius, cm
2.20	ratio of molar ratios of prod. and react.
0.15	bulk CO_2 mol fraction
1.0E-03	reaction rate constant, cm/s
1.0E-09	product layer diffusivity, cm^2/s
3.	tortuosity factor
1.0	molecular diffusivity, cm^2/s
16.8	molar volume of solid reactant, cm^3/mol
2.0	reaction time, hr
3.345	mass density of CaO, g/cm^3
10.	mass transfer coefficient, cm/s
650.	reaction temperature, C
0.1	pore diameter base, μm
0.05	maximum conversion increment
1.	total pressure, atm
0.01	equilibrium CO_2 pressure, atm
1	
2	
20	

0.1	.0
0.0907	.0006
0.0804	.0035
0.0724	.0115
0.0656	.0298
0.0604	.0504
0.0519	.1076
0.0402	.2106
0.0363	.2363
0.0303	.2607
0.0259	.268
0.0227	.2717
0.0202	.2737
0.0181	.275
0.013	.276
0.0101	.277
0.0091	.28
0.0065	.3
0.005	.34
0.004	.355

Example of Output of Computer Program

MULTIPLE PORE MODEL

TEMPERATURE(DEG C)= 650.0

INPUT DATA

PELLET RADIUS(CM)= 0.25000E-01
RATIO OF MOLAR VOLUMES= 2.2000
BULK CO2 CONCENTRATION(MOLES/CC)= 0.18481E-05
REACTION RATE CONCTANT(CM/SEC)= 0.10000E-02
PRODUCT LAYER DIFFUSIVITY(CM2/SEC)= 0.10000E-08
PELLET TURTUOSITY FACTOR= 3.00
BULK DIFFUSIVITY (CM2/SEC)= 0.10000E+01
KNUDSEN DIFFUSION COEFF. (CM/SEC)= 0.44431E+05
REACTANT MOLAR VOLUME= 16.8000
REACTION TIME(HRS)= 2.0000
VOLUME PER GRAM OF SOLID(CM3/GM)= 0.2990
MASS TRANSFER COEFF.= 10.00000
TOTAL NUMBER OF DATA POINTS= 20
MAXIMUM NUMBER OF DIVISION= 50
CONVERSION INCREMENT= 0.050

DIAMETER(CM)=	CUMVOLUME(CM3/CM3)
0.10000E-04	0.0000
0.90700E-05	0.0009
0.80400E-05	0.0054
0.72400E-05	0.0176
0.65600E-05	0.0456
0.60400E-05	0.0771
0.51900E-05	0.1645
0.40200E-05	0.3220
0.36300E-05	0.3613
0.30300E-05	0.3987
0.25900E-05	0.4098
0.22700E-05	0.4155
0.20200E-05	0.4185
0.18100E-05	0.4205
0.13000E-05	0.4220
0.10100E-05	0.4236
0.91000E-06	0.4282
0.65000E-06	0.4587
0.50000E-06	0.5199
0.40000E-06	0.5429

1

RZERO	ETASUM	EZERO
0.20000E-06	0.00000E+00	0.00000E+00
0.22500E-06	0.85246E+11	0.34098E+19
0.25000E-06	0.61061E+11	0.24424E+19
0.28750E-06	0.14337E+12	0.38231E+19
0.32500E-06	0.96886E+11	0.25836E+19
0.39000E-06	0.41160E+11	0.63323E+18
0.45500E-06	0.24936E+11	0.38362E+18
0.48000E-06	0.34268E+10	0.13707E+18
0.50500E-06	0.29310E+10	0.11724E+18
0.57750E-06	0.88173E+09	0.12162E+17
0.65000E-06	0.60472E+09	0.83409E+16

0.77750E-06	0.51572E+09	0.40449E+16
0.90500E-06	0.31498E+09	0.24704E+16
0.95750E-06	0.37473E+09	0.71377E+16
0.10100E-05	0.31787E+09	0.60548E+16
0.10725E-05	0.46187E+09	0.73900E+16
0.11350E-05	0.38778E+09	0.62045E+16
0.12150E-05	0.67346E+09	0.84183E+16
0.12950E-05	0.55271E+09	0.69089E+16
0.14050E-05	0.10125E+10	0.92042E+16
0.15150E-05	0.80043E+09	0.72766E+16
0.16650E-05	0.24530E+10	0.16354E+17
0.18150E-05	0.18718E+10	0.12478E+17
0.19125E-05	0.18461E+10	0.18935E+17
0.20100E-05	0.15843E+10	0.16249E+17
0.23025E-05	0.57261E+10	0.19576E+17
0.25950E-05	0.39095E+10	0.13366E+17
0.28075E-05	0.19791E+10	0.93132E+16
0.30200E-05	0.15769E+10	0.74206E+16
0.31500E-05	0.53757E+09	0.41352E+16
0.32800E-05	0.47496E+09	0.36535E+16
0.34500E-05	0.40293E+09	0.23702E+16
0.36200E-05	0.34755E+09	0.20444E+16
0.38200E-05	0.14434E+09	0.72171E+15
0.40200E-05	0.12336E+09	0.61679E+15
0.42775E-05	0.42226E+08	0.16399E+15
0.45350E-05	0.35247E+08	0.13688E+15
0.47675E-05	0.69128E+07	0.29732E+14
0.50000E-05	0.59717E+07	0.25685E+14

TAU	DIFFUSIVITY	RATE CONST.	POROSITY
0.00000E+00	0.14342E-01	0.11871E+04	0.54285E+00
0.36218E-01	0.14328E-01	0.11873E+04	0.54205E+00
0.81661E-01	0.14310E-01	0.11877E+04	0.54104E+00
0.12275E+00	0.14293E-01	0.11879E+04	0.54014E+00
0.18226E+00	0.14269E-01	0.11883E+04	0.53882E+00
0.22831E+00	0.14251E-01	0.11885E+04	0.53781E+00
0.31585E+00	0.14216E-01	0.11890E+04	0.53588E+00
0.36931E+00	0.14195E-01	0.11893E+04	0.53470E+00
0.47842E+00	0.14151E-01	0.11897E+04	0.53231E+00
0.53948E+00	0.14127E-01	0.11899E+04	0.53097E+00
0.72171E+00	0.14056E-01	0.11904E+04	0.52698E+00
0.79583E+00	0.14026E-01	0.11906E+04	0.52536E+00
0.10166E+01	0.13941E-01	0.11908E+04	0.52055E+00
0.11042E+01	0.13907E-01	0.11908E+04	0.51865E+00
0.12585E+01	0.13847E-01	0.11906E+04	0.51531E+00
0.13520E+01	0.13811E-01	0.11904E+04	0.51329E+00
0.15222E+01	0.13746E-01	0.11900E+04	0.50961E+00
0.16218E+01	0.13709E-01	0.11896E+04	0.50746E+00
0.19733E+01	0.13576E-01	0.11878E+04	0.49992E+00
0.20890E+01	0.13533E-01	0.11870E+04	0.49745E+00
0.24880E+01	0.13386E-01	0.11836E+04	0.48896E+00
0.26204E+01	0.13338E-01	0.11822E+04	0.48615E+00
0.33086E+01	0.13091E-01	0.11729E+04	0.47168E+00
0.34705E+01	0.13034E-01	0.11701E+04	0.46830E+00
0.42500E+01	0.12765E-01	0.11534E+04	0.45217E+00
0.44430E+01	0.12700E-01	0.11483E+04	0.44821E+00
0.49171E+01	0.12542E-01	0.11334E+04	0.43855E+00
0.51253E+01	0.12474E-01	0.11257E+04	0.43433E+00
0.56407E+01	0.12308E-01	0.10978E+04	0.42385E+00
0.58649E+01	0.12238E-01	0.10659E+04	0.41947E+00
0.64871E+01	0.12047E-01	0.95516E+03	0.40791E+00
0.67305E+01	0.11974E-01	0.92055E+03	0.40375E+00

0.74059E+01	0.11777E-01	0.80277E+03	0.39248E+00
0.76695E+01	0.11703E-01	0.75095E+03	0.38875E+00
0.85314E+01	0.11466E-01	0.58398E+03	0.37757E+00
0.88212E+01	0.11389E-01	0.54486E+03	0.37451E+00
0.97580E+01	0.11146E-01	0.43168E+03	0.36547E+00
0.10075E+02	0.11066E-01	0.41792E+03	0.36286E+00
0.11354E+02	0.10751E-01	0.36369E+03	0.35288E+00
0.11709E+02	0.10665E-01	0.34808E+03	0.35021E+00
0.13104E+02	0.10338E-01	0.30911E+03	0.34099E+00
0.13500E+02	0.10247E-01	0.29886E+03	0.33849E+00
0.15429E+02	0.98160E-02	0.26928E+03	0.32717E+00
0.15883E+02	0.97171E-02	0.26508E+03	0.32462E+00
0.17997E+02	0.92687E-02	0.25349E+03	0.31301E+00
0.18513E+02	0.91620E-02	0.25077E+03	0.31022E+00
0.20197E+02	0.88217E-02	0.24260E+03	0.30129E+00
0.20762E+02	0.87100E-02	0.23993E+03	0.29833E+00
0.22582E+02	0.83584E-02	0.23201E+03	0.28897E+00
0.23199E+02	0.82419E-02	0.22944E+03	0.28584E+00
0.27897E+02	0.73996E-02	0.21134E+03	0.26279E+00
0.28653E+02	0.72711E-02	0.20866E+03	0.25920E+00
0.33907E+02	0.64277E-02	0.19053E+03	0.23511E+00
0.34819E+02	0.62898E-02	0.18754E+03	0.23109E+00
0.39317E+02	0.56444E-02	0.17347E+03	0.21190E+00
0.40364E+02	0.55020E-02	0.17039E+03	0.20759E+00
0.45322E+02	0.48671E-02	0.15640E+03	0.18794E+00
0.46522E+02	0.47226E-02	0.15323E+03	0.18337E+00
0.50324E+02	0.42873E-02	0.14354E+03	0.16936E+00
0.51642E+02	0.41440E-02	0.14027E+03	0.16466E+00
0.55769E+02	0.37204E-02	0.13047E+03	0.15049E+00
0.57219E+02	0.35797E-02	0.12721E+03	0.14566E+00
0.62631E+02	0.30937E-02	0.11491E+03	0.12860E+00
0.64254E+02	0.29589E-02	0.11117E+03	0.12378E+00
0.70173E+02	0.25082E-02	0.98366E+02	0.10728E+00
0.71990E+02	0.23818E-02	0.94947E+02	0.10255E+00
0.79290E+02	0.19264E-02	0.81286E+02	0.84865E-01
0.81347E+02	0.18121E-02	0.77373E+02	0.80293E-01
0.89374E+02	0.14171E-02	0.62957E+02	0.63728E-01
0.91702E+02	0.13211E-02	0.59397E+02	0.59780E-01
0.10242E+03	0.94704E-03	0.44402E+02	0.43970E-01
0.10511E+03	0.86834E-03	0.40834E+02	0.40456E-01
0.11701E+03	0.59556E-03	0.29434E+02	0.28578E-01
0.12012E+03	0.53696E-03	0.26901E+02	0.25915E-01
0.13234E+03	0.35720E-03	0.18574E+02	0.17629E-01
0.13591E+03	0.31563E-03	0.16727E+02	0.15656E-01
0.14945E+03	0.19835E-03	0.10869E+02	0.10010E-01
0.15354E+03	0.17205E-03	0.94940E+01	0.87258E-02
0.15776E+03	0.14848E-03	0.81694E+01	0.75703E-02
0.16212E+03	0.12730E-03	0.69524E+01	0.65374E-02
0.16663E+03	0.10825E-03	0.60576E+01	0.55985E-02
0.17130E+03	0.91468E-04	0.52119E+01	0.47573E-02
0.17614E+03	0.76711E-04	0.44489E+01	0.40136E-02
0.18118E+03	0.63689E-04	0.37343E+01	0.33510E-02
0.18642E+03	0.52411E-04	0.31315E+01	0.27711E-02
0.19189E+03	0.42646E-04	0.26095E+01	0.22580E-02
0.19761E+03	0.34425E-04	0.21091E+01	0.18191E-02
0.20361E+03	0.27655E-04	0.16796E+01	0.14609E-02
0.20992E+03	0.21933E-04	0.12848E+01	0.11657E-02
0.21659E+03	0.17112E-04	0.99360E+00	0.92207E-03
0.22368E+03	0.13057E-04	0.80270E+00	0.71122E-03
0.23123E+03	0.97184E-05	0.61720E+00	0.53257E-03
0.23936E+03	0.71497E-05	0.45882E+00	0.39425E-03
0.24817E+03	0.51039E-05	0.31460E+00	0.28831E-03

0.25785E+03	0.34138E-05	0.22750E+00	0.20310E-03
0.26865E+03	0.20966E-05	0.16752E+00	0.13115E-03
0.28102E+03	0.11423E-05	0.10995E+00	0.74821E-04
0.29579E+03	0.52967E-06	0.58266E-01	0.36338E-04
0.31510E+03	0.15137E-06	0.24237E-01	0.13041E-04
0.35789E+03	0.00000E+00	0.00000E+00	0.00000E+00

RTEMAX= 0.803441405E-01

TAU	DIFFUSIVITY	RATE CONST.	POROSITY
0.00000E+00	0.14342E-01	0.11871E+04	0.54285E+00
0.48878E-01	0.14328E-01	0.11873E+04	0.54205E+00
0.11020E+00	0.14310E-01	0.11877E+04	0.54104E+00
0.16565E+00	0.14293E-01	0.11879E+04	0.54014E+00
0.24596E+00	0.14269E-01	0.11883E+04	0.53882E+00
0.30811E+00	0.14251E-01	0.11885E+04	0.53781E+00
0.42625E+00	0.14216E-01	0.11890E+04	0.53588E+00
0.49840E+00	0.14195E-01	0.11893E+04	0.53470E+00
0.64564E+00	0.14151E-01	0.11897E+04	0.53231E+00
0.72804E+00	0.14127E-01	0.11899E+04	0.53097E+00
0.97398E+00	0.14056E-01	0.11904E+04	0.52698E+00
0.10740E+01	0.14026E-01	0.11906E+04	0.52536E+00
0.13720E+01	0.13941E-01	0.11908E+04	0.52055E+00
0.14902E+01	0.13907E-01	0.11908E+04	0.51865E+00
0.16983E+01	0.13847E-01	0.11906E+04	0.51531E+00
0.18245E+01	0.13811E-01	0.11904E+04	0.51329E+00
0.20543E+01	0.13746E-01	0.11900E+04	0.50961E+00
0.21887E+01	0.13709E-01	0.11896E+04	0.50746E+00
0.26630E+01	0.13576E-01	0.11878E+04	0.49992E+00
0.28191E+01	0.13533E-01	0.11870E+04	0.49745E+00
0.33576E+01	0.13386E-01	0.11836E+04	0.48896E+00
0.35364E+01	0.13338E-01	0.11822E+04	0.48615E+00
0.44650E+01	0.13091E-01	0.11729E+04	0.47168E+00
0.46836E+01	0.13034E-01	0.11701E+04	0.46830E+00
0.57354E+01	0.12765E-01	0.11534E+04	0.45217E+00
0.59959E+01	0.12700E-01	0.11483E+04	0.44821E+00
0.66357E+01	0.12542E-01	0.11334E+04	0.43855E+00
0.69167E+01	0.12474E-01	0.11257E+04	0.43433E+00
0.76124E+01	0.12308E-01	0.10978E+04	0.42385E+00
0.79149E+01	0.12238E-01	0.10659E+04	0.41947E+00
0.87545E+01	0.12047E-01	0.95516E+03	0.40791E+00
0.90829E+01	0.11974E-01	0.92055E+03	0.40375E+00
0.99944E+01	0.11777E-01	0.80277E+03	0.39248E+00
0.10350E+02	0.11703E-01	0.75095E+03	0.38875E+00
0.11513E+02	0.11466E-01	0.58397E+03	0.37757E+00
0.11904E+02	0.11389E-01	0.54486E+03	0.37451E+00
0.13169E+02	0.11146E-01	0.43168E+03	0.36546E+00
0.13597E+02	0.11066E-01	0.41792E+03	0.36286E+00
0.15322E+02	0.10751E-01	0.36369E+03	0.35288E+00
0.15802E+02	0.10665E-01	0.34808E+03	0.35021E+00
0.17684E+02	0.10338E-01	0.30911E+03	0.34099E+00
0.18219E+02	0.10247E-01	0.29886E+03	0.33849E+00
0.20821E+02	0.98160E-02	0.26928E+03	0.32717E+00
0.21434E+02	0.97171E-02	0.26508E+03	0.32462E+00
0.24287E+02	0.92687E-02	0.25349E+03	0.31301E+00
0.24984E+02	0.91620E-02	0.25077E+03	0.31022E+00
0.27256E+02	0.88217E-02	0.24260E+03	0.30129E+00
0.28018E+02	0.87100E-02	0.23993E+03	0.29833E+00
0.30475E+02	0.83584E-02	0.23201E+03	0.28897E+00
0.31308E+02	0.82419E-02	0.22944E+03	0.28584E+00
0.37648E+02	0.73996E-02	0.21134E+03	0.26279E+00
0.38668E+02	0.72711E-02	0.20866E+03	0.25920E+00
0.45758E+02	0.64277E-02	0.19053E+03	0.23511E+00

```
      0.46989E+02      0.62898E-02      0.18754E+03      0.23109E+00
      0.53059E+02      0.56444E-02      0.17347E+03      0.21190E+00
      0.54473E+02      0.55020E-02      0.17039E+03      0.20759E+00
      0.61164E+02      0.48671E-02      0.15640E+03      0.18794E+00
      0.62782E+02      0.47226E-02      0.15323E+03      0.18337E+00
      0.67913E+02      0.42873E-02      0.14354E+03      0.16936E+00
      0.69693E+02      0.41440E-02      0.14027E+03      0.16466E+00
      0.75261E+02      0.37204E-02      0.13047E+03      0.15049E+00
      0.77219E+02      0.35797E-02      0.12721E+03      0.14566E+00
      0.84522E+02      0.30937E-02      0.11491E+03      0.12860E+00
      0.86713E+02      0.29589E-02      0.11117E+03      0.12378E+00
      0.94701E+02      0.25082E-02      0.98366E+02      0.10728E+00
      0.97152E+02      0.23818E-02      0.94947E+02      0.10255E+00
      0.10700E+03      0.19264E-02      0.81286E+02      0.84865E-01
      0.10978E+03      0.18121E-02      0.77373E+02      0.80293E-01
      0.12061E+03      0.14171E-02      0.62957E+02      0.63728E-01
      0.12376E+03      0.13211E-02      0.59397E+02      0.59780E-01
      0.13821E+03      0.94704E-03      0.44402E+02      0.43970E-01
      0.14185E+03      0.86834E-03      0.40834E+02      0.40456E-01
      0.15790E+03      0.59556E-03      0.29434E+02      0.28578E-01
      0.16210E+03      0.53696E-03      0.26901E+02      0.25915E-01
      0.17860E+03      0.35720E-03      0.18574E+02      0.17629E-01
      0.18341E+03      0.31563E-03      0.16727E+02      0.15656E-01
      0.20169E+03      0.19835E-03      0.10869E+02      0.10010E-01
      0.20721E+03      0.17205E-03      0.94940E+01      0.87258E-02
      0.21290E+03      0.14848E-03      0.81694E+01      0.75702E-02
      0.21878E+03      0.12730E-03      0.69524E+01      0.65374E-02
      0.22487E+03      0.10825E-03      0.60576E+01      0.55985E-02
      0.23117E+03      0.91468E-04      0.52119E+01      0.47574E-02
      0.23771E+03      0.76711E-04      0.44489E+01      0.40136E-02
      0.24450E+03      0.63689E-04      0.37343E+01      0.33510E-02
      0.25158E+03      0.52410E-04      0.31315E+01      0.27711E-02
      0.25896E+03      0.42646E-04      0.26095E+01      0.22580E-02
      0.26668E+03      0.34425E-04      0.21091E+01      0.18191E-02
      0.27478E+03      0.27655E-04      0.16796E+01      0.14609E-02
      0.28330E+03      0.21933E-04      0.12848E+01      0.11657E-02
      0.29230E+03      0.17112E-04      0.99361E+00      0.92207E-03
      0.30186E+03      0.13058E-04      0.80270E+00      0.71122E-03
      0.31206E+03      0.97185E-05      0.61720E+00      0.53257E-03
      0.32302E+03      0.71497E-05      0.45882E+00      0.39425E-03
      0.33491E+03      0.51039E-05      0.31460E+00      0.28831E-03
      0.34797E+03      0.34139E-05      0.22750E+00      0.20310E-03
      0.36255E+03      0.20966E-05      0.16752E+00      0.13115E-03
      0.37924E+03      0.11423E-05      0.10995E+00      0.74821E-04
      0.39918E+03      0.52967E-06      0.58266E-01      0.36338E-04
      0.42523E+03      0.15137E-06      0.24237E-01      0.13041E-04
      0.48298E+03      0.00000E+00      0.00000E+00      0.00000E+00
 RTEMAX=  0.595348999E-01
1              TPLUG=  0.48250E+03  RXNSEC=  0.72000E+04    AREA(CM2/G)=
0.77902E+06
     TIME (MIN.)=  0.00000E+00          CONV=  0.96701E-05
         RATE=  0.21398E-01          EFF=  0.35943E+00
         POROSITY=  0.54285E+00
 (1)RI   (2)CI   (3)DE   (4)X(I)  (5) KE  (6)EI
      0.81633E-01 0.18367E+00 0.28571E+00 0.38776E+00 0.48980E+00
 0.59184E+00 0.69388E+00 0.79592E+00 0.89796E+00 0.10000E+01

      0.85758E-02 0.10645E-01 0.15073E-01 0.23407E-01 0.38678E-01
 0.66668E-01 0.11838E+00 0.21484E+00 0.39641E+00 0.74100E+00

      0.14342E-01 0.14342E-01 0.14342E-01 0.14342E-01 0.14342E-01
 0.14342E-01 0.14342E-01 0.14342E-01 0.14342E-01 0.14342E-01
```

```
     0.96701E-05 0.96701E-05 0.96701E-05 0.96701E-05 0.96701E-05
0.96701E-05 0.96701E-05 0.96701E-05 0.96701E-05 0.96701E-05

     0.68901E-03 0.85523E-03 0.12110E-02 0.18806E-02 0.31075E-02
0.53564E-02 0.95114E-02 0.17261E-01 0.31849E-01 0.59535E-01

     0.54285E+00 0.54285E+00 0.54285E+00 0.54285E+00 0.54285E+00
0.54285E+00 0.54285E+00 0.54285E+00 0.54285E+00 0.54285E+00

    NUMBER OF ITERATIONS=   1


    TIME (MIN.)=  0.38944E-01          CONV=  0.24887E-01
        RATE=  0.21452E-01          EFF=  0.36032E+00
        POROSITY=  0.52920E+00
(1)RI   (2)CI   (3)DE   (4)X(I)  (5) KE  (6)EI
     0.81633E-01 0.18367E+00 0.28571E+00 0.38776E+00 0.48980E+00
0.59184E+00 0.69388E+00 0.79592E+00 0.89796E+00 0.10000E+01

     0.85758E-02 0.10645E-01 0.15073E-01 0.23407E-01 0.38678E-01
0.66668E-01 0.11838E+00 0.21484E+00 0.39641E+00 0.74100E+00

     0.14334E-01 0.14332E-01 0.14328E-01 0.14320E-01 0.14306E-01
0.14280E-01 0.14232E-01 0.14142E-01 0.13976E-01 0.13667E-01

     0.81772E-03 0.10125E-02 0.14294E-02 0.22137E-02 0.36497E-02
0.62811E-02 0.11135E-01 0.20163E-01 0.37063E-01 0.68805E-01

     0.68910E-03 0.85536E-03 0.12113E-02 0.18812E-02 0.31091E-02
0.53610E-02 0.95250E-02 0.17301E-01 0.31947E-01 0.59637E-01

     0.54240E+00 0.54230E+00 0.54207E+00 0.54164E+00 0.54085E+00
0.53941E+00 0.53674E+00 0.53179E+00 0.52252E+00 0.50511E+00

    NUMBER OF ITERATIONS=   1


    TIME (MIN.)=  0.77791E-01          CONV=  0.48828E-01
        RATE=  0.20936E-01          EFF=  0.35166E+00
        POROSITY=  0.51606E+00
(1)RI   (2)CI   (3)DE   (4)X(I)  (5) KE  (6)EI
     0.81633E-01 0.18367E+00 0.28571E+00 0.38776E+00 0.48980E+00
0.59184E+00 0.69388E+00 0.79592E+00 0.89796E+00 0.10000E+01

     0.80557E-02 0.10002E-01 0.14171E-01 0.22029E-01 0.36464E-01
0.63044E-01 0.11256E+00 0.20628E+00 0.38747E+00 0.74784E+00

     0.14327E-01 0.14323E-01 0.14315E-01 0.14299E-01 0.14271E-01
0.14220E-01 0.14126E-01 0.13951E-01 0.13630E-01 0.13041E-01

     0.15916E-02 0.19729E-02 0.27891E-02 0.43249E-02 0.71402E-02
0.12296E-01 0.21812E-01 0.39523E-01 0.72719E-01 0.13515E+00

     0.64737E-03 0.80383E-03 0.11390E-02 0.17709E-02 0.29325E-02
0.50731E-02 0.90650E-02 0.16625E-01 0.31171E-01 0.59241E-01

     0.54198E+00 0.54177E+00 0.54132E+00 0.54048E+00 0.53894E+00
0.53611E+00 0.53089E+00 0.52117E+00 0.50296E+00 0.46871E+00

    NUMBER OF ITERATIONS=   3
```

```
    TIME (MIN.)=  0.11759E+00          CONV=  0.72476E-01
        RATE=  0.20563E-01          EFF=  0.34540E+00
        POROSITY=  0.50309E+00
(1)RI   (2)CI   (3)DE   (4)X(I)  (5) KE  (6)EI
     0.81633E-01 0.18367E+00 0.28571E+00 0.38776E+00 0.48980E+00
0.59184E+00 0.69388E+00 0.79592E+00 0.89796E+00 0.10000E+01

     0.78618E-02 0.97627E-02 0.13836E-01 0.21518E-01 0.35648E-01
0.61722E-01 0.11048E+00 0.20339E+00 0.38511E+00 0.75301E+00

     0.14319E-01 0.14314E-01 0.14302E-01 0.14279E-01 0.14237E-01
0.14162E-01 0.14023E-01 0.13766E-01 0.13295E-01 0.12445E-01

     0.23447E-02 0.29079E-02 0.41134E-02 0.63836E-02 0.10543E-01
0.18170E-01 0.32260E-01 0.58533E-01 0.10793E+00 0.20114E+00

     0.63187E-03 0.78471E-03 0.11123E-02 0.17304E-02 0.28680E-02
0.49695E-02 0.89022E-02 0.16383E-01 0.30778E-01 0.57221E-01

     0.54157E+00 0.54126E+00 0.54060E+00 0.53935E+00 0.53707E+00
0.53288E+00 0.52515E+00 0.51074E+00 0.48364E+00 0.43251E+00

    NUMBER OF ITERATIONS=   3


    TIME (MIN.)=  0.15812E+00          CONV=  0.95698E-01
        RATE=  0.19770E-01          EFF=  0.33207E+00
        POROSITY=  0.49035E+00
(1)RI   (2)CI   (3)DE   (4)X(I)  (5) KE  (6)EI
     0.81633E-01 0.18367E+00 0.28571E+00 0.38776E+00 0.48980E+00
0.59184E+00 0.69388E+00 0.79592E+00 0.89796E+00 0.10000E+01

     0.77664E-02 0.96455E-02 0.13674E-01 0.21275E-01 0.35275E-01
0.61161E-01 0.10974E+00 0.20293E+00 0.38711E+00 0.76359E+00

     0.14312E-01 0.14304E-01 0.14288E-01 0.14259E-01 0.14204E-01
0.14104E-01 0.13922E-01 0.13585E-01 0.12971E-01 0.11893E-01

     0.30868E-02 0.38293E-02 0.54193E-02 0.84128E-02 0.13900E-01
0.23963E-01 0.42569E-01 0.77312E-01 0.14272E+00 0.26216E+00

     0.62426E-03 0.77538E-03 0.10994E-02 0.17113E-02 0.28390E-02
0.49264E-02 0.88446E-02 0.16316E-01 0.30569E-01 0.45325E-01

     0.54116E+00 0.54075E+00 0.53988E+00 0.53824E+00 0.53523E+00
0.52971E+00 0.51950E+00 0.50044E+00 0.46456E+00 0.39904E+00

    NUMBER OF ITERATIONS=   3
```

Vita

Arpaden Silaban, son of Mula Silaban and Nona B. Hutasoit, was born on November 12, 1955 in Tarutung, North Sumatra, Indonesia. He completed his Engineer's degree in Chemical Engineering at University of Sriwijaya, Palembang, Indonesia in January 1980. He joined that university following the graduation. In 1986, he was awarded from Indonesian government a scholarship on Master's degree program at Louisiana State University. He finished his Master of Science in Chemical Engineering in Spring 1989. Beginning Summer 1989 he started to pursue his doctoral degree. He is presently completing the requirements for the Doctor of Philosophy degree.

He married Doorce Sakti Batubara, daughter of M. Batubara and R. Simangunsong, on October 12, 1985. They both are blessed with a son, Athens Gomes Partogi Silaban, now 6 years old. God willing, they are now expecting the second child to be named Grace Rouge Pastima Silaban.

DOCTORAL EXAMINATION AND DISSERTATION REPORT

Candidate: Arpaden Silaban

Major Field: Chemical Engineering

Title of Dissertation: High-Temperature High-Pressure CO_2 Removal from Coal Gas

Approved:

Major Professor and Chairman

Dean of the Graduate School

EXAMINING COMMITTEE:

Date of Examination:

April 6, 1993